

**For Reference**

---

**NOT TO BE TAKEN FROM THIS ROOM**

Ex libris  
UNIVERSITATIS  
ALBERTAEASIS











THE UNIVERSITY OF ALBERTA

RELEASE FORM

NAME OF AUTHOR            MOHAMMED ZAHEERUDDIN

TITLE OF THESIS            A   SIMULATION   MODEL   FOR   DIRECT   GAIN

                                 PASSIVE   HOUSE   AND   ITS   EXPERIMENTAL

                                 VERIFICATION

DEGREE FOR WHICH THESIS WAS PRESENTED   DOCTOR OF PHILOSOPHY

YEAR THIS DEGREE GRANTED        SPRING 1983

Permission is hereby granted to THE UNIVERSITY OF ALBERTA LIBRARY to reproduce single copies of this thesis and to lend or sell such copies for private, scholarly or scientific research purposes only.

The author reserves other publication rights, and neither the thesis nor extensive extracts from it may be printed or otherwise reproduced without the author's written permission.



THE UNIVERSITY OF ALBERTA

A SIMULATION MODEL FOR DIRECT GAIN PASSIVE HOUSE AND ITS  
EXPERIMENTAL VERIFICATION

by



MOHAMMED ZAHEERUDDIN

A THESIS

SUBMITTED TO THE FACULTY OF GRADUATE STUDIES AND RESEARCH  
IN PARTIAL FULFILMENT OF THE REQUIREMENTS FOR THE DEGREE  
OF DOCTOR OF PHILOSOPHY

DEPARTMENT OF MECHANICAL ENGINEERING

EDMONTON, ALBERTA

SPRING 1983



THE UNIVERSITY OF ALBERTA  
FACULTY OF GRADUATE STUDIES AND RESEARCH

The undersigned certify that they have read, and recommend to the Faculty of Graduate Studies and Research, for acceptance, a thesis entitled A SIMULATION MODEL FOR DIRECT GAIN PASSIVE HOUSE AND ITS EXPERIMENTAL VERIFICATION submitted by MOHAMMED ZAHEERUDDIN in partial fulfilment of the requirements for the degree of DOCTOR OF PHILOSOPHY in HEAT TRANSFER.



## DEDICATION

To Late Dr.R.R. Gilpin in appreciation for his friendship, guidance and motivation which have been very valuable to me during my graduate program. This is the last of the theses Dr.Gilpin supervised during his very short span of an exemplary research and teaching career. In a small way this dedication may serve to recognize his research contributions.

M. Zaheeruddin



## ABSTRACT

A modeling and model verification study was made of the heating load reductions produced by passive solar gains. Dynamic simulation models of components were integrated together to develop an overall model for estimating the annual heating load requirements of houses designed to employ direct solar gain.

Predictions were compared against detailed measurements of heat fluxes, radiation fluxes, room air temperatures, and the power consumption rates recorded on hourly basis at the Alberta Home Heating Research Facility.

A three stage approach to the overall problem of modeling and model verification was used. First, comparisons of various components of heat loss were made with measurements in order to test and refine the model calculations for the components. In the second step the component models were put together to test the transient response of the system as a whole. Finally, comparisons of the predicted and the measured module performance were done using typical daily variations of module temperatures and most importantly the furnace heat requirements. This methodology was instrumental in developing a comprehensive validation procedure for the house heat loss models.

Several results are of interest to modeling of component heat losses. By postulating that basement heat losses can be assumed to consist of two components: one with an annual variation and one with a diurnal variation, four



basement heat loss models were developed. These models include the effects of the dynamics of the surrounding soil, the variations in the soil thermal conductivity, the deep ground temperature effects and the surface cover effects. From the model validation study it is shown that a simple and reasonably accurate strategy is to simulate the wood frame walls and ceiling as simple resistive elements and introduce their capacitance effects via a lumped capacity approach for the transient analysis of the structure. A method is described for extracting the lumped and the distributed heat capacity parameters of the structure from simple transient decay tests. It appears from the solar gains model verification study that the available methods could introduce large errors in the hourly heating load calculations. The cause for this discrepancy appears to be inadequate modeling techniques for calculating the solar gains at low sun angles. A study is also made of the window shutter thermal response characteristics and their potential impact on the hourly heating load calculations.

The component models were integrated together to test module performance as a total system. The results of the predicted and the measured module heat requirements and the room air temperatures show a good agreement.

For evaluating the module performance a logical way of extracting the seasonally averaged heating load reductions produced by solar gains is suggested. It appears that south facing windows with shutters (RSI 1.0) could reduce the



heating requirements of a typical house by about 20%. In highly insulated modules the basement and infiltration losses could account for 50% of total loss.

Finally, an attempt is made to generalize the whole study. The results of several numerical experiments were put in the form of general design curves from which optimum values of the thermal mass or window area can be related to the resistance of the thermal envelope as well as local meteorological parameters. The effects of window orientation and of window overhang are also analyzed.



## ACKNOWLEDGEMENTS

The author wishes to express his deep gratitude to Dr.R.R. Gilpin, for his supervision, guidance and encouragement throughout this thesis investigation. Dr. Gilpin's untimely death at the time when most of this work was completed, was a great personal loss to the author. It was both a pleasure and a rewarding experience to have worked with Dr.R.R.Gilpin, who led by personal example, motivated the author to develop insights into some fundamentals of heat transfer research.

Thanks are due to Dr.J.D. Dale and Dr.D.J. Wilson who took the responsibility of seeing this work completed. Their encouragement was very helpful to carry on the work as was originally proposed by Dr. Gilpin. The author is indebted for their helpful suggestions and the great understanding they exhibited during the last stages of this work.

I am grateful to my friend, M.Y. Ackerman, Manager, The Alberta Home Heating Research Facility, who was responsible for the operation and data collection at the Facility. Our discussions on measurements and the data acquisition were quite useful and rewarding learning experiences.

I also wish to express my appreciation to Professor G.W. Sadler, and Dr.T.W. Forest for several interesting discussions on clarifying some ideas.

In particular, special thanks are due to my wife, Afroz and my daughter, Tabassum for their patience and sacrifices during the course of my researches. The continued



encouragement of my parents has been greatly appreciated.

The financial assistance from the Department of Mechanical Engineering, The University of Alberta , Natural Sciences and Engineering Research Council of Canada (Grant A7795) and The Department of Energy Mines and Resources of Canada (Research agreement No. 14/9/81) are greatly acknowledged.



## Table of Contents

Chapter	Page
1. INTRODUCTION .....	1
2. LITERATURE REVIEW .....	13
2.1 Introduction .....	13
2.2 Detailed Simulation Models .....	14
2.2.1 Response Factor Approach .....	15
2.2.1.1 Limitations of Response Factor Approach .....	20
2.2.2 Harmonic Methods .....	21
2.2.2.1 Limitations of Harmonic Methods .....	22
2.2.3 Numerical Methods .....	23
2.3 Approximate Methods .....	23
2.4 Validation of Simulation Models .....	26
2.4.1 Limitations of Validation Studies .....	29
2.5 Experimental Studies .....	29
3. THE TEST FACILITY .....	31
3.1 Introduction .....	31
3.2 Specifications of The Modules .....	33
3.3 The Data .....	37
3.4 Heat Flux Gauges .....	37
3.4.1 Calibration and Time Response Characteristics of Heat Flux Gauges .....	41
4. THE THERMAL MODEL .....	45
4.1 Introduction .....	45
4.2 Walls and Ceilings .....	49
4.2.1 The Steady State Model .....	49
4.2.2 The Transient Model .....	51
4.3 Basement Models .....	56



4.3.1	The First Model .....	63
4.3.2	The Second Model .....	68
4.3.3	The Third Model .....	72
4.3.3.1	Mathematical Formulation .....	72
4.3.3.2	Difference Formulation .....	75
4.3.3.3	Solution of Discretization Equations .....	83
4.3.4	The Fourth Model .....	83
4.4	Solar Gains .....	86
4.5	Window Shutters .....	86
4.6	Infiltration .....	87
4.7	Transient Response .....	87
4.8	The Energy Balance .....	92
5.	VERIFICATION OF COMPONENT MODELS .....	95
5.1	Introduction .....	95
5.2	Walls and Ceilings .....	95
5.2.1	The Steady State Model .....	99
5.2.2	The Transient Model: .....	107
5.3	Basements .....	119
5.3.1	The First Model .....	120
5.3.2	The Second Model .....	124
5.3.3	The Third Model .....	125
5.3.4	The Fourth Model .....	136
5.3.5	Conclusions .....	137
5.4	Solar Gains .....	148
5.5	Window Shutters .....	162
5.6	Infiltration .....	169



5.7 Transient Response .....	172
5.8 Conclusions .....	180
6. PARAMETRIC STUDY .....	181
6.1 Introduction .....	181
6.2 Effect of Variations in Wall and Ceiling Resistances .....	183
6.3 Effect of the Soil Thermal Properties .....	183
6.4 Influence of Solar Gains Predictive Techniques ...	185
6.5 Effect of Thermal Shutter Resistance .....	187
6.6 Errors due to Fluctuations in Infiltration Rates .	189
6.7 Influence of Thermal Capacity .....	189
6.8 Conclusions .....	190
7. MODULE PERFORMANCE .....	192
7.1 Introduction .....	192
7.2 Solar Gains From South Facing Windows .....	192
7.3 Module Performance .....	197
7.4 Passive Solar Contributions .....	216
7.5 Component Heat Losses .....	224
8. APPLICATIONS .....	233
8.1 Introduction .....	233
8.2 General Design Curves .....	235
8.3 Physical Significance of General Design Curves ...	242
8.4 Design Considerations for Passive houses .....	244
8.4.1 Window Overhang .....	245
8.4.2 House Orientation .....	247
8.5 Conclusions .....	250
8.5.1 Window and Mass Wall Area .....	250
8.5.2 Window Overhang .....	251



8.5.3 Window Orientation .....	252
9. SUMMARY AND CONCLUSIONS .....	253
9.1 Recommendations .....	258
REFERENCES .....	260



## List of Tables

Table	Page
3.1	Design details of the modules .....34
3.2	Nominal Insulation Values for the Modules .....35
3.3	Heat flux gauge installation details .....38
5.1	Summary of the calculated and measured resistance values for the modules .....100
5.2	A summary of the measured air infiltration rates for the modules .....171
6.1	Summary of parametric study .....191
7.1	Calculated and measured heat fluxes .....196
7.2	Summary of heating degree days and energy consumption for the modules during 1980-81 and 1981-82 heating season .....199
7.3	Comparison of the measured and predicted overall U factors for the modules .....200
7.4	Effects of solar gains and shutters on module performance: monthly results .....218
7.5	Effect of solar gains and shutters on module performance: heating season results .....225
8.1	Specifications of the house designs used for numerical experiments .....234



## List of Figures

Figure		Page
1.1	Flow chart describing the model verification procedure .....	9
2.1	Heat flows at a plane wall .....	17
3.1	Typical overall dimensions of the modules .....	36
3.2	Installation of heat flux gauges .....	39
3.3	Schematic of a heat flux gauge calibration device .....	42
3.4	Typical calibration curves for heat flux gauges .....	43
4.1	Schematic of a house illustrating the heat gains and heat losses .....	46
4.2	A schematic illustration of the energy fluxes to and from the room air temperature .....	47
4.3	Cross section of frame wall in module 4 - Thermal network .....	50
4.4	Nodal point arrangement at an interface .....	53
4.5	Nodal point arrangement in a segment of a stratified medium .....	70
4.6	Basement: The North-South geometry .....	73
4.7	Basement: The East-West geometry .....	74
4.8	Control volume for an interior nodal point .....	76
4.9	Control volumes at the boundaries .....	79
4.10	Control volume at the boundaries .....	80
4.11	Simplified house model .....	90
5.1	Distribution of relative error between the measured and the calculated heat loss coefficients .....	97
5.2	Distribution of the difference in the magnitude of heat flux measured at two locations on the same wall .....	98



5.3	Variation of wall heat flux with temperature difference for module 1 .....	101
5.4	Variation of wall heat flux with temperature difference for module 3 .....	102
5.5	Variation of wall heat flux with temperature difference for module 4 .....	103
5.6	Variation of ceiling heat flux with temperature difference for module 5 .....	104
5.7	Night time heat loss with temperature difference for module 3 .....	106
5.8	Time response of the walls in module 4 .....	109
5.9	Comparison of diurnal variation of wall heat flux with the measured data .....	111
5.10	Typical diurnal variations of ambient, room, attic temperatures and ceiling heat flux for module 2 in January 1982 .....	113
5.11	Typical diurnal variations of ambient, room, attic temperatures and ceiling heat flux for module 2 in March 1982 .....	114
5.12	Comparison of the predicted and the measured ceiling heat flux for module 2 .....	115
5.13	Ceiling resistance versus time of the year for module 2 .....	117
5.14	Comparison of the measured and the predicted ceiling heat flux for module 2 .....	118
5.15	Basement heat fluxes for module 2 .....	121
5.16	Basement heat fluxes for module 4 .....	122
5.17	Comparison of the predicted and measured basement heat flux .....	126
5.18	Temperature distribution in the ground at Edmonton .....	128
5.19	Predicted and the measured heat flux from the uninsulated basement .....	130



Figure	Page
5.20 Temperature distribution at a distance of 0.3 m from the uninsulated basement .....	131
5.21 Temperature distribution at a distance of 0.3 m from the uninsulated basement .....	132
5.22 Soil isotherms for the months of November and December .....	133
5.23 Soil isotherms for the months of January and February .....	134
5.24 Soil isotherms for the months of March and April .....	135
5.25 Effects of nondimensional depth on decrement factor for an uninsulated basement .....	139
5.26 Effects of nondimensional depth on phase shift for an uninsulated basement .....	140
5.27 Effects on nondimensional depth on decrement factor for an insulated basement .....	141
5.28 Effects of nondimensional depth on phase shift for an insulated basement .....	142
5.29 Effects of the soil conductivity on the heat losses .....	145
5.30 Comparison of the measured heat losses through the uninsulated and the insulated basement .....	147
5.31 Plot of the ratio of diffuse horizontal to horizontal total versus sun altitude .....	150
5.32 Plot of the ratio of vertical total to horizontal total for various sun altitudes .....	151
5.33 Ratio of the horizontal diffuse to horizontal total versus clearness index .....	154
5.34 Ratio of diffuse horizontal to horizontal total versus clearness index .....	156
5.35 Ratio of diffuse horizontal to extraterrestrial insolation versus	



Figure	Page
clearness index .....	157
5.36 Ratio of diffuse horizontal to extraterrestrial insolation for various sun altitudes .....	159
5.37 Transmissivity of insitu double glass .....	161
5.38 Sensor locations in window shutter cavity .....	163
5.39 Temperature distribution inside shutter cavity .....	164
5.40 Change in air temperature inside shutter cavity after shutter is closed .....	167
5.41 Change in measured resistance value of the window shutters after shutter is closed .....	168
5.42 Transient response of the modules .....	175
5.43 Transient response of the modules .....	177
5.44 Diurnal input heat flux to the basement walls .....	179
6.1 Effect of wall resistance and the soil properties on module 3 heat requirements .....	184
6.2 Effect of solar gains and transmissivity on module 3 heat requirements .....	186
6.3 effect of shutter resistance and infiltration rate on module 3 heat requirements .....	188
7.1 Window gain factors resulting from south facing windows .....	194
7.2 Overall U-Factors for modules 2 and 4 .....	201
7.3 Comparison of the predicted and the measured module temperatures and furnace heat requirement on a hourly basis .....	205
7.4 Performance of module 3 for various months of the heating season .....	207
7.5 Performance of module 3 for various months of the heating season .....	208



Figure	Page
7.6	Performance of module 3 for various months of the heating season .....209
7.7	Performance of module 4 for various months of the heating season .....210
7.8	Performance of module 4 for various months of the heating season .....211
7.9	Performance of module 4 for various months of the heating season .....212
7.10	Performance of module 2 for various months of the heating season .....213
7.11	Performance of module 2 for various months of the heating season .....214
7.12	Performance of module 2 for various months of the heating season .....215
7.13	Monthly heating load reductions produced by modules 3 and 4 .....222
7.14	Component heat losses for module 3 without shutters .....227
7.15	Component heat losses for module 3 with shutters .....228
7.16	Component heat losses for module 4 without shutters .....229
7.17	Component heat losses for module 4 with shutters .....230
7.18	Component heat losses for module 2 .....231
8.1	Simplified version of the thermal model .....236
8.2	General design curves for estimating heating load reduction produced by passive solar gain .....241
8.3	Effect of window overhang .....246
8.4	Effect of house orientation for a house with all heat gain windows in one wall .....248
8.5	Performace of a house with window area



split equally between two walls of the  
house .....249



## List of Plates

Plate	Page
3.1 View of the test facility: molules 1 through 6 numbered from left .....	32
3.2 A typical heat flux gauge - and its installation on the basement wall .....	40



## NOMENCLATURE

Symbol	Definition
A	Area ( $m^2$ )
<div style="display: flex; align-items: center;"> <div style="display: flex; flex-direction: column; align-items: center; margin-right: 10px;"> A B C D </div> <div style="font-size: 4em; line-height: 1;">}</div> </div>	Elements of transmission matrix
AHLR	Annual Heating Load Reduction Factor (Equation 8.8)
Bi	Biot Modulus ( $h \Delta x/k$ )
C	Final concentration (ppm)
Co	Initial concentration (ppm)
$C_T$	Total heat energy stored (J/K)
C	Specific heat (J/Kg-K)
D(Z)	Polynomial
E	Energy stored ( $W/^\circ C$ )
F	Transfer function
H	Horizontal Insolation ( $W/m^2$ )
H	Combined convective and radiative heat transfer coefficient ( $W/m^2-K$ )
$H_d$	Diffuse Radiation ( $W/m^2$ )
HdHr	Heating Degree Hours (Equation 8.3) (Hr- $^\circ C$ )
HHr	Heating Hours (Equation 8.4) (Hr)



HLR	Heating Load Reduction Factor
$H_o$	Extraterrestrial Insolation ( $W/m^2$ )
$I$	Intensity of Solar Radiation ( $W/m^2$ )
$I$	Internal Loads (W)
$I_f$	Fluctuating Internal Load (W)
$I_c$	Constant Component of Internal Load (W)
$I'_f$	Fluctuating Internal Load (Equation 8.9) (W)
$I'_c$	Constant Internal Load (Equation 8.10) (W)
ISHGF	Integrated Solar Heat Gain Factor ( $W/m^2$ )
$K$	Defined by Equation 5.8
$K_d$	Defined by Equation 5.7
$K$	$\equiv \sqrt{\omega/2\alpha}$ (in Equation 2.7)
$K$	Clearness Index (Equation 5.7)
$L$	Left Hand Node
$M$	Nodal Point
$M$	Mass Wall Area ( $m^2$ )
$N$	Number of Elements
$N(Z)$	Polynomial
$O$	Output
$Q$	Heat Flux ( $W/m^2$ )
$Q_A$	Energy Stored In Air (W)
$Q_L$	Energy Stored in Lumped Capacity (W)
$Q_S$	Energy Stored in Distributed Capacity (W)
$Q_{LOSS}$	Steady State Heat Loss (W)



$Q_{fan}$	Fan Load (W)
$Q_{fu}$	Furnace Heat (W)
$R$	Resistance (English units: $\text{Hr-ft}^2\text{-}^\circ\text{F/Btu}$ )
$RSI$	Resistance (SI units: $\text{K-m}^2/\text{W}$ )
$R_e$	Effective Resistance ( $\text{K-m}^2/\text{W}$ )
$R_s$	Steady State Resistance (Shutter Open) ( $\text{K-m}^2/\text{W}$ )
$R$	Initial Resistance ( $\text{K-m}^2/\text{W}$ )
$SHG$	Solar Heat Gain (W)
$SHF$	Solar Heating Fraction
$SIG$	Solar and Internal Gain Factor
$SLR$	Solar Load Ratio
$T$	Temperature ( $^\circ\text{C}$ )
$T_R$	Room Temperature ( $^\circ\text{C}$ )
$T_{min}$	Minimum Allowable Temperature ( $^\circ\text{C}$ )
$T_{max}$	Maximum Allowable Temperature ( $^\circ\text{C}$ )
$T_\infty$	Ambient Temperature ( $^\circ\text{C}$ )
$\bar{T}_y, \bar{T}_e$	Average Ground Surface Temperature ( $^\circ\text{C}$ )
$U$	Steady State Heat Loss Coefficient (Table 7.2) ( $\text{W}/^\circ\text{C}$ )
$V$	Temperature
$W$	Heat Energy Stored (W)
$W_A$	Window Area ( $\text{m}^2$ )
$WGF$	Window Gain Factor
$Y_n$	Defined by Equation 4.34
$Z_n$	Defined by Equation 4.35
$a$	Absorbtivity



$f_I$	Fraction of area through insulation path
$f_w$	Fraction of area through wood path
$h$	Heat Transfer Coefficient ( $W/m^2-K$ )
$h$	Enthalpy ( $J/m^3$ )
$k$	Thermal Conductivity ( $W/m-K$ )
$\ell$	Length (m)
$q$	Heat Flow Rate (W) (Equation 4.47)
$q$	Heat Loss Rate ( $W/^\circ C$ ) (Equation 4.83)
$t$	Time (s)
$t$	Temperature ( $^\circ C$ )
$x$	Spatial Coordinate (m)

#### Greek Letters

$\alpha$	Thermal Diffusivity ( $m^2/s$ )
$\beta$	Time Costant Parameter ( Equation 8.5)
$\gamma$	Air Change Rate
$\theta$	Temperature ( $^\circ C$ )
$\theta$	Time (s)
$\tau$	Time Constant (Hr)
$\rho$	Density ( $Kg/m^3$ )
$\omega$	Angular Frequency ( $1/s$ )
$\Delta t$	Time Increment (s)
$\Delta x$	Spatial Increment (m)
$\Delta Fo$	Fourier Number $\equiv \alpha \Delta t / (\Delta x)^2$
$\phi$	Phase Lag of Sol-Air Temperature Cycle (Radians)



$\phi$	Phase Shift (Equation 4.36) (Radians)
$\lambda$	Decrement Factor (Equation 4.32)

## Subscripts

b	Bottom
conv	Convection
e	Effective
f	Frozen
grnd	Ground
i	i <sup>th</sup> Node
i	Inside
i-1,i	Heat flow from i to i-1
i,i+1	Heat flow from i to i+1
I	Insulation Path
j	j <sup>th</sup> Node
j,j-1	Heat flow from j to j-1
j+1,j	Heat flow from j+1 to j
l	Left side
o	Outside
L	Left Hand Node
L,R	Heat flow from node L to R
L-1,R	Heat flow from L-1 to R
r	Right side
R	Right Hand Node
R,R+1	Heat flow from R to R+1
s	Stored



s	Saturated
t	Top
uf	Unfrozen
y	Sol-Air Temperature Cycle
W	Wood Path

## Superscripts

$\gamma$	Time Step
$\gamma+1$	New Time Step



## 1. INTRODUCTION

The impact of World's depleting fossil fuel reserves and the prevalent rates of energy usage have created a growing awareness in the area of energy management techniques in four major energy-consuming sectors: Electricity generation, Transportation, Production, and Heating and Cooling of the buildings.

It is recognized that high grade energy should not be used for low grade applications such as used in the last of the above sectors namely, the heating and cooling of buildings [1]. These considerations have been the motivation for research into two parallel fields.

1. Finding alternative sources of energy for space conditioning.
2. Designing buildings for energy conservation.

In this context the direct gain passive house design is a conceptual outcome of the strategy of combining the tasks of utilizing an alternative source of energy such as solar radiation and disposing the available energy by way of storing, redirecting, enhancing, and inhibiting, to achieve an indoor environment compatible with the comfort level of its inhabitants.

The passive heating and cooling systems may take a variety of forms as discussed in [2,3]. However the system analyzed in this thesis is usually referred to as Direct Gain Passive System. In general a simple direct gain passive house consists of the following elements: walls, ceiling,



basement, windows with thermal shutters, overhang, doors and thermal storage walls etc. The problem of practical interest is to predict the heating requirement of such a house exposed to temporal variations in ambient air temperatures, solar radiation fluxes, intermittent internal heat sources and furnace heat requirements.

A review of the literature shows that there are a large number of simulation models of varying degree of details for estimating the house heating requirements. These include the public domain programs [4,5,6,7,8,9], some of which are capable of simulating not only the building thermal loads but also the HVAC air distribution systems and the central plant systems. The next level of programs are those which explore the use of passive solar gains to reduce the residential house heating requirements [10,11,12,13,13A]. This study essentially falls into this latter category. However, the building thermal load calculations are common to all the models. To develop an overview of the problem the general limitations of the above studies will have to be first examined. For clarity these general limitations will be grouped into three categories.

1. The component modeling and the overall modeling of house heating requirements.
2. The model validation studies.
3. The overall thermal performance studies.

The first category limitations of the above referred models concerning the theoretical modeling aspects can be



summarized as follows.

1. Most of the models do not have the capability of modeling below grade basement losses. The studies which do include basement losses into their models have used either simple empirical relations, or have used a steady state conductance approach. As an improvement over the steady state methods, recent studies have utilized two dimensional numerical techniques for analyzing basement heat losses. However, no efforts are made in these studies to integrate the basement models with the overall energy analysis of houses.
2. Most of the simplified models neglect the internal heat capacity of the structure.
3. The internal heat sources are either neglected or assumed to have all been utilized in directly replacing the furnace heat.
4. The actual thermal capacity in the house is largely unknown because of the nonhomogeneities associated with the building materials. In this regard no efforts have been made to theoretically justify the transient response of the structure.
5. The studies directed towards prediction of building thermal resistance have used simple first order models for the transient analysis. The air heat capacity in such cases is almost always neglected.

The second category of the limitations concerning the model validation studies can be summarized as follows.



1. The usual method of validation of computer models based on agreement between the predicted and the measured room air temperatures appears to be not a sound validation technique, because of the fact that in the calculation of house heat requirements several uncertainties are involved in the prediction of solar gains, basement and infiltration losses.
2. No efforts have so far been made in the direction of establishing a comprehensive verification procedure for models predicting house heating requirements.
3. It is noted that many model verification studies have based their conclusions on the accuracy of their models from a few days measured data. This type of limited analysis may not be good indicator of the accuracy of the model in predicting the seasonal thermal performance of houses.
4. Most of the models have been verified from the data on test cells which are above grade structures.
5. Seasonal thermal performance data analyses either on the above grade or on the below grade elements of houses are lacking.

Finally, the third category limitations of the studies concerning the overall thermal performance evaluation of houses can be summarized as follows.

1. Almost no method is available in the literature by which the heating load reductions produced by the passive solar gains can be evaluated from the routine



measurements of room temperatures and furnace heat requirements. This is one of the major limitations of the previous studies due to which there is controversy on the actual magnitudes of the heating load reductions that can be obtained from passive solar gains.

2. Efforts are lacking in the direction of a generalized study by which several passive house designs could be compared. Such a study would be of value in developing a criterion of thermal similarity between different designs or between different design parameters of a house.

These limitations were the motivators for carrying out a detailed investigation into the theoretical modeling, model verification and performance evaluation study of direct gain passive houses. The starting point of the present work was the model developed by the author [14]. This model is capable of simulating the dynamic behaviour of a direct gain passive house exposed to temporal variations in ambient air temperatures and solar radiation fluxes. In general most of the previously mentioned limitations are also applicable to this model. A further limitation was that the walls and ceilings in this model were simulated as simple resistive elements and no attempts were made to develop transient models for these elements. However, the two improvements of this model relative to the previous studies were its ability to account for the building thermal mass, internal heat sources and an exploratory attempt was made to set a trend



in developing certain general results from this model. In view of the general limitations of the previous studies including the authors' previous model the objectives set out for the present work were: to introduce refinements to the previous model, to adequately test this refined model and to investigate methods of generalizing the results. As a consequence of this approach several different methods of modeling and techniques for analyzing the models were developed. These proposed methods will be briefly summarized into the following three groups.

1. The refinements introduced into the previous model [14] by way of improved techniques for modeling the component and as well as the overall house heat losses.
2. Proposed methods for model verification.
3. Methods of data analysis for performance evaluation of a direct gain passive house and attempts to generalize the whole study by which the performance of direct gain houses can be compared.

The first group of proposed methods referred to as refinements to the previous model can be summarized as follows.

1. By postulating that the basement heat losses can be divided into two components: one with a diurnal variation and one with an annual variation, four basement models were examined. These models were developed to include the effects of the dynamics of surrounding soil, surface cover variations and the



freezing and thawing effects of the soil on the basement heat losses.

2. A simple method of integrating the above basement models with the overall house model is presented.
3. Simple one dimensional transient numerical models for the walls and ceiling are proposed.
4. A simplified model is proposed through which the effects of thermal resistance and capacitance of the structure on its transient response can be investigated. This model when combined with the transient temperature decay tests yields such important information as the actual magnitudes of the lumped and the distributed heat capacities in the structure.

The second group of the proposed methods suggest the following set of criterion for adequately validating the direct gain passive models.

1. A fundamental criterion for validating the simulation model has to be based not only on the verification of the overall model but also on the verification of the component models.
2. A second criterion for validating the simulation model has to be based on the verification of the transient response of the structure.
3. A third step in the verification procedure is to check if the overall energy balance equation is satisfied. This can be done by performing a check to see if the heat losses and storages balance the heat gains.



4. The last step in the verification of the models be based on the comparison of the accuracy of the predicted and the measured room air temperatures and the furnace heat requirements under different modes of shutter operation.

In order to fully appreciate the validation procedure followed, a flow chart describing the various tests and their sequence is depicted in Figure 1.1. During the process of model verification for the components several different methods of analyzing the data are suggested. These include:

1. Analysis of the steady state and the transient heat losses from the walls and ceilings to identify problems associated in modeling of walls and ceiling heat losses.
2. Generally it is assumed that thermal shutters on windows instantaneously provide the expected resistance value upon closing. The evidence gathered from experimental data analysis shows that due to infiltration and thermal capacitance effects of the window-shutter combination, the actual resistance provided by the shutters is significantly less than its expected nominal resistance value.
3. Several short comings of the available solar gain models have been identified. A three step criterion for verifying the window gains model is proposed. It is shown that the window gain factor can be used to compare the performance of different windows.

Finally the third group of the proposed methods on the evaluation of the thermal performance of passive houses can



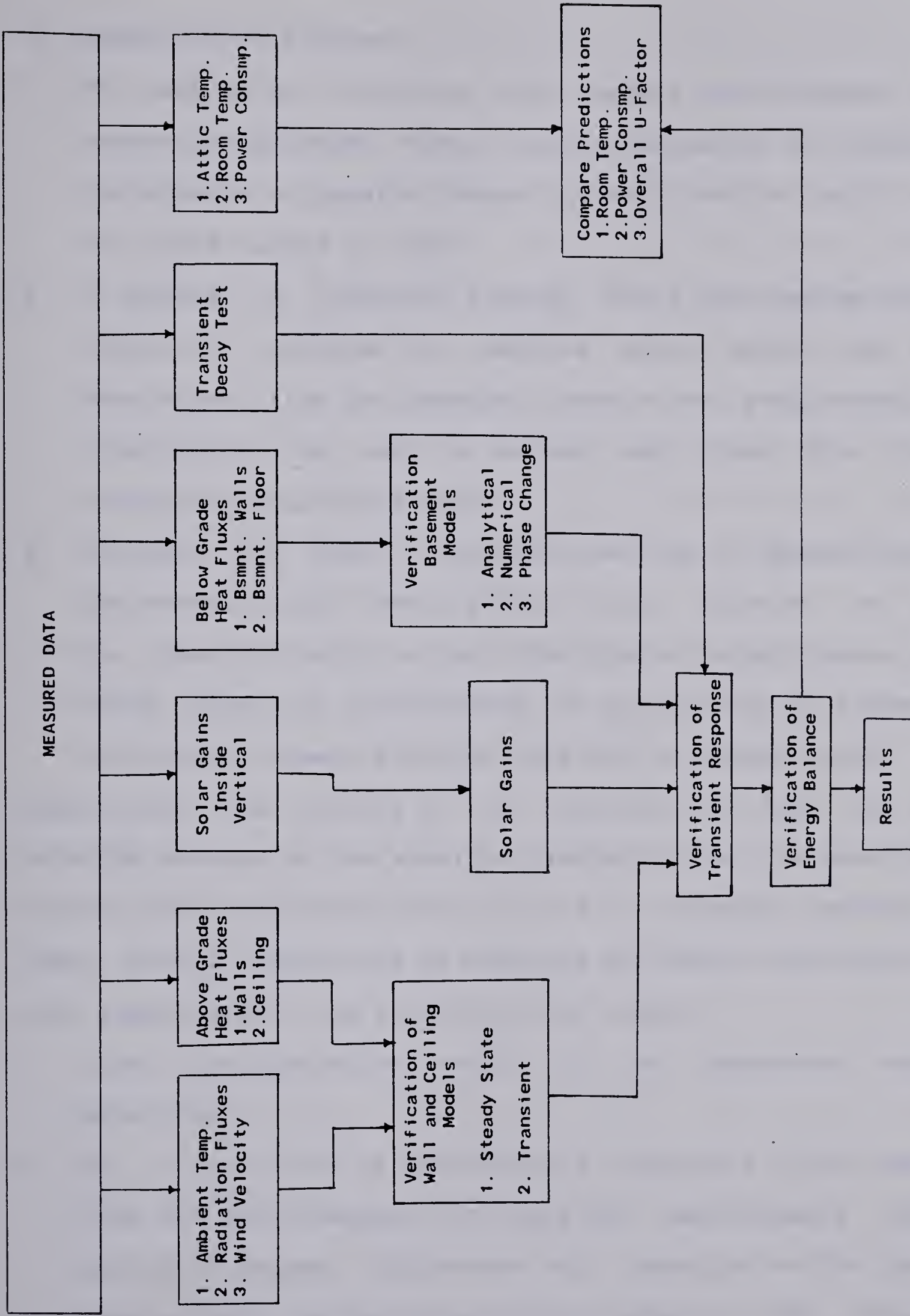


Figure 1.1 Flow Chart Describing the Model Verification Procedure



be summarized as follows.

1. Two methods of analyzing the thermal performance of houses are proposed. These include evaluation of thermal performance of passive houses for small and as well as for large values of time.
2. A method is proposed through which the heating load reductions produced by passive solar gains can be determined from the measured furnace heat requirements. A rationale for such a method was drawn from the theoretical considerations.
3. Attempts are made to explore the idea of generalizing the overall study into a set of curves referred to as the general design curves. The physical significance of these curves are examined and the possibility of thermal similarity between different designs is investigated.

Essentially, what follows in the chapters to come is an extended version of the specific limitations of the previous studies and a detailed description of the proposed methods. These overall objectives of modeling and model verification were approached in the following four steps.

1. First, the theoretical models of the components were developed.
2. The calculation of the various components of the heat loss was then compared with detailed measurements from heat flux gauges, radiometers etc., measured on the test modules built at the University of Alberta [15]. These comparisons were used to test and refine the model



calculations for the components.

3. The next step was to compare the predicted and the measured module performance as a whole where all of the components were involved. This was done using typical daily variations of module temperatures and furnace heat requirements. These comparisons check the time constant behaviour, solar gains as well as heat losses.
4. Finally, the heating season summary of the results were obtained which included the percentages of heating load resulting from each component of the heat loss as well as the percentage contributions to heating load reduction made by solar gains.

These ideas together with the theory and the data analysis have been organized as follows.

In chapter 2 the specific limitations of the available models have been pointed out. A brief description of the experimental test facility and the data collection procedure is discussed in Chapter 3. Theoretical considerations in modeling the thermal performance of the enclosures together with the proposed models are described in chapter 4. Chapter 5 compares the accuracy of the component models with the detailed measurements. A parametric study illustrating the effects of certain parameters on the module heat requirements is presented in Chapter 6. In Chapter 7 the predicted and the measured module performances are compared, and a summary of the monthly and as well as the annual heating load contributions made by solar gains to these



modules are presented. An attempt is made in Chapter 8 to explore the idea of generalizing the results of this study. This is followed by a summary and conclusions in Chapter 9.



## 2. LITERATURE REVIEW

### 2.1 Introduction

A large body of information in the field of energy consumption for residential space heating is available in the literature. Since the building heat transfer problem involves multimode heat transfer processes, a wide range of other studies in heat transfer area are also of interest to the modeling of house heating requirements. The task then was to choose the appropriate papers and introduce them to the reader in a logical way. In order to be consistent with the overall objective of this thesis, it was desired to place emphasis on the modeling of overall house and as well as on its components. This led to the organization of the literature review into two stages.

1. Studies related to the overall house.

2. Studies related to the component modeling of a house.

This chapter deals with the studies related to the overall house. An overview of the available predictive models, and their limitations can be obtained from this first stage review of the literature. Later, in chapter 4, on the development of the thermal model, the second stage review of the literature dealing with the component modeling of houses will be introduced at appropriate places.

The first stage review of the literature in the field of energy consumption for residential space heating can be



arranged into the following four easily identifiable groups.

1. Detailed simulation models.
2. Approximate methods.
3. Validation of simulation models.
4. Experimental studies.

## 2.2 Detailed Simulation Models

There are quite a few computer models capable of simulating in great detail the energy analysis of commercial and residential buildings. These are some times referred to as public domain programs namely: DOE [7], NBSLD [4], BLAST-2 [5], ENCORE-CANADA [6]. Other programs like, TRNSYS [8], PASOLE [10], and the algorithms developed by the ASHRAE task group on energy requirements for heating and cooling of buildings [9] are some of the major ones available for energy analysis.

The discussion with reference to these programs is limited to the techniques employed in heat loss calculations, because this part is of interest to the present study. With the exception of reference [6], most of these models appear to be concentrating their efforts on the slab on grade type of construction which is commonly found in the United States. Although Encore-Canada [6] model includes basement heat loss calculations, the methods employed are similar to steady state type calculations. Therefore the only comparison that can be made between these



models and the present study is the method of calculating the heat losses through the above grade elements of a house. In this respect most of these models employ response factor approach for solving the heat conduction equation. As pointed out by Gupta, Spencer and Muncey [16], the techniques employed for the solution of heat conduction equation in the energy analysis programs can be grouped into three categories:

1. Response factor approach.
2. Harmonic analysis.
3. Numerical methods.

A brief comparative study of these methods is very instructive for an understanding of the limitations or the approximations that these methods could introduce into the heat loss calculations.

### 2.2.1 Response Factor Approach

Mathematically, the response factor concept implies that a system output  $O$  can be related to the input  $I$ , through a transfer function  $F$  [17,18,19,20,7]

$$O(Z) = F(Z) \cdot I(Z) \quad (2.1)$$

Assuming that such a transfer function exists it can be expressed as the ratio of two polynomials  $N(z)$  and  $D(z)$  ie.



$$F(Z) = \frac{N(Z)}{D(Z)} \quad (2.2)$$

In order to find the coefficients of the polynomials  $N(Z)$  and  $D(Z)$  one has to consider the heat transfer mechanisms taking place in the system.

Consider for example a homogeneous plane wall as the system subjected to convective boundary conditions as shown in Figure 2.1. The differential equation and the boundary conditions describing the system are:

$$\frac{\partial T}{\partial t} = \alpha \frac{\partial^2 T}{\partial x^2} \quad (2.3)$$

$$k \left. \frac{\partial T}{\partial x} \right|_{x=L} = h_i (T - T_R) \quad (2.4)$$

$$k \left. \frac{\partial T}{\partial x} \right|_{x=0} = h_o (T - T_e(t)) \quad (2.5)$$

Where  $T_e$  is the sol-air temperature, first introduced by Mackey and Wright [21]. The sol-air temperature accounts for the radiation fluxes received by the surface. Note that  $T_e$  is time dependent fluctuating temperature, however for the moment it is considered to be constant.

Drawing an analogy between an electrical and thermal phenomenon, Von Gorcum [22] showed that the temperature and the heat flow can be treated as conjugate variables much the



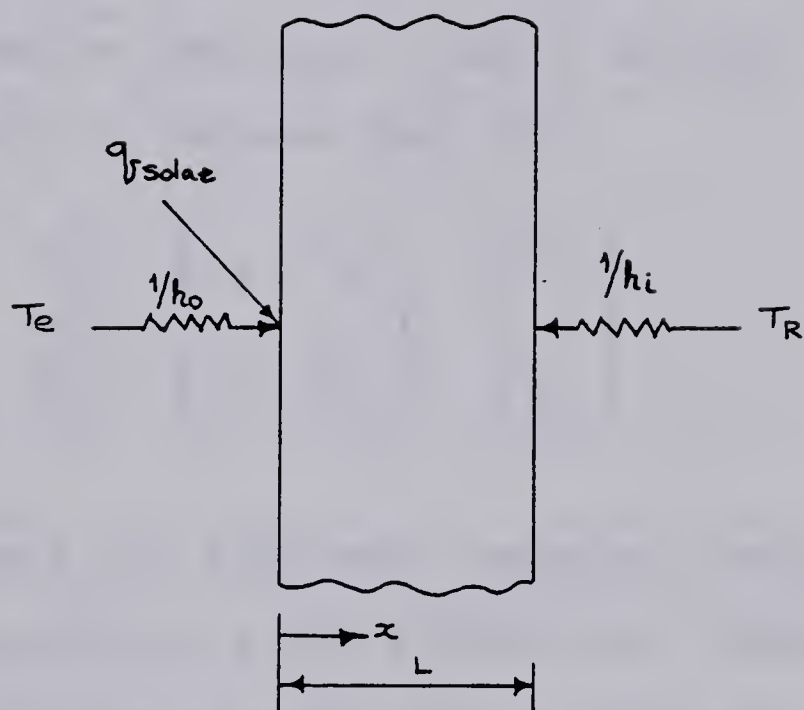


Figure 2.1 Heat flows at a plane wall



same way as voltage and current, with a certain time lag or phase difference. This analogy enables one to go somewhat further in solving the heat conduction Equation 2.3 by the familiar method known in electrical networks as four-poles technique.

Based on these considerations Von Gorcum showed that for a given input, say for simplicity a sinusoidal input function, the amplitudes of the transformed temperature  $T'_o$  and heat flux  $q'_o$  at one side of the slab are linearly related to those at the other side  $T'_i$  and  $q'_i$ . In general for a composite wall it follows that [23],

$$\begin{bmatrix} T'_o \\ q'_o \end{bmatrix} = \begin{bmatrix} A_1 & B_1 \\ C_1 & D_1 \end{bmatrix} \begin{bmatrix} A_2 & B_2 \\ C_2 & D_2 \end{bmatrix} \dots \begin{bmatrix} T'_i \\ q'_i \end{bmatrix} \quad (2.6)$$

The effects of film heat transfer coefficients  $h_i$  and  $h_o$  used in Equations 2.4 and 2.5 can be treated as simple resistive layers one on each side of the wall. Therefore the homogeneous plane wall with convective boundary conditions can now be treated as a composite three layer wall. The transformed solution of which has the form,

$$\begin{bmatrix} T_o \\ q_o \end{bmatrix} \begin{bmatrix} 0 & 1/h_o \\ 0 & 1 \end{bmatrix} \begin{bmatrix} \cosh KL(1+i) & -\frac{\sinh KL(1+i)}{kK(1+i)} \\ -kK(1+i)\sinh KL(1+i) & \cosh KL(1+i) \end{bmatrix} \begin{bmatrix} 1 & 1/h_i \\ 0 & 1 \end{bmatrix} \begin{bmatrix} T_i \\ q_i \end{bmatrix} \quad (2.7)$$



Solution of Equation 2.7 is now merely an exercise in finding the inverse transform. Closed form solutions of Equation 2.7 with a sinusoidal input function can be found. However, the algebra gets involved as more and more layers are added. An analytical solution to Equation 2.3 was given by Alford et al. [24]. Mackey and Wright [25,26] extended this solution to a plane wall consisting of three layers.

Mitalas and Stephenson in a series of papers [17,18,19,20], showed the technique of numerically inverting the matrix Equation 2.7, which results in a set of factors generally known as weighting factors or response factors.

Thus finding response factors for each of the elements of the thermal envelope is the first step towards writing an overall energy balance equation.

For example the energy balance equation in the DOE-2 computer program [7] is written based on the transfer functions for each of the processes participating in the overall heat balance such as:

1. Instantaneous heat gains from solar radiation.
2. Energy from lights.
3. Energy from people and appliances.
4. Energy entering by conduction through walls.

The main difference between these heat gain processes is the relative amounts of energy appearing as convection to the room air and radiation on different walls and furniture.

At this point a thermal network describing the energy balance on the inside surfaces of the wall is constructed.



This network is employed to determine the contributions from the individual process heat gain weighting factors. This is a common approach employed in all the cooling load calculations.

However, another approach to writing energy balance on the room air is to balance the heat losses to the corresponding heat gains. This is a more direct approach employed in ENCORE-CANADA computer program [6].

#### 2.2.1.1 Limitations of Response Factor Approach

Even though the idea of response factors may appear simple, the calculation procedure is quite complex. Apart from this the other limitations of this method are:

1. It is applicable only to processes that can be represented by linear differential equations.
2. Constant property assumption is invariably necessary.
3. Non-linear processes such as natural convection and radiation have to be linearly approximated.
4. Use of response factors requires familiarity with the probable inaccuracies introduced by inappropriate selection of time step.

In view of the above limitations of the response factor approach it is apparent that this method cannot be used for analyzing the effects of changing soil conductivity, surface cover variations or the freezing and thawing of soil on the basement heat losses. Further the ventilated attics cannot be adequately analyzed by response factor approach.



### 2.2.2 Harmonic Methods

Solution to Equation 2.3 was given by Alford et al. [24] for a sinusoidal input function consisting of a steady term and a sufficient number of harmonics. Considering each of the harmonics as a separate input, the heat conduction Equation 2.3 with the boundary conditions given by Equations 2.4 and 2.5 was solved. The solution has the form,

$$T_i = T_R + \frac{1}{h_i} [U(\bar{T}_e - T_R) + U\lambda\Delta T_e \cos(\omega\theta - \psi - \phi)] \quad (2.8)$$

Equation 2.8 gives the inside surface temperature  $T_i$  for the fundamental component of the input function. More harmonics could be added to improve the accuracy.

The elegance and simplicity of Equation 2.8 are of interest. Physically, it implies that a sinusoidally varying input temperature gives rise to a sinusoidal output that is decreased in amplitude and lagging behind by  $(\phi)$  with the input function.

The decrement factor,  $\lambda$  and the phase angle,  $\phi$  are the characteristic parameters that describe the behaviour of the wall. This discussion will be later followed up in Chapter 4 on component modeling.

Using harmonic analysis, Mackey and Wright [25,26] later developed exact solutions for single homogeneous, and two and three layered composite walls. Generalizing their results they introduced the concept of representing the multi-layered walls by a single equivalent homogeneous wall.



A recent thesis by Sonderegger [27], deals exclusively with harmonic methods and their application in developing equivalent thermal parameters for modeling the dynamic behaviour of buildings.

Yet, in another recent thesis, Goldstein [28], utilizes the harmonic methods for developing some theoretical models to design of energy conserving buildings.

#### 2.2.2.1 Limitations of Harmonic Methods

The limitations of harmonic method are:

1. The input function must be of periodic nature. For greater accuracies the climatic data have to be analysed using large number of harmonics which makes this method impractical for accurate analysis.
2. The main restriction as the with the response factor approach is that the system parameters must be time invariant.
3. Linearization approximations have to be used for convective and radiative boundary conditions.
4. For better accuracy [29], the time period of the design climatic cycle has to be at least twice the thermal time constant of the system.

Since hourly climatological input data are rarely periodic, predictions from the models using the harmonic method will only be approximate.



### 2.2.3 Numerical Methods

Numerical methods are extremely valuable for solving heat transfer problems that are not susceptible to analytical solutions. The transient building heat transfer calculations can be easily performed using any of the following three finite difference methods.

1. Explicit Methods.
2. Crank-Nicholson's Method.
3. Implicit Methods.

The advantages and limitations of each of these methods are well known [30,31,32]. Particularly, the implicit method offers the choice of selecting large time steps which is very much desired in yearly heating load calculations for buildings.

The limitations of the response factor methods or the frequency response methods can be largely overcome through the use of numerical methods. In this thesis the numerical methods are extensively used particularly in basement heat loss calculations.

### 2.3 Approximate Methods

Much of the work in developing simplified methods for heating load calculations stems from the fact that the actual calculations of energy analysis are too complex to be handled by practising engineers. In this section two commonly used methods will be discussed. For the other



papers the interested reader is referred to the following references [37,38,39,40,41,42,43,44].

In series of papers Balcomb and MacFarland et al. [33,34], have discussed a simple empirical method for estimating the performance of a passive solar heated building. The simplified method relies on the use of an appropriate correlating parameter called Solar Load Ratio (SLR) and an empirical fit to the large ensemble of hour by hour detailed simulation results. The SLR and the SHF (Solar Heating Fraction) are defined as,

$$\text{SLR} = \frac{\text{Energy absorbed by thermal mass}}{\text{Monthly steady state building load}} \quad (2.9)$$

$$\text{Annual SHF} = 1 - \frac{\text{Annual auxiliary energy}}{(\text{Annual degree days}) * (\text{building heat loss coefficient})} \quad (2.10)$$

Accuracy of this method is reported to be within 3% of computer simulation results.

However, the limitation of this method are:

1. Building thermal mass is neglected.
2. Correlations are valid only for the predefined temperature swing.



3. It assumes that all the internal heat sources contribute to solar heating fraction.
4. Below grade basement calculations are not included.

In a similar study, Mitalas [35,36] used computer simulations to generate correlating parameters identified as Net Annual Heat Loss Factors (NAHLF).

The NAHLF's were determined using a computer Model [6] by evaluating the annual heating requirements of a standard and a modified house exposed to a test year weather cycle. The NAHLF was defined as the ratio of difference between the standard and the modified design divided by the numerical value of the parameter causing the difference.

Graphical results of NAHLF as a function of degree days for individual components such as windows, walls , ceilings etc. were presented.

As with the other methods, this technique is limited in scope in that it does not account for internal heat sources or the interior thermal storage capacity. The below grade basement calculations are also excluded. It is desired to be stressed here that the above simplified methods are susceptible to inaccuracies and that they represent more or less average best fits obtained from detailed simulation analysis. Often, these simplified correlations are valid for certain specific design situation and therefore are limited in their application. Attempts are made in this study to overcome these limitations and generalize the results so that the results are more widely applicable.



## 2.4 Validation of Simulation Models

Even though there have been extensive studies using computer simulations, data on validation of computer models is lacking. The reasons for this are obvious considering the cost of constructing and monitoring a test facility. In this section some of the published results on validation of computer models will be discussed.

The validation of the NBSLD public domain program from the results on dynamic thermal performance of an experimental masonry building constructed inside a 70,000 cu.ft. environmental laboratory are of interest [45]. Under controlled environmental conditions, the simulated diurnal sol-air temperature cycle was imposed on the building for 3 to 4 days before measurements like temperatures, heat fluxes and electrical power consumption rates were made. A total of ten different tests were designed and performed: five under thermostated conditions and the other five under free floating conditions. In each of these five tests the effects of placing insulation on the inside or outside of the structure with window and internal mass either added or removed were studied.

The predictions based on response factor approach were compared with the measurements. The results under thermostated conditions showed a maximum of 8% difference in computed and measured heating load with an average difference of 4.5%. The heating load predictions were lagging behind the measurements by 1 to 3 hours. This



discrepancy was acknowledged in the study but no probable reasons were given.

The window losses investigated (note that no solar gains were simulated in the chamber) showed the accuracy of predictions to be within 4%.

Two conclusions drawn from the study were:

1. The steady state methods overestimate the heating load by as much as 30%.
2. Placement of insulation on the outside of walls and roof is shown to be effective in reducing the heating load and controlling the inside temperature.

The room temperature fluctuations for the free floating conditions showed good agreement. However the heating loads, as in the previous case, were reported to be not in phase. The results of this study although of importance cannot be extrapolated to insitu thermal performance of residential houses.

Chen et al. [46] in an experimental study on a direct gain passive test cell measured the room temperatures for a period of two weeks. This data was used in validating the PCAP, Princeton University Circuit Analysis Program [12]. The conclusions drawn by Chen et al. were that the Trombe wall on an average maintained the room air temperature about 3°C higher than that of a direct gain system.

Field validation studies of the DEROB/PASOLE models by Arumi-Noe [47] were based on seven test units built and monitored at Los Alamos laboratory for a period of 7 days:



Comparisons between the measured and the predicted room temperature on a direct gain test unit showed an error of about 4°F. It is observed from Arumi-Noe's study that there is a phase difference between the measured and the predicted room temperature. Obviously, this is an effect of improper modeling of the time constant of the test units.

Hunn et al. [48], have used the above one week data measured on LASL passive test units to validate the two computer models: DOE-1 and SUNSPOT. They showed that the room temperatures predicted by DOE-1 were consistently higher than those predicted by the SUNSPOT. This was attributed to inaccuracies in room thermal response factors used in DOE-1. The numerical predictions of SUNSPOT were compared with the measurements done over a period of 30 days. The agreement is reported to be satisfactory with a maximum difference of 2°F.

Wheeling et al. [49], reported the performance of passive test unit from the results of data gathered for a complete heating season. Measurements, such as solar radiation, air temperatures, thermal storage wall temperature were used to validate the SUNCAT computer model [11]. The maximum error between the predicted and the measured room temperature was reported to be 5°F. Energy consumption rates were not monitored.

Balcomb et al. [50], have also used a similar approach for verifying their simulation model by comparing with the test room temperatures. A satisfactory agreement was



reported.

#### 2.4.1 Limitations of Validation Studies

From the above studies three major limitations can be identified. First, it can be noted that the validation of computer models were based on room air temperatures measured over a few days. This type of validation technique is not sound because it overlooks the complexities involved in the predictions of three major components in the heating load calculations: namely, solar gains, basement and infiltration losses. Secondly, the actual thermal capacity of a structure is generally not known. Incorrect modeling of this parameter would introduce phase lag between the measured and the predicted values [47]. Finally, it appears unrealistic to make any conclusions on the seasonal thermal performance of houses from a few days measured data.

#### 2.5 Experimental Studies

In this section a few independent experimental results will be discussed. Even though these results were not used for verifying any computer models, they are in themselves important and give an indication of annual space heating requirements of occupied dwellings.

From a survey of approximately 50 low energy houses in Saskatoon, Dumont et al. [51] have reported the average total energy consumption of the houses incorporating passive



design features as about 218 MJ/sq.m. The passive features included improved insulation levels, improved air tightness with controlled ventilation and use of south facing windows for passive solar gains.

Performance results of 'Saskatchewan Energy Conservation House', have been reported by Besant et al. [52]. The space heating requirement of this house was reported to be 5.1 GJ/year compared to approximately 140 GJ/year for an average pre 1975 house. On an yearly basis it appears that 44% of the total energy required is supplied by the passive solar gains and about 41% is provided by the internal heat gains.

To this end it must be pointed out that there are a large number of papers on validation of computer models together with some theoretical and experimental studies. In this review a few papers, which were of direct interest to this study were considered. For other studies the reader is referred to the review of Moore and McFarland [53], which gives a survey of the passive solar test modules built and monitored throughout the United States and Canada.

Although not exhaustive, this first stage review shows the specific limitations of the above studies. These limitations were summarized in the introduction to this thesis. The methods proposed in this study will attempt to overcome such limitations. This will form the discussion of Chapters 4, 5, 6 and 7. But before doing so, a brief description of the experimental facility will be presented in the following chapter.



### 3. THE TEST FACILITY

#### 3.1 Introduction

The Test Facility, known as The Alberta Home Heating Research Facility, consists of six, 22 foot by 24 foot single story modules with full basements, located on the University of Alberta farm in a single East-West row as shown in Plate 3.1. The overall objectives of this facility, its design, construction and monitoring were performed under the direct supervision of Dr.R.R.Gilpin, Professor, Department of Mechanical Engineering, The University of Alberta. Several members of the group [15,54] were also involved in this endeavour. As a member of this group the author was responsible in assisting Dr.R.R.Gilpin by way of conducting numerous numerical experiments on several house models. The results of these numerical experiments were very useful in the decision making process concerning several experimental aspects of the facility. However, the authors' modest contributions with regards to the experimental work on the test facility were:

1. Calibration and installation of heat flux gauges.
2. Preparation of formatted files for the data of the year 1980-1981, transfered from the data acquisition system to the main computer at the university.
3. Periodic analysis and interpretation of data to check for inconsistencies or questionable inaccuracies etc.





Plate 3.1 View of the test facility: modules 1 through 6  
numbered from left



A complete description on the design and construction of the test facility can be found in references [15,54]. In this chapter a limited description of the facility, no more than required for understanding of this thesis, will be presented.

### 3.2 Specifications of The Modules

The overall physical dimensions of all the six modules are identical. The typical dimensions are shown in Figure 3.1. Table 3.1 supplements Figure 3.1 in that it gives the design details. As each module was built to test a different design strategy, their thermal characteristics are different. Each module has different insulation levels on above grade basement walls with partially or fully insulated below grade basements. The nominal resistance values for walls, ceiling, windows, doors, above grade basements etc. are listed in Table 3.2. These values together with the module overall heat loss coefficient were calculated using traditional steady state methods [55]. For calculating the module overall heat loss coefficients, the contribution of infiltration component was based on a limited measured air change rates [56].



Table 3.1 Design details of the modules

Module	Floor area (Sq m)	Window area (Sq m)				Shutters	Door area (Sq m)	Total basement wall area (Sq m)	Basement floor area (Sq m)	House volume (Cu m)
		N	S	E	W					
1	49	1.62	-	1.67	1.67	none	1.86	68.5	49	239
2	49	1.62	-	1.67	1.67	none	1.86	68.5	49	239
3	49	-	5.06	0.95	-	on south facing window	1.86	68.5	49	239
4	49	-	10.1	0.96	-	on south facing window	1.86	68.5	49	239
5	49	1.62	-	1.67	1.67	none	1.86	68.5	49	239
6	49	1.62	-	1.67	1.67	none	1.86	68.5	49	239

N - North, S - South, E - East, W - West

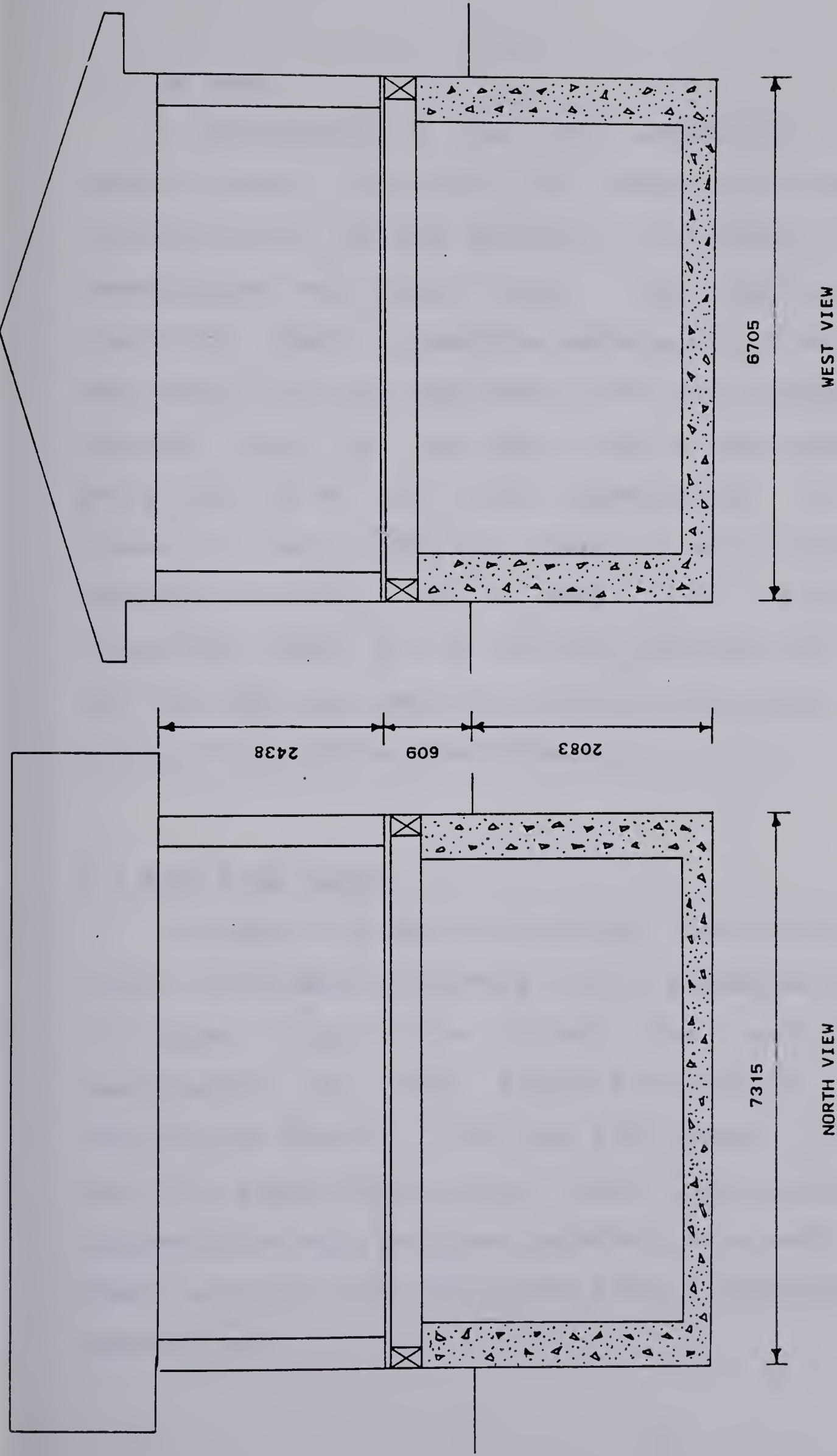


Table 3.2 Nominal Insulation Values for the Modules

Module	Walls RSI (R)	Ceiling	Window Shutters	Door	Additional Insulation on Basement Walls		
					Above grade	Below grade	Floor
1	1.76	2.11	-	0.475	1.76	1.76	none
	(10)	(12)		(2.7)	(10)	(10) 0.6m below grade	
2	1.41	2.11	-	0.475	none	none	none
	(8)	(12)		(2.7)			
3	7	14.1	1.76	0.925	1.76	3.52	none
	(40)	(80)	(10)	(5.26)	(20)	(20) full height	
4	3.52	7	1.76	0.925	1.76	1.76	none
	(20)	(40)	(10)	(5.26)	(10)	(10)	
5	1.76	2.11		0.925	1.76	1.76	none
	(10)	(12)		(5.26)	(10)	(10) 0.6m below grade	
6	1.76	5.63	-	0.925	1.76	1.76	none
	(10)	(32)		(5.26)	(10)	(10) 0.6m below grade	

Note: Values in brakets are in English units. (English units(R):Hr-deg.F-sq.ft/BTU);(SI units(RSI):=K-sq.m/W)





Dimensions are in mm

Figure 3.1 Typical overall dimensions of the modules



### 3.3 The Data

A description of the data acquisition system, the method of data collection and storage are described in reference [54]. The data gathered in this study consisted of temperatures, wall heat fluxes, solar radiation fluxes, electrical power consumption rates and wind velocities. An idea about the total magnitude of the data analyzed can be obtained from the fact that of the 93 measurements stored every hour, 34 of them were temperatures, 37 were heat fluxes, 5 were radiation fluxes, 6 were electrical power consumption rates, and 10 were wind velocities and directions. Almost all of the data collected over two years, 1981 and 1982, was used for verifying the present component models or the main simulation model.

### 3.4 Heat Flux Gauges

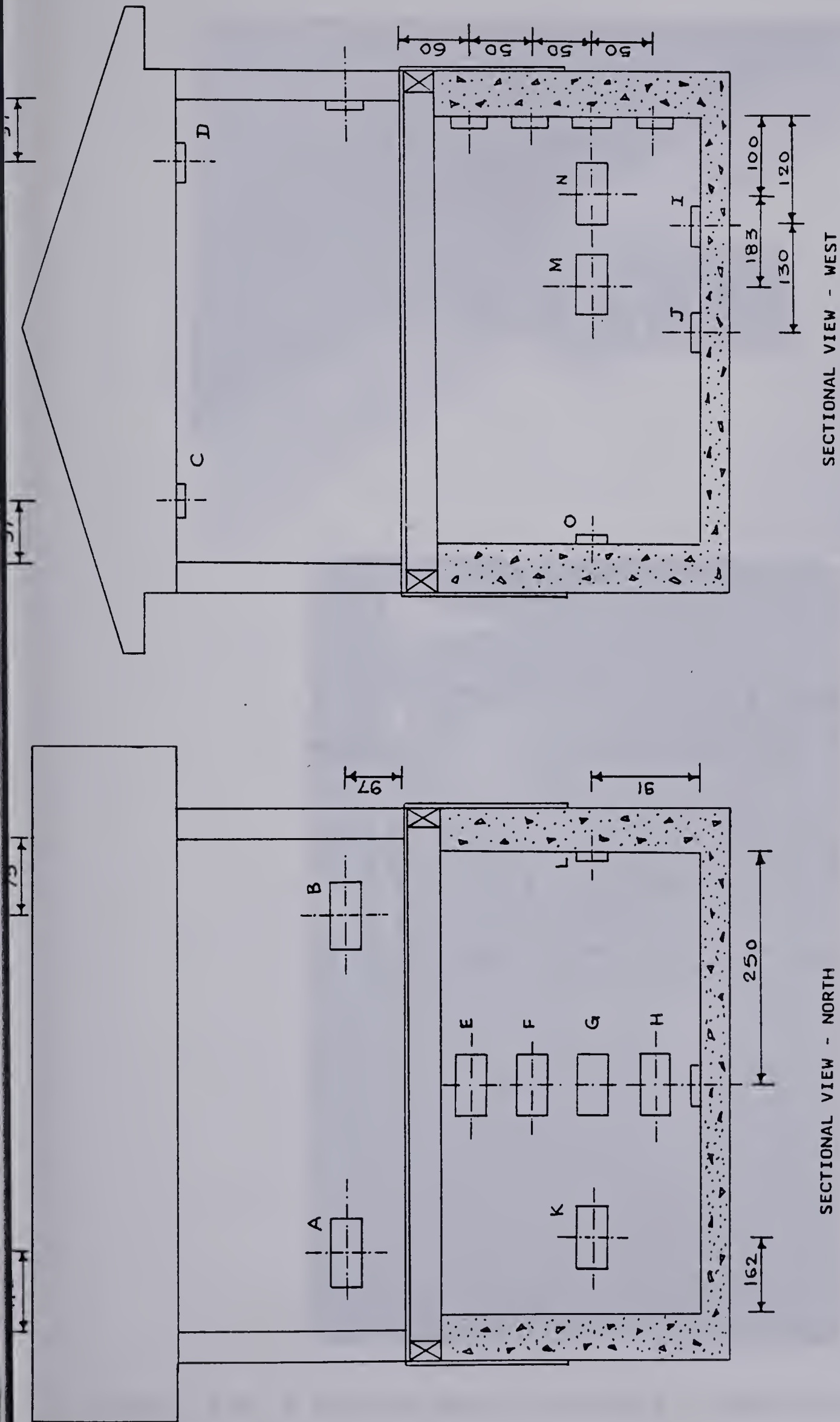
In order to study the heat loss characteristics of a number of building components, and to establish the dynamics of diurnal fluctuations through them, wall heat flux measurements were used. Figure 3.2 and Table 3.3 give the installation details of the heat flux gauges. A total of 42 heat flux gauges (40 by 15 cm), built from a single batch of thermocouples and plexiglass materials were used. Plate 3.2 shows a typical heat flux gauge and its installation on the basement wall.



Table 3.3 Heat flux gauge installation details

Module	Heat Flux Gauge Numbers														
	A	B	C	D	E	F	G	H	I	J	K	L	M	N	O
1	1	23	-	-	-	-	-	-	-	-	-	-	-	-	-
2	2	15	6	19	20	31	28	38	26	12	7	39	21	14	10
3	3	32	-	22	-	-	-	-	-	-	-	-	16	-	-
4	4	18	-	5	24	33	34	37	30	29	-	13	-	-	-
5	9	8	-	6	-	-	-	-	-	-	-	-	-	-	-
6	11	25	-	27	-	-	-	-	-	-	-	-	-	-	-





Dimensions are in cm

Figure 3.2 Installation of heat flux gauges



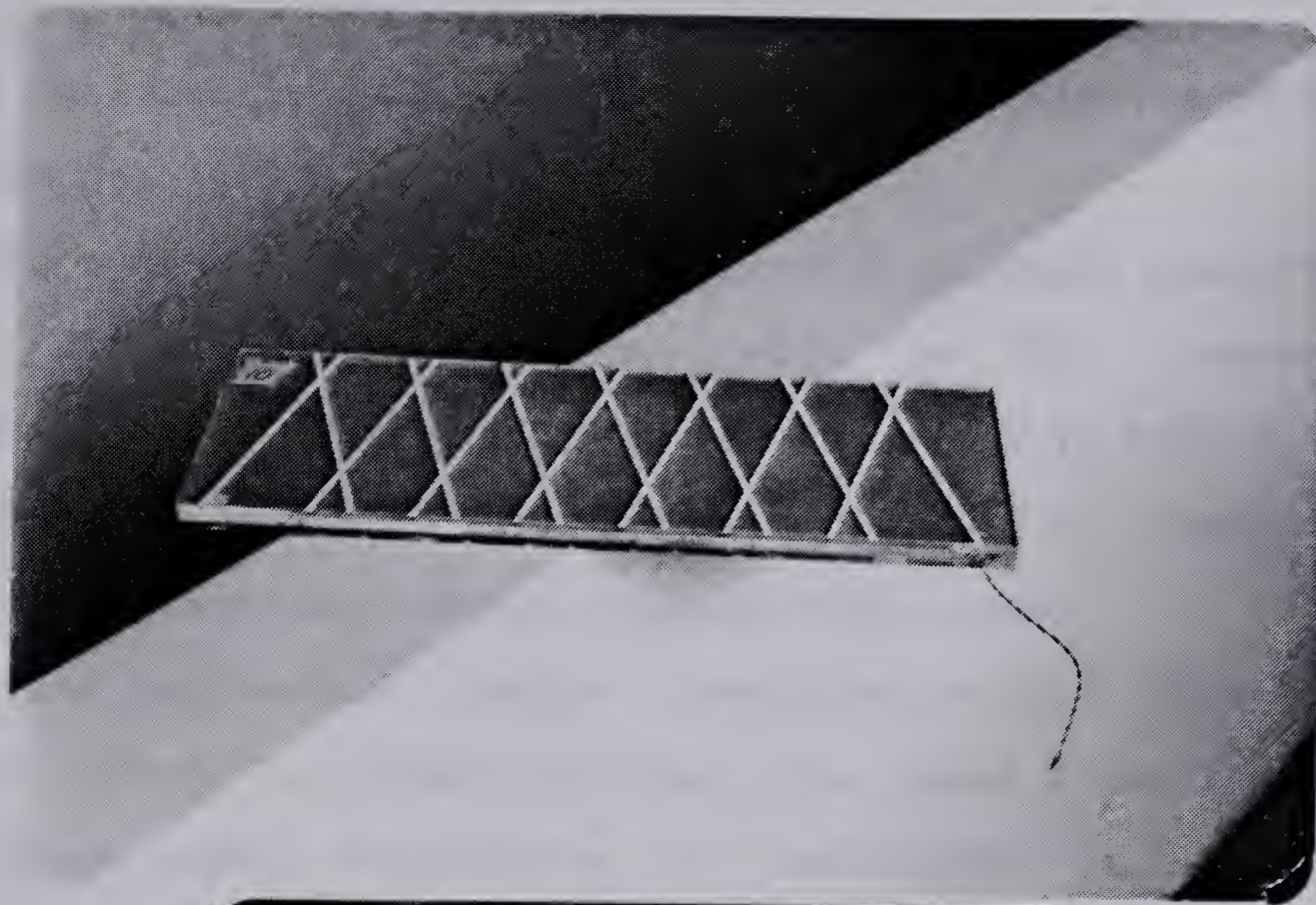


Plate 3.2 A typical heat flux gauge - and its installation on the basement wall



### 3.4.1 Calibration and Time Response Characteristics of Heat Flux Gauges

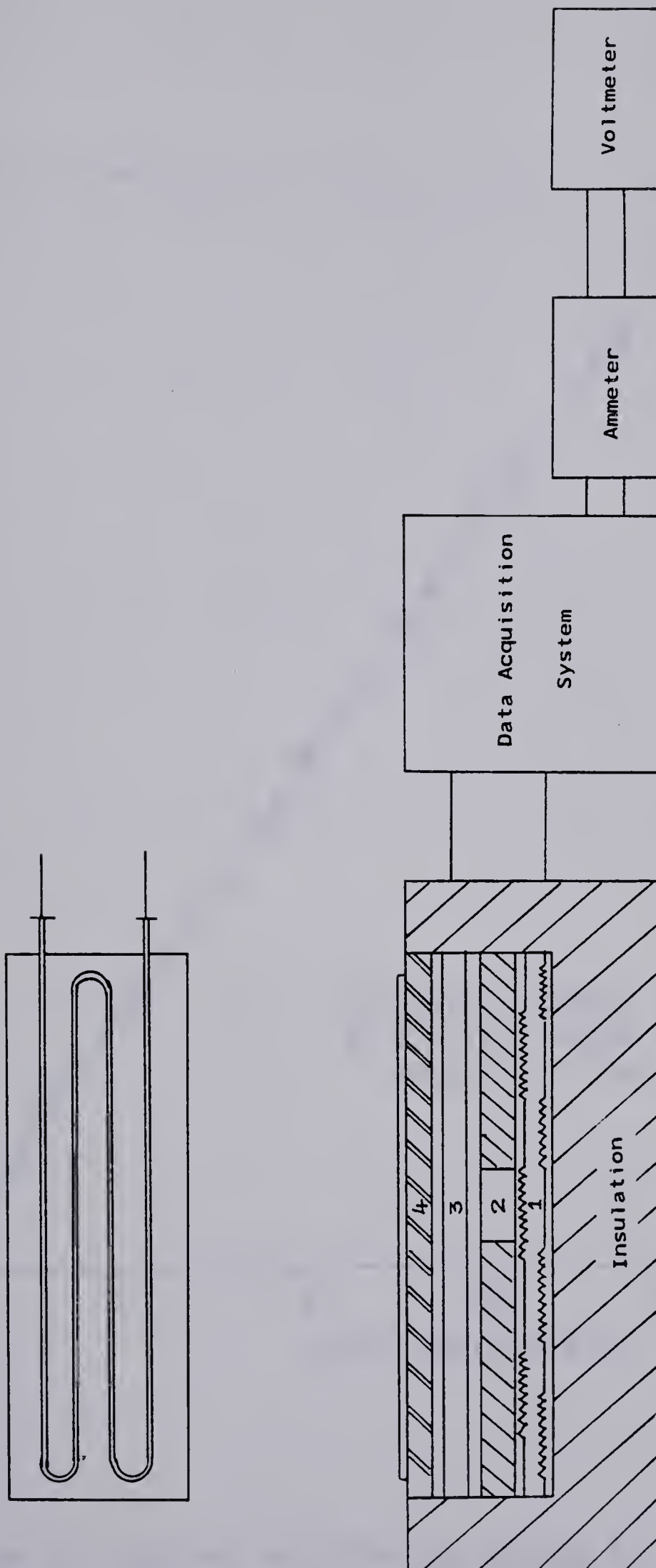
Each gauge was calibrated against a standard commercial gauge which was provided by with a NBS traceable calibration. A calibration device, as shown in Figure 3.3, was used in which heat flux gauges could also be tested at least approximately against an electrical input.

The calibration device consisted of an electrical heater plate 1, commercial heat flux gauge 2 and the heat flux gauge under calibration 3, positioned as shown in Figure 3.3. Cooling water was circulated through the tubes on the plate 4 so as to aid in establishing steady state conditions.

By increasing the input to the heater, the output from the heat flux gauges were recorded using a HP 3052A data acquisition system. The output from the commercial heat flux gauge together with its calibration constant was used for calibrating the heat flux gauges. The sensitivity of the as built gauges varied between 0.66 to 0.74 mv per  $W/m^2$  with most gauges having sensitivities within 4.9% of the mean. This consistency between the gauges was very convenient in that it meant one calibration constant could be used for all the gauges. A typical calibration curve is shown in Figure 3.4.

The gauges, as built, have a resistance value of RSI 0.18. This means that they can be expected to produce a 8% effect on a standard wall of RSI 2.11. However, for most of





1. Heater
2. Commercial Heat Flux Gauge
3. Heat Flux Gauge under Calibration
4. Copper Plate

Figure 3.3 Schematic of a heat flux gauge calibration device



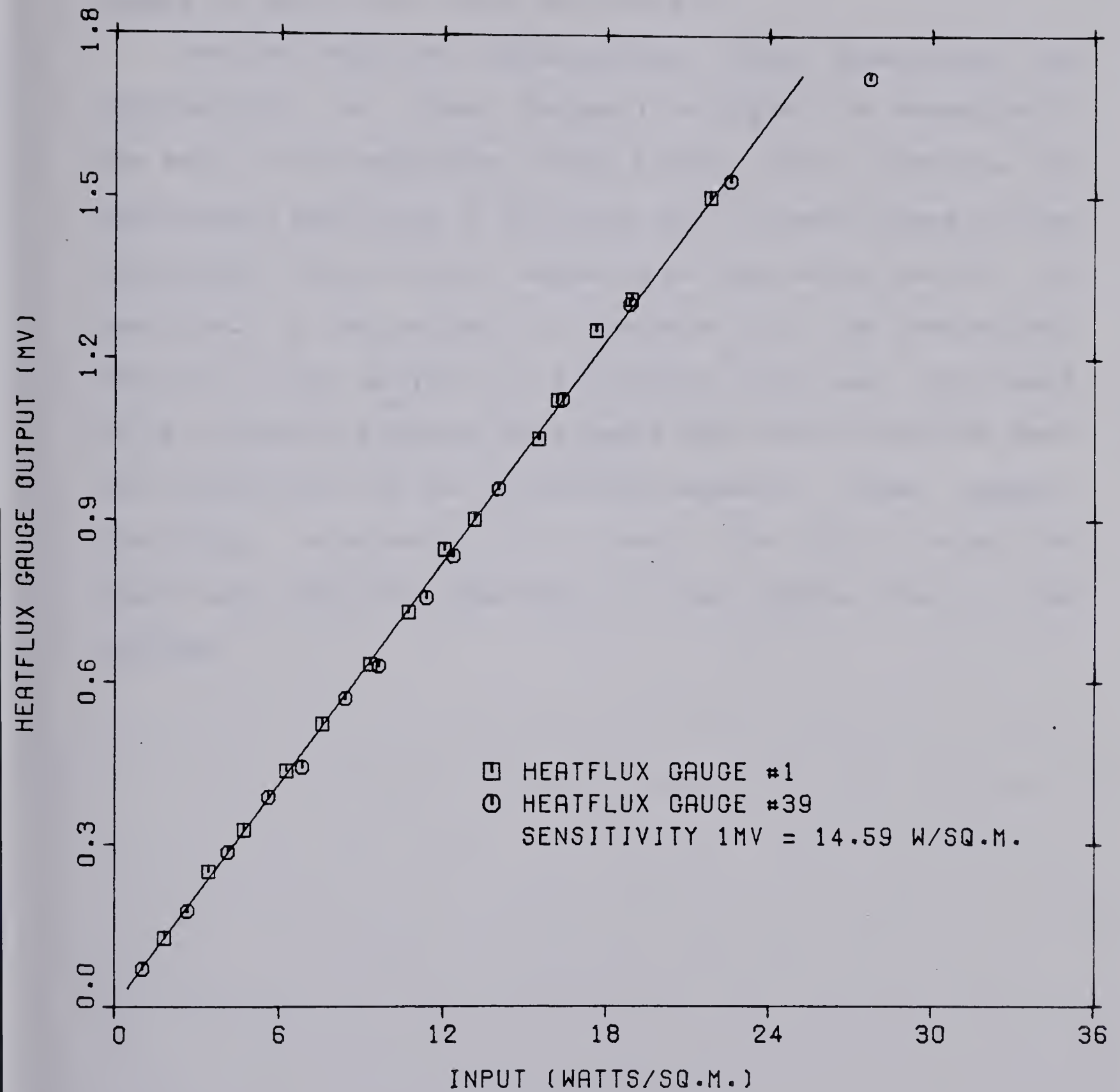


Figure 3.4 Typical calibration curves for heat flux gauges



the other measurements made the RSI values of the elements were around 5. This means the errors introduced by these gauges in such cases would be around 3%.

Another important characteristic that determines the applicability of these gauges in studying the dynamics of the wall is the magnitude of its thermal time constant. An approximate magnitude of the time lag of these gauges can be determined theoretically. Assuming an equivalent section as described by the methods in reference [26], the theoretical time lag of the gauges to a sinusoidal input was calculated to be around 24 minutes. This means that short duration heat flux variations are not accurately sensed by these gauges. Therefore, interpretation of heat flux data to study the short term transient behaviour of the modules has to be avoided.



## 4. THE THERMAL MODEL

### 4.1 Introduction

The analyses in this chapter begin with the thermal model which was developed as a part of the author's MSc. thesis work, a detailed description of which can be found in reference [14]. However, before attempting to discuss the refinements that will be introduced to this model, it is instructive to restate very briefly the previous thermal model so that the overall problem of modeling house heat losses can be better appreciated.

Figure 4.1 shows the physical model which was used to develop the previous simulation model [14]. The various heat losses and heat gains through the elements of this house have been shown therein. The energy balance equation for describing the overall behaviour of this house was written to consider the dynamic interactions between the different elements of the house and its micro climate. A method of formulating the energy balance equation and its solution procedure was shown in the above reference. Fundamental to the development of this procedure was the understanding of the 'to' and 'from' nature of the interactions taking place between the various energy fluxes and the room air. This is illustrated in Figure 4.2. Consequently the quantities of interest such as room air temperatures, furnace heat requirements, the hours of potential over heating etc. were



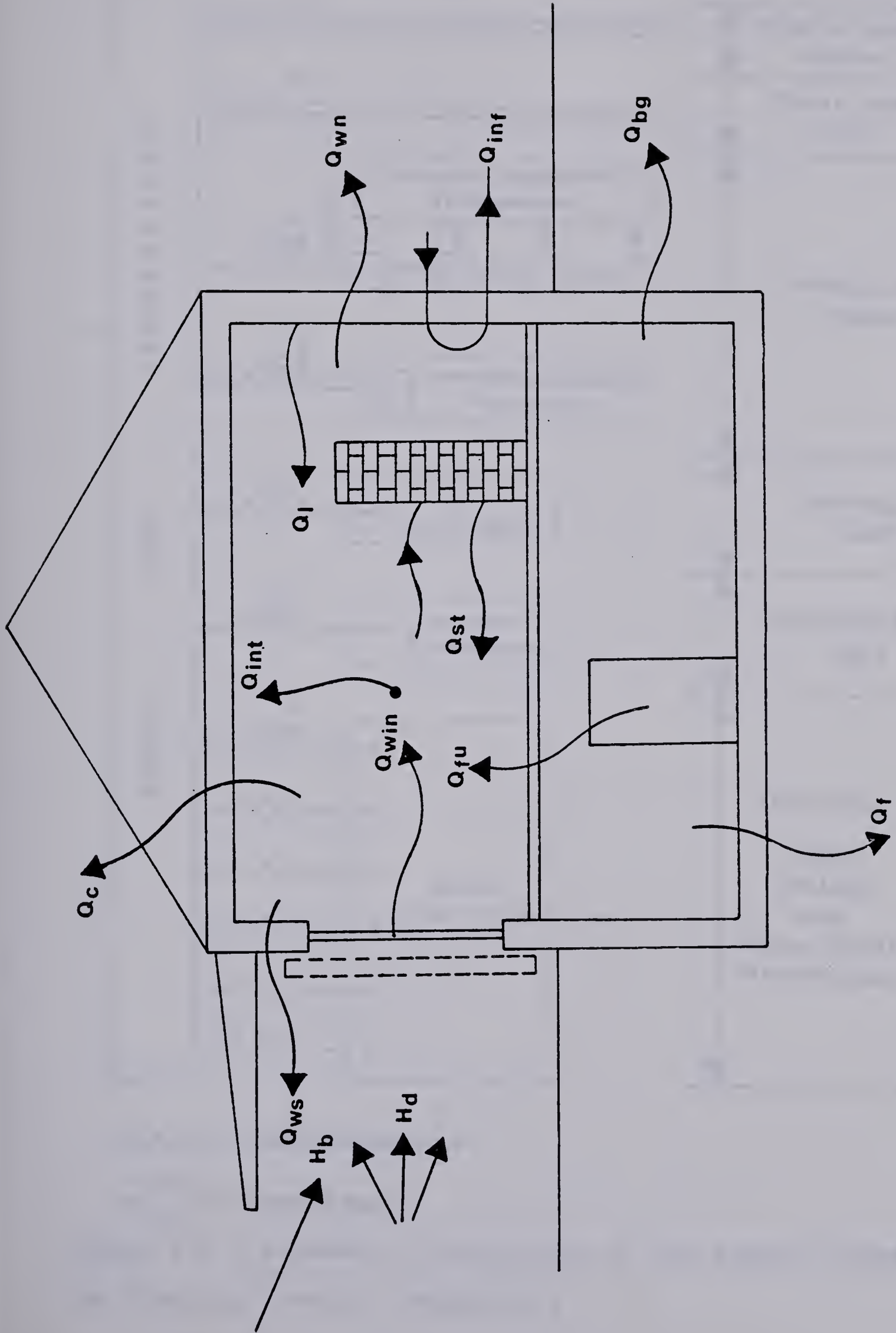


Figure 4.1 Schematic of a house illustrating the heat gains and heat losses



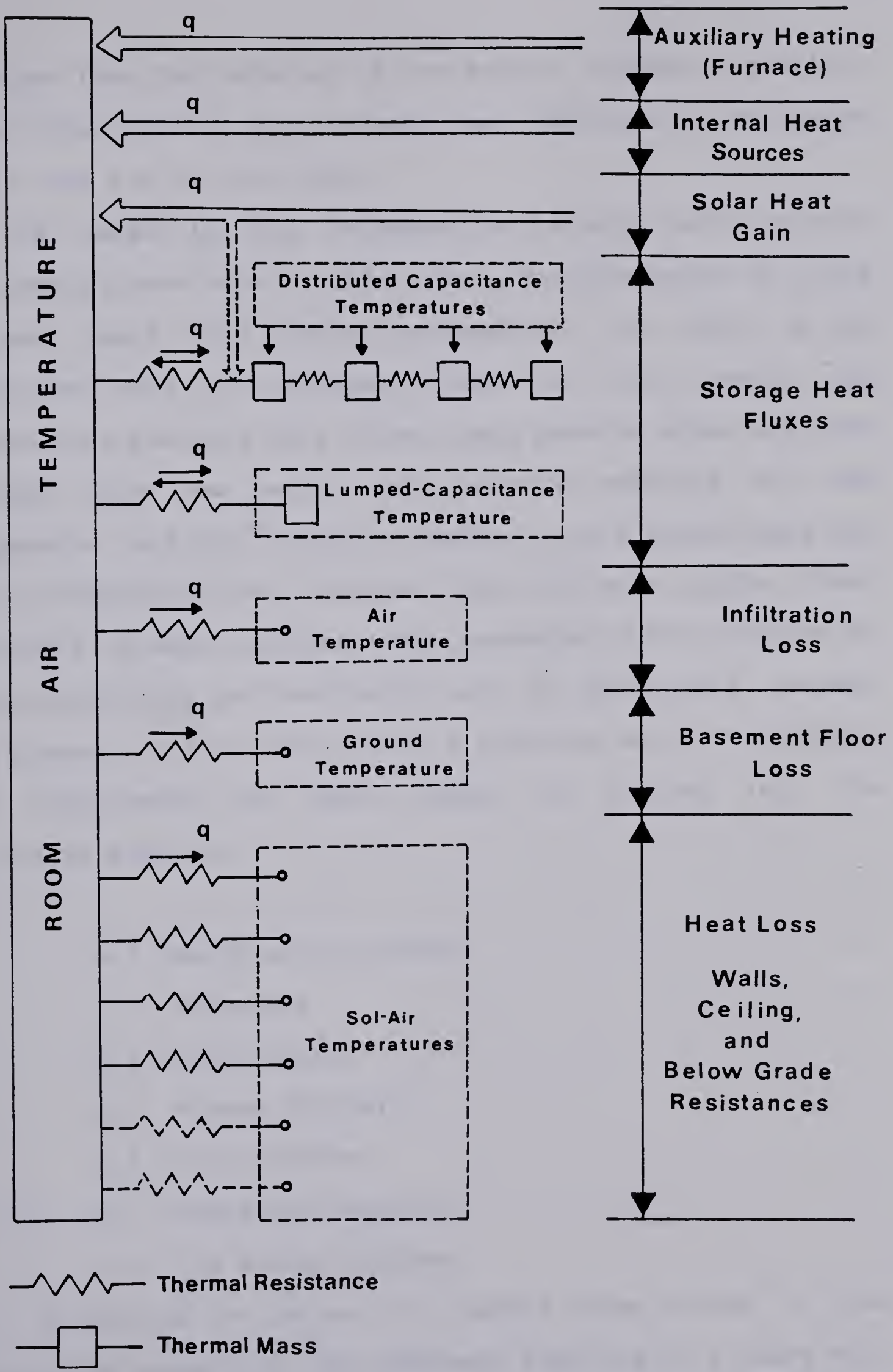


Figure 4.2 A schematic illustration of the energy fluxes to and from the room air temperature



obtained from the solution of the energy balance equation. Since these details have already been described in reference [14], they are omitted here.

As noted in the introduction to this thesis several refinements were made to this model. The discussion of this chapter deals with these refinements. In order to be consistent with the approach taken in this study, the theoretical analysis of a direct gain passive house has been divided into two parts; the thermal modeling of the components, and the integral response of the house where all of the components are involved. With this as a guide line, an effort is made to present the contents of this chapter so that consistency and continuity can be maintained between the present work and the author's previous work. To this end the organization of this chapter is divided into the following sections.

#### 4.2 Walls and Ceilings.

#### 4.3 Basements.

#### 4.4 Solar Gains

#### 4.5 Window Shutters

#### 4.6 Infiltration

#### 4.7 Transient Response

#### 4.8 The Energy Balance

As pointed out before, the second stage review of the literature concerning the component modeling of a house will now be introduced in this chapter at appropriate places in



the above sections.

## 4.2 Walls and Ceilings

Two methods of modeling the walls and ceilings were considered. In the first approach the walls and ceilings were treated as simple resistive elements (The Steady State Model) and their thermal capacity effects were included in the transient response of the structure via a lumped capacity approach. In the second method a more rigorous approach was taken in which, the heat conduction equation for each layer of the composite wall was solved (The Transient Model).

### 4.2.1 The Steady State Model

Consider the typical wall section of module 4 shown in Figure 4.3. The thermal network diagram for this wall section is shown there in. The choice of two different heat transfer paths appear to be appropriate. The steady state heat loss rate through the unit area of the wall is given by,

$$q = \frac{\Delta T}{R_e} \quad (4.1)$$

Where  $R_e$  the effective resistance is given by,

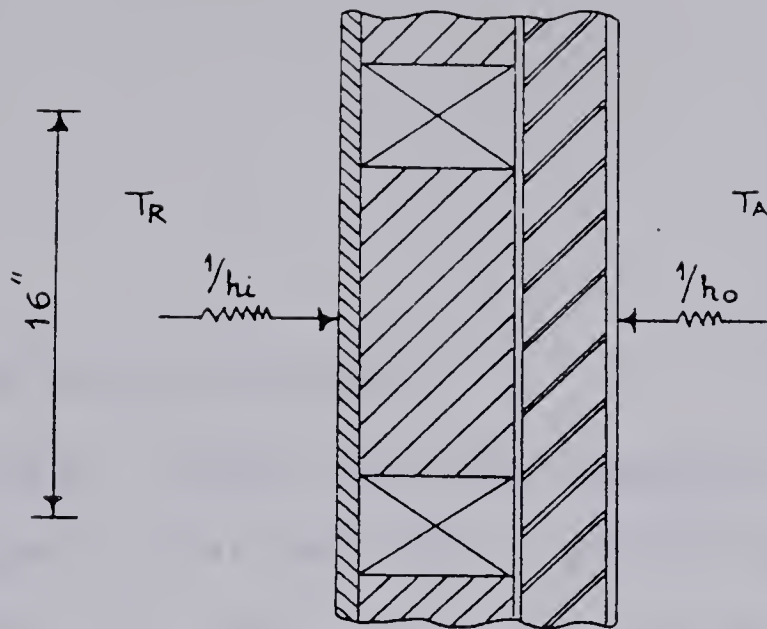
$$R_e = \frac{R_I R_W}{R_I + R_W}$$

and

$$R_I = \left( \frac{1}{h_i} + \sum_{i=1}^N \frac{l_i}{k_i} + \frac{1}{h_o} \right) / f_I \quad (4.2)$$

$$R_W = \left( \frac{1}{h_i} + \sum_{i=1}^N \frac{l_i}{k_i} + \frac{1}{h_o} \right) / f_w \quad (4.3)$$



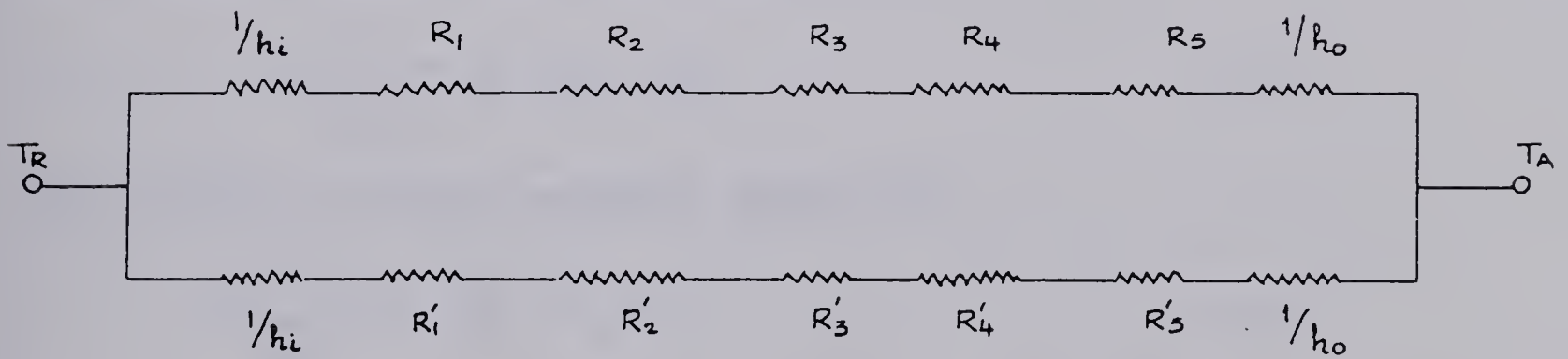


Insulation path  
(from left to right)

1. Dry wall
2. Fibreglass insulation
3. Ply wood
4. Styrofoam
5. Ply wood

Wood Path  
(from left to right)

1. Dry wall
2. Wood stud
3. Ply wood
4. Styrofoam
5. Ply wood



R - Insulation Path

R' - Wood Path

Figure 4.3 Cross section of frame wall in module 4 - Thermal network



#### 4.2.2 The Transient Model

Consider again the same composite wall shown in Figure 4.3. Assuming that heat flow is one dimensional and that the properties of the wall and as well as the heat transfer coefficients are constant, the appropriate equation describing the conduction heat transfer mechanism in each layer can be written as:

$$\frac{\partial T_i}{\partial t} = \alpha_i \frac{\partial^2 T_i}{\partial x_i^2} \quad (4.4)$$

The inside surface boundary condition:

$$k_i \frac{\partial T_i}{\partial x_i} = h_i (T_i - T_R) \quad (4.5)$$

The outside surface boundary condition:

$$k_i \frac{\partial T_i}{\partial x_i} = h_o (T_i - T_y(t)) \quad (4.6)$$

At the interface, temperature and heat flows are continuous:

$$k_i \frac{\partial T_i}{\partial x_i} = k_{i+1} \frac{\partial T_{i+1}}{\partial x_{i+1}} \quad (4.7)$$

The initial condition:

$$T_i(x, 0) = T_R \quad (4.8)$$

Where  $i = 1, 2, 3, \dots, N$  represent the number of layers making up the composite wall.



There are a number of methods available for solving Equation 4.4. In this model, a finite difference fully implicit method was selected because the fully implicit scheme is stable for all values of time steps. This is a great advantage especially when hourly heating loads have to be computed over a period of one year.

Difference formulation of Equations 4.4 through 4.8 is quite straight forward, the details of which can be found in references [31,32]. With a little manipulation, the resulting difference equations can be put in the form shown below.

Interior Nodes:

$$T_i^{v+1} = [T_i^v + \Delta Fo (T_{i+1}^{v+1} + T_{i-1}^{v+1})] / (1 + 2\Delta Fo) \quad (4.9)$$

Room side boundary condition:

$$T_i^{v+1} = [T_i^v + 2\Delta Fo T_{i-1}^{v+1} + 2Bi_i \Delta Fo T_R^{v+1}] / (1 + 2\Delta Fo + 2Bi_i \Delta Fo) \quad (4.10)$$

Outside boundary condition:

$$T_i^{v+1} = [T_i^v + 2\Delta Fo T_{i+1}^{v+1} + 2Bi_o \Delta Fo T_y^{v+1}] / (1 + 2\Delta Fo + 2Bi_o \Delta Fo) \quad (4.11)$$

The interface boundary condition needs some consideration. A typical interface is shown in Figure 4.4.

Let the nodal points be designated as L for the node to the left of the interface and as R to the right of the



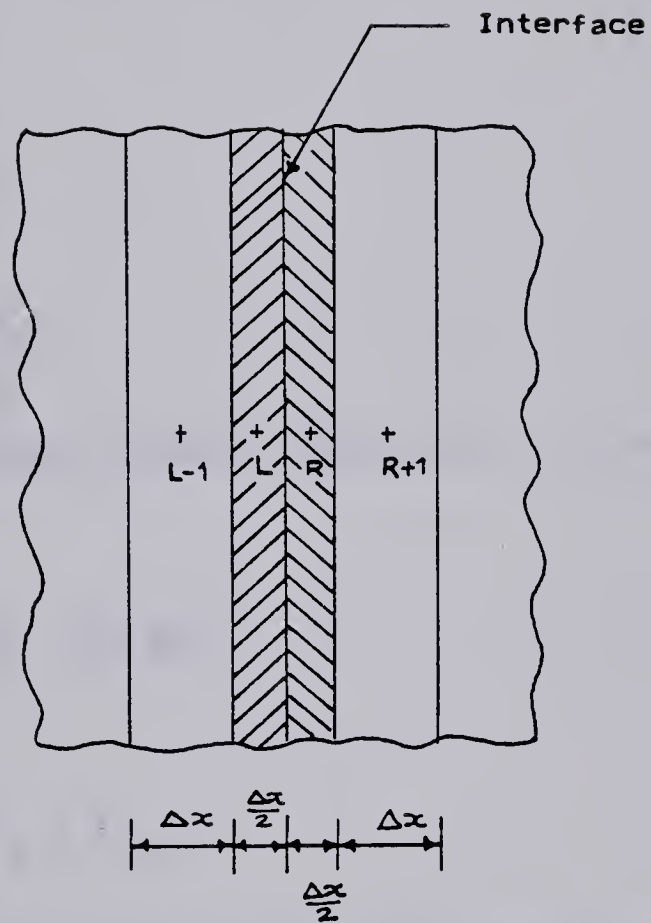


Figure 4.4 Nodal point arrangement at an interface



interface.

Energy balance on node L can be written as:

$$\rho c \left( \frac{\Delta x}{2} \right) \frac{dT_L}{dt} = q_{L-1,L} - q_{L,R} \quad (4.12)$$

$$q_{L-1,L} = \frac{k_L}{\Delta x_L} (T_{L-1} - T_L) \quad (4.13)$$

$$q_{L,R} = U (T_L - T_R) \quad (4.14)$$

$$U = 1 / \left( \frac{\Delta x_L}{2k_L} + \frac{\Delta x_R}{2k_R} \right) \quad (4.15)$$

Similarly, the energy balance equation on node R yields,

$$\rho c \left( \frac{\Delta x}{2} \right)_R \frac{dT_R}{dt} = q_{L,R} - q_{R,R+1} \quad (4.16)$$

Where,

$$q_{R,R+1} = \left( \frac{k}{\Delta x} \right)_R (T_R - T_{R+1}) \quad (4.17)$$

Equations 4.12 and 4.16 can now be written in difference form:

$$T_L^{v+1} = T_L^v + \frac{2\Delta t}{(\rho C \Delta x)_L} \left[ \left( \frac{k}{\Delta x} \right)_L (T_{L-1}^{v+1} - T_L^{v+1}) - U (T_L^{v+1} - T_R^{v+1}) \right] \quad (4.18)$$

and

$$T_R^{v+1} = T_R^v + \frac{2\Delta t}{(\rho C \Delta x)_R} \left[ \left( \frac{k}{\Delta x} \right)_R (T_R^{v+1} - T_{R-1}^{v+1}) - U (T_L^{v+1} - T_R^{v+1}) \right] \quad (4.19)$$

Note that Equations 4.18 and 4.19 were derived from simple physical considerations by writing energy balance equations



on a particular node under investigation.

It is of interest to rearrange Equations 4.18 and 4.19 as follows:

From Equation 4.15 for a uniform grid spacing, with ideal contact

$$U = \left( \frac{2k_L k_R}{k_L + k_R} \right) \frac{1}{(\Delta x)} \quad (4.20)$$

The bracketed term in Equation 4.20 is a harmonic mean of the left and the right side nodal conductivities. This is what is referred to as interface conductivity by Patankar [35]. Therefore, Equation 4.18 can be written as:

$$T_L^{v+1} = T_L^{v+1} + \frac{2\Delta t}{\rho C \Delta x_L^2} [ke_L (T_{L-1}^{v+1} - T_L^{v+1}) - ke_R (T_L^{v+1} - T_R^{v+1})] \quad (4.21)$$

Comparing Equations 4.21 and 4.18

$$ke_L = k_L \quad (4.22)$$

and

$$ke_R = \left( \frac{2k_L k_R}{k_L + k_R} \right) \quad (4.23)$$

The advantage of the rearrangement is at once clear in that the nonuniform conductivities introduced by nonhomogeneity of materials or due to composite slabs can be taken care of throughout the calculation domain by simply invoking the boundary condition Equation 4.7 at every interface.



### 4.3 Basement Models

One of the most difficult heat losses to evaluate with any degree of certainty is the basement heat loss. The earliest study of Houghton et al. [57], based on experimental tests had proposed a very simple method in that the basement floor was assumed to loose heat to mean ground temperature and the wall heat losses were taken as twice the floor loss assuming it to be uniform over the height of the wall.

Later Brown [58], from steady state considerations developed a graphical method for determining the temperature distribution underneath heated or cooled slabs on the ground surface. Based on Brown's work, Boileau and Latta [59,60], proposed an analytical method for calculating the heat losses from the portion of the basement below grade. This method, which was adopted by ASHRAE, is based on steady state analysis and thus eliminates the dynamic interaction of the basement from the rest of the structure. Secondly, such important parametric studies as the effects of soil properties, the influence of deep ground temperature etc. cannot be analyzed with such a simplistic model.

In a more recent study McBride et al. [61] have used an explicit finite difference calculation to solve the two dimensional unsteady heat conduction equation applied to a basement geometry. The predictions were compared with measured ground temperatures. In their analysis, the outside boundary condition neglected the solar radiation and



seasonal surface cover effects. With assumed values of soil properties, the accuracy of this model was reported to be within 2°F. This method is a definite improvement in the analysis of basement heat loss calculations in that it is a transient model and secondly one year daily measured temperatures were used in the study. However, no heat flux measurements were made.

Shipp [62], in his thesis on thermal characteristics of large earth sheltered structures, presented experimental results on wall heat fluxes, surface temperatures and ground temperatures measured in and around the underground experimental research centre, at the University of Minnesota. These measurements were used to develop a two dimensional finite difference implicit model. From his study, Shipp concluded that the transient conduction model can predict the heat losses from the underground walls and ceiling with "reasonable accuracy."

Other studies on basement heat losses include an empirical method developed by Swinton and Platts [63], a shape factor approach to basement heat losses by Mitalas [63A], and the numerical study of Kusuda and Achenbach [64]. Swinton and Platts's method is an empirical fit to the measured data and as such cannot be called a real predictive method. On the other hand Kusuda and Achenbach's three dimensional model is quite complex rendering it unsuitable for heat loss calculations for the buildings. The shape factor approach of Mitalas is somewhat practical but limited



in scope because of its simplifying assumptions.

In order to fully appreciate the approximations involved in the above studies or those that will be introduced in the present study, it is necessary to consider the problem in a more general form. A cavity like a heated basement in the undisturbed ground thermal regime creates an unsteady temperature field of its own in the surrounding soil. Depending upon the soil properties and the surface cover effects, a considerable time is required before the quasi-steady state conditions can be established.

In general, therefore, the two important areas in the study of ground thermal regime problems are: The heat exchange mechanisms at the earth's surface and the mechanism of heat and mass transfer in the soil which is essentially a porous medium.

Among the studies concerning the first aspect of the ground thermal regime, is a study of Gilpin [65] on the ground temperature boundary condition provided by a vegetation covered surface. Gilpin concluded that the conventional single surface energy balance can lead to significant errors when applied to a vegetation covered surface that is not completely saturated with water. With experimental observations Gilpin demonstrated the existence of two distinct surfaces: a radiation surface and an evaporation surface and thus proposed a two surface model.

In an another study, Gilpin and Wong [66] studied the effects of ground surface cover and some factors that



influence the ground temperature. In what they called a heat valve effect, Gilpin and Wong showed that the effect of surface cover and the freezing and thawing in the active layer would tend to keep the mean ground temperature 3-4 °C higher than the mean air temperature. In a parametric study on some factors influencing the ground temperature Gilpin and Wong [67] published an order of magnitude analysis of the average surface temperatures and the ground temperatures due to perturbations in the input parameters. These effects were tabulated as influence coefficients which were obtained by dividing the change in temperature by the factor responsible for the change. It was shown that changes by a factor of two in the average properties of winter and summer surface cover produced changes in the mean ground temperature from about 2 to 7°C depending on location and type of change involved.

The second part of the problem concerns itself with heat and mass transfer processes in a porous medium such as the soil. Currently, this is one of the most actively pursued research area. Studies of de Vries [68] on heat transfer in soils and Philip's study [69] on water movement in the soil are of considerable interest. de Vries studies show that heat is transferred in the soil mainly by conduction. The mechanisms of heat transfer in the soil are in order of importance: conduction, convection and radiation. Conduction occurs throughout the soil but the main flow of heat is through solid parts. Convection in the



usual sense is at most times negligible with the exception of rapid infiltration of water after heavy rain or melting of winter snow cover. However, the transport of latent heat by water vapour greatly contributes to the heat transfer in gas filled pores. Radiation heat transfer is only of importance in dry soils at high temperatures.

When the combined transport of heat and moisture must be considered, two coupled partial differential equations must be solved which are non-linear in nature.

It should be recognized that each of the above studies though complex are still based on a number of simplifying assumptions. Therefore one has to be careful in applying these results to the building heat transfer problems as the one encountered in the prediction of basement heat losses.

Consequently the recent trend is to analyze the basement heat losses through two dimensional numerical techniques. As an example recently Eckert, Bligh and Pefender [70] have used a two dimensional conduction model to analyze heat losses through large earth sheltered structures. In view of the complexity of the problem, the approach taken in this thesis was to first establish certain guide lines within which basement heat loss models could be developed.

Firstly, the existing ASHRAE calculation procedure [59], on basement heat losses can be improved. A guide line used in selection of this approach was that the first model should give the results only to the minimum of detail and



accuracy required and no more. Application of this guideline eliminated some of the more complex calculation procedures. In the procedure chosen, the heat exchange to the basement walls was divided into two components. One with a diurnal variation and one with an annual variation. The diurnal component represents heat flow into and out of the basement walls that occur due to room temperature variations. The mean value of these flows is zero; thus they are not in themselves a net heat loss, however, they do play an important part in determining the transient behaviour of the house.

The annual variation of heat flow from the basement results in a net heat loss if the average ground temperature is below the indoor air temperature. To treat this component of heat loss it was assumed that heat flows out of the basement through a layered path consisting of an inside film coefficient, the concrete basement wall, a basement insulation layer where applicable, the ground and an effective ground surface layer to the sol-air temperature for a horizontal surface. The temperature input data can be obtained by fitting a sinusoidal curve with a period of one year to the climatological data for sol-air temperature. The advantage as far as simplicity is concerned of this approach is that the heat flux through a layered medium can be analytically calculated for a simple sinusoidal input. The result is that the calculated heat flux at the basement wall is also a sinusoid with a mean amplitude and phase shift



relative to the sol-air temperature cycle. Thus this first model, is an improvement over the ASHRAE steady state method in that it goes one step further to include the thermal mass effects of the ground in the calculation procedure.

A second guide line comes from the considerations of surface boundary conditions and the variations in the soil conductivity. That is the first model, the mathematical formulation of which will be discussed shortly, is not capable of taking into account such variations as effective ground surface cover, and conductivity of the soil in relation to the moisture content, both of which vary with location and time. Therefore, a second model which, while still relying on one dimensional analysis, includes provision to adjust the soil conductivity and the surface cover effects externally to the model. Since numerical solution schemes offer such a flexibility, a finite difference implicit calculation technique was used in developing the second model.

A third guide line can be formulated by recognizing that the heat losses from the basement walls cannot be truly represented by one dimensional model. In fact a general three dimensional analysis of the problem may be required. However, the numerical solution of a three dimensional conduction model is not warranted because of the fact that the soil properties are not known to any great accuracy. This however does not preclude the possibility of developing a two dimensional conduction model so that deep ground



temperature and the far field temperature boundary conditions may be taken into consideration.

Therefore, in line with the above two models, the next guideline was, to develop a third model, a two dimensional conduction model, with a flexibility for adjusting the soil conductivity and the ground surface cover variations.

A fourth guide line comes from the reasoning that adjustment of soil conductivity values external to the model is not completely realistic considering the freezing and thawing effects in the ground. Therefore, a fourth guideline was to try a simple one dimensional phase change conduction model for making comparisons with the previous three models. The results of these comparisons would give necessary information on further attempts towards refining basements heat loss models.

In the sections to follow the mathematical and the finite difference formulation of the above four models will be presented.

#### 4.3.1 The First Model

Let the layered paths be identified by:

$i = 1$  inside concrete wall

$i = 2$  insulation layer where appropriate

$i = 3$  path through the ground

Heat flow through a homogeneous, constant property medium



can be represented by:

$$\frac{\partial T_i}{\partial t} = \alpha_i \frac{\partial^2 T_i}{\partial x_i^2} \quad (4.24)$$

The room side boundary condition: for  $i=1$ ,

$$-k_i \frac{\partial T_i}{\partial x_i} = h_i (T_i - T_R) \quad (4.25)$$

The weather side boundary condition for  $i=3$  can be expressed as:

$$-k_i \frac{\partial T_i}{\partial x_i} = h_o (T_i - T_y) \quad (4.26)$$

Where,

$$T_y = \bar{T}_y + \Delta T_y \cos (Wt - \phi_y) \quad (4.27)$$

In the above formulation  $h$  is the appropriate heat transfer coefficient approximated to include convective and radiative effects.

$T_y$  in Equation 4.27 represents the annual sol-air temperature cycle with mean amplitude of  $\bar{T}_y$  and a fluctuating component represented by second term in the equation.

Solution of Equation 4.24 for a homogeneous single medium was given by Alford et al. [24]. They treated the room side boundary condition similar to Equation 4.25 but



the weather side boundary condition was treated as consisting of two distinct components: one due to ambient temperature and the other due to solar radiation.

The final result which was also derived by the author to check for the correctness is of interest to this study. Reproducing their equation:

$$\begin{aligned}
 q_2 = & U [t_m + \{\lambda_o t_o \cos(W_o \theta - \alpha_o - \phi_o) + \lambda_1 t_1 \cos(W_1 \theta - \alpha_1 - \phi_1) \\
 & + \dots\}] + U \left[ \frac{1}{H} (aI_m - \xi \Delta R_b) + \frac{a}{H} \{ \lambda_o I_o \cos(W_o \theta - \beta_o - \phi_o) + \right. \\
 & \left. \lambda_1 \cos(W_1 \theta - \beta_1 - \phi_1) + \dots \} \right]
 \end{aligned}
 \tag{4.28}$$

Where,

- $q_2$  inside wall heat flux
- $U$  overall heat transfer coefficient of the medium
- $t_m$  mean temperature of the air temperature cycle
- $\lambda$  decrement factor defined by equation 4.32.
- $\xi \Delta R_b$  product of emmissivity and net long wave radiation
- $\alpha$  displacement angle of air temperature
- $\phi$  phase angle of inside heat flux
- $\beta$  displacement angle of solar intensity
- $I$  intensity of solar radiation
- $H$  combined convective and radiative heat transfer coefficient
- $w$  angular velocity and its harmonics
- $\theta$  time



In deriving Equation 4.28, the room temperature was arbitrarily set equal to zero. Equation 4.28 has to be modified so that it could be applied to the first model. Fortunately the modifications are simple.

By introducing the concept of sol-air temperature [21], the two component input function used by Alford et al. can be merged into a single component whose effects are equivalent to those contributed by the above two components: that is, air temperature and solar radiation can be combined into one component.

Introduction of sol-air temperature concept eliminates the second part of the Equation 4.28 which can now be written as:

$$q_2 = Ut_m + U [\lambda_n t_n \cos(W_n \theta - \alpha_n - \phi_n)] \quad (4.29)$$

Where subscript n stands for 0, 1, 2, ...., n harmonics.

With room temperature set at a constant value,  $t_r$ , Equation 4.29 can be written as:

$$q_2 = U [t_m + \{\lambda_n t_n \cos(W_n \theta - \alpha_n - \phi_n)\} - t_r] \quad (4.30)$$

Where,

$$U = \frac{1}{h_i} + \frac{l_i}{k_i} + \frac{1}{h_o} \quad (4.31)$$

and  $\lambda$  can be shown to be equal to,  $\lambda_n = \frac{h_o h_i}{k \sigma_n \sqrt{Y_n^2 + Z_n^2}} \quad (4.32)$



Where,

$$\sigma_n = \frac{\sqrt{\rho C W_n}}{2k} \quad (4.33)$$

and:

$$Y_n = \left(1 + \frac{h_o h_i}{2\sigma_n^2 k_n^2}\right) \cos\sigma_n L \sinh\sigma_n L + \left(1 - \frac{h_o h_i}{2\sigma_n^2 k_n^2}\right) \sin\sigma_n L \cosh\sigma_n L + \frac{(h_o + h_i)}{\sigma_n k_n} \cos\sigma_n L \cosh\sigma_n L \quad (4.34)$$

$$Z_n = \left(1 + \frac{h_o h_i}{2\sigma_n^2 k_n^2}\right) \cos\sigma_n L \sinh\sigma_n L + \left(1 - \frac{h_o h_i}{2\sigma_n^2 k_n^2}\right) \sin\sigma_n L \cosh\sigma_n L + \frac{(h_o + h_i)}{\sigma_n k_n} \sin\sigma_n L \sinh\sigma_n L \quad (4.35)$$

$$\phi_n = \tan^{-1} \left( \frac{Z_n}{Y_n} \right) \quad (4.36)$$

Rearrangement of Equation 4.30 is at once clear: in that the addition of layers to a single homogeneous layer should not alter the form of the Equation 4.30. However, the task of determining  $\lambda$  and  $\phi$  with addition of each layer becomes progressively complicated.

Mackey and Wright in their studies on periodic heat flow through homogeneous walls and roofs [25] and later on composite walls and roofs [26] defined an equivalent homogeneous wall or roof which will have the same variation in indoor surface temperature with time as does the actual composite wall or roof under identical ambient conditions..



While developing their method Mackey and Wright solved the basic problem given by Equations 4.24 through 4.27 for two and three layered walls. A little consideration would suggest that advantage can be taken of their solution by utilizing the equations for decrement factor and phase angle for a two and three layered sections and substituting them into Equation 4.32 to calculate the inside wall heat flux.

The equations for  $\lambda$  and  $\phi$  which are quite involved can be obtained from Figures A and B given in [26].

Thus the first model can be applied to each of the precalculated path lengths using appropriate two layered or three layered equations. The advantage as far as the simplicity is concerned of this first model is that it is an analytical model and requires very little computer time. In addition it provides a basis for comparing the more complicated numerical models.

#### 4.3.2 The Second Model

Formulation of the second model is based on the second guide line discussed earlier. In implementing this guide line it is necessary to decide on the degree of nonhomogeneity of the soil that one would like to consider. Once this is done, the discretization equations can be developed using the interface conductivity concept discussed in section 4.2.3. In fact it is very tempting to consider the soil as completely nonhomogeneous medium and develop a general numerical model for the heat flow through the soil as



was done Mexiel and Shipp et. al.[71,72]. However, such an approach appears to be unrealistic. The reason for this stems from the difficulties involved in measuring the soil conductivities over small increments in spatial coordinates.

In view of the above considerations it was necessary to decide a scheme on which the formulation of basement numerical models can be based. The rationale for the approach adopted in the present numerical models came from Lachenbruchs' study [73] on periodic heat flow in a stratified medium with applications to permafrost problems. Lachenbruch maintains that it is more realistic to consider the ground as a stratified medium. Application of this concept requires that the numerical models be able to accomodate the non uniformity in soil conductivity.

Formulation of the second model is therefore based on two considerations: use of the second guide line stated before and the rationale drawn from Lachenbruchs' study. Consider, for example, a general situation represented in Figure 4.5. Using one dimensional analysis, the appropriate equations for describing the heat flow can be written as:

$$(\rho C) \frac{\partial T}{\partial t} = \frac{\partial}{\partial x} \left( k \frac{\partial T}{\partial x} \right) \quad (4.37)$$

$$-k \left. \frac{\partial T}{\partial x} \right|_{x=0} = h_o (T - T_y(t)) \quad (4.38)$$

$$-k \left. \frac{\partial T}{\partial x} \right|_{x=L} = h_i (T - T_R) \quad (4.39)$$

$$T_y = \bar{T}_y + \Delta T_y \cos (Wt - \phi_y) \quad (4.40)$$



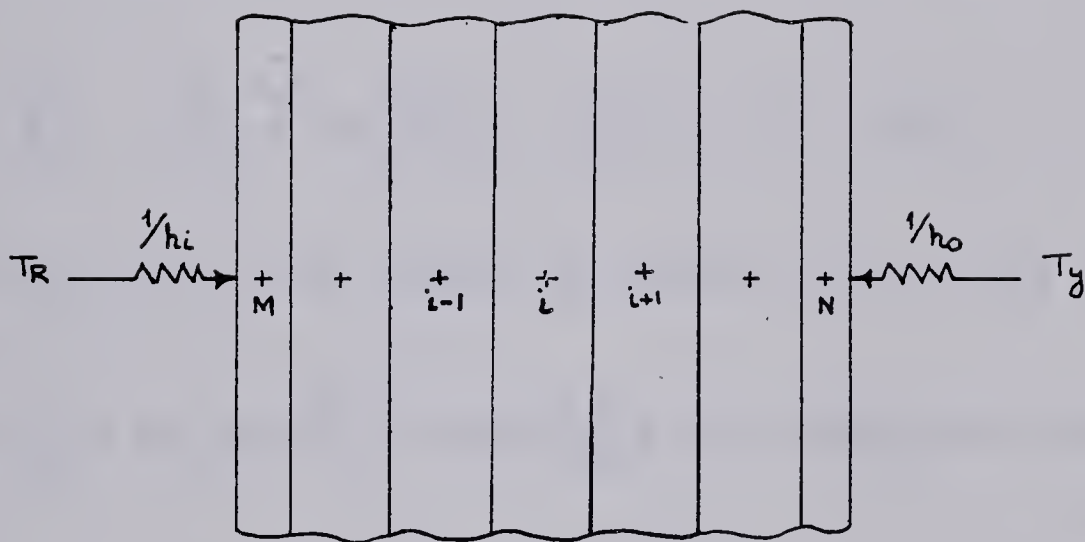


Figure 4.5 Nodal point arrangement in a segment of a stratified medium



Since the ground is considered as a stratified medium the heat flow path can be divided into a number of segments. Within each segment the ground will be considered as a homogeneous medium. At the interface between the two segments the interface conductivity concept will be applied to develop the discretization equations.

The fully implicit difference equations within a segment on a node such as  $i$  in Figure 4.5 can be written as:

$$T_i^{v+1} = [T_i^v + \Delta Fo (T_{i-1}^{v+1} + T_{i+1}^{v+1})] / (1 + 2\Delta Fo) \quad (4.41)$$

The room side boundary condition can be written as :

$$T_M^{v+1} = [T_M^v + 2Bi_i \Delta Fo T_R^{v+1} + 2\Delta Fo T_{M+1}^{v+1}] / (1 + 2Bi_i \Delta Fo + 2\Delta Fo) \quad (4.42)$$

The weather side boundary condition can be written as:

$$T_N^{v+1} = [T_N^v + 2Bi_o \Delta Fo T_y^{v+1} + 2\Delta Fo T_{N-1}^{v+1}] / (1 + 2Bi_o \Delta Fo + 2\Delta Fo) \quad (4.43)$$

At the interface between the two segments, the equations are similar to Equations 4.19 and 4.21 given in section 4.2.2. That is:

$$T_L^{v+1} = T_L^v + \frac{2\Delta t}{\rho C \Delta x_L^2} [ke_L (T_{L-1}^{v+1} - T_L^{v+1}) - ke_R (T_L^{v+1} - T_R^{v+1})] \quad (4.44)$$

and,

$$T_R^{v+1} = T_R^v + \frac{2\Delta t}{\rho C \Delta x_R^2} [ke_R (T_R^{v+1} - T_{R-1}^{v+1}) - ke_L (T_L^{v+1} - T_R^{v+1})] \quad (4.45)$$



Where  $\kappa_{e_L}$  and  $\kappa_{e_R}$  are effective interface conductivities. Equations 4.41 through 4.45 were solved using Gauss-Siedel iterative technique with a relaxation parameter to aid in faster convergence.

#### 4.3.3 The Third Model

The motivation for developing the third model, the two dimensional conduction model, comes from two considerations. Firstly, the deep ground temperature and the far field temperature regimes have a definite influence on the basement heat losses, and secondly, the one dimensional path length concept may not truly represent the overall dynamics of the basement heat losses.

Therefore, using the third guideline and considering the ground to be a stratified medium, a two dimensional fully implicit transient conduction model will be developed.

##### 4.3.3.1 Mathematical Formulation

The appropriate equation is:

$$(\rho C) \frac{\partial T}{\partial t} = \frac{\partial}{\partial x} \left( k \frac{\partial T}{\partial x} \right) + \frac{\partial}{\partial y} \left( k \frac{\partial T}{\partial y} \right) \quad (4.46)$$

While the relevant boundary conditions are shown in Figures 4.6 and 4.7. These figures represent a one half of the basement geometry about the line of symmetry when viewed from the East and the West directions respectively.



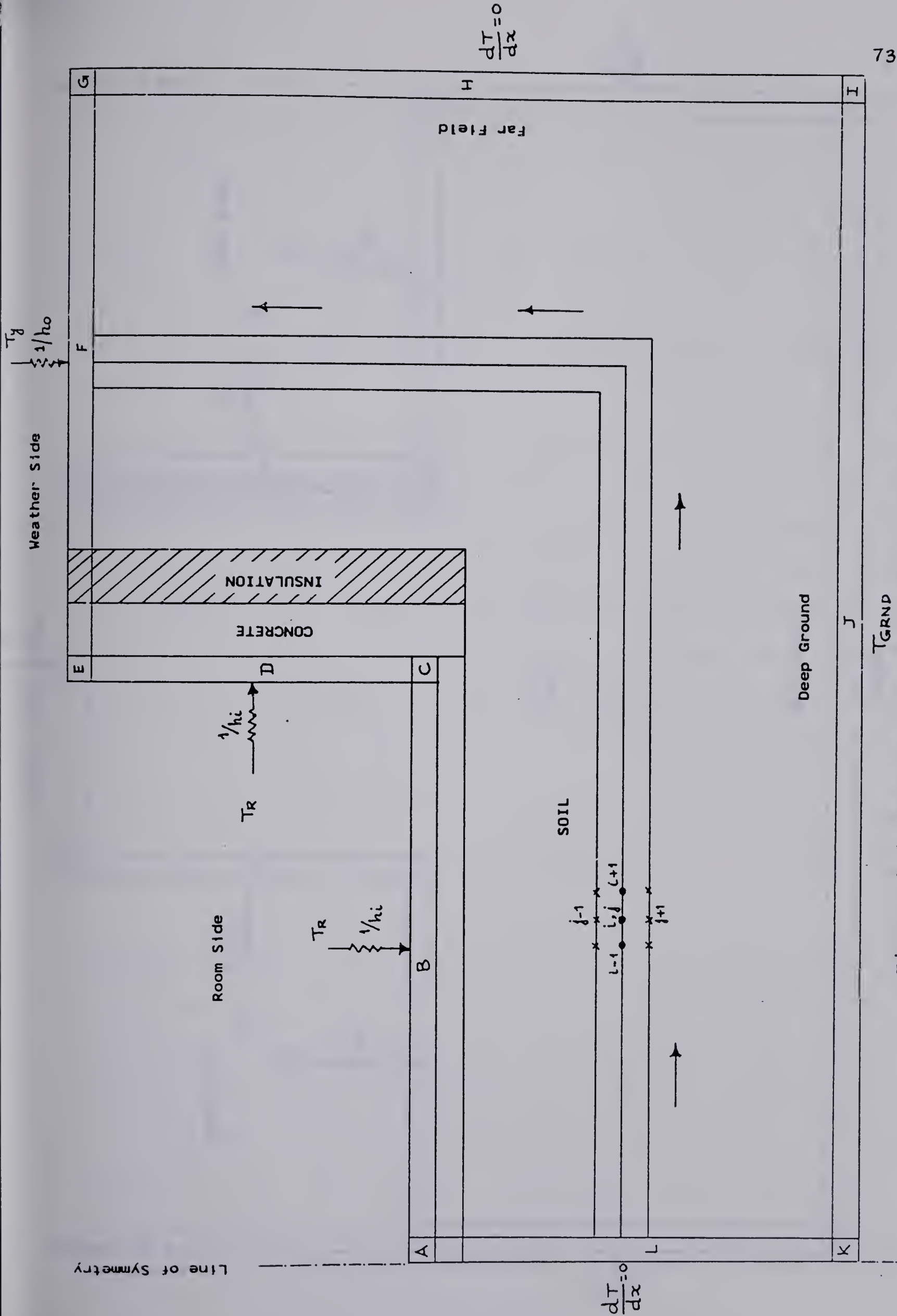


Figure 4.6 Basement: The North-South geometry



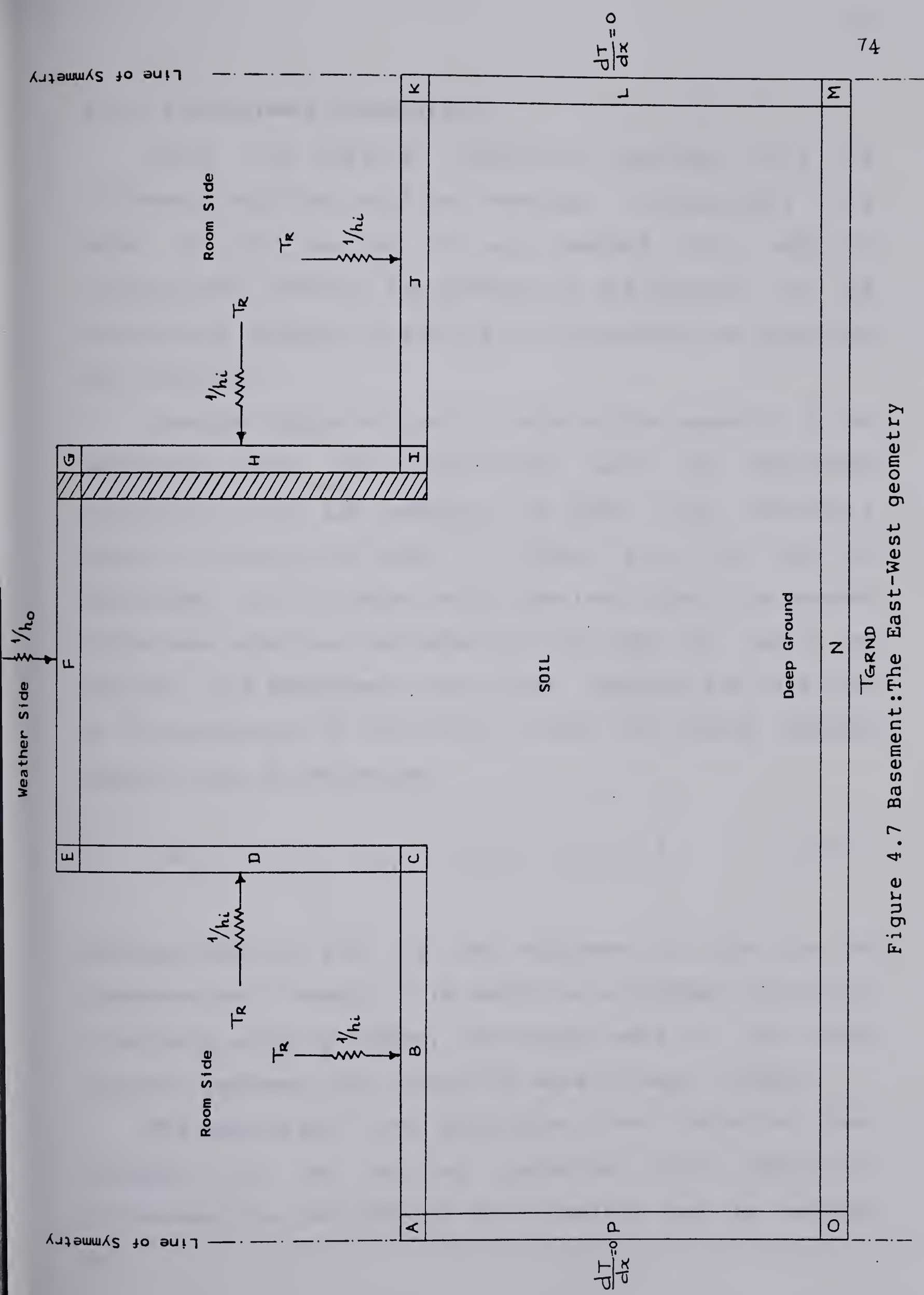


Figure 4.7 Basement: The East-West geometry



#### 4.3.3.2 Difference Formulation

Using the physical formulation approach [31] the difference equations will be developed. Conceptually this model is very similar to any standard fully implicit formulations. However, the geometry of the problem and the methodology adopted in solving the discretization equations are different.

Consider Figure 4.6 and 4.7 showing the geometry of the basements along the North-South and the East-West orientation for the modules. To begin with consider a typical interior node shown in Figure 4.8. Let this be surrounded by interfaces on all the four sides. The general difference equations developed for this case can easily be reduced to a homogeneous case later. Applying the first law of thermodynamics to the control volume, the energy balance equation may be written as:

$$E_{s_{i,j}} + q_{i-1,i} + q_{j+1,j} - q_{j,j-1} - q_{i,i+1} = 0 \quad (4.47)$$

Because equation 4.47 is the statement of the law of conservation of energy it is valid for a constant as well as a variable property medium. The energy terms in the above equation represent the conduction mode of heat transfer.

The appropriate law describing the conduction heat transfer to the driving potential (the temperature difference) via the property of the medium can be written as:



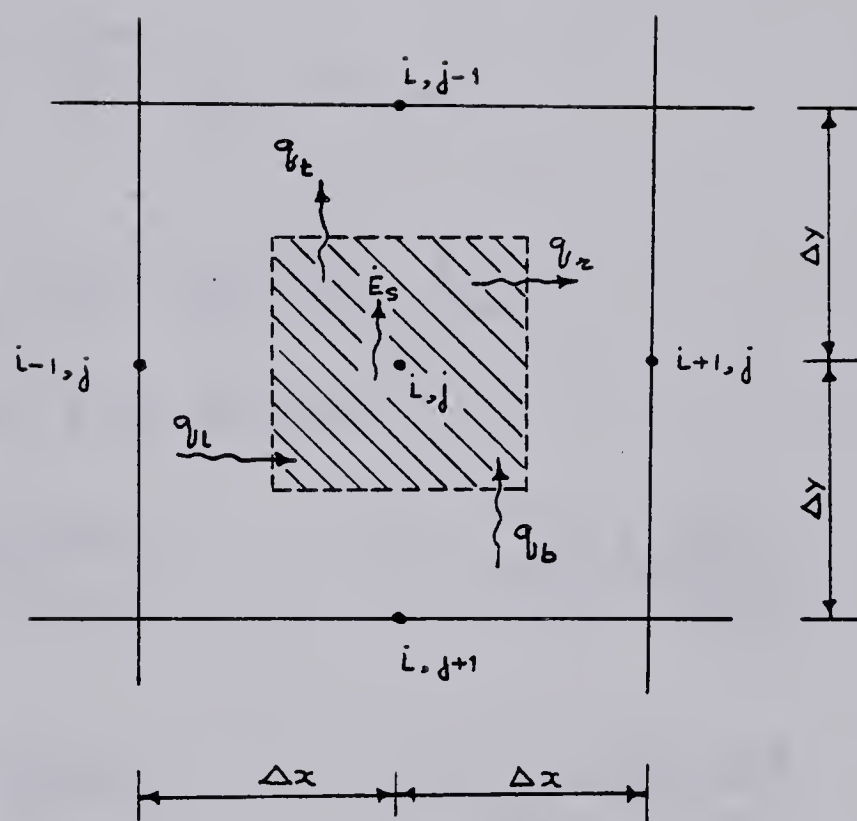


Figure 4.8 Control volume for an interior nodal point



$$q_{i-1,i} = -k_{\ell} A \frac{dT}{dx}$$

(4.48)

$$q_{i-1,i} = \frac{k_{\ell} \Delta y}{\Delta x} (T_{i-1,j} - T_{i,j})$$

Similarly:

$$q_{i,i+1} = \frac{k_r \Delta y}{\Delta x} (T_{i,j} - T_{i+1,j})$$

$$q_{j+1,j} = \frac{k_b \Delta x}{\Delta y} (T_{i,j+1} - T_{i,j}) \quad (4.49)$$

$$q_{j,j-1} = \frac{k_t \Delta x}{\Delta y} (T_{i,j} - T_{i,j-1})$$

and:

$$Es_{i,j} = (\rho C) \Delta x \Delta y \left( \frac{T_{i,j}^{v+1} - T_{i,j}^v}{\Delta t} \right) \quad (4.50)$$

Where, for equal grid spacing,

$$k_{\ell} = \frac{2 k_{i,j} k_{i-1,j}}{k_{i,j} + k_{i-1,j}}$$

$$k_r = \frac{2 k_{i,j} k_{i+1,j}}{k_{i,j} + k_{i+1,j}}$$

(4.51)

$$k_t = \frac{2 k_{i,j} k_{i,j-1}}{k_{i,j} + k_{i,j-1}}$$

$$k_b = \frac{2 k_{i,j} k_{i,j+1}}{k_{i,j} + k_{i,j+1}}$$

The suffix  $\ell$ ,  $r$ ,  $t$ ,  $b$  stand for approaching the node  $i, j$  from left, right, top and bottom respectively.

Substituting the above energy terms into the energy balance Equation 4.47, the fully implicit difference equations can be written as:

$$\rho C (\Delta x)^2 \frac{T_{i,j}^{v+1} - T_{i,j}^v}{\Delta t} = [k_{\ell} (T_{i-1,j}^{v+1} - T_{i,j}^v) - k_r (T_{i,j}^{v+1} - T_{i+1,j}^{v+1}) - k_t (T_{i,j}^{v+1} - T_{i,j-1}^{v+1}) + k_b (T_{i,j+1}^{v+1} - T_{i,j}^v)]$$

Rearranging:

$$T_{i,j}^{v+1} = [T_{i,j}^v + (\Delta Fo_{\ell} T_{i-1,j}^{v+1} + \Delta Fo_r T_{i+1,j}^{v+1} + \Delta Fo_t T_{i,j-1}^{v+1} + \Delta Fo_b T_{i,j+1}^{v+1})] / (1 + \Delta Fo_{\ell} + \Delta Fo_r + \Delta Fo_t + \Delta Fo_b) \quad (4.52)$$



Where:

$$\begin{aligned}
 \Delta Fo_{\ell} &= \frac{k_{\ell} \Delta t}{\rho C \Delta x}^2 & \Delta Fo_t &= \frac{k_t \Delta t}{\rho C \Delta x}^2 \\
 \Delta Fo_r &= \frac{k_r \Delta t}{\rho C \Delta x}^2 & \Delta Fo_b &= \frac{k_b \Delta b}{\rho C \Delta x}^2
 \end{aligned}
 \tag{4.53}$$

With a little modification Equation 4.52 can be applied to a homogeneous medium. This would imply that the Fourier numbers appearing in the Equation 4.52 due to the nonhomogeneity will be equal for a homogeneous medium. Therefore rewriting Equation 4.52 for a homogenous medium,

$$T_{i,j}^{v+1} = [T_{i,j}^v + \Delta Fo (T_{i-1,j}^{v+1} + T_{i+1,j}^{v+1} + T_{i,j-1}^{v+1} + T_{i,j+1}^{v+1})] / (1 + 4\Delta Fo)
 \tag{4.54}$$

The difference formulation of the boundary nodes shown in Figures 4.9 and 4.10 can be developed as follows:

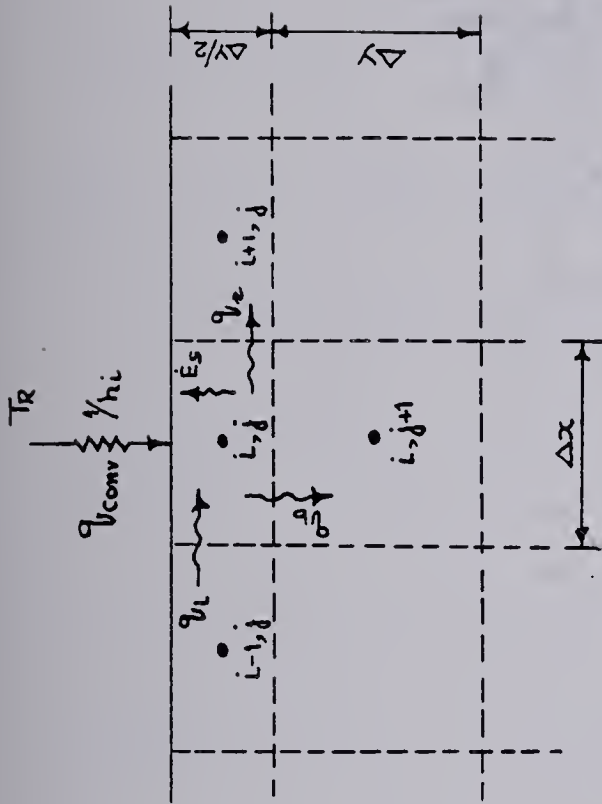
Control volume 3 of Figure 4.9:

$$E_s = q_{\text{conv}} - q_b - q_r
 \tag{4.55}$$

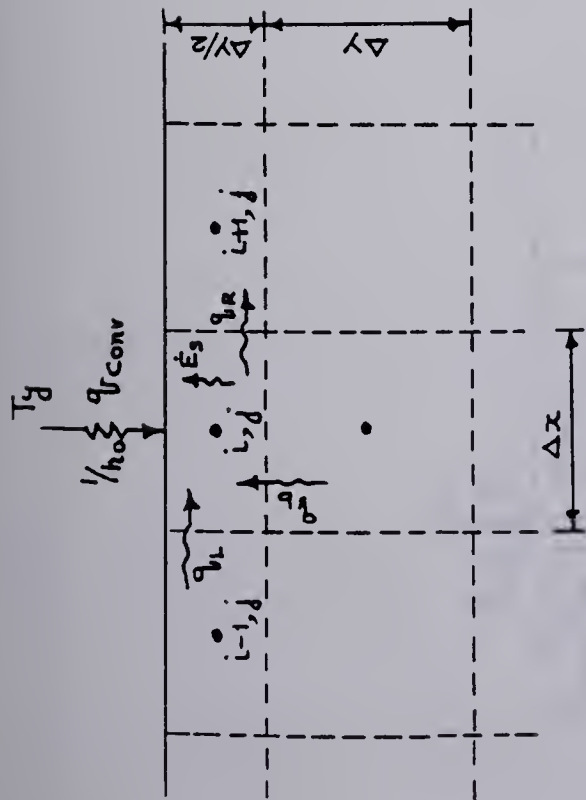
Substituting for energy terms and rearranging:

$$T_{i,j}^{v+1} = [T_{i,j}^v + 2Bi_i \Delta Fo T_R^{v+1} + 2 \Delta Fo (T_{i,j+1}^{v+1} + T_{i+1,j}^{v+1})] / (1 + 2Bi_i \Delta Fo + 2\Delta Fo)
 \tag{4.56}$$

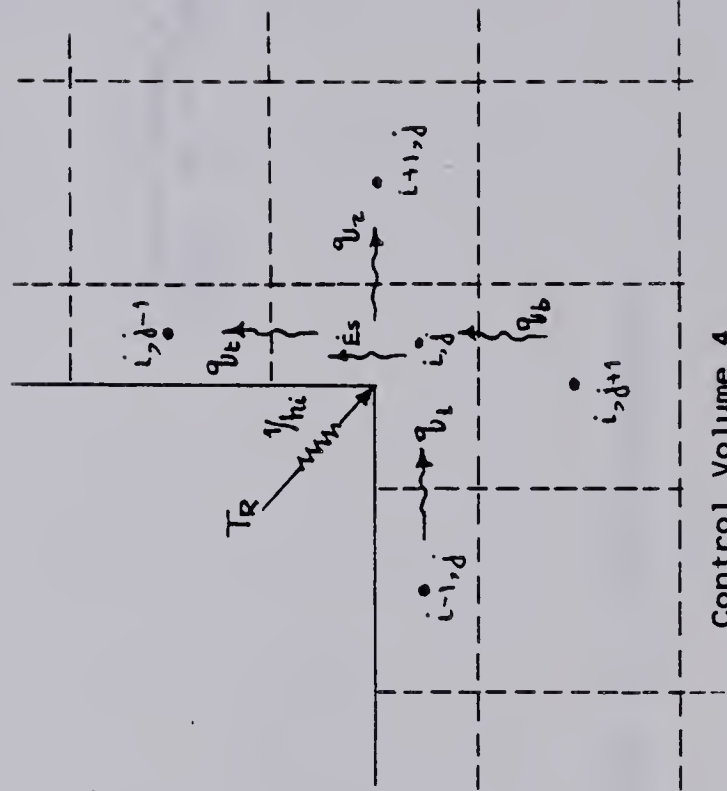




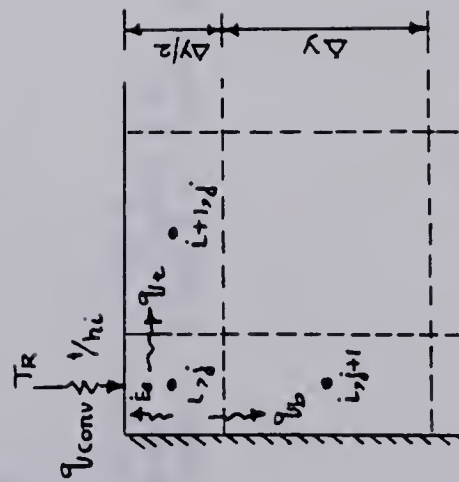
Control Volume 2  
Nodes - B and D of Figure 4.6  
Nodes - B,D,H and J of Figure 4.7



Control Volume 1  
Node - F of Figures 4.6 and 4.7



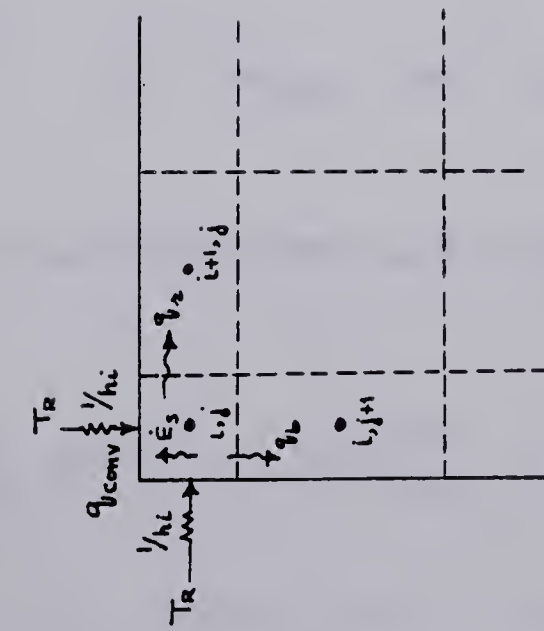
Control Volume 4  
Node - C of Figure 4.6  
Nodes - C and I of Figure 4.7



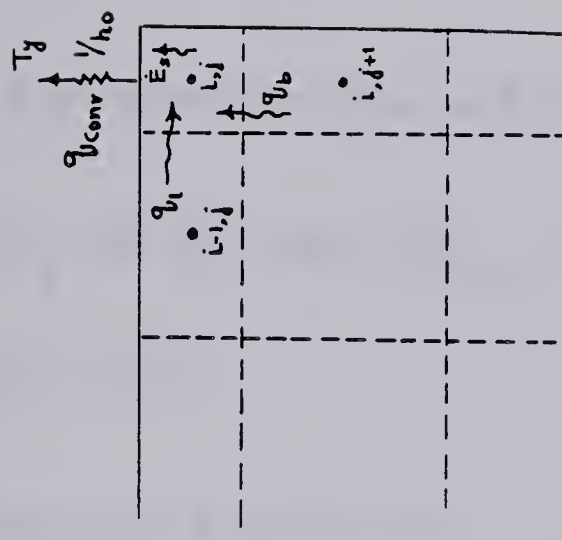
Control Volume 3  
Node - A of Figure 4.6  
Nodes - A and K of Figure 4.7

Figure 4.9 Control volumes at the boundaries





Control Volume 5  
Node - E of Figure 4.6  
Nodes - E and G of Figure 4.7



Control Volume 6  
Node - G' of Figure 4.6

Figure 4.10 Control volume at the boundaries



Control Volume 2 of Figure 4.9

$$E_s = q_{\text{conv}} + q_{\ell} - q_r - q_b \quad (4.57)$$

Substituting for energy terms and rearranging:

$$T_{i,j}^{v+1} = [T_{i,j}^v + 2Bi_i \Delta Fo T_R^{v+1} + 2\Delta Fo (T_{i-1,j}^{v+1} + T_{i+1,j}^{v+1} + 2 T_{i,j+1}^{v+1})] / (1 + 2 Bi_i \Delta Fo + 4\Delta Fo) \quad (4.58)$$

Control Volume 4 of Figure 4.9

$$E_s = q_{\text{conv}} + q_{\ell} + q_b - q_t - q_r \quad (4.59)$$

Substituting for energy terms and rearranging:

$$T_{i,j}^{v+1} = [T_{i,j}^v + \frac{2}{3} Bi_i \Delta Fo T_R^{v+1} + \frac{2}{3} \Delta Fo (T_{i-1,j}^{v+1} + 2 T_{i,j+1}^{v+1} + 2 T_{i+1,j}^{v+1} + T_{i,j-1}^{v+1})] / (1 + \frac{2}{3} Bi_i \Delta Fo + 4\Delta Fo) \quad (4.60)$$

Control Volume 5 of Figure 4.10:

$$E_s = 2q_{\text{conv}} - q_b - q_r \quad (4.61)$$

Substituting for energy terms and rearranging:

$$T_{i,j}^{v+1} = [T_{i,j}^v + 2 Bi_i \Delta Fo T_R^{v+1} + 2 \Delta Fo (T_{i+1,j}^{v+1} + T_{i,j+1}^{v+1})] / (1 + 2 Bi_i \Delta Fo + 4\Delta Fo) \quad (4.62)$$



Control Volume 1 of Figure 4.9

$$E_s = q_b - q_{\text{conv}} + q_\ell - q_r \quad (4.63)$$

Substituting for energy terms and rearranging:

$$T_{i,j}^{v+1} = [T_{i,j}^v + 2\Delta Fo (T_{i,j+1}^{v+1} + \frac{1}{2} T_{i-1,j}^{v+1} + \frac{1}{2} T_{i+1,j}^{v+1}) + 2Bi_o \Delta Fo T_y^{v+1}] / (1 + 2Bi_i \Delta Fo + 4\Delta Fo) \quad (4.64)$$

Control Volume 6 of Figure 4.10

$$E_s = q_b + q_\ell - q_{\text{conv}} \quad (4.65)$$

Substituting for energy terms and rearranging:

$$T_{i,j}^{v+1} = [T_{i,j}^v + 2 Bi_o \Delta Fo T_y^{v+1} + 2\Delta Fo (T_{i,j+1}^{v+1} + T_{i-1,j}^{v+1})] / (1 + 2Bi_o \Delta Fo + 4\Delta Fo) \quad (4.66)$$

Nodes H,L of Figure 4.6 and L,P of Figure 4.7:

Far from the basement the heat flow is essentially one dimensional as it is at the line of symmetry. This boundary condition is generally known as adiabatic boundary condition.

$$\frac{dT}{dx} = 0 \quad (4.67)$$

$$T_{i,j}^{v+1} = T_{i-1,j}^{v+1}$$

Nodes I,J and K of Figure 4.6 and M,N,O of Figure 4.7:

The mean ground temperature recorded by environmental services or from other sources can be used as an imposed



boundary condition.

$$T_{i,j}^{v+1} = T_{\text{grnd}} \quad (4.68)$$

#### 4.3.3.3 Solution of Discretization Equations

There are a number of schemes for solving system of algebraic equations. An important criterion for faster convergence is to march along the direction of heat flow. Taking advantage of this concept, a L - shaped marching scheme was developed. The advantage of this method over the conventional methods will be discussed in Chapter 5.

#### 4.3.4 The Fourth Model

By applying the fourth guideline a one dimensional phase change model was formulated. To fix ideas, suppose that the heat losses through the basements can be modeled using a simple one dimensional system in which two phases exist. This is true of a ground thermal regime subjected to a freeze thaw situation. Therefore, these two phases can be identified as frozen and unfrozen states.

An essential feature of the problems with a change of phase is the existence of a moving surface of separation between the two phases. Heat is liberated or absorbed at this surface and the thermal properties of the two phases on different sides of it may be different. Following the approach of Gilpin and Wong [66] the problem was formulated as follows.



In the ground, freezing of the soil moisture will be assumed to occur at a discrete temperature  $T_f$ . The equations of heat conduction and energy conservation then give an expression for the time rate of change of enthalpy. The enthalpy  $h$  can be related to temperatures by the non-linear expressions:

$$\frac{\partial h}{\partial t} = k \frac{\partial^2 T}{\partial x^2} \quad (4.69)$$

$$k = k_{uf} \quad \text{for } T > T_f \quad (4.70)$$

$$k = k_f \quad \text{for } T < T_f \quad (4.71)$$

$$h = \rho C_f (T - T_f) ; T < T_f \quad (4.72)$$

$$h = \rho C_{uf} (T - T_f) + \rho L_s ; T > T_f \quad (4.73)$$

Where the enthalpy was defined as zero for the soil in its frozen state at  $T=T_f$ .

The boundary conditions can be written as :

The weather side boundary condition:

$$-k \frac{\partial T}{\partial x} = H_o (T - T_y) \quad (4.74)$$

The room side boundary condition:

$$-k \frac{\partial T}{\partial x} = H_R (T - T_R) \quad (4.75)$$



The Difference Formulation:

Using a straight forward Euler scheme for time stepping the solution ahead, Equation 4.69 in difference form becomes,

$$h_i^{v+1} = h_i^v + \frac{\Delta t}{\Delta x} [k(T_{i-1}^v - T_i^v) - k(T_i^v - T_{i+1}^v)] \quad (4.76)$$

Where,

$$\begin{aligned} k &= k_f ; T < T_f \\ k &= k_{uf} ; T > T_f \end{aligned} \quad (4.77)$$

Equations 4.72 and 4.73 can be used to calculate the values of T at the new time step. That is,

$$T_i^{v+1} = T_f + \frac{h^{v+1}}{\rho C_f} ; h < 0 \quad (4.78)$$

$$T_i^{v+1} = T_f ; 0 < h < \rho L_s \quad (4.79)$$

$$T_i^{v+1} = T_f + \frac{h^{v+1} - L_s}{\rho C_{uf}} ; h > \rho L_s \quad (4.80)$$

Similarly the boundary conditions can be written as,

The weather side boundary condition:

$$h_i^{v+1} = h_i^v + \left\{ k \left( \frac{T_{i-1}^v - T_i^v}{\Delta x} \right) - H_o (T_i^v - T_y^v) \right\} \left( \frac{2\Delta t}{\Delta x} \right) \quad (4.81)$$

The room side boundary condition can be written as,

$$h_i^{v+1} = h_i^v + \left\{ H_R (T_R^v - T_i^v) - k \left( \frac{T_i^v - T_{i+1}^v}{\Delta x} \right) \right\} \left( \frac{2\Delta t}{\Delta x} \right) \quad (4.82)$$



#### 4.4 Solar Gains

Calculation of solar gains from measured horizontal total insolation consisted of three steps:

1. Breaking the horizontal total into its direct and diffuse components.
2. Calculation of vertical components of these fluxes.
3. Calculating the transmitted fractions of these fluxes.

Using the predictive models proposed by Liu and Jordan [74], Hay [75] and Threlkeld [76], a solar gains model was developed [14]. A discussion on the comparisons between the predicted and the measured solar gains will be made in Chapter 5.

#### 4.5 Window Shutters

The overall resistance of the window shutter combination for the modules 3 and 4, calculated from simple steady state analysis gave a resistance value of RSI 2.30. However, it would be expected that the actual resistance provided by the shutters will be less due to air infiltration around the shutter seals. This is a major uncertainty which cannot be handled adequately by theoretical models. In order to try and determine the effective resistance provided by the shutters, several measurements were made on the window shutter of module 3. In Chapter 5 the results of the above measurements will be analyzed so that a simple window shutter model consistent



with the measurements can be included in the simulation model.

#### 4.6 Infiltration

The importance of developing improved techniques for air infiltration modeling in estimating the heating or cooling load calculations for buildings cannot be over emphasized. Even though the mechanism of infiltration is conceptually simple, the hydrodynamic nature of the problem is quite complex. Therefore, much of the research efforts these days are directed towards developing simple empirical models based on experimental observations.

The approach taken for modeling the air infiltration losses in the present model was to use the results of the experiments performed on the modules [56] to establish the typical air infiltration rates. A brief description of the above experiment and the results will be presented in Chapter 5.

#### 4.7 Transient Response

In simulation studies on heating load calculations the heat losses from the enclosure and its thermal capacity play an important role. Often the enclosure materials are nonhomogenous and therefore theoretical analysis of compounding the effects of different heat capacities of the enclosure are not quite accurate.



In this regard, Pratt and Ball's [77] analytical study on transient cooling of a heated enclosure is of interest. Assuming a distributed and a lumped heat capacity model and neglecting the heat capacity of room air, Pratt and Ball derived an analytical expression for the transient change in air temperature inside an enclosure following a step change in outside temperature.

For a perfectly sealed enclosure with no internal storage, the ratio of energy stored to rate of heat loss from the enclosure has been shown to control the inside temperature. This ratio is referred to as time constant of the enclosure. The simplified equation for the temperature distribution has the form:

$$\frac{\theta_i(o) - \theta_i(t)}{\theta_o} = 1 - \exp [-t/(W/q)] \quad (4.83)$$

Where  $\theta_i$ ,  $\theta_o$  are inside, outside temperatures

$t$  is the time

$W$  Energy stored

$q$  heat loss rate

Extending the analysis of Pratt and Ball, Warsi and Choudhury [78,79], developed weighting functions to study the transient response of a homogeneous and as well as a composite structure subjected to any arbitrary input function.

Experimental techniques to determine the approximate time constant of a house have been used by Janssen [80] and Besant et al. [52]. Using a first order model Janssen



formulated the following expression for time constant.

$$\tau = \frac{t}{\ln \frac{Q_f - UA (T_r - T_o)}{Q_f - UA (T - T_o)}} \quad (4.84)$$

Where,

$Q_f$  fan load (W)

$T_r$  reference temperature ( $^{\circ}\text{C}$ )

$T_o$  outside temperature ( $^{\circ}\text{C}$ )

$U$  overall heat transfer coefficient ( $\text{W/m}^2\text{-}^{\circ}\text{C}$ )

The above investigations neglect the heat capacity of room air. This assumption, often justified in heating load calculations, can become important as will be shown later, when comparing the predicted and the measured transient temperature decay curves.

To supplement the detailed simulation model used in this study, it is instructive to develop a very simplified version of a house thermal model to study its transient temperature decay characteristics. Consider a house model shown in Figure 4.11. By postulating that the thermal mass existing in a building can be classified into a lumped heat capacity and a distributed heat capacity, an energy balance equation describing the system at any instant of time can be written as:

$$Q_s + Q_a + Q_L + Q_{fan} - Q_{loss} = 0 \quad (4.85)$$

The rate equations describing the processes can be written



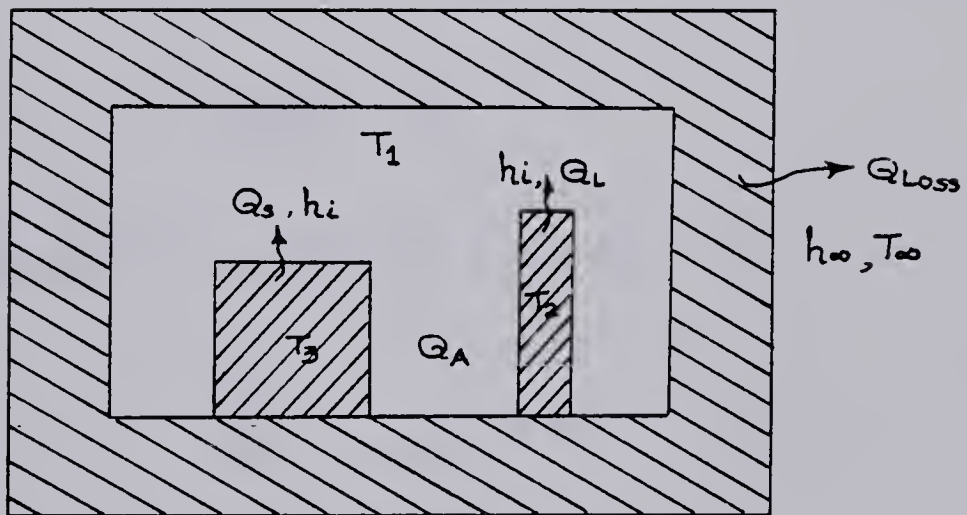


Figure 4.11 Simplified house model



as:

Lumped capacity:

$$(\rho CV)_2 \frac{dT_2}{dt} = - h_i A_2 (T_2 - T_i) \quad (4.86)$$

$$T_2 = T_i ; t = 0 \quad (4.87)$$

Distributed capacity:

$$(\rho CV)_3 \frac{\partial T_3}{\partial t} = k \left( \frac{\partial^2 T_3}{\partial x^2} \right) \quad (4.88)$$

$$T_3(x, 0) = T_i \quad (4.89)$$

$$- k A_3 \frac{dT_3}{dx} = h_i A_3 (T_3 - T_i) ; x = 0, t > 0 \quad (4.90)$$

$$\frac{dT_3}{dx} \bigg|_{x = L/2} = 0 \quad (4.91)$$

Air capacity:

$$-(\rho CV)_1 \frac{dT_1}{dt} = UA(T_1 - T_\infty) + h_i A_2 (T_1 - T_2) + h_i A_3 (T_1 - T_3) + Q_{fan} \quad (4.92)$$

Where,

$T_1$  air temperature

$T_2$  temperature of lumped capacity

$T_3$  temperature of distributed capacity

$T_\infty$  ambient temperature

Equation 4.92 can be solved for air temperature together with Equations 4.86 through 4.91. Note that solar gains or sol-air temperature effects have been omitted.



because the transient tests were conducted on the modules during night time.

A simple finite difference explicit numerical scheme was adopted for solving Equation 4.88. The details of which have been described in [14]. A straight forward Euler scheme was used for time stepping the solution of Equations 4.86 through 4.91. In the chapter to follow the results of this model will be compared with the measurements.

#### 4.8 The Energy Balance

The energy balance equation is the statement of the first law of thermodynamics. A method of formulating the energy balance equation for a house model is to combine the heat losses and heat gains with the storage heat.

Employing the above method, the energy balance equation describing the heat exchange between the building and its surroundings was written. Alternatively this step represents the process of integrating the component models to form an overall model. Using numerical techniques the overall energy balance equation was solved. Since these details have been adequately described in the authors' previous work [14], they have been omitted here. However, during the process of integrating the basement model with the main model a very important concept was introduced which led to a considerable simplification in that the overall character of the energy balance equation or its solution procedure described in the



above reference remained unaltered. This concept can be best illustrated by drawing certain analogies.

During the formulation of the basement models it was postulated that the basement heat losses could be divided into two components. One with a diurnal variation and one with an annual variation. This concept is very similar to the idea of uncoupling the equations. That is the dynamics of the diurnal variations were uncoupled from the dynamics of the annual variations. However, such a uncoupling has to satisfy the energy conservation principle.

To fix ideas consider two independent systems A and D. Let the dynamics of both the systems be known or can be modeled independently. Further suppose that the dynamics of the system D are influenced on a short time scale and that of the system A are influenced only on a large time scale. Now it is desired to study the dynamics of the system D under the influence of the system A. The problem of coupling may appear complex, however a little consideration suggests that as far as the dynamics of system D are concerned, the influence of system A is similar to bringing in contact a constant energy reservoir (such as system A) with the system D.

The correspondence between the house model and the above example can now be explored. The system D referred to above can be thought of as the dynamics of the diurnal fluctuations taking place in the house. The system A can thought of as the annual variations in the basement heat



losses calculated independently but introduced into the overall dynamics of the house in much the same way as bringing in contact a cold reservoir with the house.

The advantage as far as the simplicity of this method is concerned is that the overall basement heat loss problem was divided into two simpler problems and the solutions of the individual problems were superposed to obtain the solution to the overall energy balance equation. It is to be noted here that the models available in the literature employ the routine solution techniques for the energy analysis of houses. It is believed that application of the above concepts can lead to significant simplifications. In the chapters to follow these ideas which were incorporated into the main simulation model will be tested for the accuracy of the predictions.



## 5. VERIFICATION OF COMPONENT MODELS

### 5.1 Introduction

The validity of the component simulation models developed in chapter 4 will now be tested. The results will be analyzed from two aspects: Firstly, a comparison of the predictions and the measurements will be made, secondly, several methods of analyzing the data will be explored which will aid in better understanding of house heat losses and gains.

The organization of this chapter is identical to Chapter 4 in that the component models follow essentially the same order.

5.2 Walls and Ceilings

5.3 Basements

5.4 Solar Gains

5.5 Window Shutters

5.6 Infiltration

5.7 Transient Response

5.8 Conclusions

### 5.2 Walls and Ceilings

The insitu performance of wood frame walls and ceilings is difficult to measure. Yet the most important parameter needed to be accurately known in heating load calculations is the heat loss coefficient of these elements. For this



reason measurements of wall heat fluxes through the North end of the walls and ceilings were made. Heat flux gauges were installed at two locations on the North wall and at one location on the ceiling in each of the six modules. The location of heat flux gauges are shown in Figures 3.3. Data collected over the 1980-1982 heating seasons will now be analyzed and compared using the two proposed models: the steady state model and the transient model.

Before attempting to develop correlations from the wall heat flux data, it is appropriate to perform certain accuracy checks on the large amount of data collected over these two heating seasons. The accuracy test was performed by calculating the relative error between the measured and the calculated heat loss coefficient using steady state methods. Figure 5.1 illustrates the distribution of relative error between the measured and the calculated heat loss coefficients. It can be seen that for the most of the data (greater than 75%) the relative error is less than 5%.

A second check on the data can be performed to see if the heat flux data measured on a single wall at two locations is consistent. Such a test will also give some indication of the non uniformity in the thermal resistance offered by the same wall at two different locations. Consider for example heat flux gauges 1 and 23 installed on the North wall of the module 1. Figure 5.2 shows that for the most of the data (greater than 80%) the difference in the measured heat fluxes is less than 1.5 W/sq.m. The above



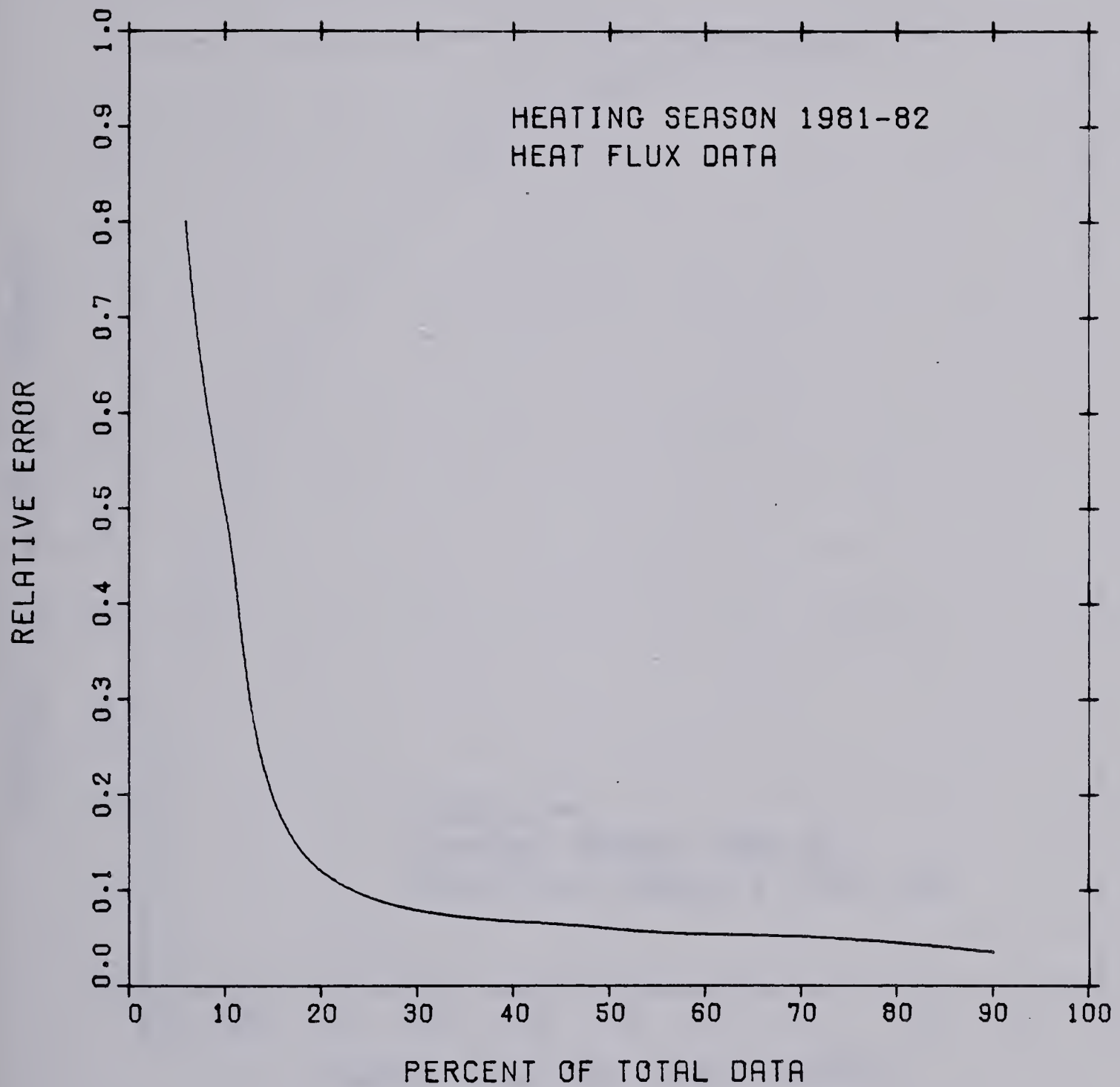


Figure 5.1 Distribution of relative error between the measured and the calculated heat loss coefficients



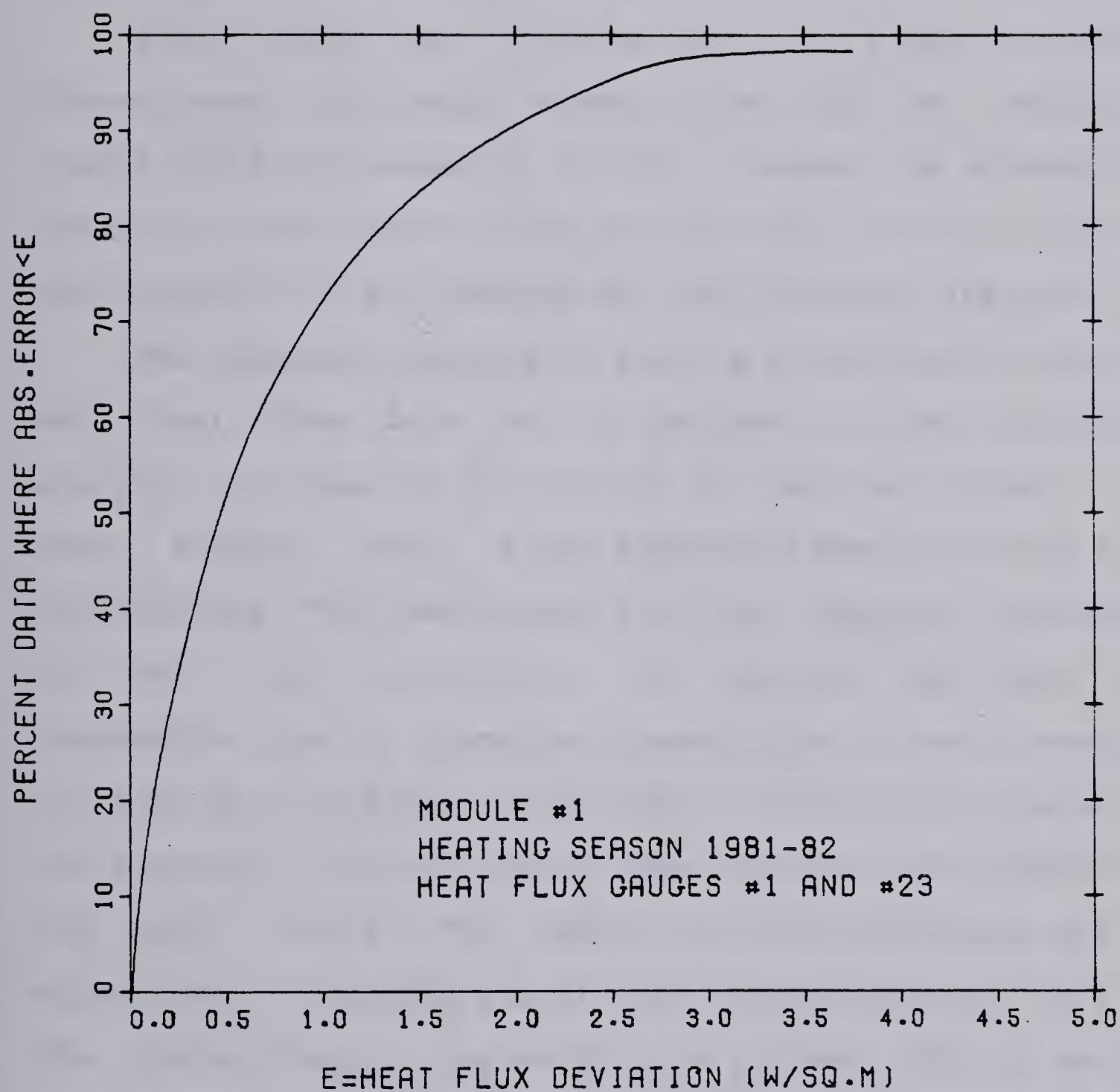


Figure 5.2 Distribution of the difference in the magnitude of heat flux measured at two locations on the same wall



results give some indication of the degree of certainty with which the present heat flux data can be analyzed.

### 5.2.1 The Steady State Model

Since walls and ceilings have only a small amount of thermal mass, to a large extent they can be treated as simple resistive elements. It will, however, be assumed that there is a contribution from the dry wall to the effective heat capacity of the modules for the transient analysis.

The simplest approach to finding a correlation from the wall heat flux data is to perform a linear regression analysis. An equation of the form  $Y = Ax + B$  was fitted to the data. Normally this is the approach taken in steady state calculations. The coefficient A in the equation represents the heat loss coefficient. To compress the data to a manageable form for graphical presentation it was necessary to take daily averages. Note that a guide line in selecting the averaging interval has to come from the time constant of the walls itself. The choice of daily averaging has the advantages of reducing the diurnal fluctuations as well as the thermal lags of the walls to a minimum. This is because of the fact that the time constant of the frame walls in most cases is less than two hours. With these considerations the daily average heat flux is plotted against temperature difference in Figures 5.3 through 5.6 for a few typical cases. A complete summary of the measured and the calculated heat loss coefficients is given in Table 5.1. The heat loss



Table 5.1 Summary of the calculated and measured resistance values for the modules

Wall RSI		Ceiling RSI		Remarks
Module	Steady State Calculated+	Measured	Steady State Calculated	
1	1.84	1.74	2.27	* * not measured
2	1.58	1.43	2.16	2.29
3	7.52	8.33	14.52	** Large scatter in data. Regression not attempted
4	3.75	3.60	7.55	**
5	1.84	2.10	2.16	1.93
6	1.84	1.85	5.77	**

+ ASHRAE Method



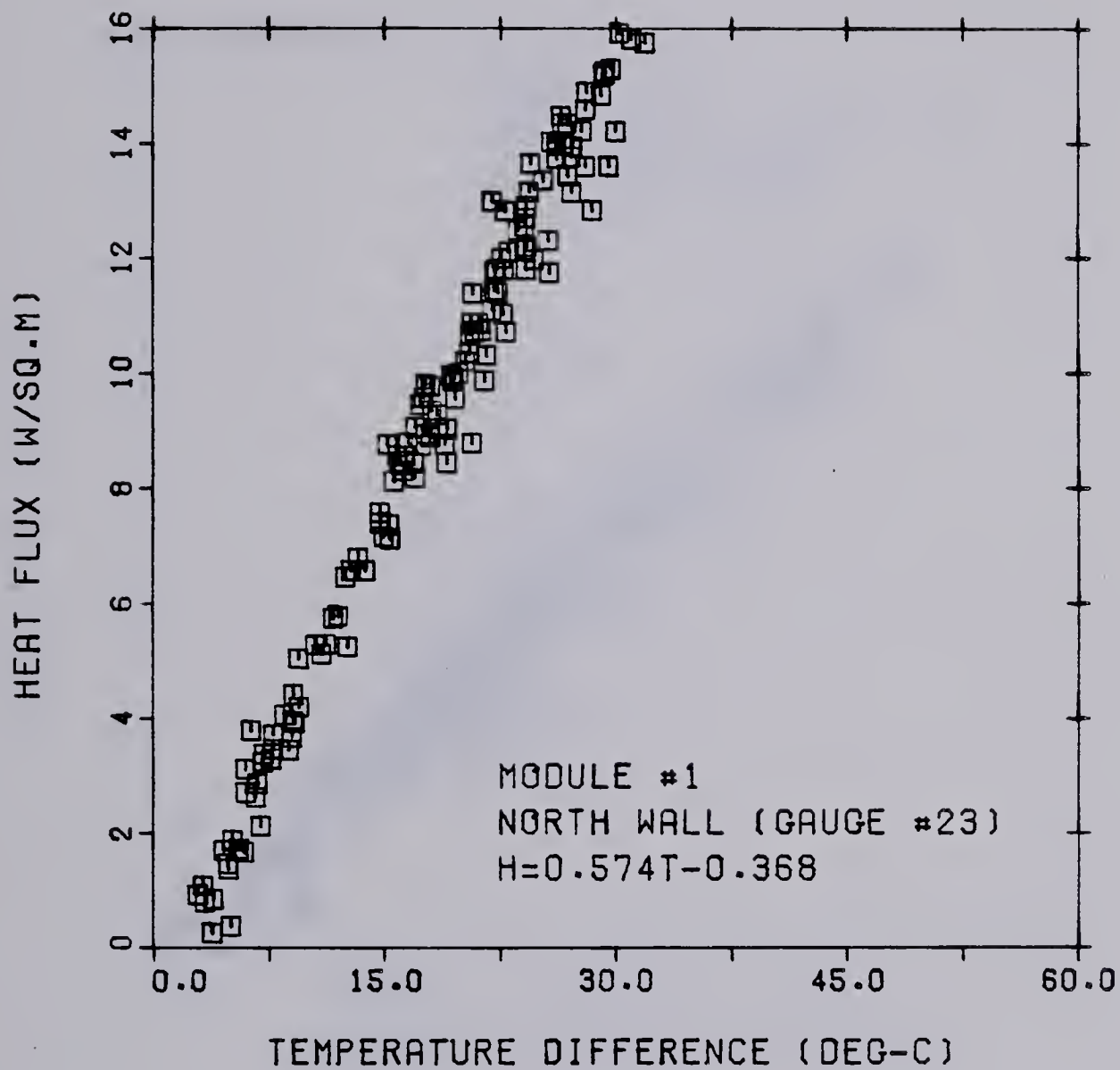


Figure 5.3 Variation of wall heat flux with temperature difference for module 1



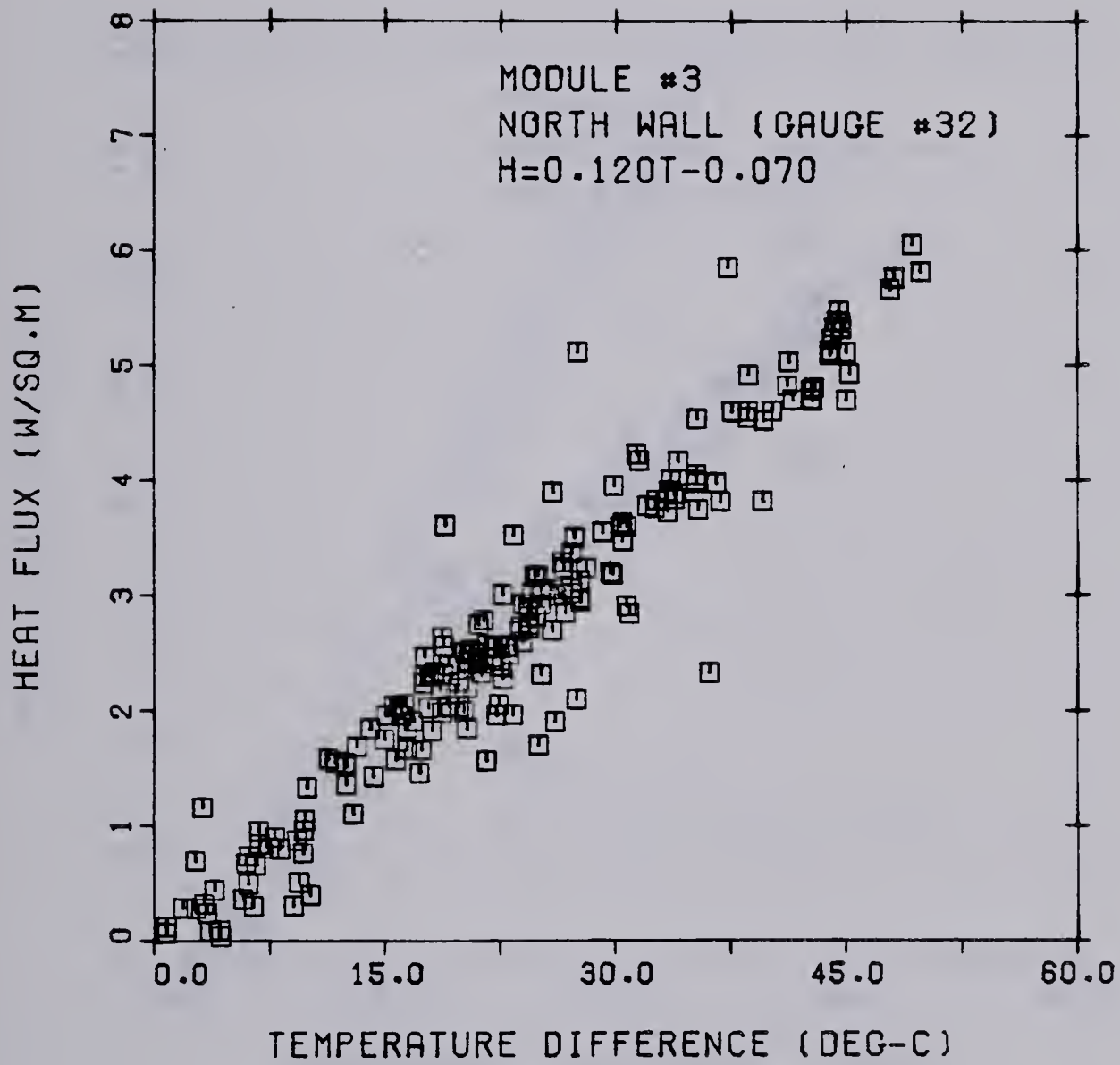


Figure 5.4 Variation of wall heat flux with temperature difference for module 3



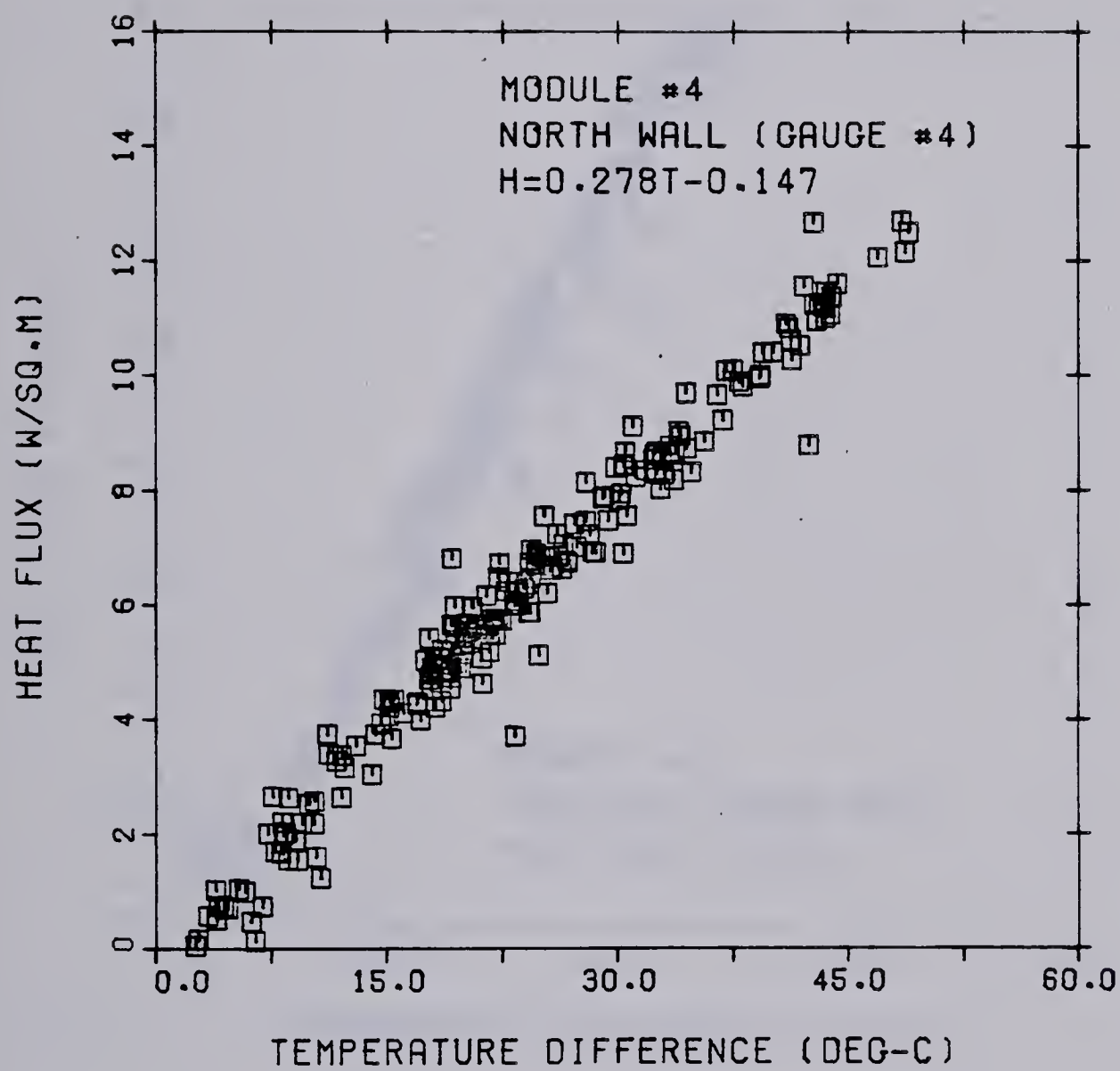


Figure 5.5 Variation of wall heat flux with temperature difference for module 4



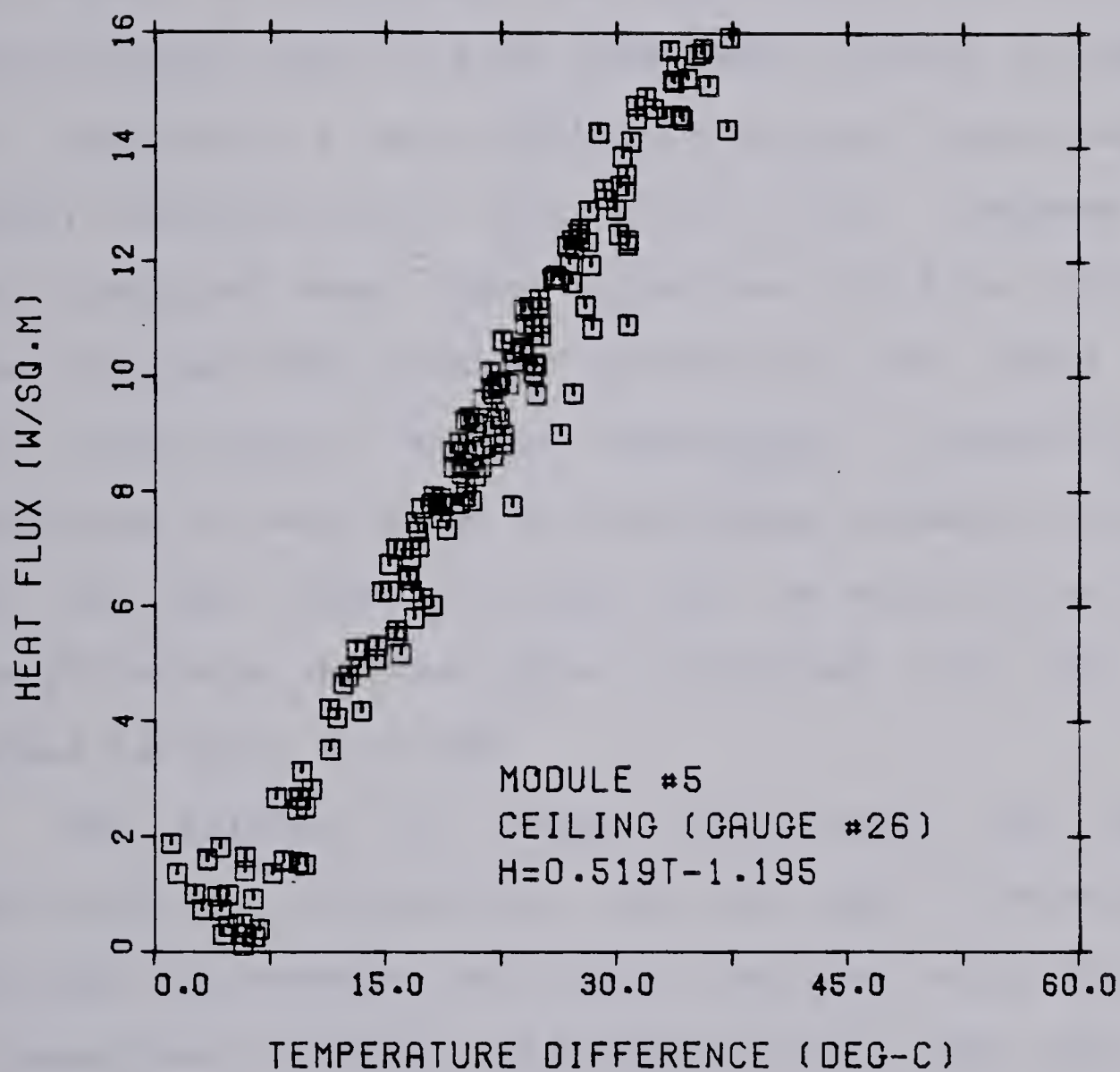


Figure 5.6 Variation of ceiling heat flux with temperature difference for module 5



coefficients of these elements were calculated using the steady state model and the thermal property data given in the ASHRAE Hand Book of Fundamentals [55].

First thing to note from these figures is that daily averaging of the heat flux data can be advantageously used to obtain a reasonably accurate measure of the heat loss coefficients. Also to note from these figures is that there is relatively a large variation in heat fluxes measured on highly insulated walls (Figure 5.4) than compared to the less insulated ones. These variations could be attributed to the increased time constant effects of the walls together with experimental errors associated in measuring the low magnitude of heat losses through these elements. However, as can be seen from the table, for the majority of the cases the difference between the calculated and the measured values is about 5 to 6%.

The effects of thermal capacitance can be partly decreased by considering only the night time heat losses. Consider for example the highly insulated walls of module 3. A comparison of Figures 5.4 and 5.7 shows that the variation in heat losses is reduced. This therefore, suggests that night time heat loss alone could be used as an approximate direct measure of steady state heat loss.



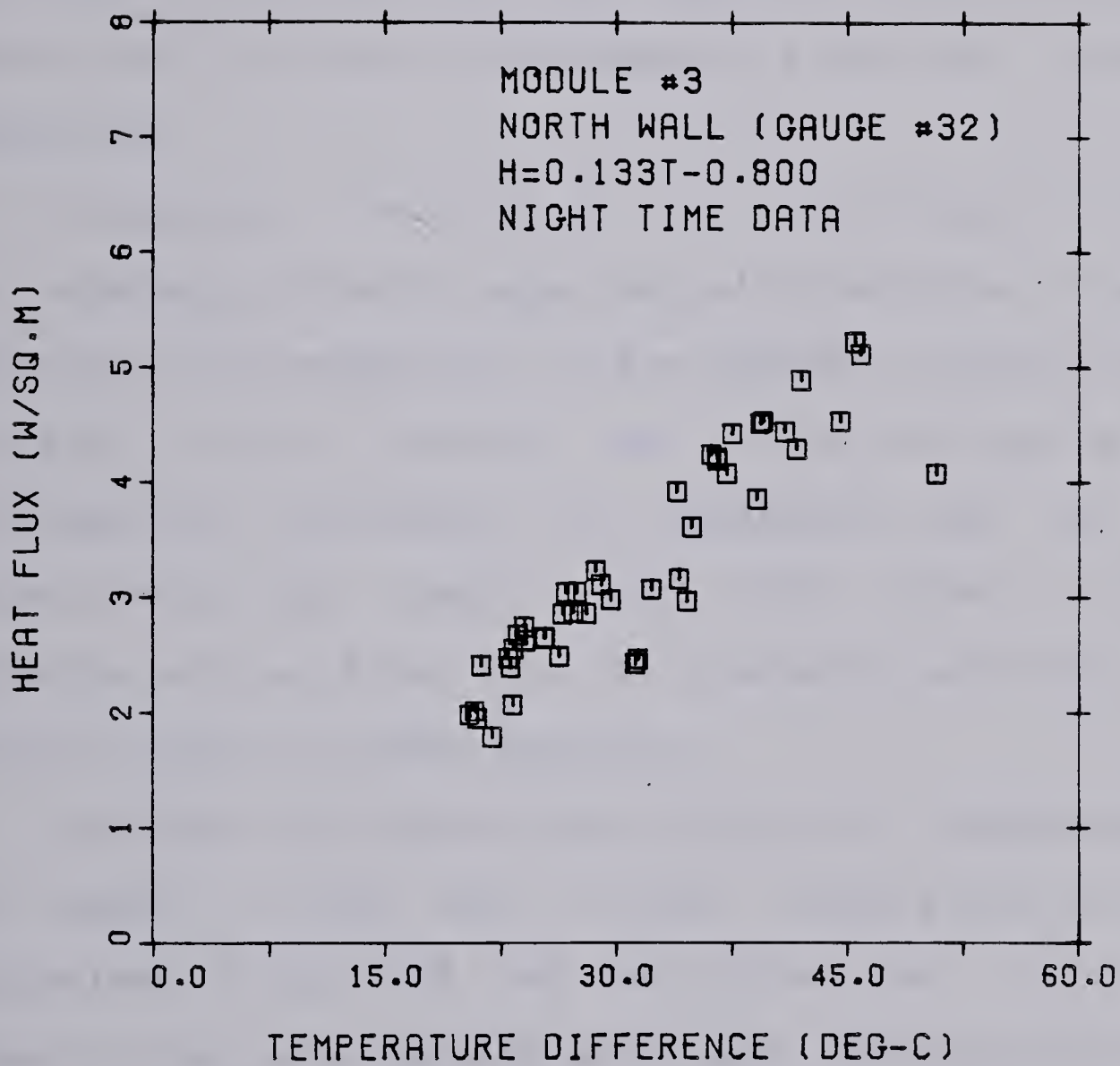


Figure 5.7 Night time heat loss with temperature difference for module 3



### 5.2.2 The Transient Model:

Determination of dynamic thermal performance of wood frame walls from insitu measurements has been recently investigated by Brown and Schuyler [81], Sherman, Sonderegger and Adams [82] and Roberts and Reinke [83]. In all these investigations, the important characteristic which determines the dynamic performance is the time constant of the walls.

Frequently, knowledge of the time constant of the walls is necessary to avoid experimental errors due to capacitive effects or for comparison of the transient behaviors of two different walls. Broadly what is required may be a simple arithmetical calculation to determine the time lag in establishing the steady state. With this in view, some guidance will be drawn from the available solutions of the classical heat transfer problems.

Consider for example the solution of homogeneous slab of length  $\ell$  with zero initial temperature and with  $x=0$  maintained at zero and  $x=\ell$  maintained at  $V$  for time  $t$  greater than zero. Carslaw and Jaeger [23] give the solution of this problem for the quantities of heat which cross a unit area of the faces  $x=0$  and  $x=\ell$  respectively up to time  $t$  as:

$$Q_0 = \frac{KV}{\ell} \left( t + \frac{\ell^2}{3\alpha} \right) - \frac{2KV\ell}{\alpha\pi^2} \sum_{n=1}^{\infty} \frac{1}{n^2} \exp \left( -\alpha n^2 \pi^2 t / \ell^2 \right) \quad (5.1)$$

$$Q_\ell = \frac{KV}{\ell} \left( t - \frac{\ell^2}{6\alpha} \right) - \frac{2KV\ell}{\alpha\pi^2} \sum_{n=1}^{\infty} \frac{(-1)^n}{n^2} \exp \left( -\alpha n^2 \pi^2 t / \ell^2 \right) \quad (5.2)$$



It is at once clear from these equations that for larger values of time  $Q_0$  and  $Q_1$  are the values of steady state heat flow for times  $t-\tau_0$  and  $t-\tau_l$  Where,

$$\tau_0 = -l^2/3\alpha \quad (5.3)$$

$$\tau_l = l^2/6\alpha \quad (5.4)$$

These are the characteristic time lags in establishing the steady states.

Extending these ideas in much the same way, Jaeger [84] gave the solution to a composite wall consisting of  $n$  layers. The formulae derived for time lags of composite sections can be obtained from this reference.

From this view point, the first thing that remains to be seen is the ability of the transient model developed in this section in predicting the transient behavior of the composite walls. To illustrate, Figure 5.8 shows the time required in establishing steady state for two different walls. It can be seen that the above grade basement walls have a time lag of approximately three hours. This is the order of magnitude predicted by Equation 5.4. Note also that the time lag of the frame walls is about an hour. This is an additional verification for considering the frame walls as simple resistive elements, while introducing their small time lags via a lumped capacity model for the transient analysis of the modules.



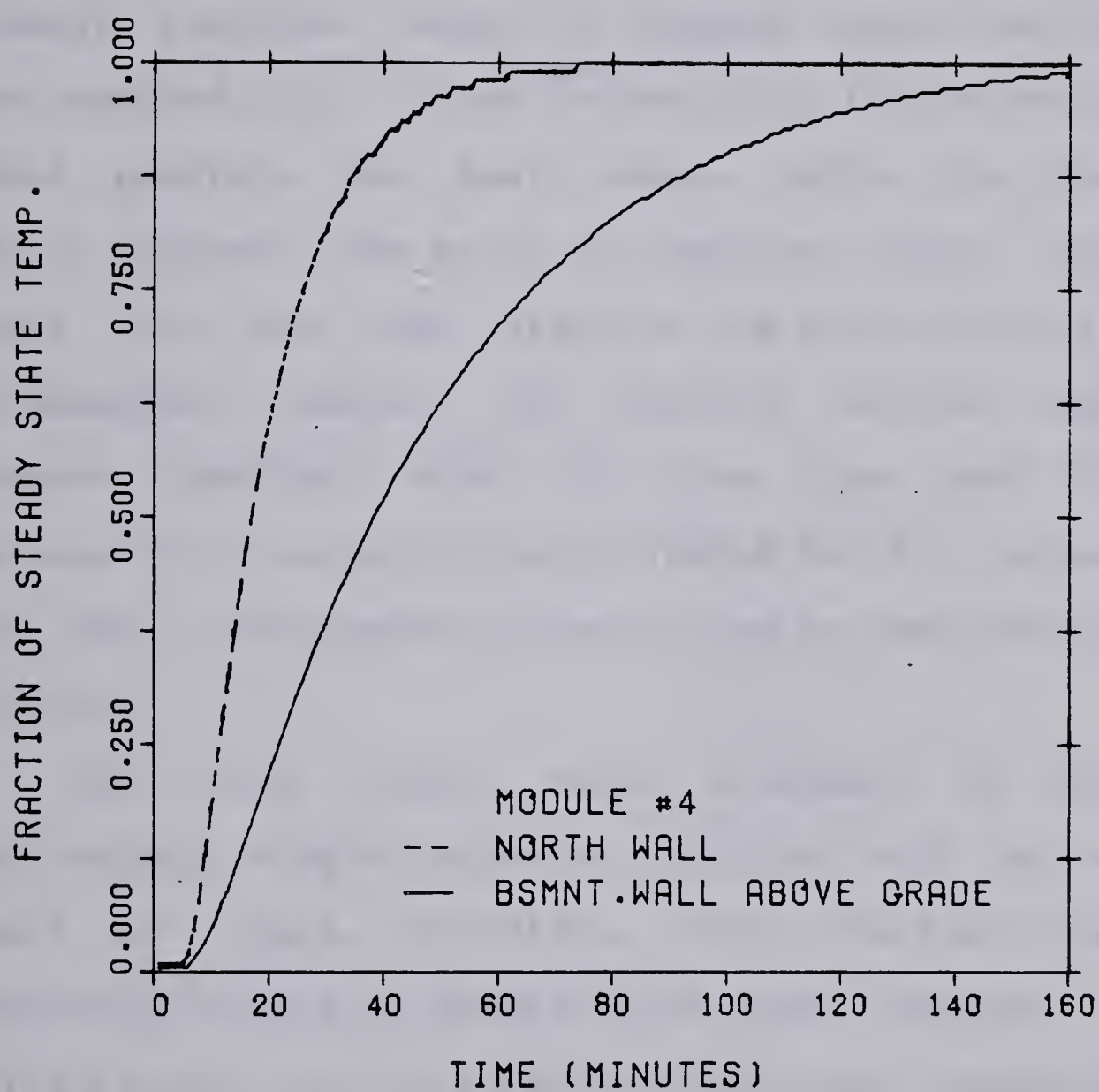


Figure 5.8 Time response of the walls in module 4



Even though the magnitude of the time constant of wood frame walls is small, they do introduce thermal time lags. These effects can be studied by analyzing the diurnal variations in wall heat fluxes. Consider Figure 5.9, in which comparisons are made of the predictions from the present transient model, a response factor calculation and the measured data. It can be seen that the present transient model predicts the heat losses better than the response factor approach. The error in response factor calculations comes from the time steps of one hour which is generally recommended. However, the implicit scheme used in the present transient model is free from such limitations because it is unconditionally stable for all values of time and that convergence criterion can be specified for better accuracy.

The wood frame walls discussed so far form a particularly simple composite section with or without a small air space. Therefore, their transient analysis are relatively simple as demonstrated above. However, the same thing is not true for a ceiling-attic-roof combination.

Modeling of ceiling-attic-roof combination is only straight forward in so far as ceiling and or roof sections are concerned. However, the major uncertainty comes from lack of knowledge of infiltration rates of ventilated attics and the thermal stratification of attic air itself. Recently Wilkes [85] has made comparison of the results from several ventilated attic models. It appears that all the models are



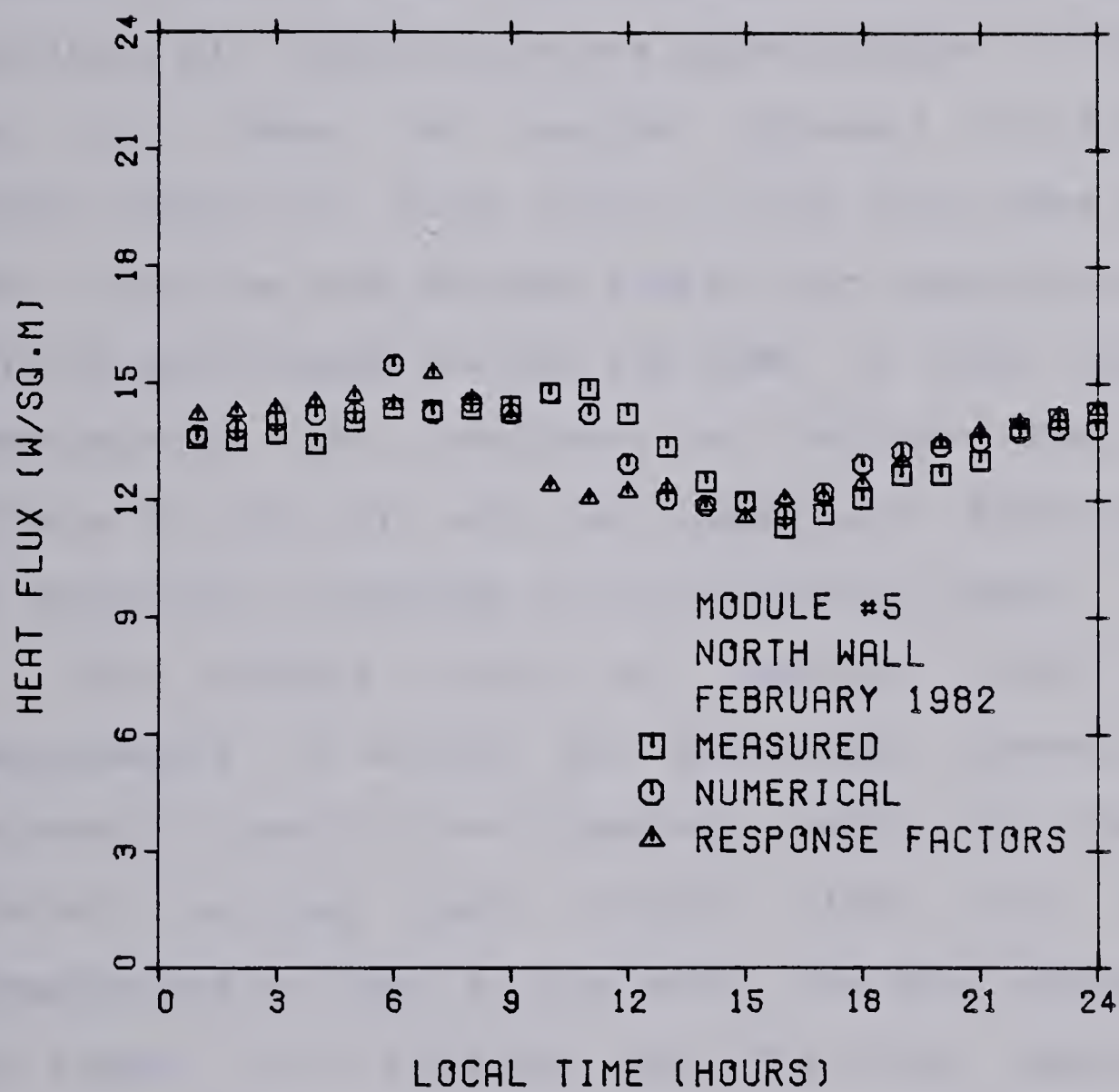


Figure 5.9 Comparison of diurnal variation of wall heat flux with the measured data



over predicting the ceiling heat losses.

In view of this complexity, it is necessary to draw some guidance from the experimental results so that a direction can be set in approaching the problem of modeling a ceiling-attic-roof combination. To illustrate, a typical diurnal ceiling heat flux together with the ambient, room and attic air temperatures are shown plotted in Figures 5.10 and 5.11. These two results represent the mid and late winter conditions. First thing to note from these figures is that the time lags between ambient air temperatures and the ceiling heat fluxes are not the same in both cases. This demonstrates the importance of variable heat capacity effects of attic air with the temperature difference. Also of importance is perhaps the infiltration rates.

This problem cannot be resolved until detailed measurements on attics are performed. However, it is of interest to see if the transient model can predict the diurnal ceiling heat fluxes given attic space air temperatures as input to the model. The good agreement shown in Figure 5.12 suggests that the heat capacity of the ceiling is correctly modeled.

Since data on attic temperatures is rarely available, it is not suggestive to use attic space air temperatures for predicting ceiling heat fluxes. Therefore it is worth while to explore approximate methods of modeling ceiling-attic-roof combination. Two such methods were investigated.



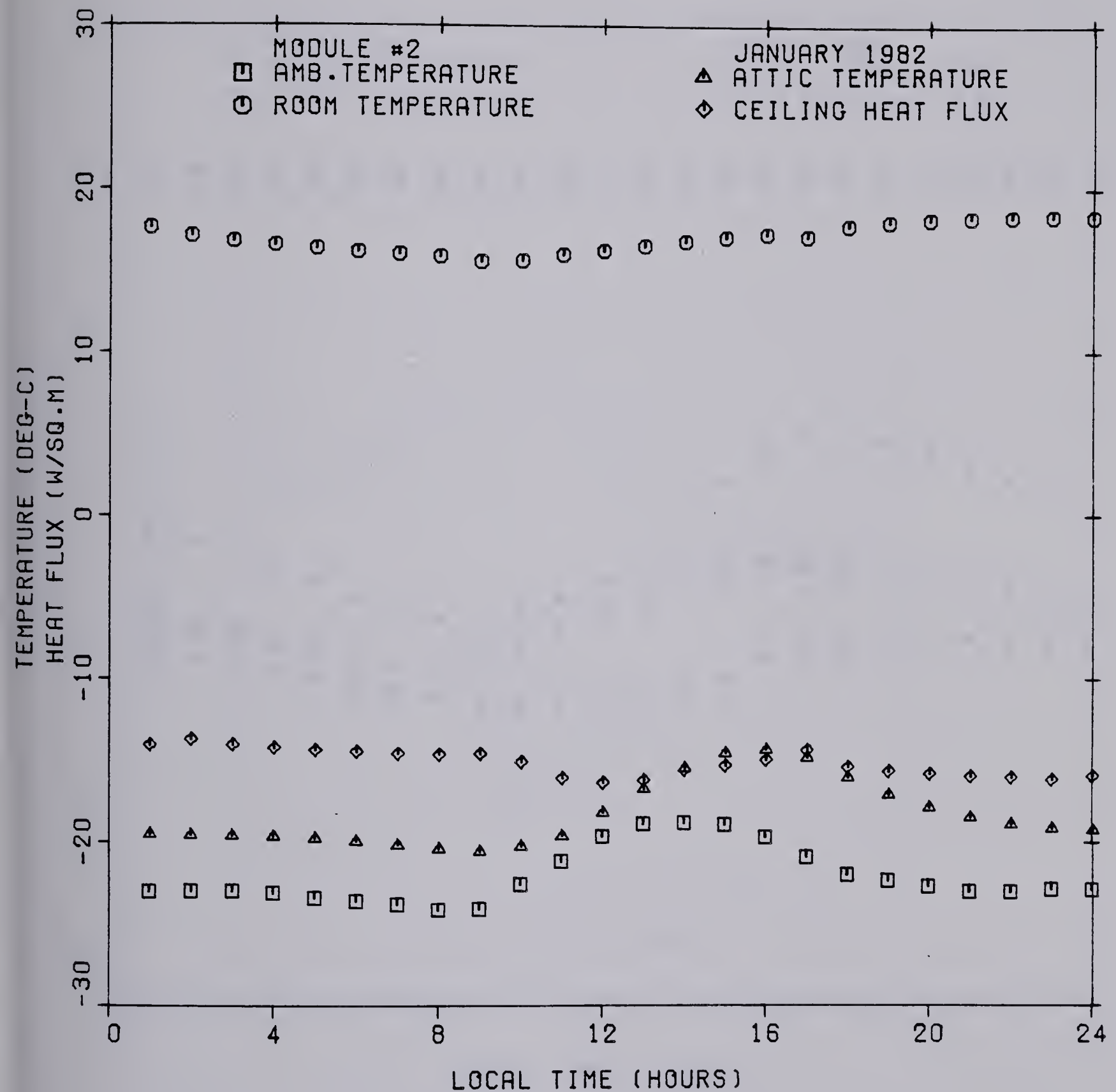


Figure 5.10 Typical diurnal variations of ambient, room, attic temperatures and ceiling heat flux for module 2 in January 1982



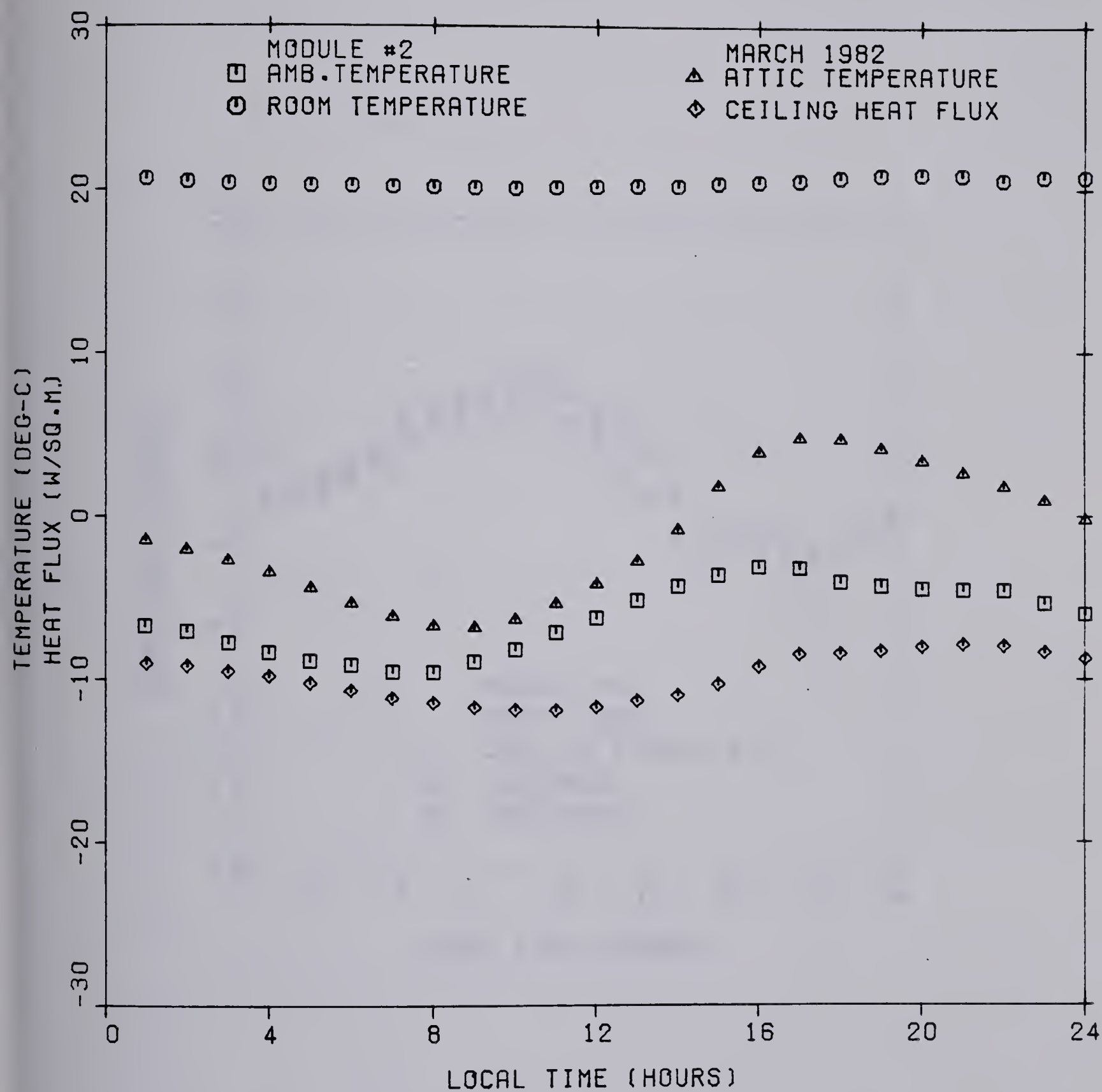


Figure 5.11 Typical diurnal variations of ambient, room, attic temperatures and ceiling heat flux for module 2 in March 1982



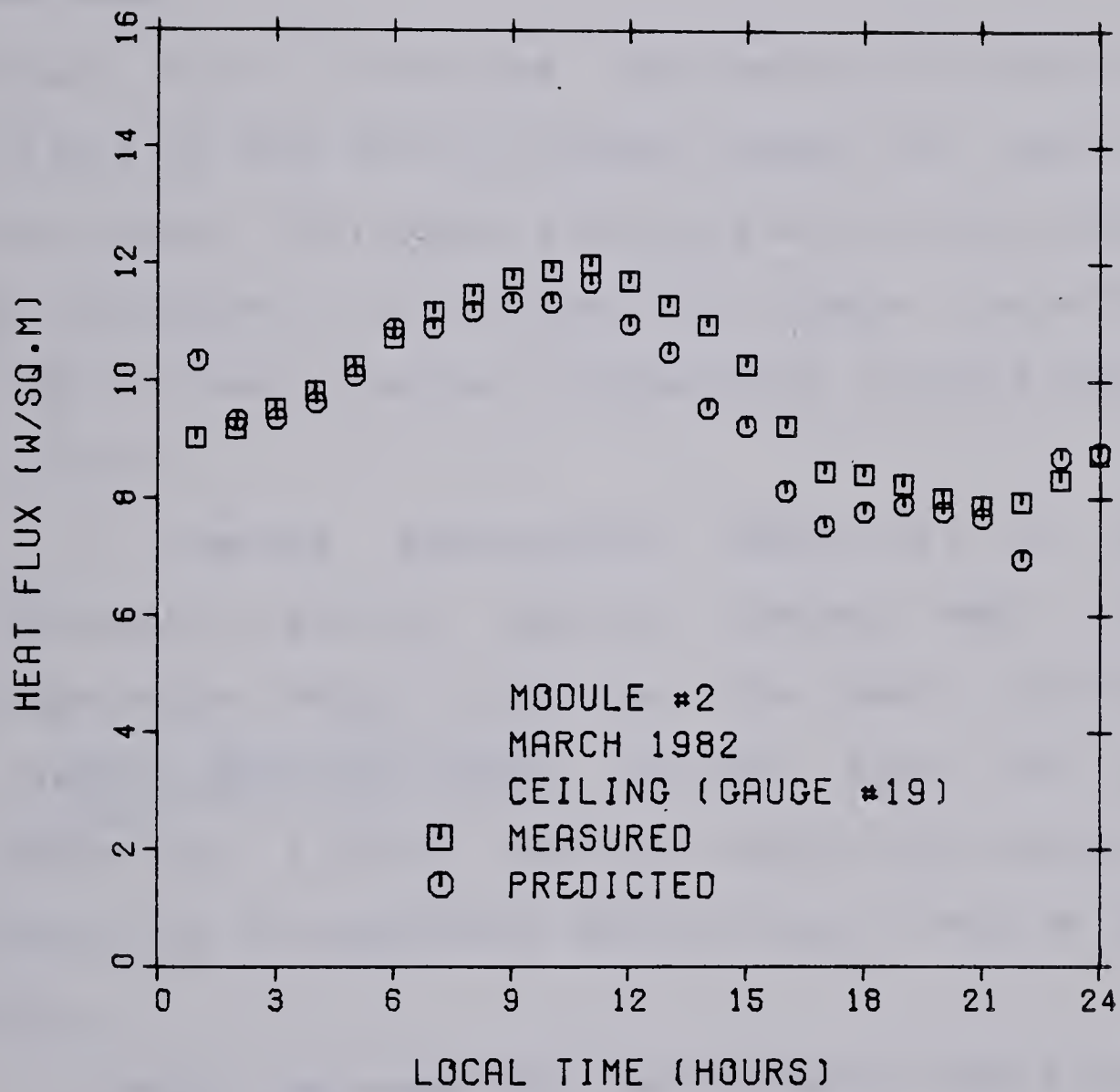


Figure 5.12 Comparison of the predicted and the measured ceiling heat flux for module 2



In the first method, a gross time constant of the ceiling-attic-roof combination was approximately estimated from the measured data and an equation of the form

$$Q = \frac{A}{R} (T_t - T_{\infty(t-\tau)}) \quad (5.5)$$

was used.

Figure 5.13 illustrates this method. The total RSI of the ceiling is very nearly constant except for some extraneous data points. Therefore, a ceiling-attic-roof combination can be considered in a gross way as a simple resistive element loosing heat to sol-air temperature,  $\tau$  hours lagging behind in time.

A second approximate method is to consider an equivalent ceiling section losing heat to sol-air temperature which will have the same variation in heat fluxes as does the actual ceiling. Since the theoretical models for a real ceiling section are rarely exact, the definition of equivalent section has to rely on the measured data.

Taking the measured time constants from Figure 5.10 an equivalent section was approximately simulated as shown in Figure 5.14. It can be seen that for winter conditions, this concept can be employed without a great sacrifice in the accuracy. However, with increasing outdoor temperatures, the heat capacity effects of attic air could become important.

To conclude this section, firstly it can be stated that the apparent differences in the measured and the nominal



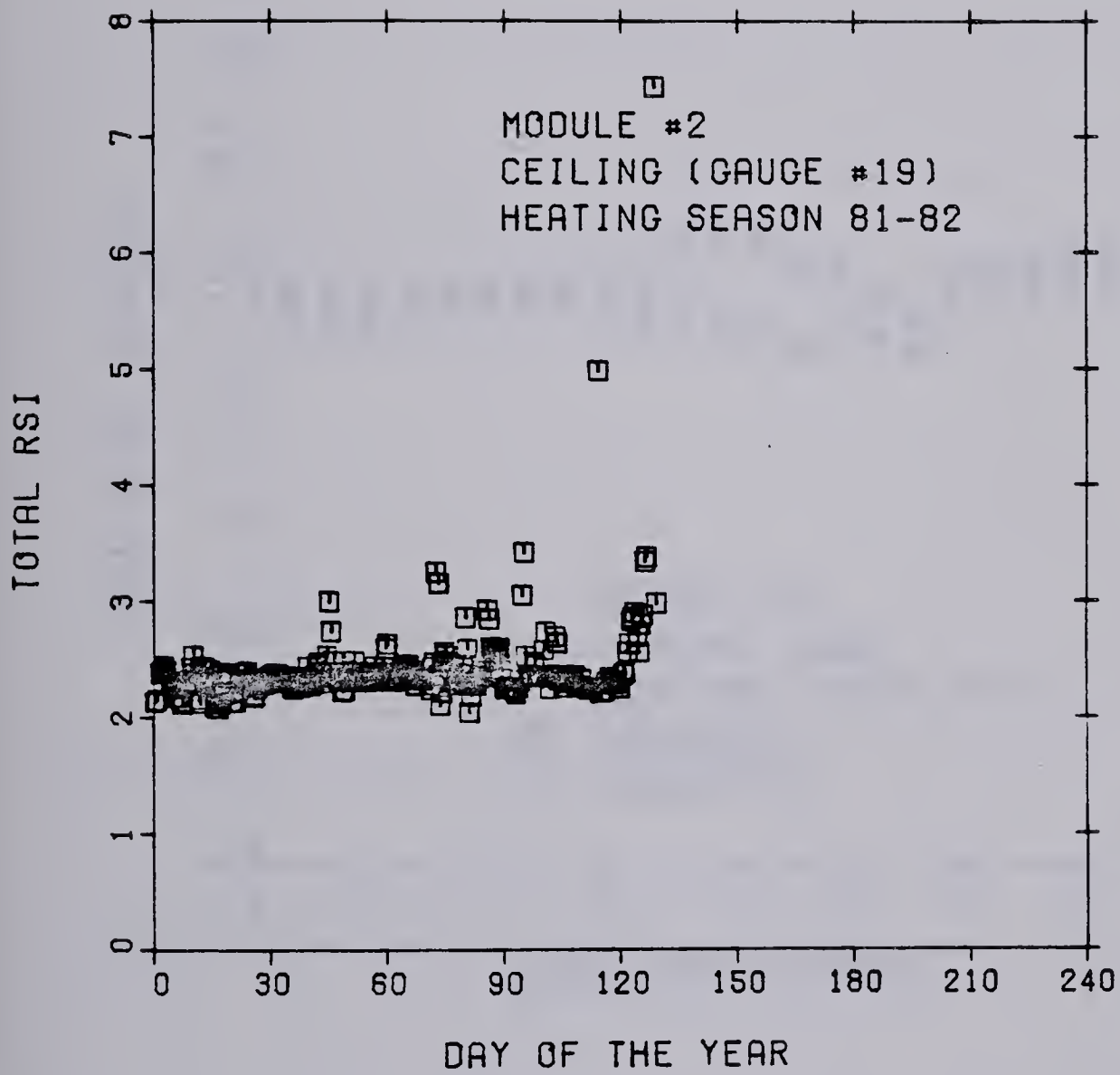


Figure 5.13 Ceiling resistance versus time of the year for module 2



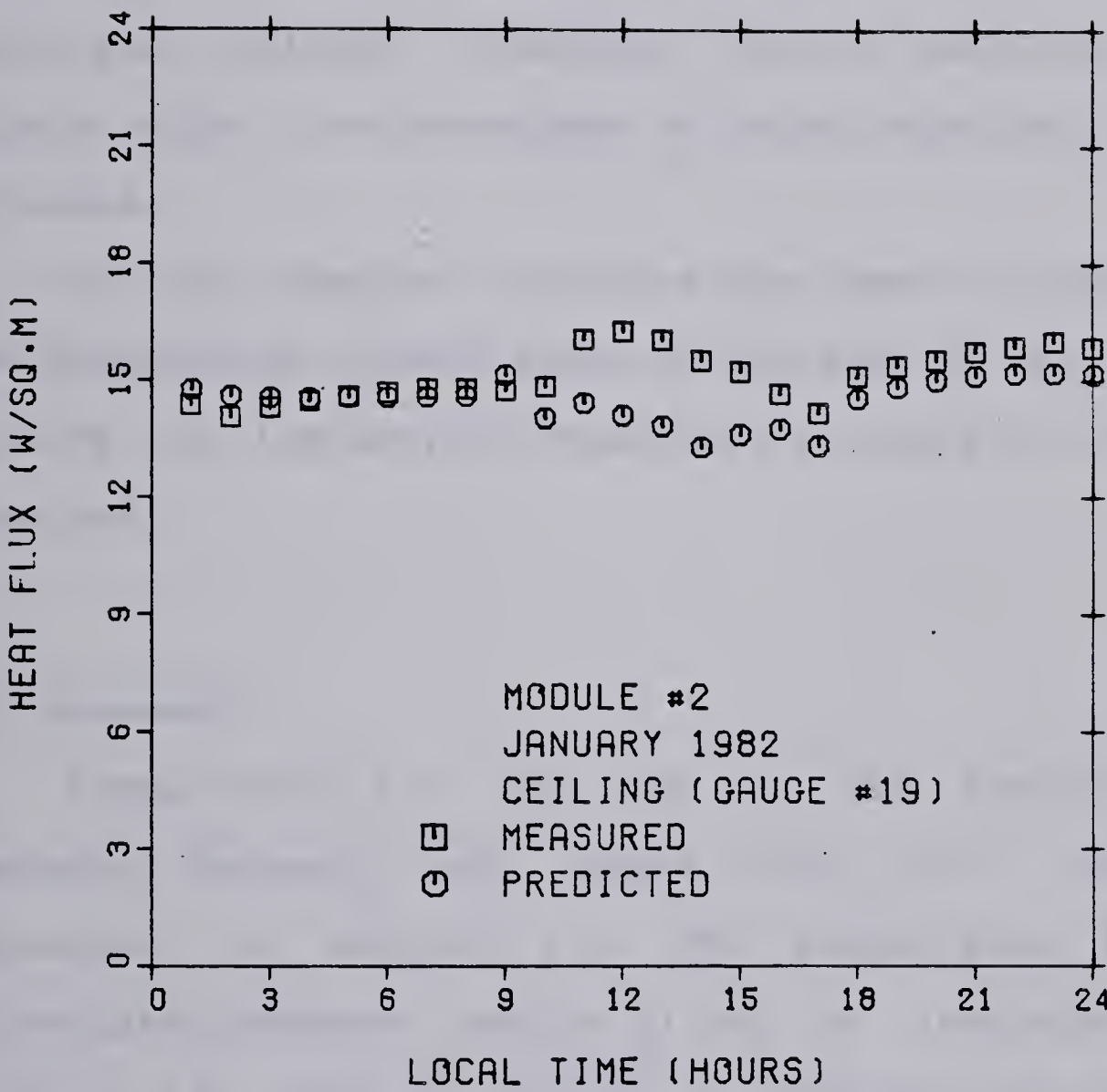


Figure 5.14 Comparison of the measured and the predicted ceiling heat flux for module 2



heat loss coefficients of the walls and ceilings sets limits on the accuracy of any practical calculations. Secondly, to a large extent walls and ceiling can be treated as simple resistive elements and their time lags can be accounted for in the transient analysis of the module via a lumped capacity approach. Finally, for more accurate modeling of walls and ceilings, transient finite numerical implicit models offer the advantages of being relatively simple and accurate.

In the chapter to follow the impact of the errors in the calculation of heat loss coefficients of the walls and ceiling on the overall house heat loss predictions will be examined.

### 5.3 Basements

Comparisons will be made of the predicted and the measured basement heat losses using the four models developed in section 4.3. The comparisons between an uninsulated basement (Module 2) and an insulated basement (Module 4), will be made to estimate the magnitude of heating load reductions obtained by insulating the basements. Heat flux data together with the ground temperatures measured near the uninsulated basement will be used to test the third model. This will be followed by a conclusion on the basement models.



### 5.3.1 The First Model

Five input parameters are required for this model: the sol-air temperature cycle, weather side film coefficient, the path lengths, properties of the layered mediums, the inside film coefficient, and the inside air temperature.

Sufficiently accurate results can be obtained by fitting a sinusoidal curve with a period of one year to the climatological data to obtain the annual temperature cycle. The steady state path lengths for the heat flux gauge locations shown in Figure 3.3 can be calculated using the method described in [59]. One of the major uncertainties in selecting any particular value for the soil conductivity is the soil moisture content. This parameter strongly effects both the conductivity and the heat capacity of the soil. The range of possible values for the soil conductivity are between  $0.8 \text{ W/m-K}$  for a dry soil with  $m$ , the mass of water per unit mass of the soil, equal to 10% to  $1.36 \text{ W/m-K}$  for a wet soil ( $m = 35\%$ ) [54]. It is to be expected that the soil moisture content and hence the soil conductivity will increase with increasing depth.

By varying the conductivity within the above range, the predicted annual basement heat losses together with one week average of the measured heat flux data for the year 1981 are plotted in Figures 5.15 and 5.16 for modules 2 and 4 respectively.

Barring a large scatter during mid July which appears to be the instrumentation problem, it can be seen from



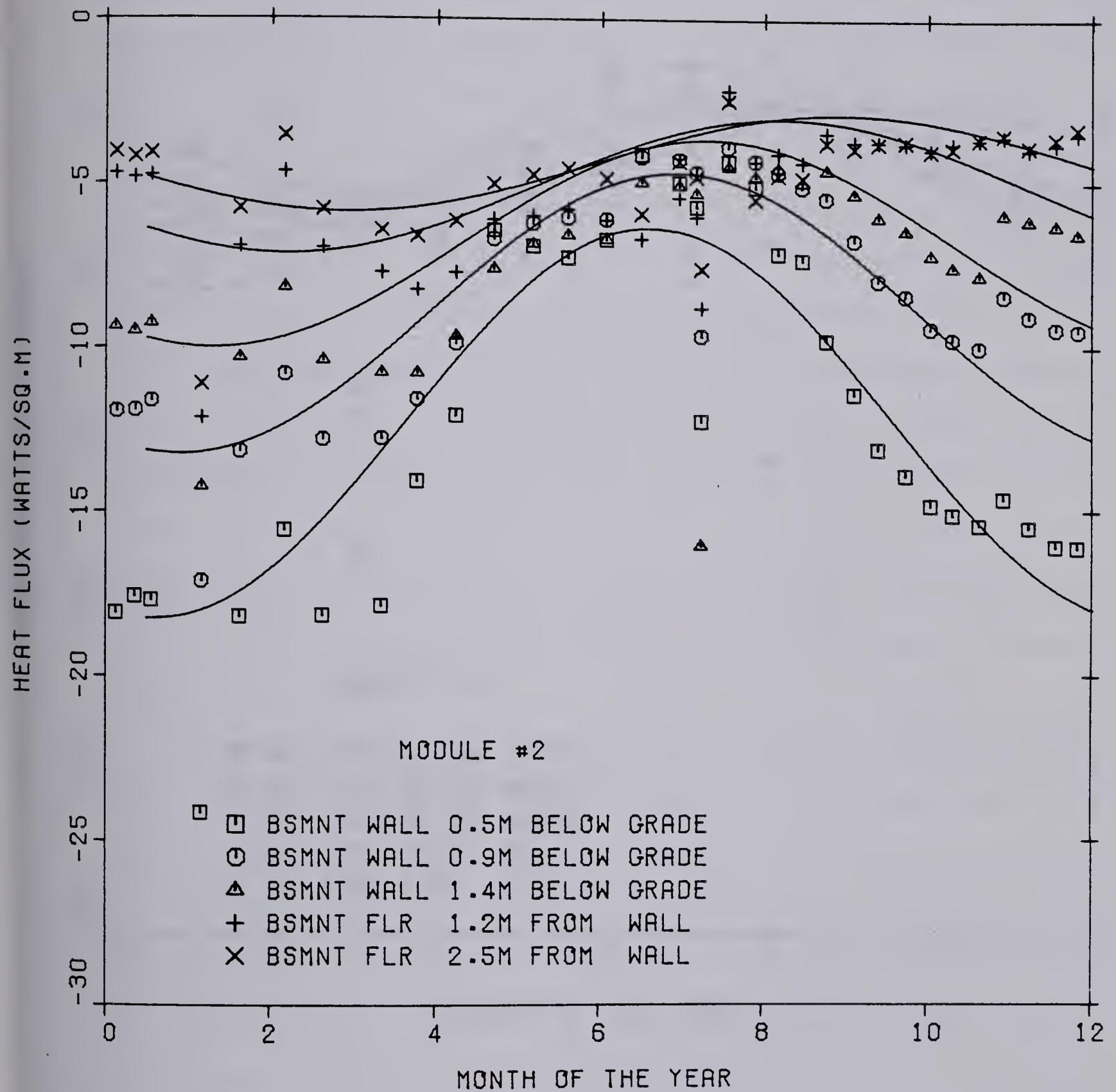


Figure 5.15 Basement heat fluxes for module 2

(solid lines are predictions)



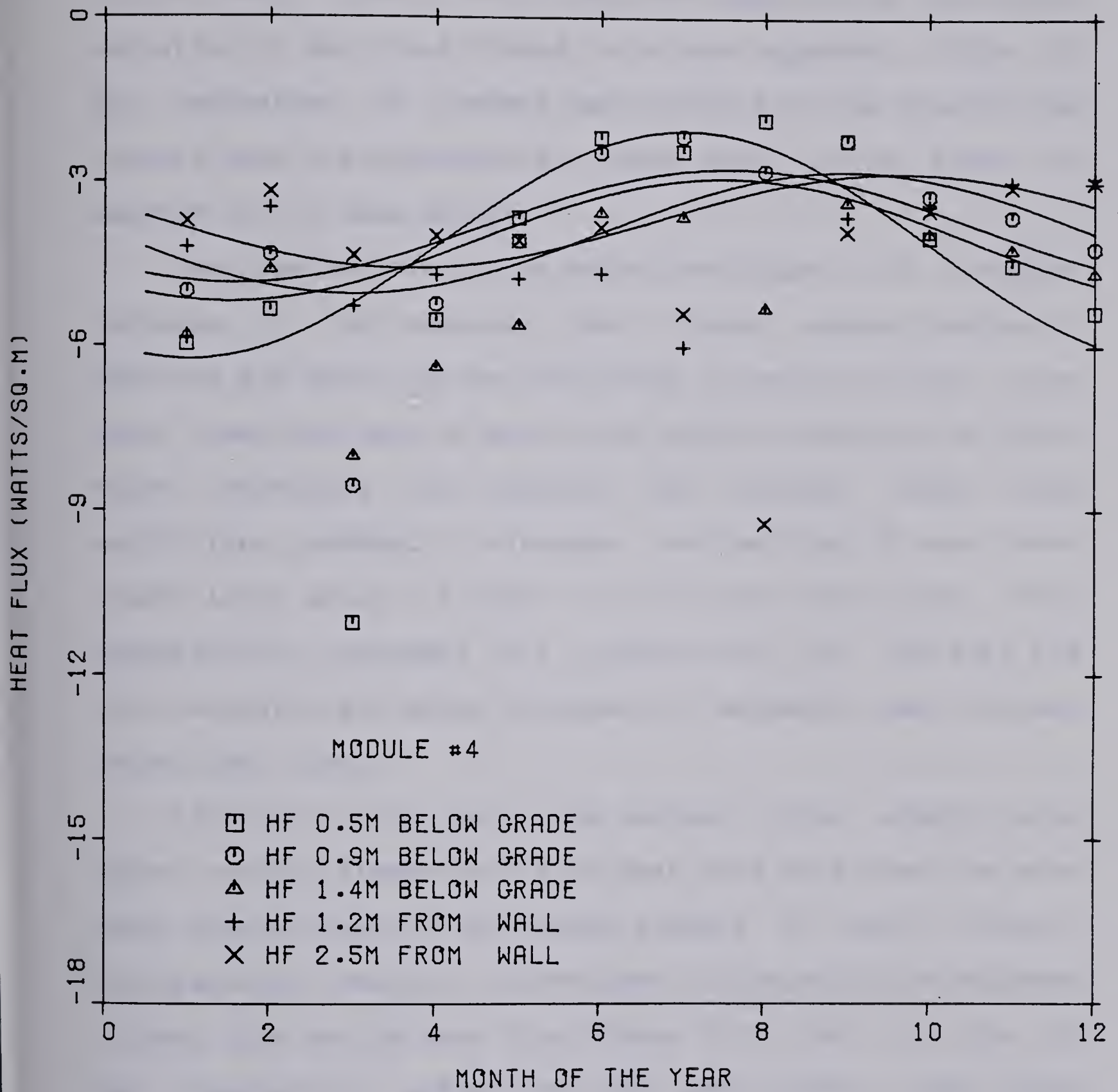


Figure 5.16 Basement heat fluxes for module 4  
(solid lines are predictions)



Figure 5.15 that the predicted and the measured heat fluxes follow very closely and that most importantly the annual variation in wall heat fluxes is at once apparent. This is the indication of thermal mass effects of the ground. The thermal mass also produces the phase shift in the times of maximum in the heat fluxes.

Few observations can be made from Figure 5.15. A sudden increase in the measured heat fluxes between months of February and March can be attributed to melting of the snow cover (recorded date of snow cover melting February 16, 1981) which introduces two changes: The weather side film coefficient suddenly increases, and melting of snow cover causes large amount of water to infiltrate the ground. This dramatically increases the conductivity of the soil and hence explains the sharp increase in basement heat losses during that time.

If this is true the ground surface cover should also cause another discontinuity in heat flux data when the snow cover starts covering the ground surface in early winter. Interestingly enough, in November a discontinuous decrease in heat flux can be seen from Figure 5.15. This is due to the insulating effect of the snow cover, the first appearance of which was recorded in November 1981 at the facility.

Admittedly, the first model based on constant property approximation cannot follow the measured heat flux point by point, but it does closely predict the annual trends caused



by sol-air temperature cycle.

The results for the insulated basement are plotted in Figure 5.16. Due to the large scatter in data only the monthly average values are shown in the figure. The scatter in the heat flux data appears to be due to the difficulties associated in measuring the low magnitudes of heat fluxes with these gauges. The heat fluxes are much lower and their variability through winter is much less. In fact a reasonable approximation would be to assume constant heat loss paths and the ground can be described in a very gross way by the average resistance to the heat flow it provides through these paths.

### 5.3.2 The Second Model

As noted before, advantage will be taken of the flexibility offered by numerical technique adopted in the second model. The monthly average outside film coefficients and the average soil conductivities used as input to the model were varied. Soil conductivities ranging from 0.86 W/m-K to 1.36 W/m-K and average heat transfer coefficient ranging from 2 W/sq. m-K to 16 W/sq. m-K gave sufficiently accurate fit to the measured heat fluxes. The sol-air temperature cycle, the path lengths, the inside film coefficient, and the inside air temperature were kept the same as in the First Model.

A comparison of the predicted and the measured basement heat fluxes through the uninsulated basement is shown in



Figure 5.17. For clarity results for one heat flux gauge (0.9M below grade) are shown. At the outset it can be seen that the surface cover effects are correctly modeled and there is a definite indication that the predictions are following the actual heat flux data points.

However, a complete verification of this model still have to wait till the surface cover data and the soil conductivity measurements are made for at least one year. Even though, the moisture content has a strong influence on the soil properties, as a first approximation, the changes in heat losses due to moisture content can be represented to a large extent by the changes in conductivity alone.

### 5.3.3 The Third Model

Comparisons will be made of the predicted and the measured heat fluxes and the ground temperatures surrounding the uninsulated basement. Some advantages of the present implicit model and the L-shaped marching scheme will be discussed.

To analyze the basement geometry shown in Figure 4.6, about 6000 nodes of 100 mm square were used. Important information required for starting the numerical solution is the initial ground temperature distribution. In general a better initial distribution insures faster convergence. Since the temperature distribution in a undisturbed soil is a function of soil conductivity, surface cover effects, and phase change phenomenon, it was decided to use the Fourth



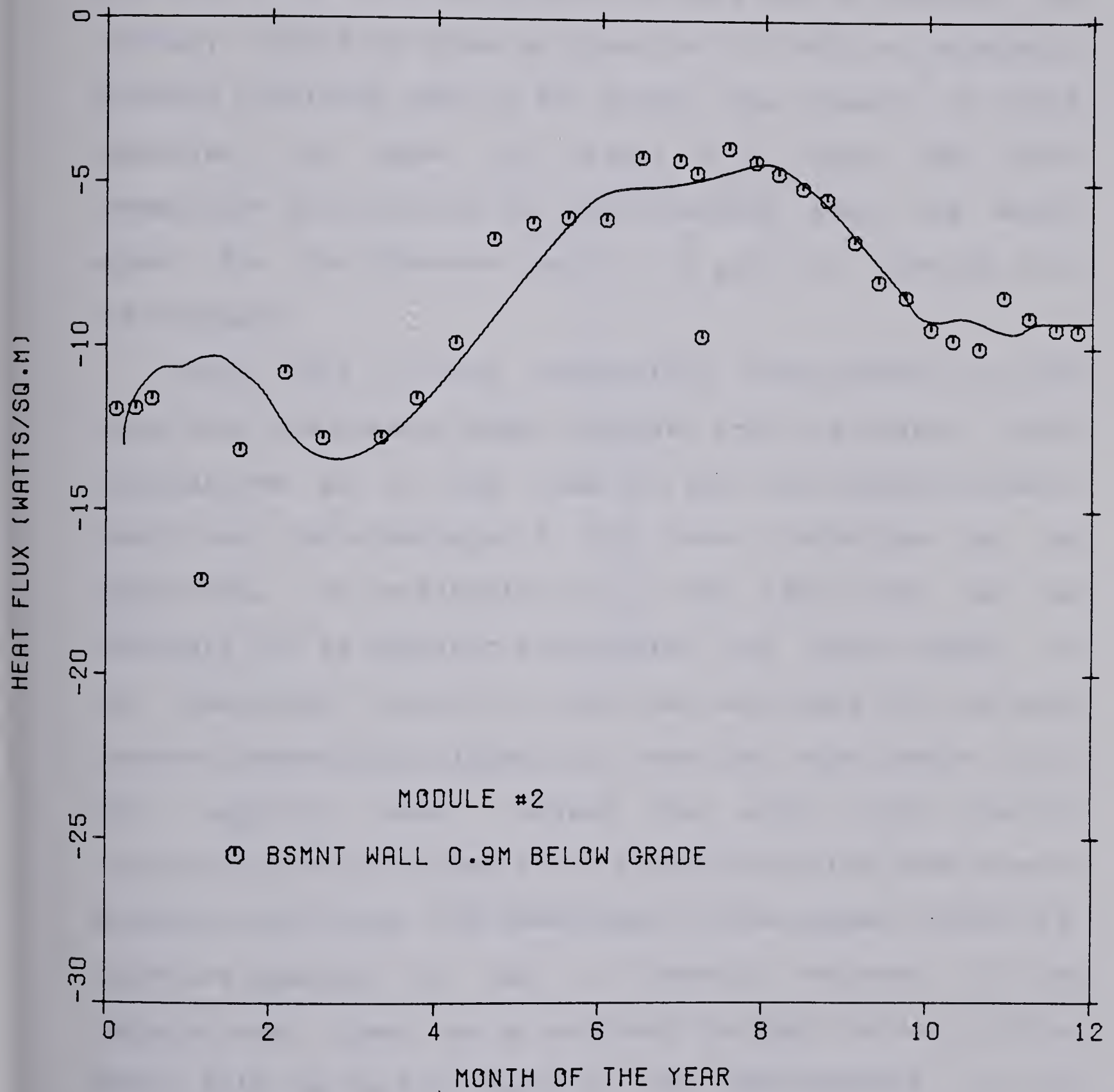


Figure 5.17 Comparison of the predicted and measured basement heat flux



Model, the phase change model, to simulate the initial temperature distribution. The only modifications that were required for the fourth model to do this was to replace the boundary condition given by Equation 4.75 with an adiabatic boundary condition deep in the ground. The result of this exercise is shown in Figure 5.18. Note that this temperature distribution is approximately what one would expect for the Edmonton region at a point far removed from the basement.

Using this initial temperature distribution, it was found that the present model required only one yearly cycle calculations as a lead time to reach the steady periodic conditions. The advantage of the above technique can be appreciated by estimating the lead time that may be necessary for an explicit calculation. For this reason, a two dimensional explicit model was developed for the same basement geometry of Figure 4.6. Numerical experiments with this explicit model showed that about three yearly calculations were necessary for establishing the same steady periodic conditions. The advantages of the present model are therefore apparent in that a dramatic decrease in the computational time can be achieved through the use of this model. This can be attributed to two improvements in the third model : a better initial distribution and the L-shaped marching scheme.

The results that are of immediate interest from this model are the comparisons between the predicted and the



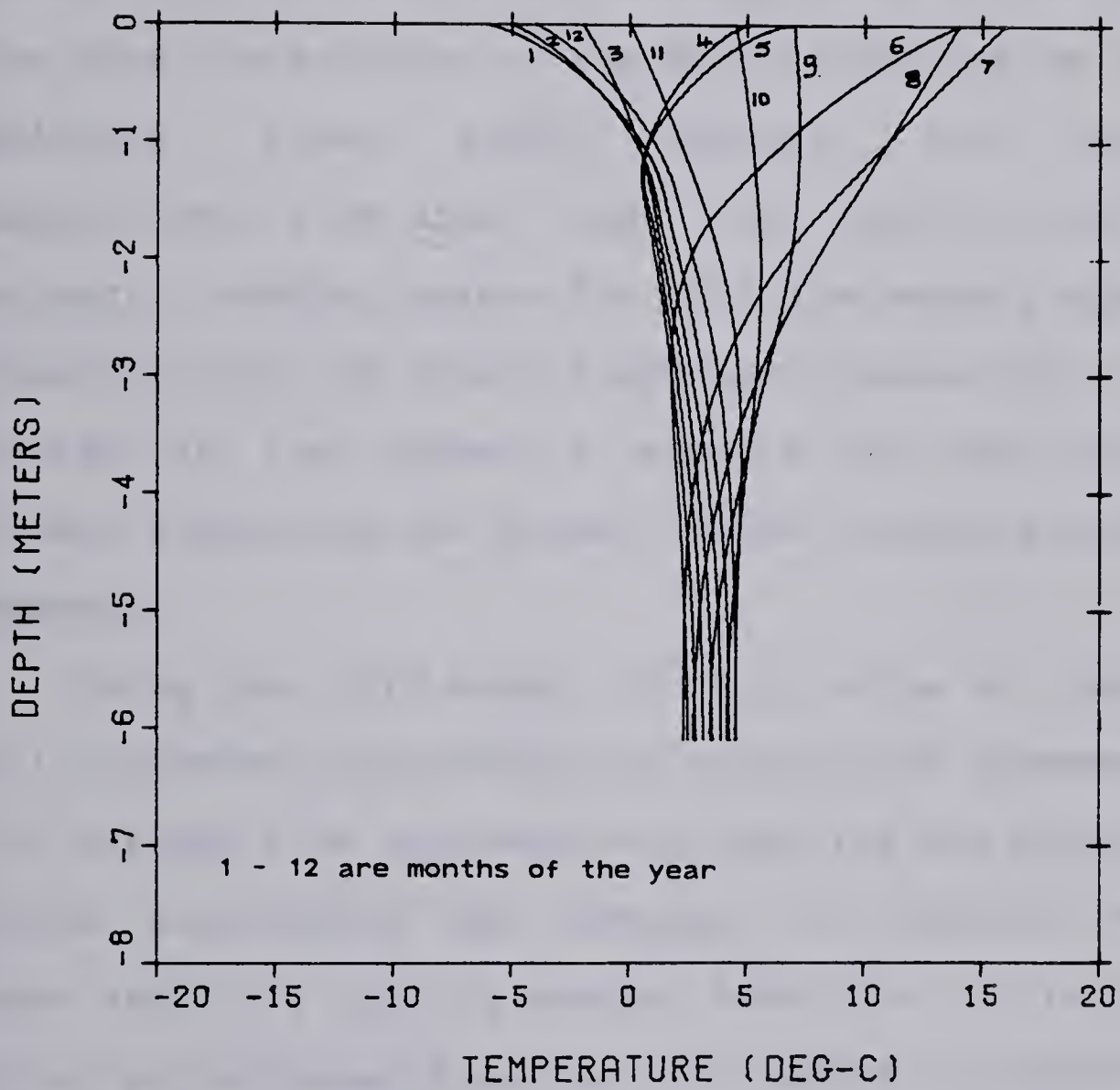


Figure 5.18 Temperature distribution in the ground at Edmonton



measured heat fluxes and the ground temperatures shown in Figures 5.19, 5.20 and 5.21. The predicted heat flux shown in Figure 5.19 is in good agreement with the measurements. However, the predicted ground temperatures shown in Figures 5.20 and 5.21 seem to be slightly warmer than the measured values for the months of January, February and March 1982. Note that the accuracy of the predictions can be improved by employing finer grids, however, the increase in computational time often does not justify the increased accuracy. Another reason for this discrepancy appears to be resulting from the ground temperature measuring techniques. However, for the present it appears that the third model is closely simulating the ground thermal regime surrounding the basement.

Using the third model, it is of value to generate the soil isotherms surrounding the uninsulated basement. Figures 5.22 through 5.24 approximately describe the ground thermal regime surrounding the basement of module 2. The results shown are for a heating season. Note that the isotherms are either pulled upwards during mid winters or pushed downwards as the ambient temperatures start to warm up. In general these isotherms appear very similar to the steady state isotherms except that the deep ground temperature effects are felt more with increasing depth. It can also be seen from these figures that the isotherms closer to the basement floor stay relatively constant throughout the year. This is the indication of a constant heat loss through this portion



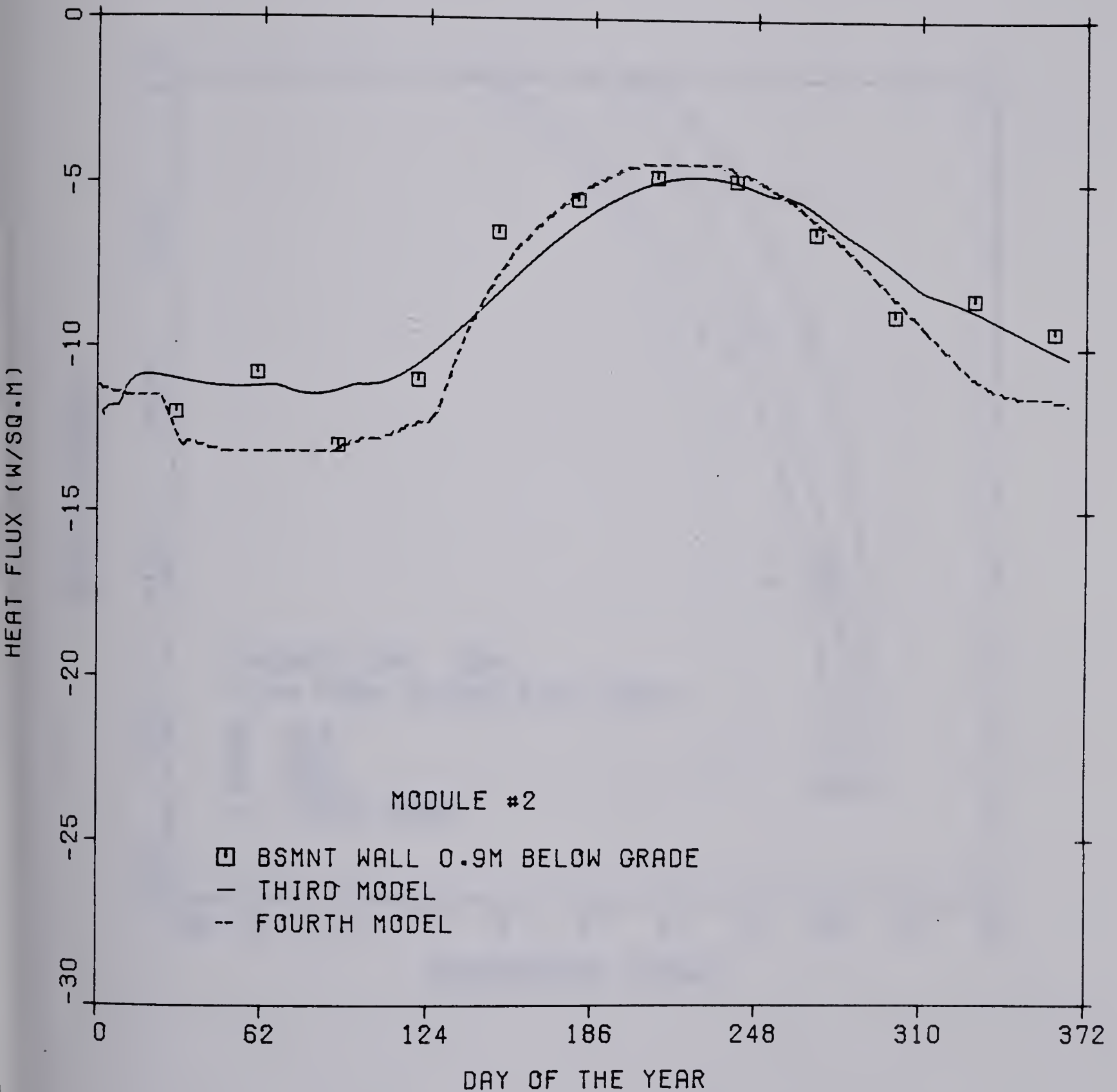


Figure 5.19 Predicted and the measured heat flux from the uninsulated basement



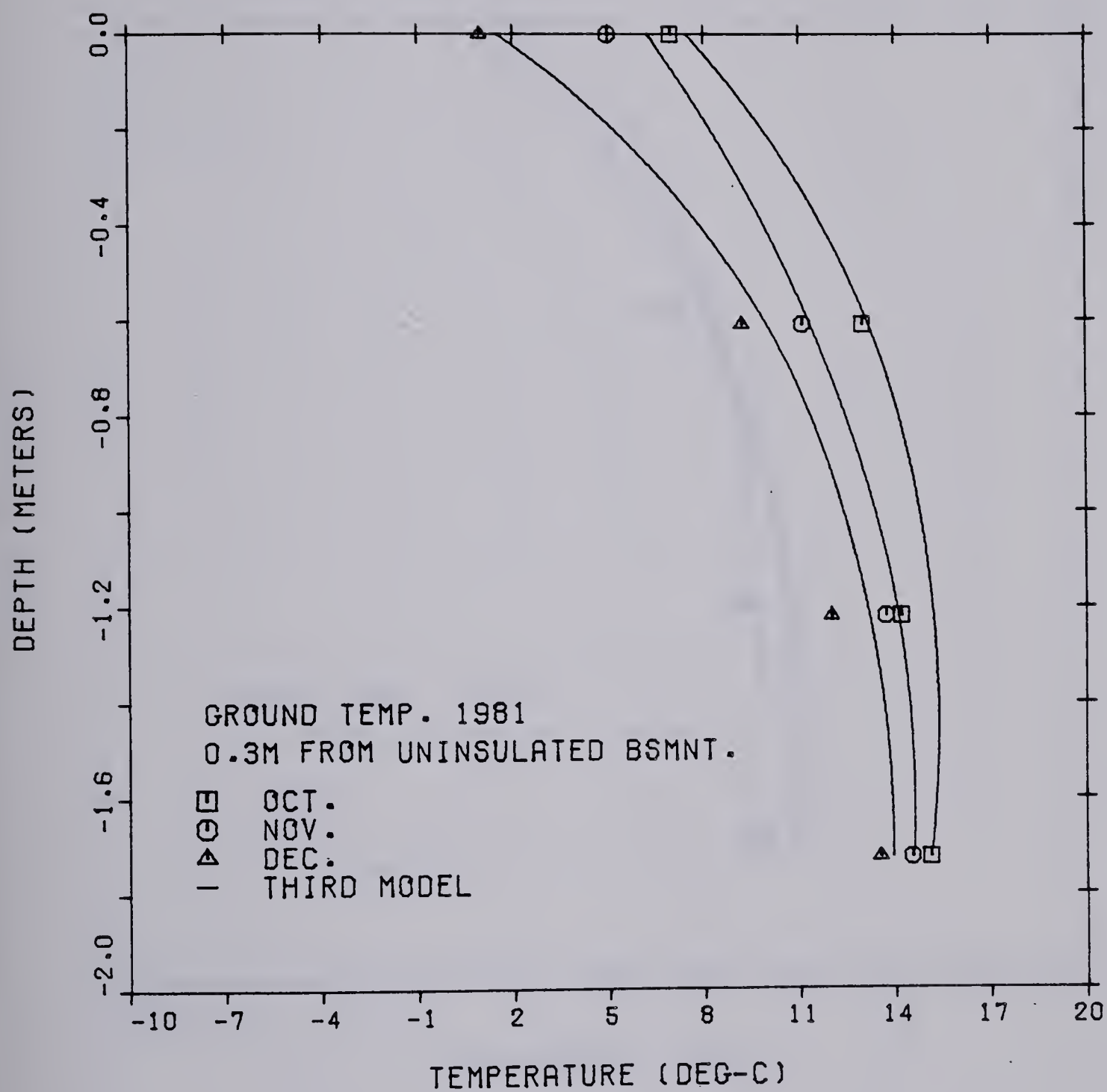


Figure 5.20 Temperature distribution at a distance of 0.3 m from the uninsulated basement



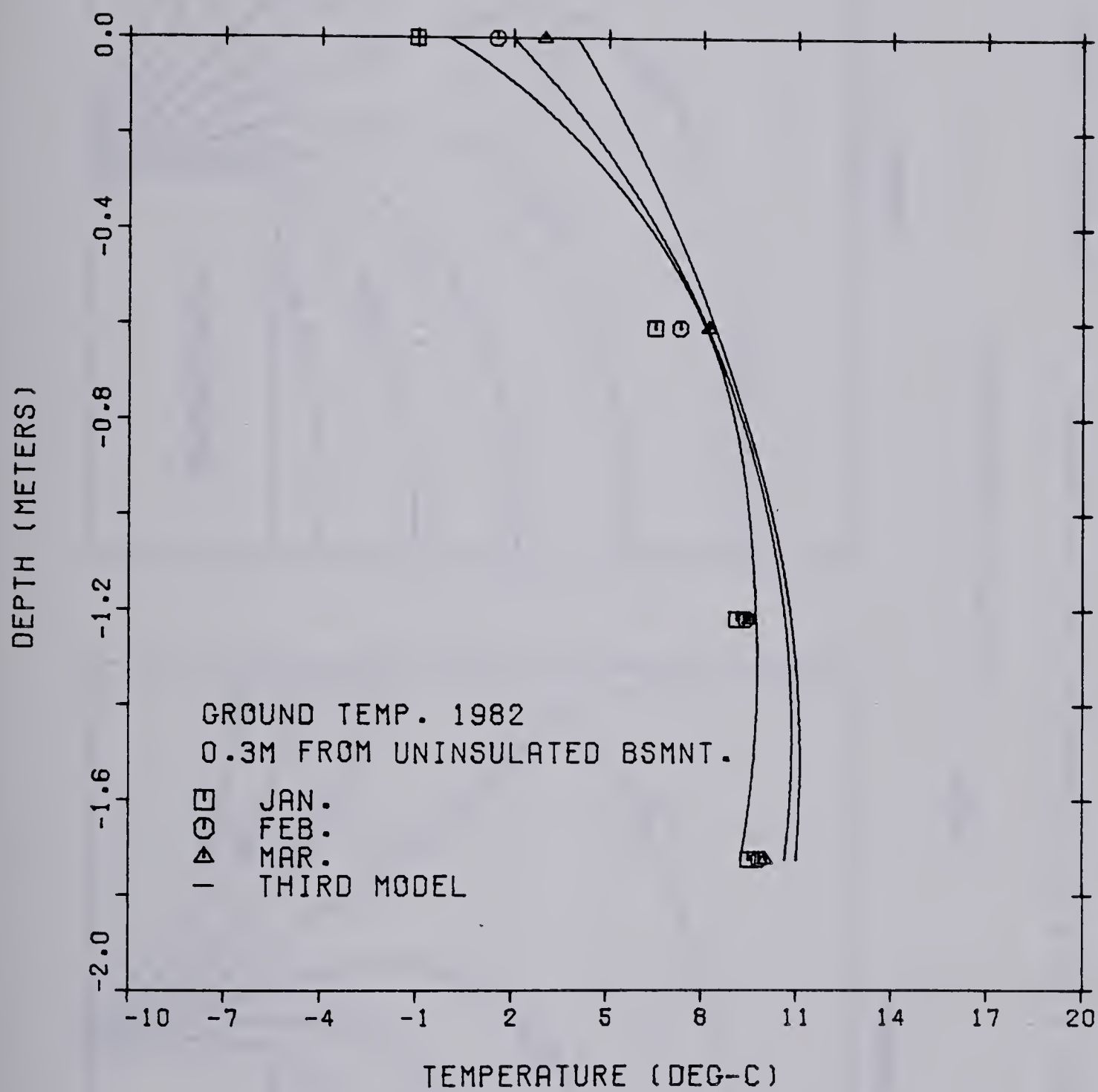


Figure 5.21 Temperature distribution at a distance of 0.3 m from the uninsulated basement



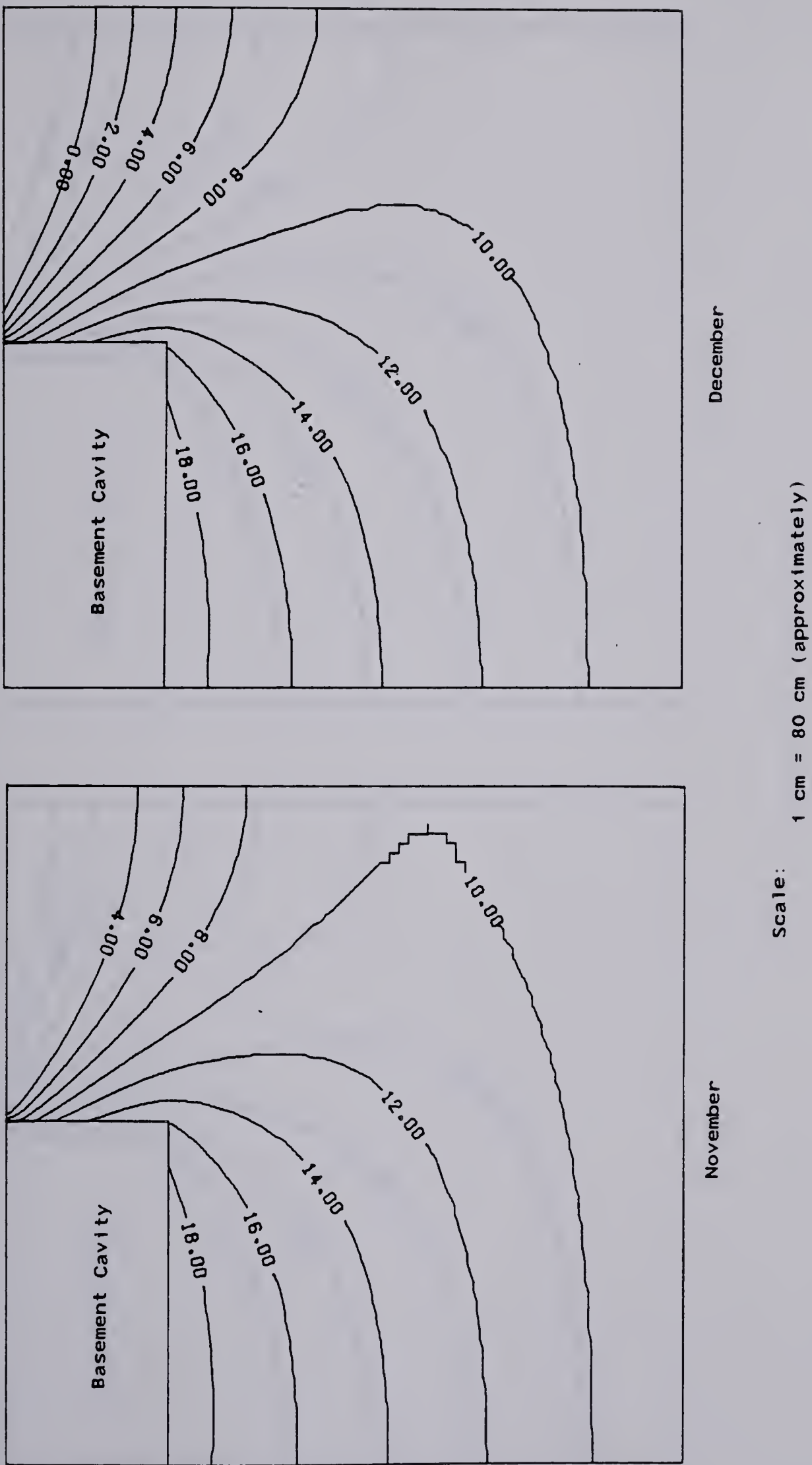
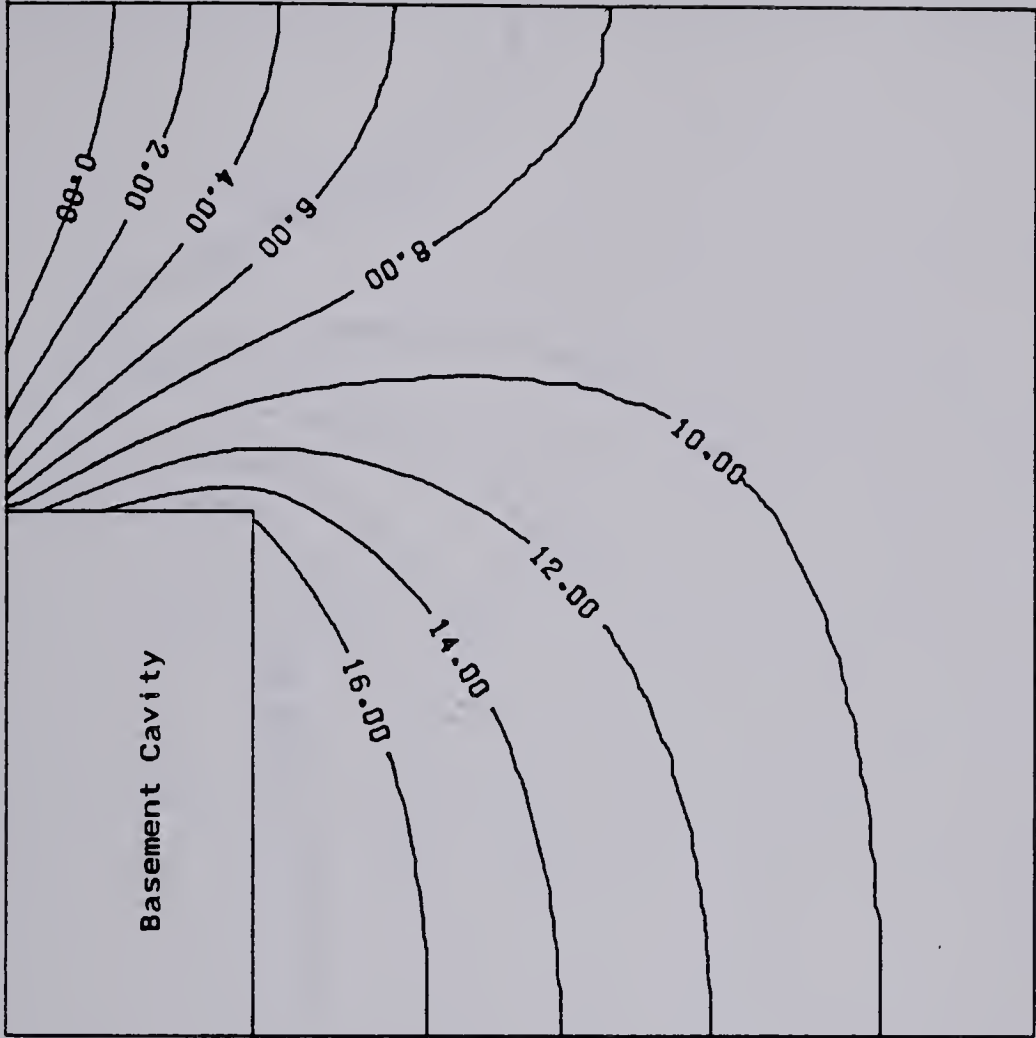


Figure 5.22 Soil isotherms for the months of November and December (in degrees C)





January

February

Scale: 1 cm = 80 cm (approximately)

Figure 5.23 Soil isotherms for the months of January and February (in degrees C)



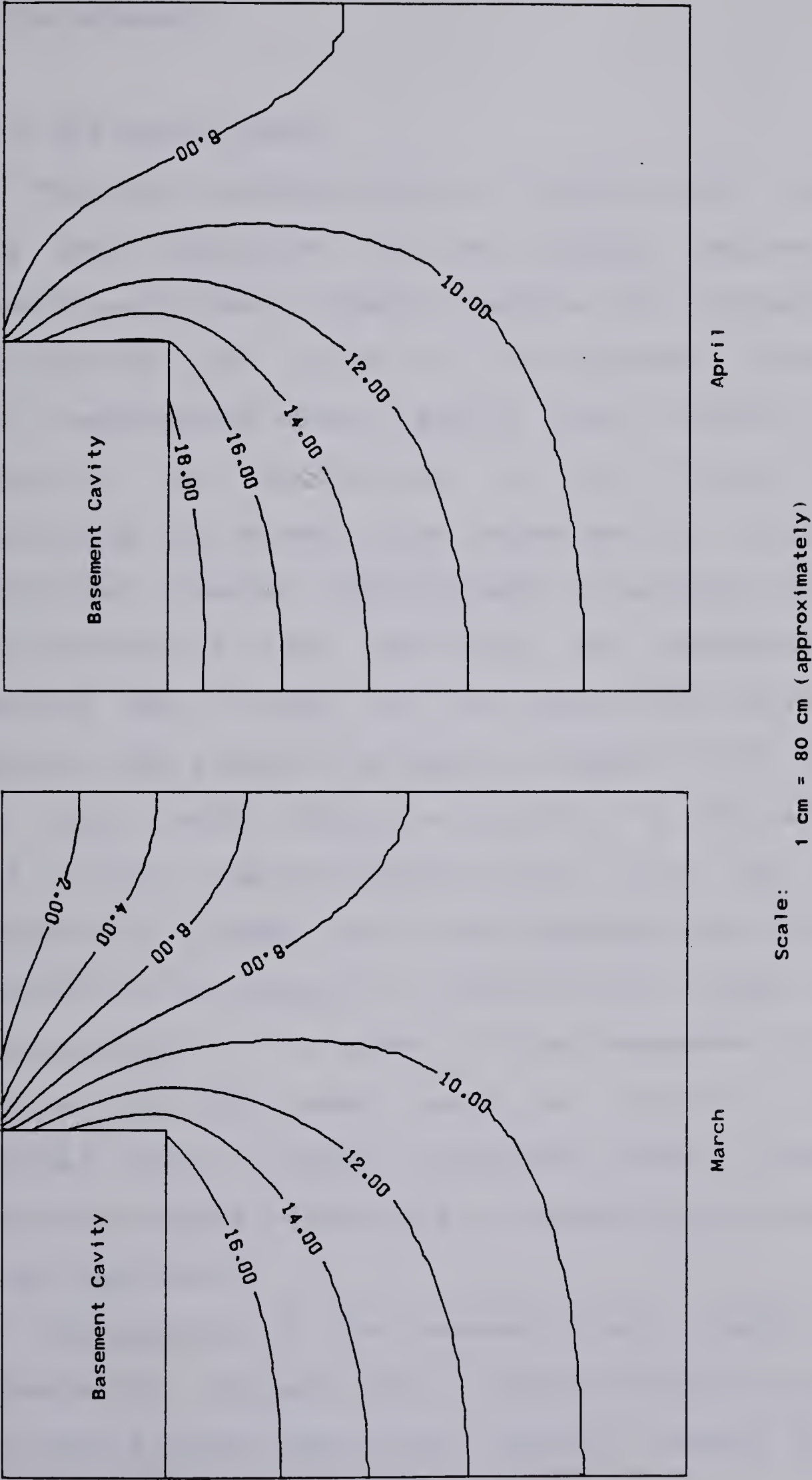


Figure 5.24 Soil isotherms for the months of March and April  
(in degrees C)



of the basement.

#### 5.3.4 The Fourth Model

The soil isotherms shown in Figures 5.22 through 5.24 give some indication of the probable regions where the freezing and thawing effects could be felt. Indeed it is to be expected that closer to the basement, throughout the year, temperatures above freezing would prevail. In this situation the application of the fourth model for calculating the basement heat losses may not introduce any significant changes. Nevertheless, to explore the potential applications of this technique, the predicted and the measured heat fluxes at one location for the uninsulated basement were compared as shown in Figure 5.19. Note that the fourth model behaved very similar to the second model. This is to be expected because of the fact that the soil temperature through this path remained above freezing and therefore in the absence of discontinuous changes that are characteristic of a phase change phenomenon, the results obtained with this model would be similar to the ones obtained from a simple conduction model. However, for increasing depths the effects of freezing and thawing could become important.

The analysis of the basement heat losses thus far presented do suggest that simple conduction models could very well simulate the ground thermal regimes surrounding the heated basements.



### 5.3.5 Conclusions

The above discussion on the four basement models was essentially limited to check the four guide lines that were proposed while developing the basement models. Indeed the results largely substantiate these ideas.

One observation that can be brought forth from Figures 5.16 and 5.19 is that the annual trends in the basement heat losses did not change much due to the two dimensionality of the problem. This means that the heat flux from the two dimensional model can still be represented by a sinusoid reduced in amplitude and lagging behind in time similar to the results obtained from the first model. This observation suggests that some conclusions on the basement heat losses can be made by considering the possibility of generalizing the results from the first model.

Consider the first model. An examination in its solution suggests that most of the parameters can be grouped to form a non dimensional depth parameter such as :

$$x \sqrt{\frac{\omega}{2\alpha}} \quad (5.6)$$

The effects of the nondimensional depth on heat losses can be indirectly investigated by observing two dependent variables: the decrement factor and the phase shift. The decrement factor was defined by Equation 4.32. Physically it signifies the relative importance of the periodic component of the heat loss rate to its steady state value.



To show the generality of this approach the variation in decrement factor as a function of nondimensional depth, representing the conditions of the uninsulated basement is shown in Figure 5.25. Note the decrease in decrement factor with increasing depth. This in terms of heat losses would mean that there is a large difference between the periodic heat losses and the steady state losses.

The influence of surface cover effects on the decrement factor can be studied in a very simplified way by varying the weather side heat transfer coefficient. This is shown by Biot numbers based on maximum depth. A Biot number of 135.0 shown in Figure 5.25 corresponds to an average value of weather side heat transfer coefficient of 5 W/sq.m. It can be seen that a decrease in Biot number decreases the decrement factor considerably. However, increasing the Biot number cannot produce the same increase in the decrement factor. This is because in the limit with the Biot number tending to infinity the surface temperature cycle tend to follow the sol-air temperature cycle closely.

The variation in phase lag as a function of nondimensional depth with the Biot number as a parameter is shown in Figure 5.26. Notice that the phase lag increases almost linearly with increasing depth. Thus as the nondimensional depth increases the ground temperature lags more and more behind the sol-air temperature cycle.

Extension of these results to the insulated basement are shown in Figures 5.27 and 5.28. Note that the effect of



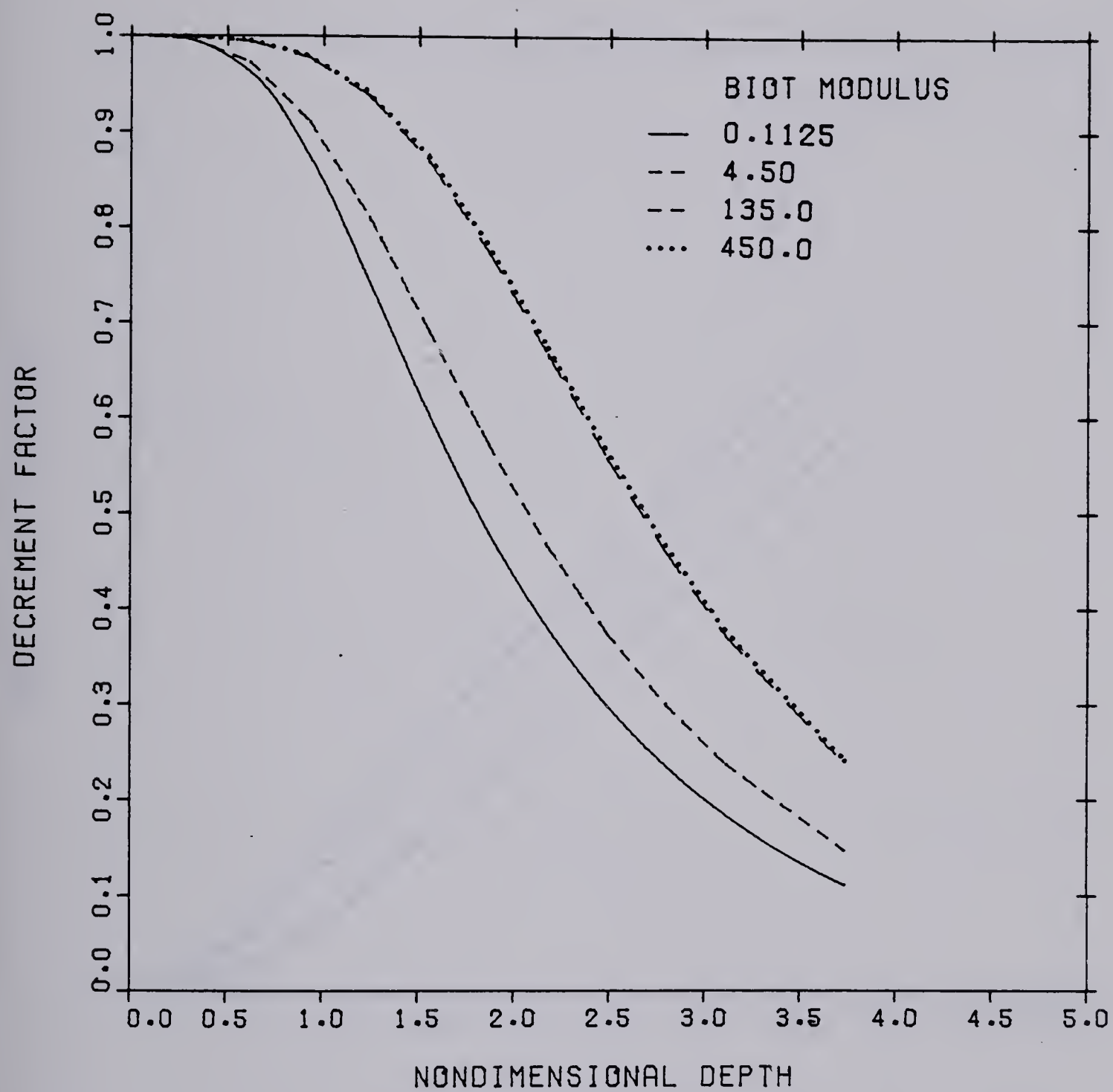


Figure 5.25 Effects of nondimensional depth on decrement factor for an uninsulated basement



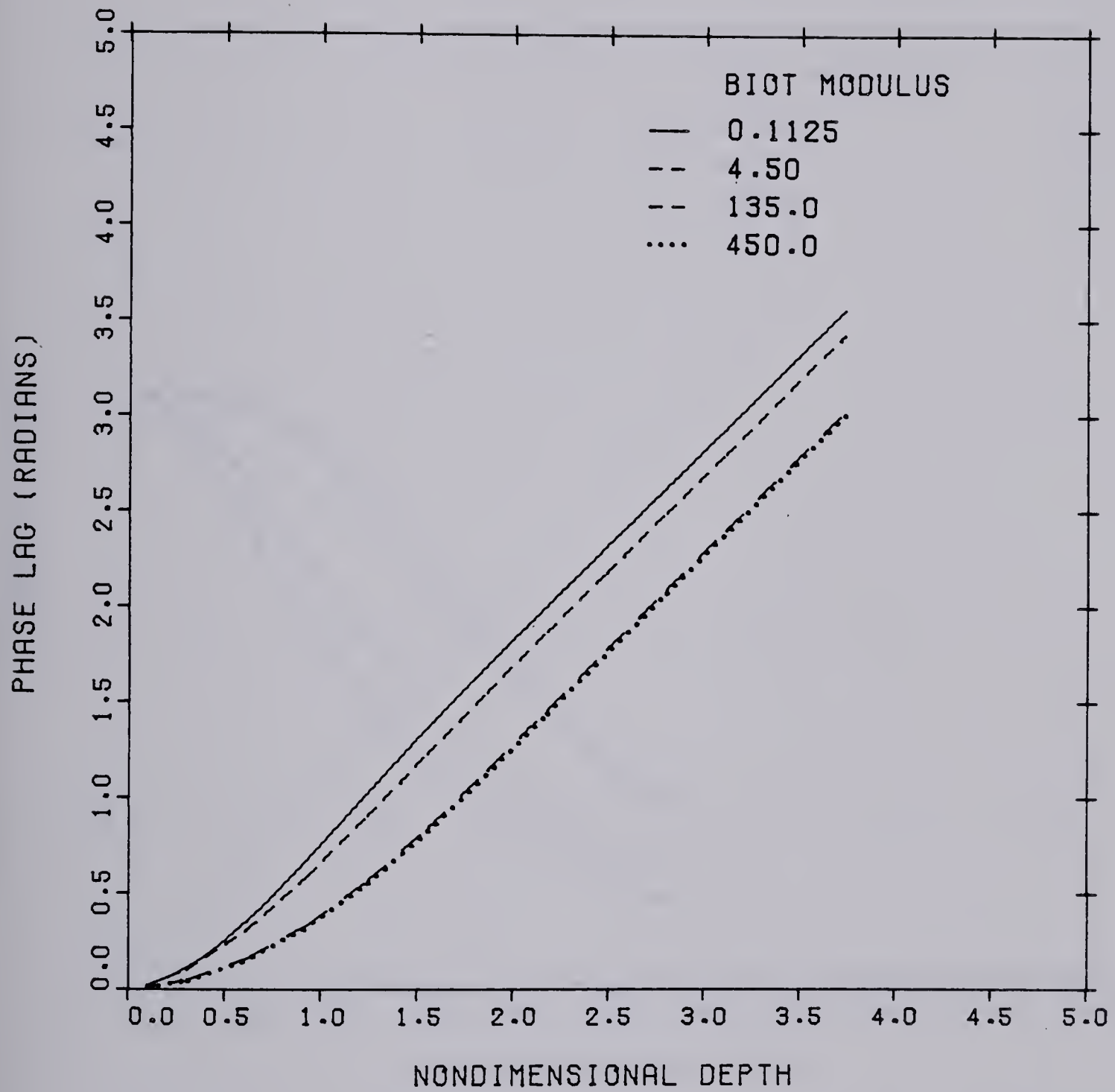


Figure 5.26 Effects of nondimensional depth on phase shift for an uninsulated basement



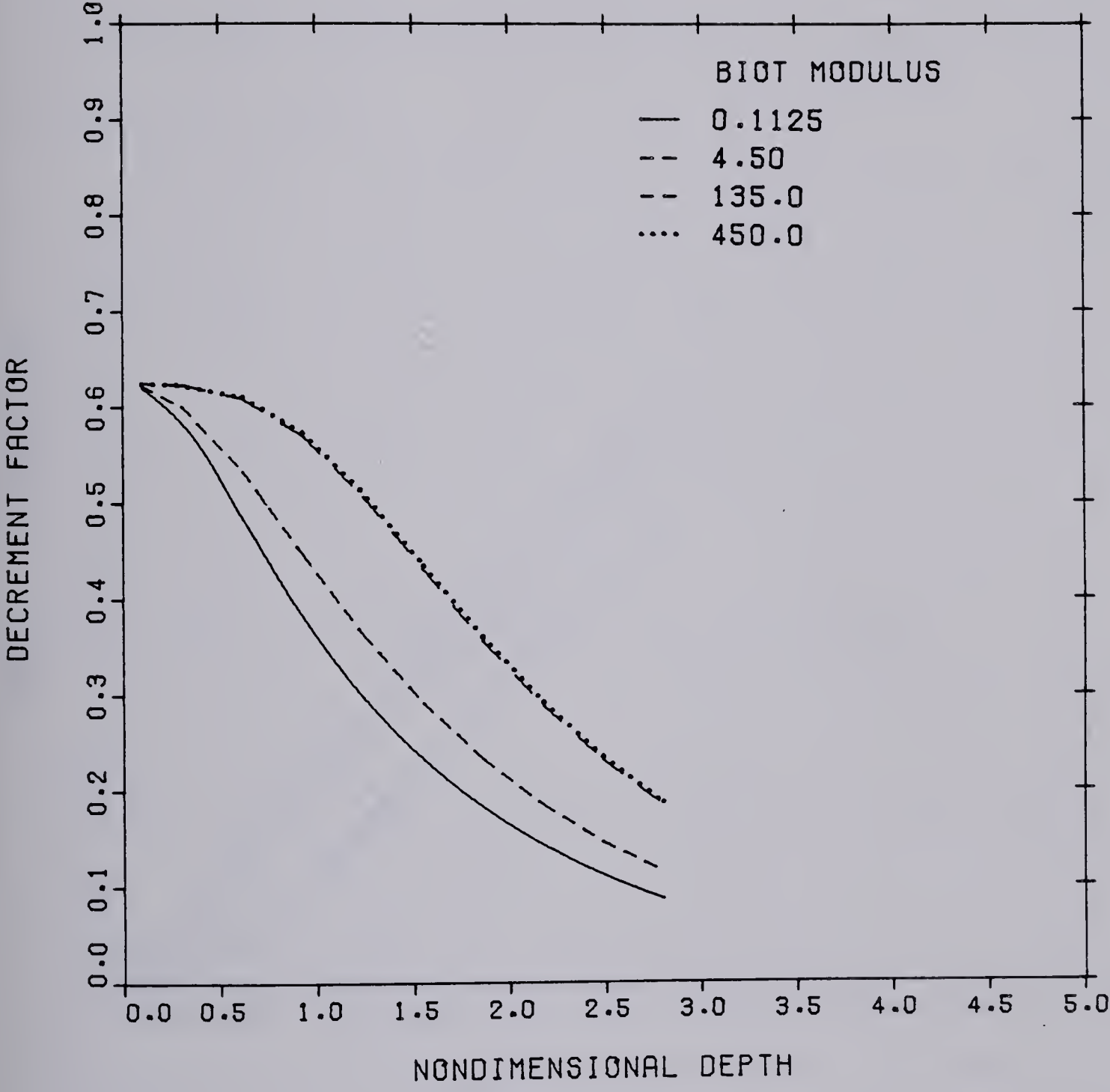


Figure 5.27 Effects on nondimensional depth on decrement factor for an insulated basement



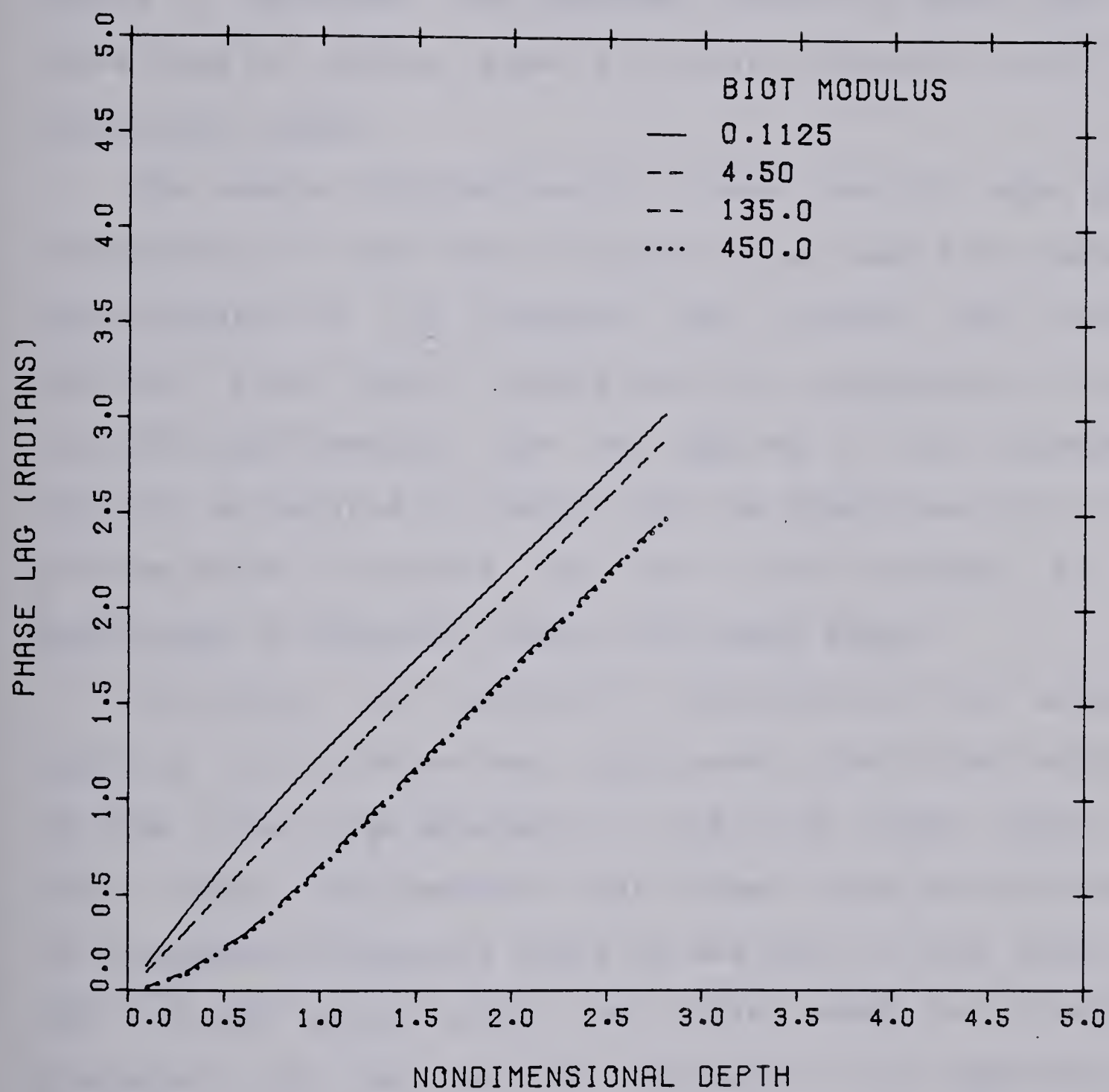


Figure 5.28 Effects of nondimensional depth on phase shift for an insulated basement



insulating the basement on the decrement factor is to decrease its magnitude considerably as shown in Figure 5.27. In fact an insulation of RSI 1.76 on the basement walls of module 4 decreases the decrement factor by about 30%. The phase lags as before show a linear variation with non dimensional depth.

The general implications of these results are quite interesting, in that these figures can be used for a general understanding of the basement heat losses. The results obtained from these figures would be independent of input function and therefore can be applied to any basement. Further as pointed out before the two dimensionality of the problem would introduce but only minor changes in the magnitudes of decrement factor and phase angle.

Therefore, one method of approaching the basement modeling in the house heat requirement predictions would be to take a two stage approach. In the first stage, using the third model, the basement heat losses could be analyzed as an independent component model as was done in this study. In the second stage using the first model an iterative procedure could be used to determine the approximately equivalent path lengths that could reproduce the results of the third model. These equivalent path lengths once found can be transferred to the main simulation model. This approach offers both the advantages of accuracy and a considerable reduction in the computational time.



Using the equivalent path lengths, the heat losses through the basements could be determined and their variations due to changes in the soil conductivity could be studied. Suppose it is desired to study the change in basement heat loss at a depth of 0.9 meter below grade of basement of module 2 due to a change in conductivity of the soil by 25%. The results shown in the Figure 5.29 suggest that on an annual basis a 25% increase in conductivity of the soil produces a 15% increase in the basement heat losses through this path of the basement.

The implications of the above analysis are that the soil conductivity is a major uncertain parameter which has a direct influence on the basement heat losses. Therefore, in order that the above models can be called as real predictive models a soil conductivity model may have to be included in them. Nevertheless the previous results show that the basement heat losses can be predicted with a reasonable accuracy by assuming average conductivity values for the soil. For example one method of applications of the above basement models would be to measure the soil thermal properties at different depths about four different times of the year. This data can be used as an input to the third model. Through the results of this model the equivalent path lengths could be determined.

More practical information of interest is the reduction in heat losses that can be achieved by insulating the basements. To answer this question the monthly averages of



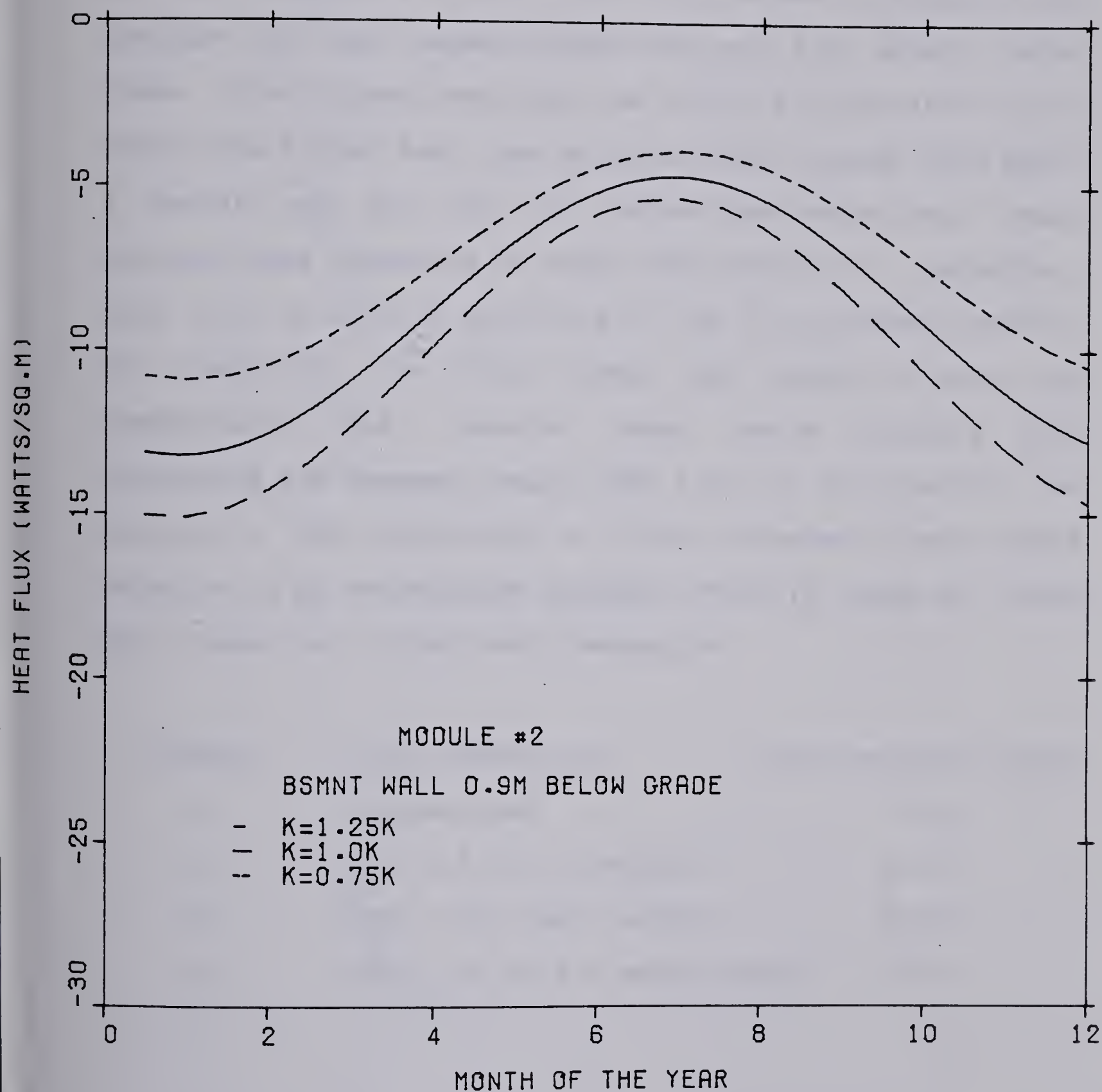


Figure 5.29 Effects of the soil conductivity on the heat losses



the previous basement heat loss data, measured at identical locations on module 2 (uninsulated) and module 4 (insulated to full height to RSI 1.76) are plotted in Figure 5.30. Consider the heat losses through the wall 0.9 meters below grade. The figures show that the effect of insulation is to reduce the winter heat loss by about 50%. through this path. A better way will be to compare the annual heat losses through these basements to study the effects of insulation. This can be done by using any of the four basement models. For simplicity the first model was used to make the comparisons. The results shown below indicate that insulating the basement walls (RSI 1.76) to full height can achieve a 50% reduction in total basement heat losses relative to an uninsulated basement. This in terms of house heat losses is a significant reduction.

module	wall insulation	relative heat losses
2	uninsulated	1.00
3	RSI 3.5 (full height)	0.47
4	RSI 1.76 (full height)	0.57
5	RSI 1.76 (0.6 m below grade)	0.77



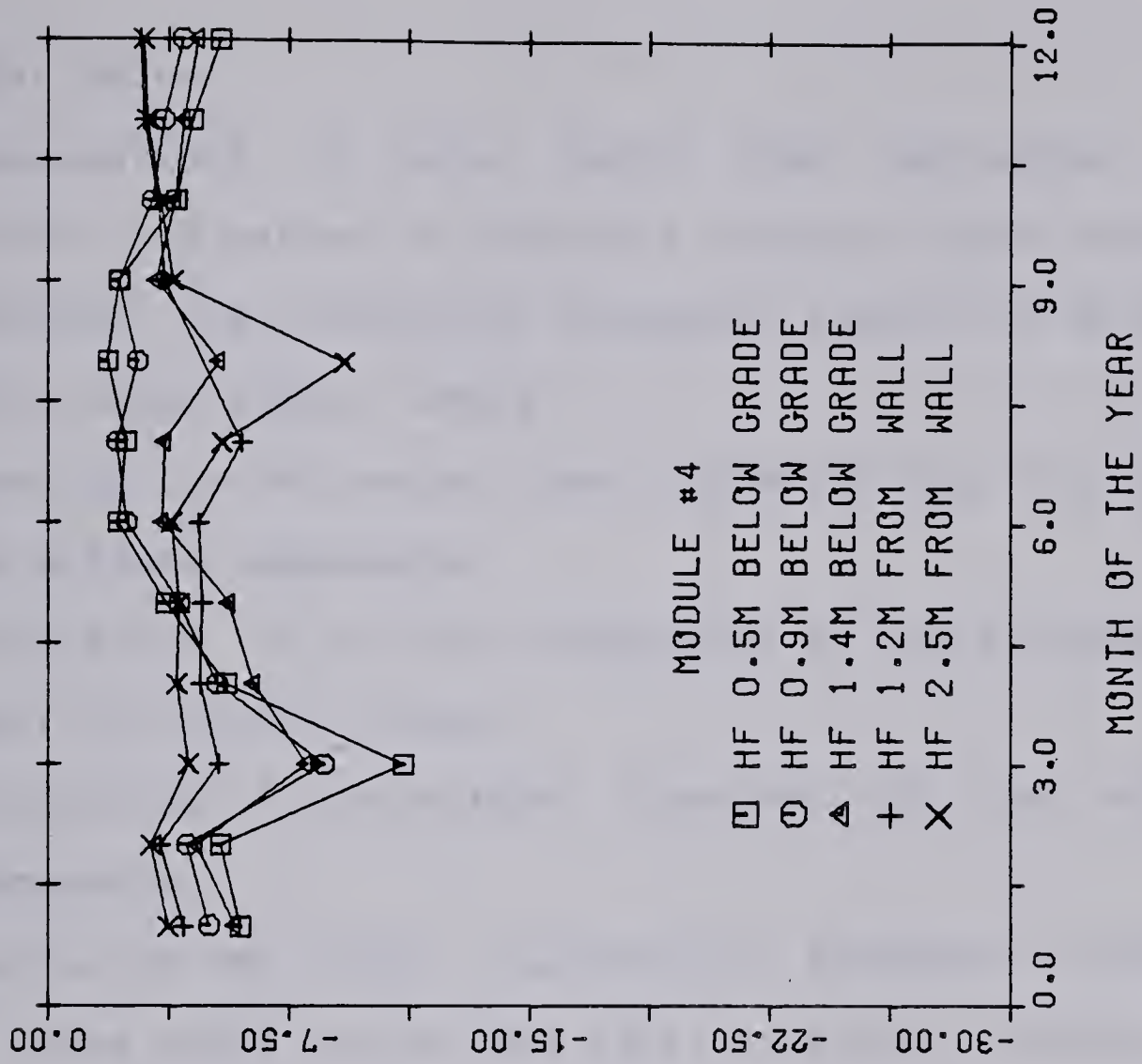
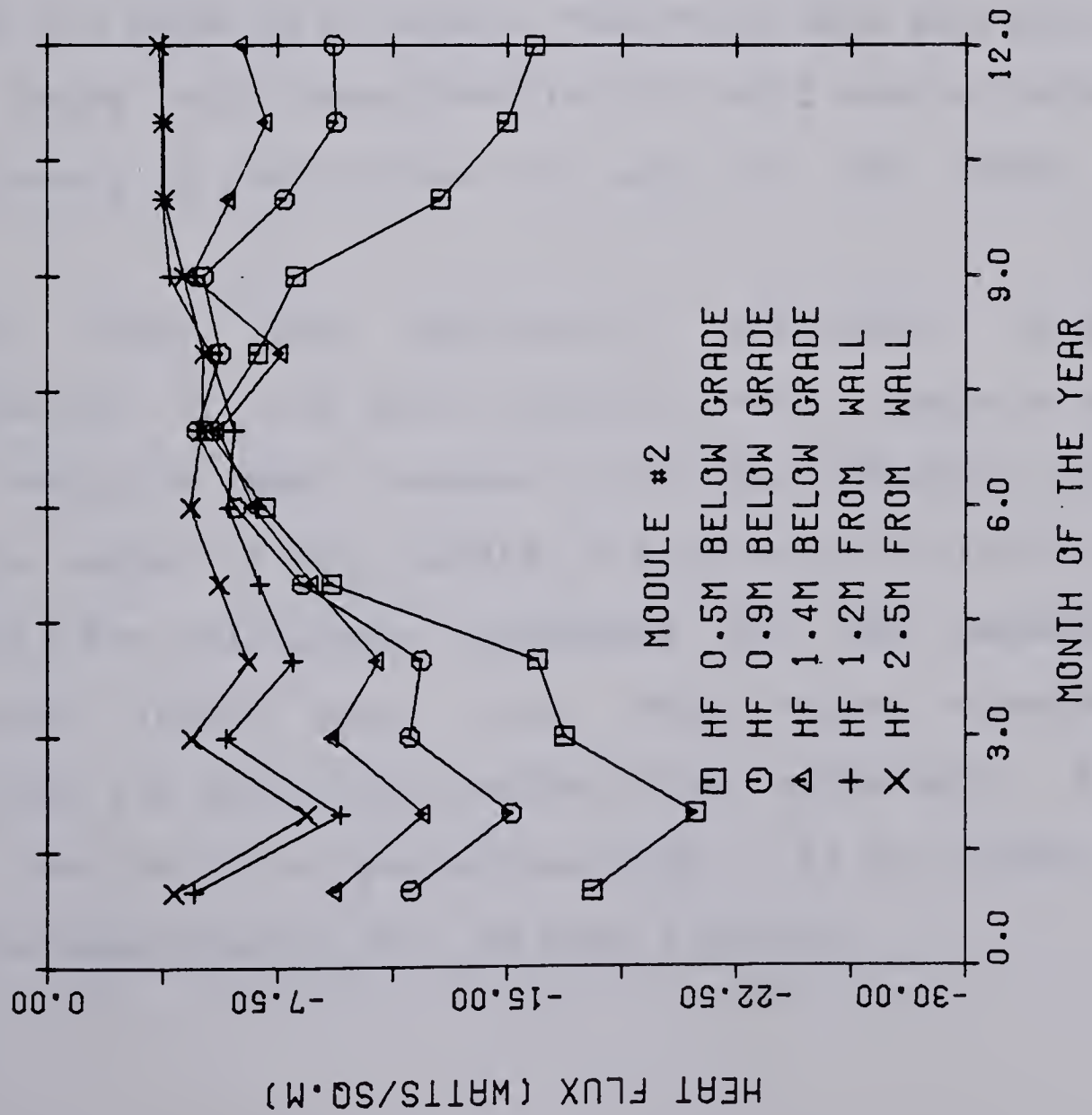


Figure 5.30 Comparison of the measured heat losses through the uninsulated and the insulated basement



## 5.4 Solar Gains

calculations of solar gains from horizontal total insolation is a matter of extensive research these days. As noted before, the calculation procedure itself can be broken down into three steps, namely:

1. Breaking the horizontal total radiation into its direct and diffuse components.
2. Calculation of vertical components of these fluxes from their horizontal fluxes.
3. Calculation of transmitted fractions of the vertical components.

Delineation of the total calculation procedure into the above three steps can be used as an excellent criterion for testing the solar gain models. Following this approach, the solar gains model described in [14] will now be tested for its accuracy of predictions for each of the above three steps.

To check the calculation procedure graphical presentation of the hourly results over a complete heating season would be ideal. However, this would involve plotting a large number of data points. A much better alternative is to verify the calculation procedure for the measurements made only around solar noon. These values represent the conditions for which the greatest solar gains occur for at least the mid winter period and also it is for these values that the measurements will be most accurate.



Figure 5.31 shows the ratio of diffuse horizontal to horizontal total, calculated and measured for various sun altitudes. For clarity, data with  $H_d/H \leq 0.20$  was used for plotting. Clearly the predictions are high, particularly at low sun altitudes. Note, however, that sun angles may not be the only factor involved since for sun angles less than  $20^\circ$  the ground also had snow cover.

Similarly, the results from the second criterion of the verification procedure are shown plotted in Figure 5.32. This time the ratio of total on a vertical surface to horizontal total is plotted against sun altitude. Again predictions are different from measurements for low sun angles. The cause of this discrepancy is not quite clear. However, it appears that the predictions do not adequately describe the largely anisotropic nature of reflected light from snow cover for low sun angles. It should also be noted here that the solar radiation models are generally based on a long term average correlations and therefore do not accurately predict the diurnal variations.

Before attempting to further explore the measured data, it is instructive to examine the fundamental nature of the problem and the various attempts made by several authors to simplify the problem.

The diffuse radiation reaching the ground is a complex function of such phenomenon as scattering effects of air molecules and particulate matter, absorbing effects of ozone, water vapour and other gases in the atmosphere. Of greater



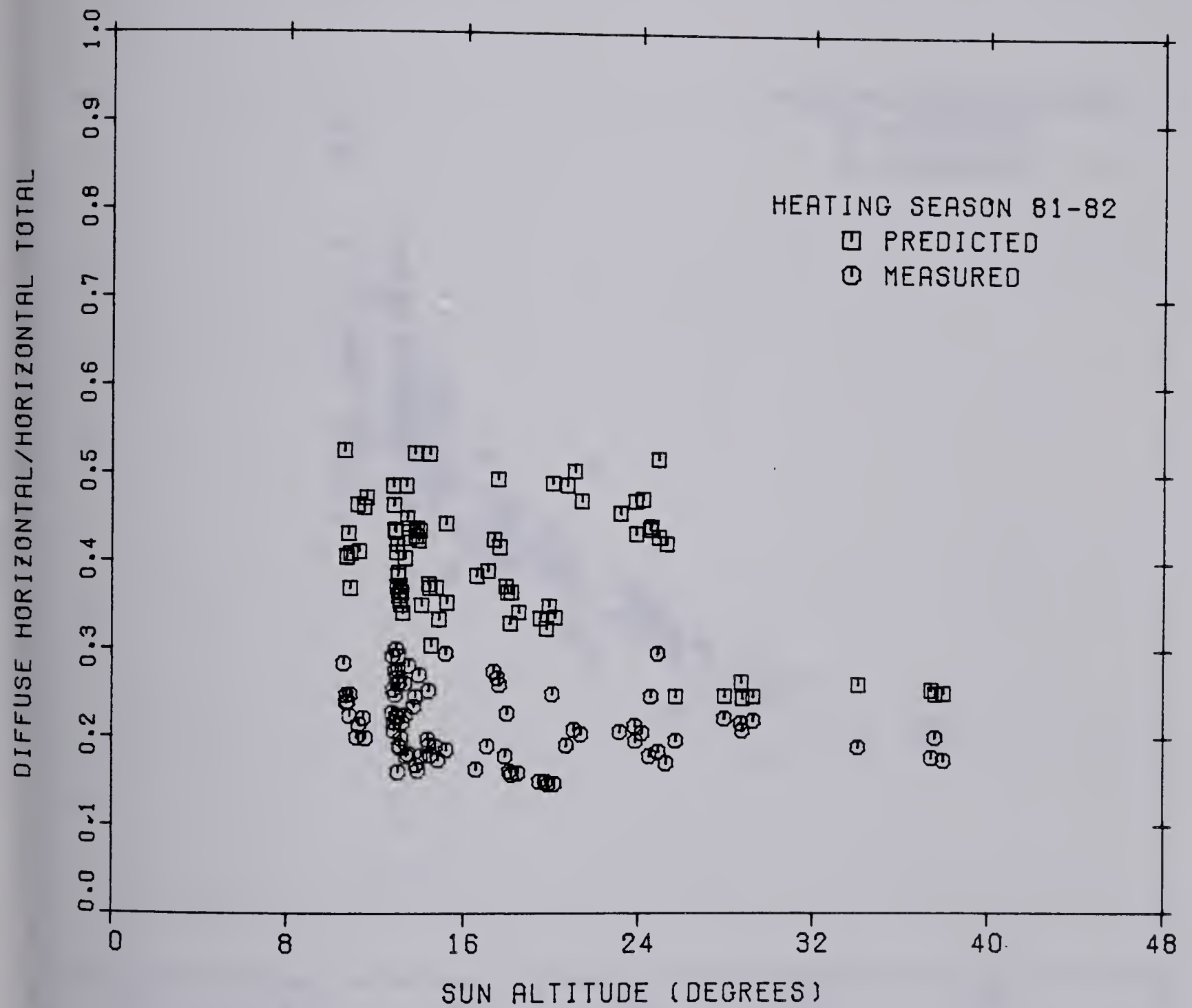


Figure 5.31 Plot of the ratio of diffuse horizontal to horizontal total versus sun altitude



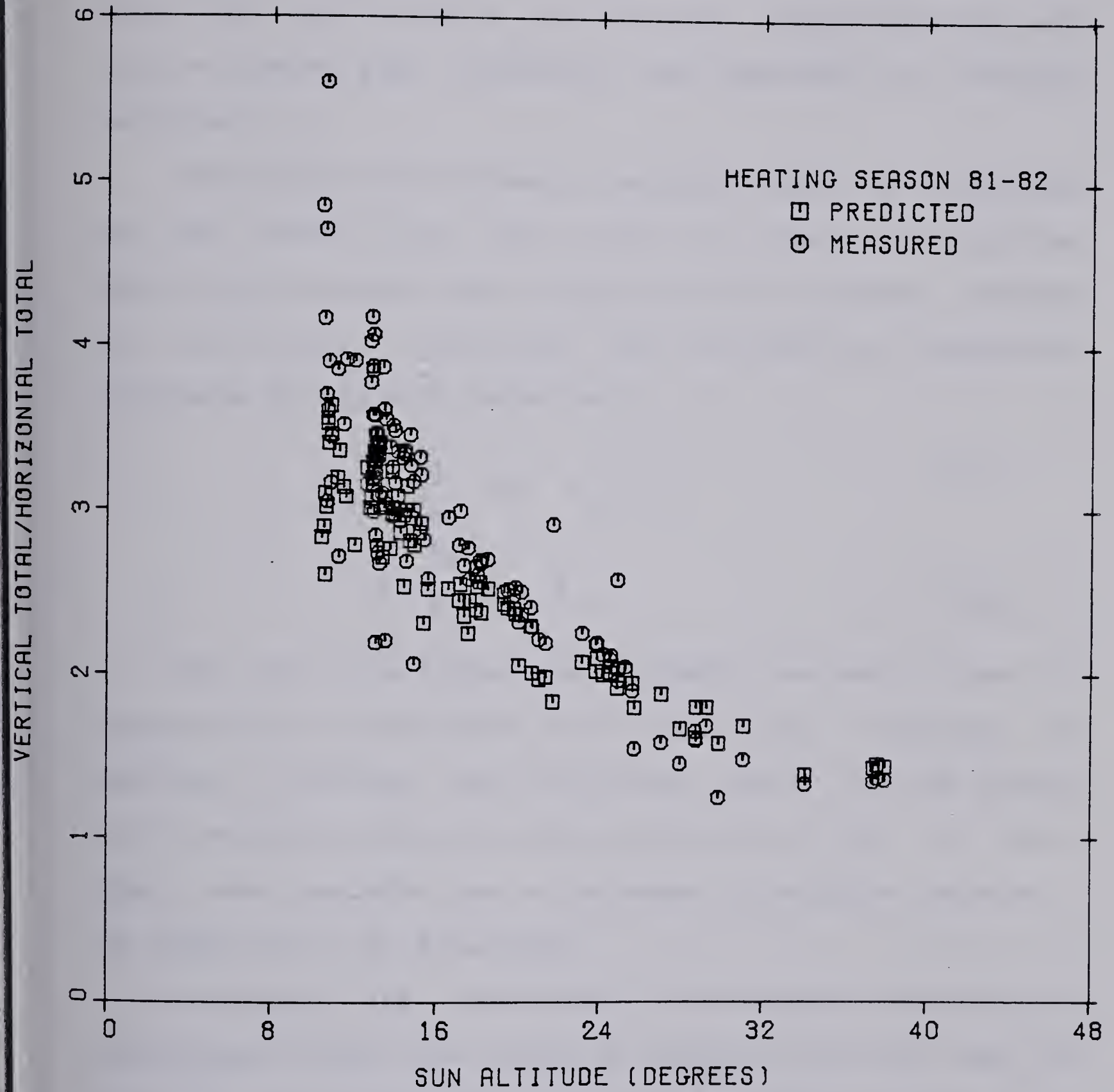


Figure 5.32 Plot of the ratio of vertical total to horizontal total for various sun altitudes



importance is the overwhelming role played by clouds in modifying the diffuse radiation. Recent studies [86,87] have identified that effects of latitude, average air mass and surface albedos also influence the magnitude of diffuse radiation.

Recognizing the extremely variable nature of cloudiness Liu and Jordan [74] were first to show from long time statistical averages that a relation exists between diffuse and horizontal insolation. The correlating parameters introduced by Liu and Jordan were:

$$K_d = \frac{H_d}{H_o} \quad \text{and} \quad K_T = \frac{H}{H_o} \quad (5.7)$$

$$K = \frac{H_d}{H} \quad \text{and} \quad K_T \quad (5.8)$$

Thus the functional relationship between  $K$  and  $K_T$  proposed by Liu and Jordan has since been a subject of continuous scrutiny over different parts of the World [86,87,88,89,90]. Recently Klein and Duffie [91] in their paper have concluded that a universal correlation between  $K$  and  $K_T$  has yet to be developed.

Even though the correlation coefficients describing  $K$  and  $K_T$  might differ from region to region or from one year to the next, the general nature of functional relationship shown by Liu and Jordan has been verified by many authors.

Contrary to dealing with long term averages, most heating load calculations using computers are done on hour by hour basis. This would require that the solar gains model



be able to correctly predict the hourly values of diffuse radiation from the hourly horizontal insolation. As a first approximation the practice is [8] to use the same functional relationship between  $K$  and  $K_T$  which was developed from long term averages.

The limitations of this approach are therefore evident in that the predicted radiation would give an average hourly diffuse radiation but not the instantaneous value. In an attempt to elevate this problem recent studies [87,88,89,90] have been directed at correlating the hourly diffuse and hourly total insolation just the same way as was proposed by Liu and Jordan.

Buglars [87] study shows that the data points scatter as much as 30-50 percent about certain mean value. Therefore any attempts to correlate the hourly data would necessarily have a large variation associated with it. However, what is important from Buglars study is that the correlation between  $K$  and  $K_T$  does appear to show dependence on average air mass. This observation is also supported by Iqbal [88].

Within the context of these limitations, a guide line used in this study was to carry out analyses of the hourly diffuse and horizontal insolation data with a view to explore correlations between  $K$  and  $K_T$ .

In an attempt to seek the correlation between  $K$  and  $K_T$  from the hourly data recorded at the test facility, the ratio of diffuse radiation to horizontal total insolation was plotted against clearness index in Figure 5.33. For



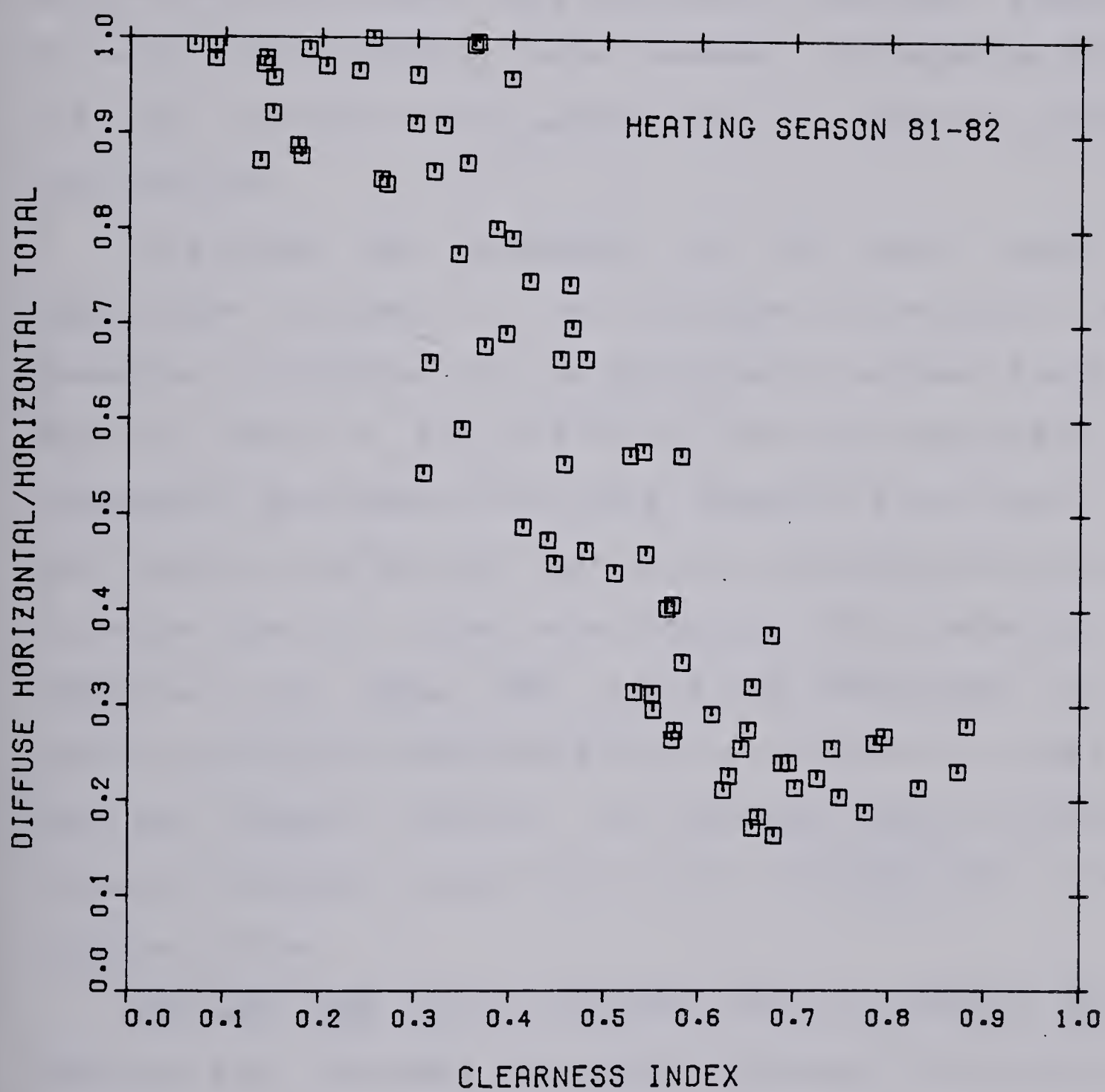


Figure 5.33 Ratio of the horizontal diffuse to horizontal total versus clearness index



clarity measurements made around solar noon were used for plotting. It can be seen that on an average, there appears to be three distinct regions of slopes around which the data points are distributed. This observation has been supported by many investigators. Note, however, the expected errors one might encounter while using a best fit equation through these points.

To analyse the randomness of the above result an appropriate strategy is to introduce an average air mass parameter in representing the distribution between  $K$  and  $K_T$ . This is done in Figure 5.34 for the data recorded by the Atmospheric Environment Services at Edmonton Stony Plain. At the outset it can be seen that at low sun angles the scatter is larger than for higher solar angles. This behaviour as explained by Iqbal [88] could be attributed to the scattering effects associated with the thicker air mass at low sun angles. However, no definite pattern could be extracted from the figure which could relate  $K$  and  $K_T$  with solar altitude.

The same data can be plotted with  $K_d$  against  $K_T$  for various sun altitudes as shown in Figure 5.35. It can be seen that sun altitude dependence in the region of  $K_T$  less than 0.4 is almost non-existent. This is characteristic of mainly cloudy weather in which most of the radiation reaching ground is diffuse in nature. The next region of  $K_T$  between 0.4 and 0.75 can be characterized by partly clear and partly cloudy region, shows that even though solar altitude



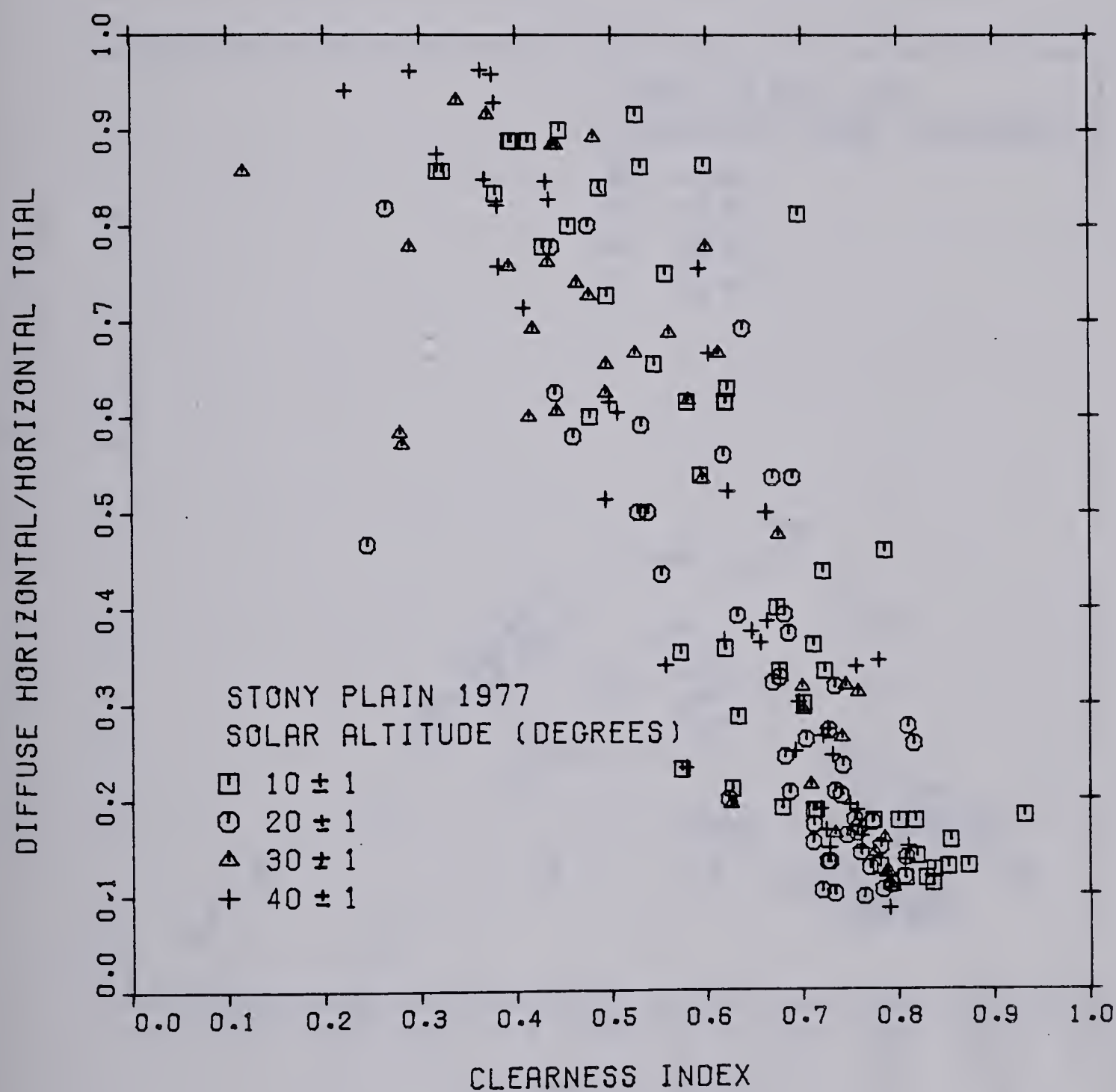


Figure 5.34 Ratio of diffuse horizontal to horizontal total versus clearness index



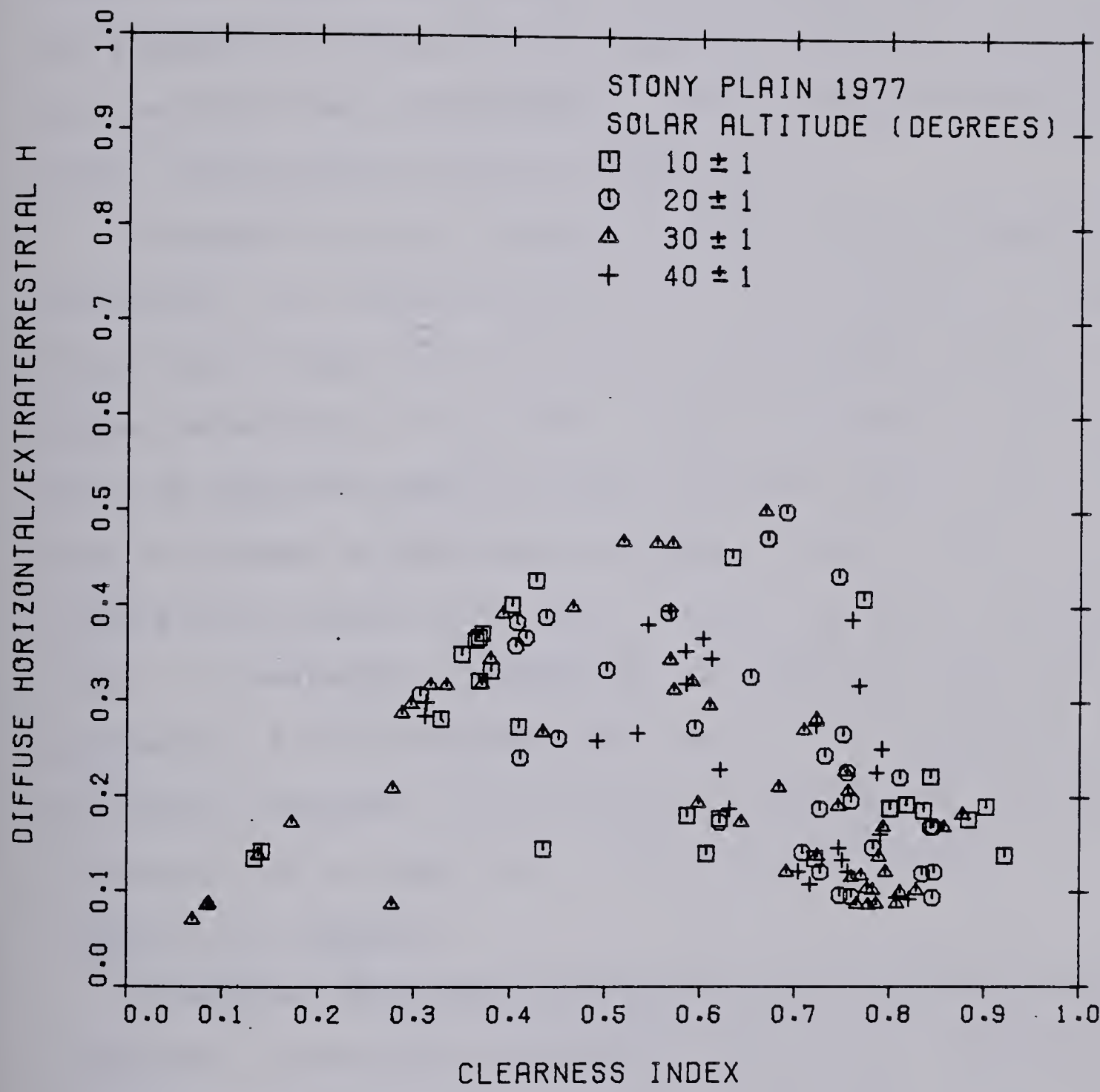


Figure 5.35 Ratio of diffuse horizontal to extraterrestrial insolation versus clearness index



may be a factor in modifying  $K_d$  no definite pattern can be attributed to solar altitudes. In this regard Iqbal [88] has recently made a number of possible explanations for this behaviour. Lastly the region with  $K_T$  greater than 0.75 can be classified as mainly clear weather region. In this region most authors have recommended to use a constant fraction of total insolation as diffuse radiation.

However it is of interest to see if this assumption of constancy of diffuse radiation is true. Because it appears from Figure 5.34 that for  $K_T > 0.75$  the probable range of  $K$  value is between 0.1 to 0.20. Figure 5.36 shows the data for  $K_T > 0.75$  replotted against solar altitude while identifying the  $K_T$  values by different legends. It can be seen from the figure that except for a small scatter, majority of  $K_d$  values show a remarkable dependence on solar altitude with  $K_T$  as parameter. It is believed that use of this approach would certainly minimize the errors in estimation of diffuse radiation for at least 30% of the data which falls in the region of  $0.75 \leq K_T < 1.0$ .

The above analyses demonstrate that the hourly diffuse radiation cannot be accurately predicted because of its random nature. Therefore, one has to be aware of the errors that might result when using an average correlation between  $K$  and  $K_T$ . The impact of this error on heating load predictions will not be significant because solar gains represents a small fraction of heat losses unless the house was highly insulated. To avoid such uncertainties it was



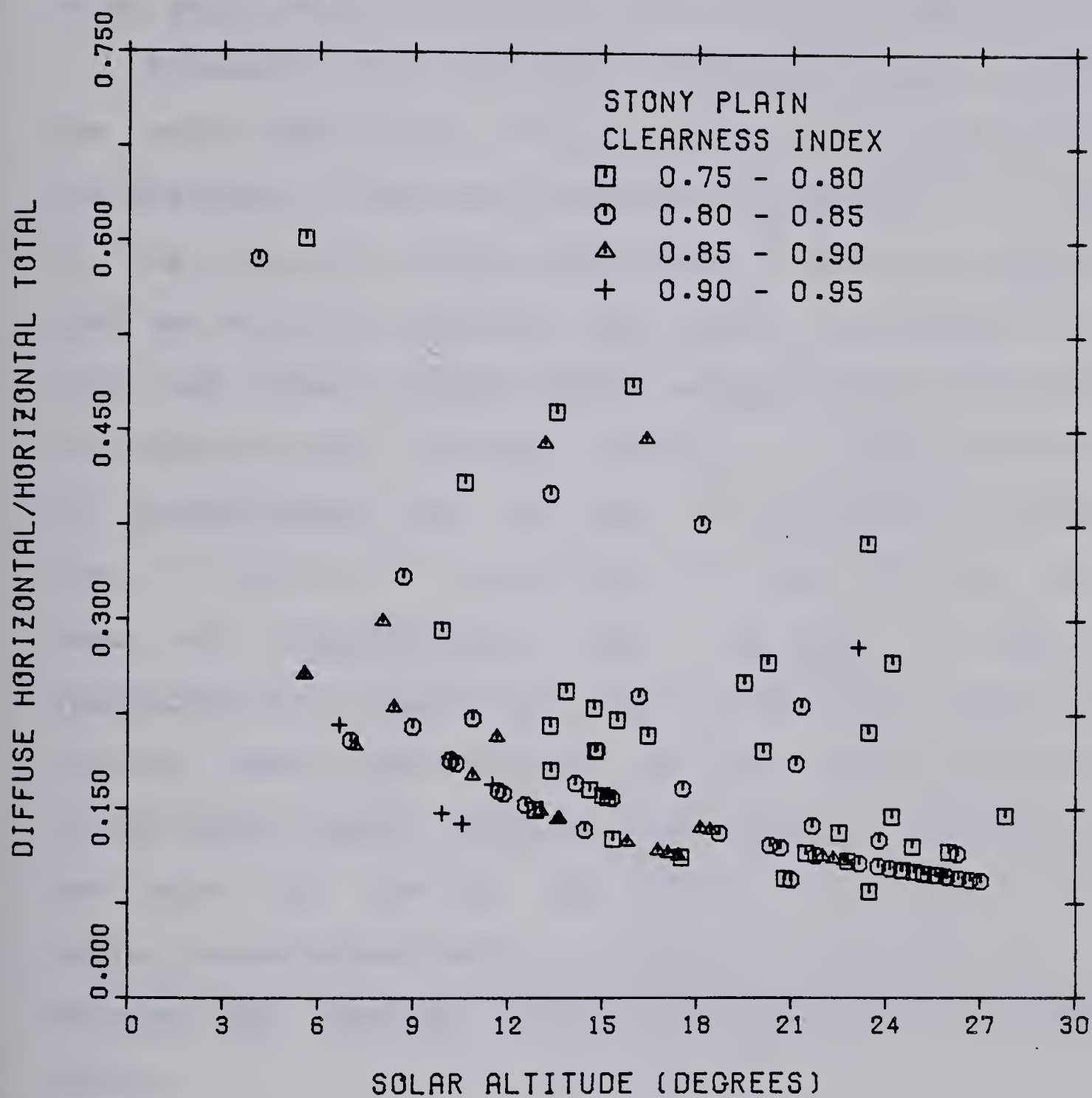


Figure 5.36 Ratio of diffuse horizontal to horizontal total for various sun altitudes



decided to use the measured vertical radiation for calculating the solar heat gains through the window. However, The sol-air temperatures were calculated using the solar gains model developed in the previous study [14].

Proceeding with the last of the criteria for verifying the solar gains model, it can be seen from Figure 5.37 that the predicted transmitted component (predicted-1 in figure) of the radiation through the window is about 8% higher than that was actually measured. This can be attributed to the dust and other surface layers on the glass which decrease its transmittance. Clearly, one has to be aware of the loss of transmittance due to such ever persisting problem of dust. In Figure 5.37, the effects of dust, dirt etc, on the loss of transmittance were adjusted in the model (predicted-2 in figure) by using an equivalent clear double glazing having approximately the same transmittance as that of the insitu double glazing. This approach although does not take into account the effects of air mass at low sun angles, nonetheless tends to keep the transmissivity curve between the expected theoretical maximum and the measured value.

The uncertainties in the prediction of solar gains through windows are expected to introduce some error in the calculation of hourly house heat requirements. The magnitude of the error itself can be determined. This will be discussed in the following chapter.



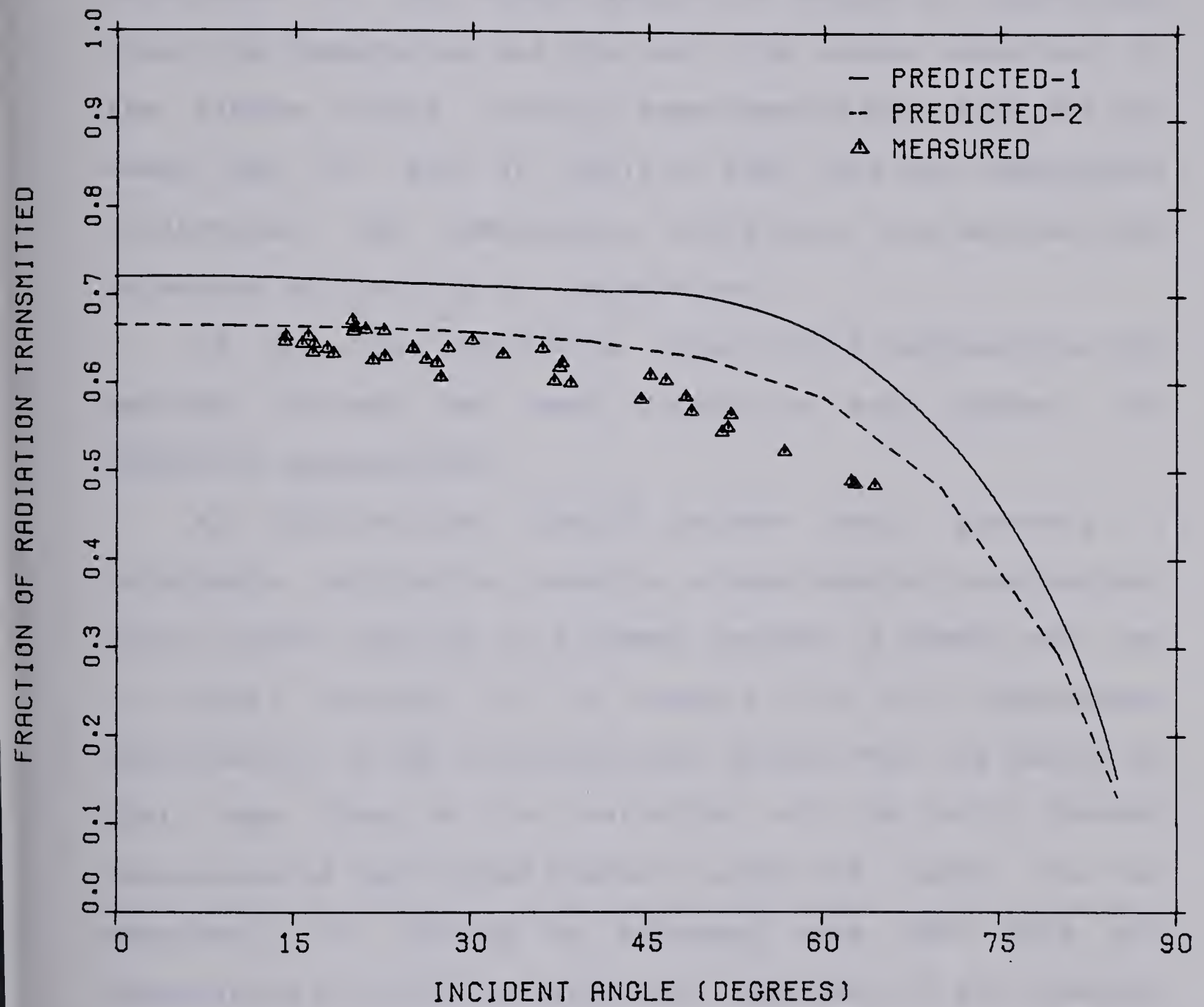


Figure 5.37 Transmissivity of insitu double glass



## 5.5 Window Shutters

To draw some guide lines in correctly modeling the window shutter combination several measurements were undertaken on the window shutter of module 3. Figure 5.38 shows the temperature and the heat flux sensor locations in the window shutter cavity. Measurements were made for two weeks (Jan. 29 - Feb. 10, 1981) of heat flux and temperature differences. The temperature difference was defined with reference to the room air temperature.

Of the two weeks data, three nights representing the maximum, minimum and mean conditions were chosen for graphical presentation.

Air infiltration around shutter seal presents a formidable problem for modeling window-shutter combination. Since shutter sealing is a common concern, a simple and yet a logical strategy is to measure the air temperature distribution in the window-shutter cavity over its height so that some idea of the variation of the insitu thermal resistance of the window shutters along its height can be obtained. It should be stressed here that this air temperature distribution gives the magnitude of the combined effects of air infiltration and as well as the temperature difference.

Figure 5.39 shows the quasi-steady variation of temperature difference (between the air temperature in shutter cavity and the inside room temperature) over the window height. This temperature distribution is a complex



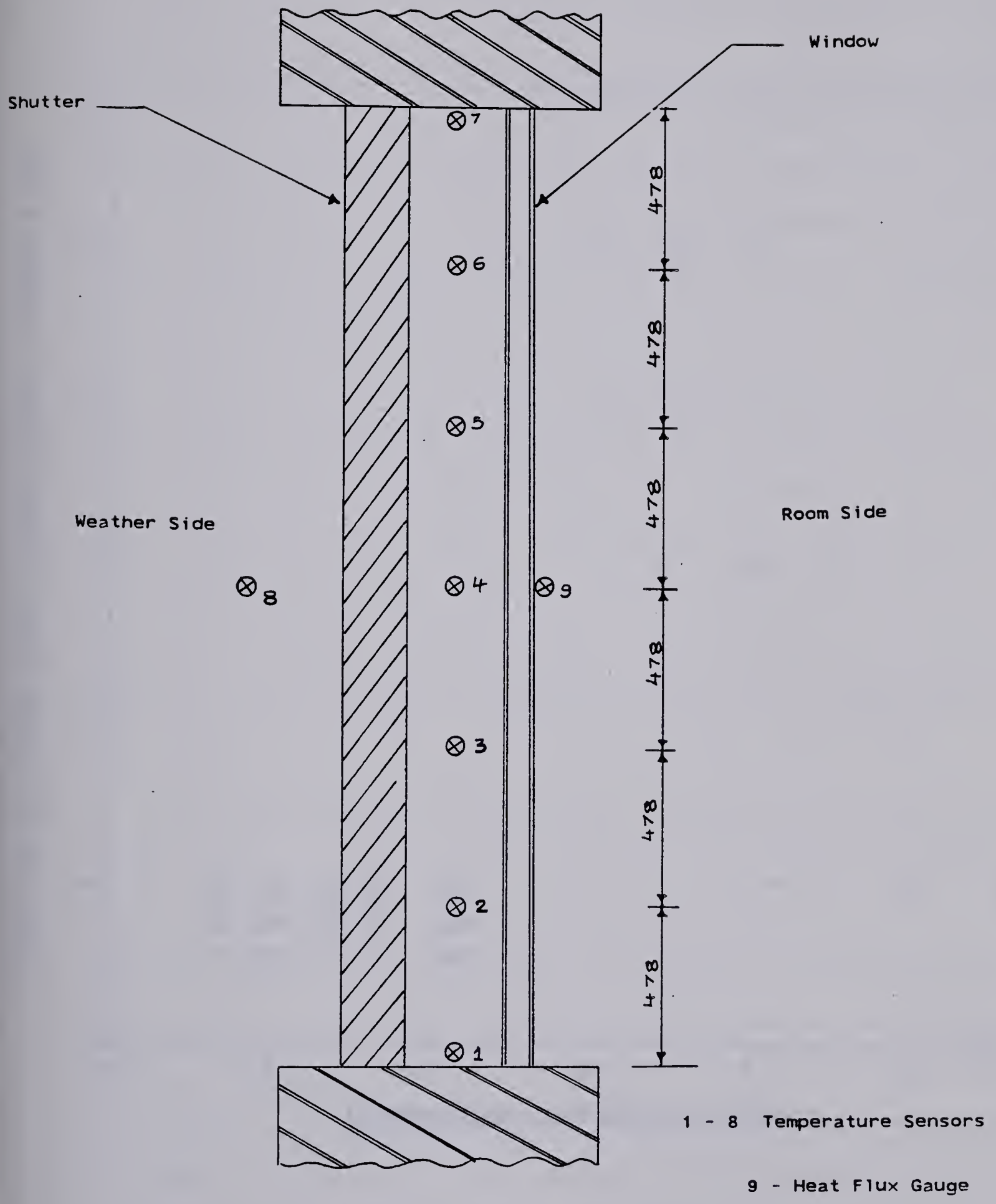


Figure 5.38 Sensor locations in window shutter cavity



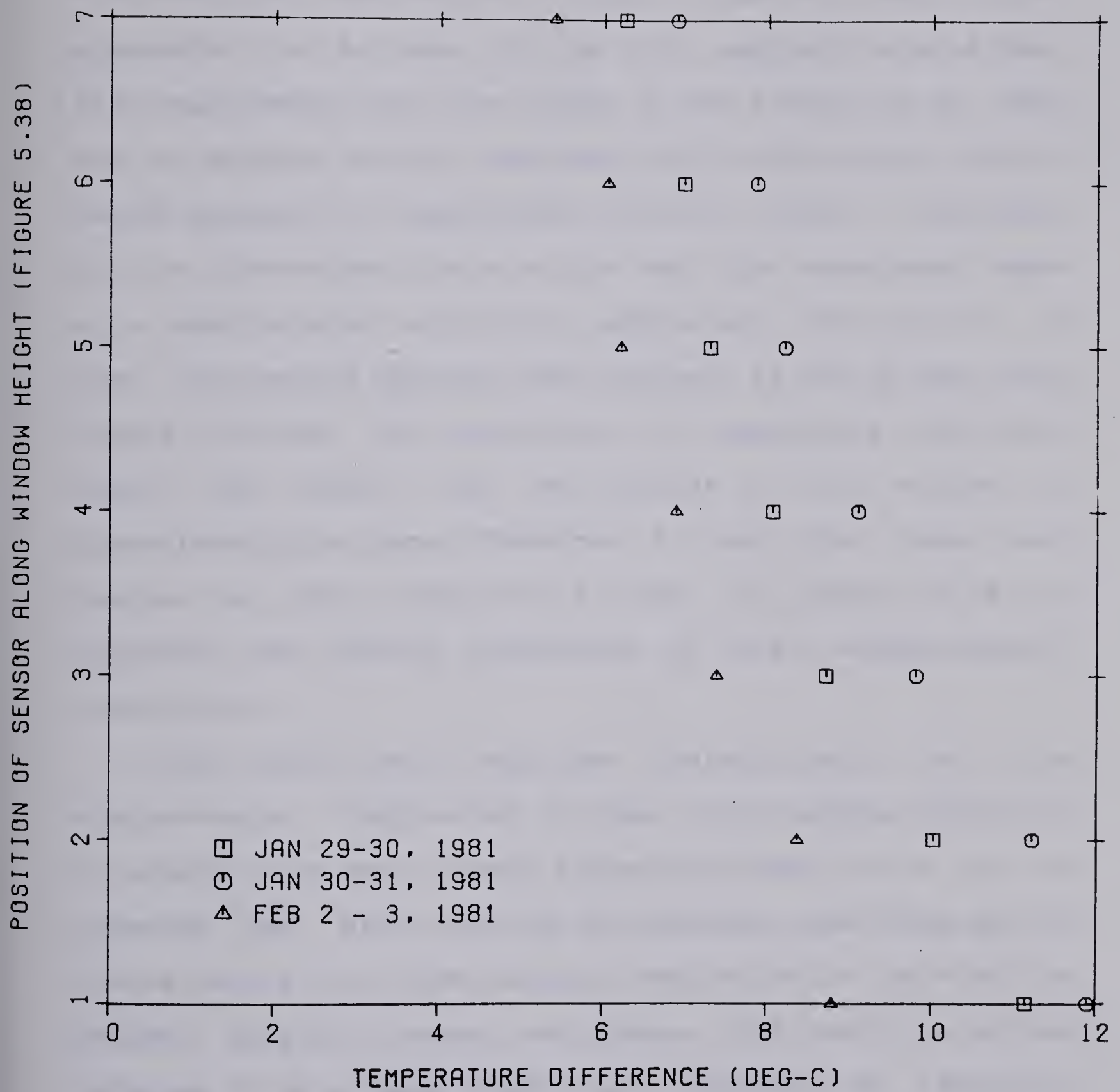


Figure 5.39 Temperature difference between the shutter cavity and the room temperature along the window height



function of convective and infiltrative fields.

To determine an average thermal resistance of the window-shutter combination in this situation one of two approaches can be taken. In the first approach several heat flux measurements over the height of the window can be made and an average overall resistance can be determined. In the second approach, an approximate overall thermal resistance can be determined from a single heat flux measurement made at a location about which the temperature distribution is even. The second approach was followed. It can be seen from Figure 5.39 that the magnitude of temperature variation above and below the mid height of the window is approximately the same. Therefore, a heat flux gauge was mounted at this location as shown in Figure 5.38 to determine an average resistance of the window-shutter combination.

The second most important characteristic of the window-shutter combination is their time response behaviour in establishing quasi-steady state conditions. It is to be expected that after closing the shutters, some time has to elapse before the window-shutter combination can provide its maximum possible thermal resistance. This condition can be referred to as a quasi steady state condition. To establish the time response of the window-shutter combination, the temperature difference between the air in the shutter cavity and the room is plotted as a function of the time elapsed after closing of the shutter. It can be seen from Figure



5.40 that about 3-4 hours may be required before quasi-steady state conditions can be established.

The impact of transient behaviour of window-shutters in terms of its thermal resistance is shown in Figure 5.41. Relatively large scatter in the data is caused by room temperature variations that occur during the furnace cycle. These temperature variations even though small, the heat flux gauges amplify them. It can be seen from Figure 5.41 that the effective shutter R value varies by as much as 30% depending on temperature difference and wind velocity. These results show a resistance value of RSI 0.3 for windows with shutters open and an average value of RSI 1.5 with shutters closed. The expected value with shutter closed is RSI 2.30. That is the effective steady state R value of the window shutter combination is about 35% less than the theoretical.

The impact of the transient nature of the window-shutter thermal resistance could be important on the hourly heating load calculations. This is because of the fact that the window losses represent a significant portion of the total loss [54]. Here it is desired to be stressed that in nearly all of the simulation studies for heating loading calculations, the transient behavior of window shutters is often ignored and the assumption of 'perfect' shutters is invariably used. The above analysis demonstrate that such an assumption is likely to introduce errors in the overall heat loss predictions. The magnitude of the error itself can be established. A discussion on the probable



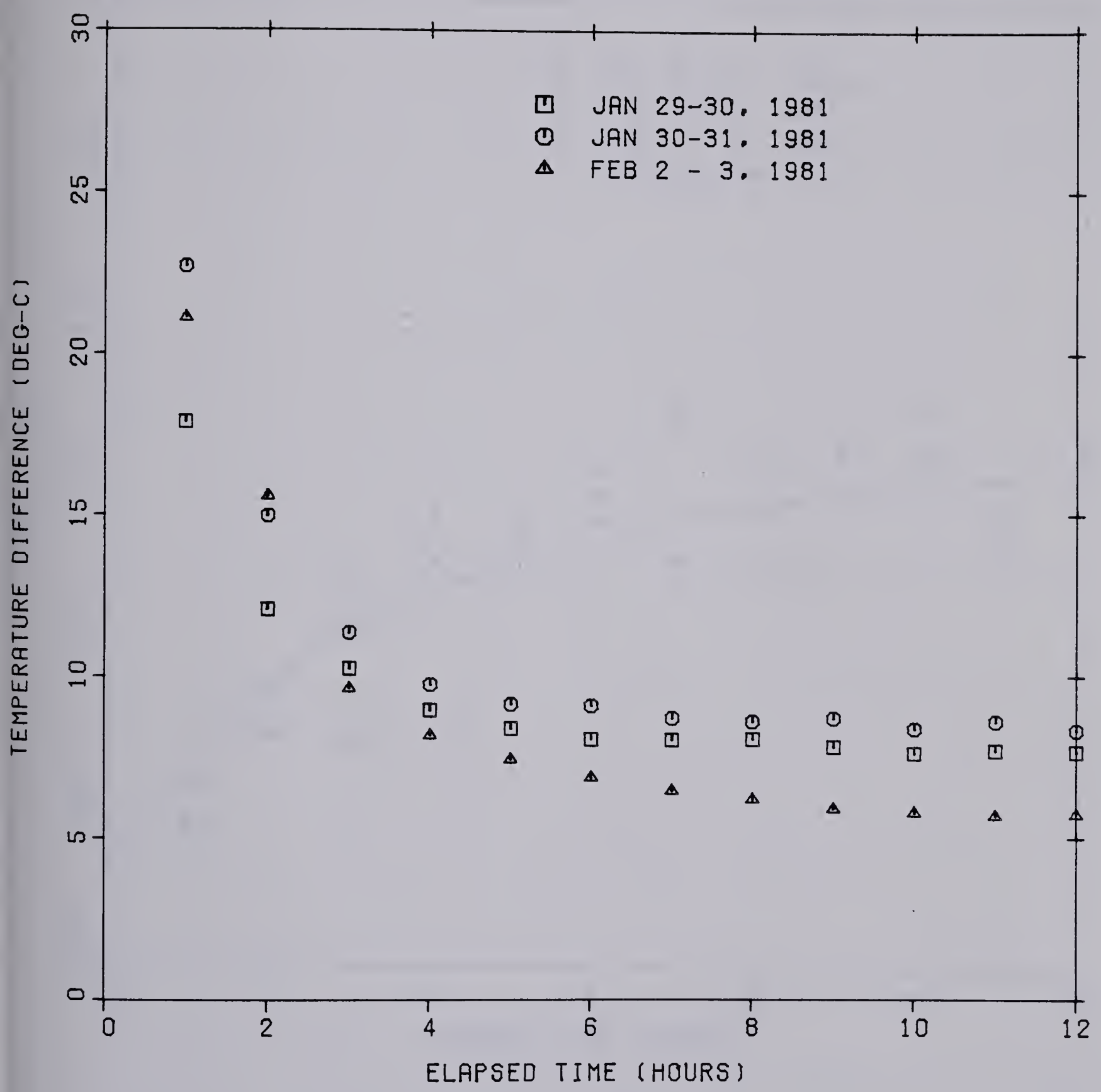


Figure 5.40 Change in air temperature inside shutter cavity after shutter is closed



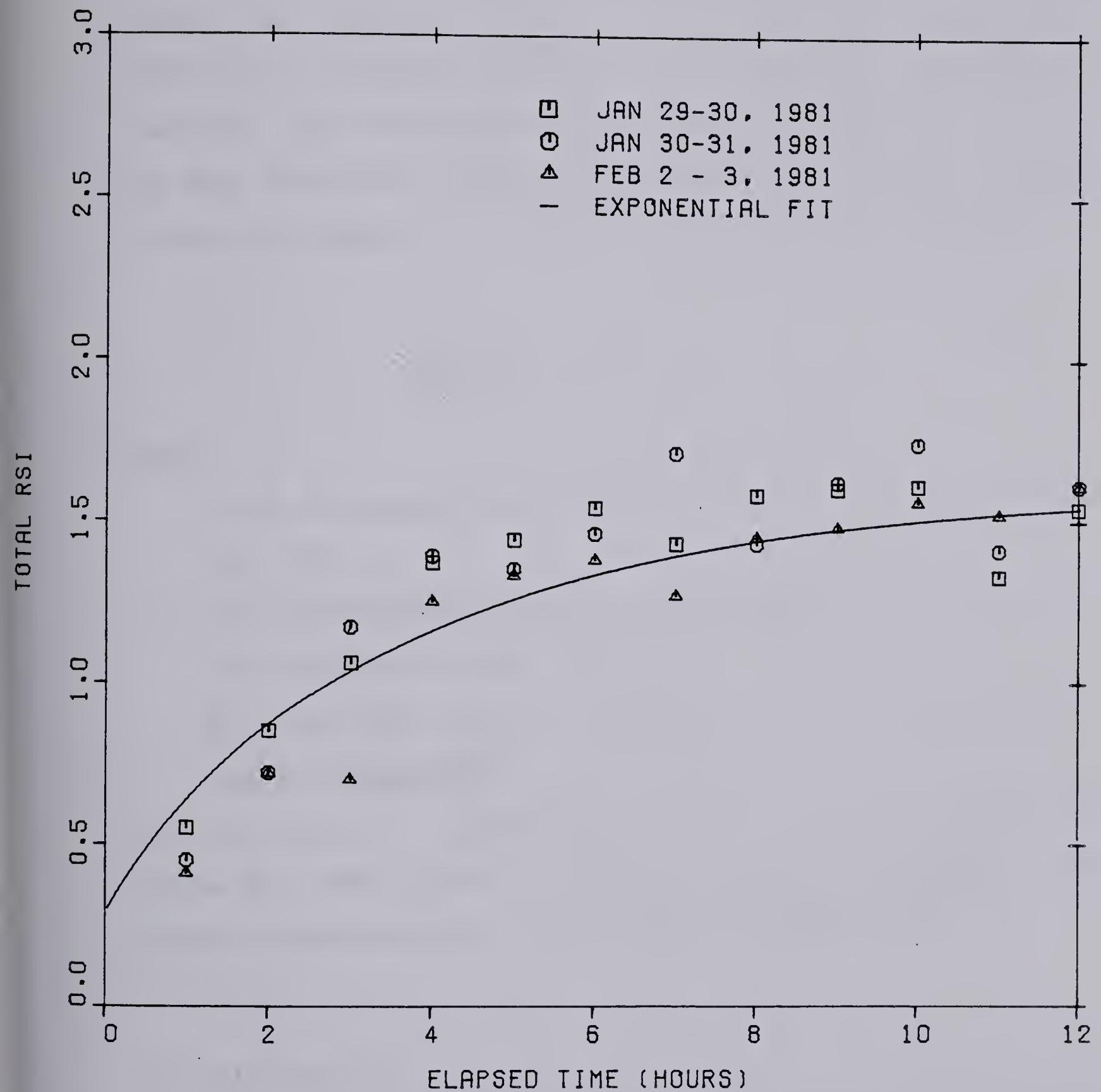


Figure 5.41 Change in measured resistance value of the window shutters after shutter is closed



errors will be taken up in the following chapter.

From these observations it is believed that until the problem of shutter seals is rectified any theoretical modeling of window shutters will not be meaningful. Therefore for the present investigation an empirical fit to the data would be a logical step. With this in view a simple correlating equation of the following form was attempted:

$$\frac{R - R_o}{\bar{R}_s - R_o} = 1 - e^{-\beta t} \quad (5.9)$$

Where

$R_o$  is the measured  $R$  value for the window with shutters open (RSI 0.3)

$R_s$  is the measured average quasi-steady state  $R$  value with shutters closed. (RSI 1.5)

$\beta$  is the time constant parameter of the window shutter combination( $\text{hours}^{-1}$ )

With  $\beta$  equal to approximately 0.25, it can be seen from Figure 5.41 that Equation 5.9 can be used to represent the present window shutter  $R$  value quite satisfactorily.

## 5.6 Infiltration

The typical infiltration rates for each module were arrived at from the results of a separate experimental study performed on the modules [56]. This experimental technique, known as the tracer gas technique, consisted of injecting



SF6 tracer gas into the return air duct of the electrical furnace until the concentration reached about 5 ppm. The circulating fan on the furnace was operated continuously. With the use of a Wilkes Miran 1A infra-red spectrometer the concentration time profile was plotted on a strip chart recorder. The experiment was conducted for a period of three weeks during which time the typical weather conditions were:

Out door temperature                      -10°C to -20°C

Wind speed                                      3 to 6 m/s

Assuming a perfect mixing, the air change rates of the modules were calculated from the following equation.

$$C = C_0 e^{-\gamma(\Delta t)} \quad (5.10)$$

Where  $C_0$  and  $C$  are the initial and final concentrations over a time interval of  $\Delta t$ .

$\gamma$ , is the air change rate.

Table 5.2 summarizes the typical average infiltration rates obtained from this study. These values were used in the main simulation model. This approach implies that the infiltration rates were considered as weather independent. Consequences of this assumption can only be evaluated either from theoretical models or from experimental studies.

A review of the literature suggests that there are yet no general theoretical models available which could relate the infiltration rates with the weather parameters. However, the trend now is to measure the leakage characteristics of



Table 5.2 A summary of the measured air infiltration rates  
for the modules

Module	Air changes per hour
1	0.50
2	0.50
3	0.10
4	0.30
5	0.40
6	0.40



the enclosures and apply physical principles in order to compute the air flows through the openings [92,93,94,95,96,97,98]. Two common methods used are: tracer gas techniques [93,94,97] and pressurization tests [95,96]. It should however be emphasized that application of these methods would require that an actual experiment be carried out to determine the empirical constants that correlate infiltration rate with the weather parameters. Currently, a parallel study is under way at the University of Alberta to determine such correlation constants for these modules [99].

Although speculative, it appears that the errors resulting in the heating load calculations due to the assumption of constant infiltration rates would be small for large values of time. This is because of the fact that the fluctuations in infiltration rates would average out on a large time period. However, the impact of the uncertainties in the magnitudes of the infiltration rates on the hourly heating requirements of the modules can be studied in a very simplified way. This discussion will be continued later in Chapter 6.

## 5.7 Transient Response

The next step in the verification of the simulation model was to check its time response characteristics as a whole where all of the previous component models are involved. Conceptually, this is the last of the tests to see



if the compounding of the different elemental models is properly done. From heat transfer considerations this means verification of the time constant of the structure which consists of materials having different heat capacities with different degrees of nonhomogeneity. Since the theoretical models use equations valid strictly for homogeneous materials, this limitation can be overcome by introducing the effects of nonhomogeneity of the structure into the model from the results obtained from the transient decay tests.

To verify the transient behaviour of the main simulation model, it would be advantageous to first work with a simplified version of the house model developed with an idea of verifying the three major parameters namely: the steady state UA value, the distributed capacity and the lumped capacity of the overall structure. Once the range of these parameters are established from the decay curves, they can be transformed to the main simulation model to check for its time response characteristics.

It is desired to be stressed here that of the three parameters, the steady state UA value and the distributed heat capacity of the modules are known to a greater degree of accuracy. However, the actual heat capacity contributions made by the wood and the dry wall in the structure are uncertain to assess. Therefore, one way of extracting this parameter will be to perform the transient temperature decay tests.



Following this approach, the predicted and the measured decay curves for modules 2, 3, 4 and 5 are plotted in Figure 5.42. It can be seen that to a fair degree of accuracy the model described in section 4.6 can be used to predict the transient temperature decay characteristics of a structure. A small variation after the hours 7 and 8 is presumably due to the assumption of constant heat transfer coefficient used in the model. Since the heat transfer coefficient is also a function of temperature difference it is reasonable to expect that during the decay tests, due to decreasing temperature difference, the heat transfer coefficient would decrease as well. Since the above assumption of constant heat transfer coefficient gives quite satisfactory results no attempts were made to introduce variable heat transfer coefficient in the model.

The general implication of the above result is of significant value. Generally it has been thought that basement walls do not contribute significantly to the thermal mass of a house. There has been a good deal of controversy and very little data related to this matter. From the present tests it is apparent that basement contributes to the thermal mass of these modules. This is evident from the decay curves in Figure 5.42 not being linear on a semi-log plot since the basement walls cannot be considered as simple lumped masses at a uniform temperature.

From the results of several transient temperature decay curves on these modules certain guide lines in selecting the



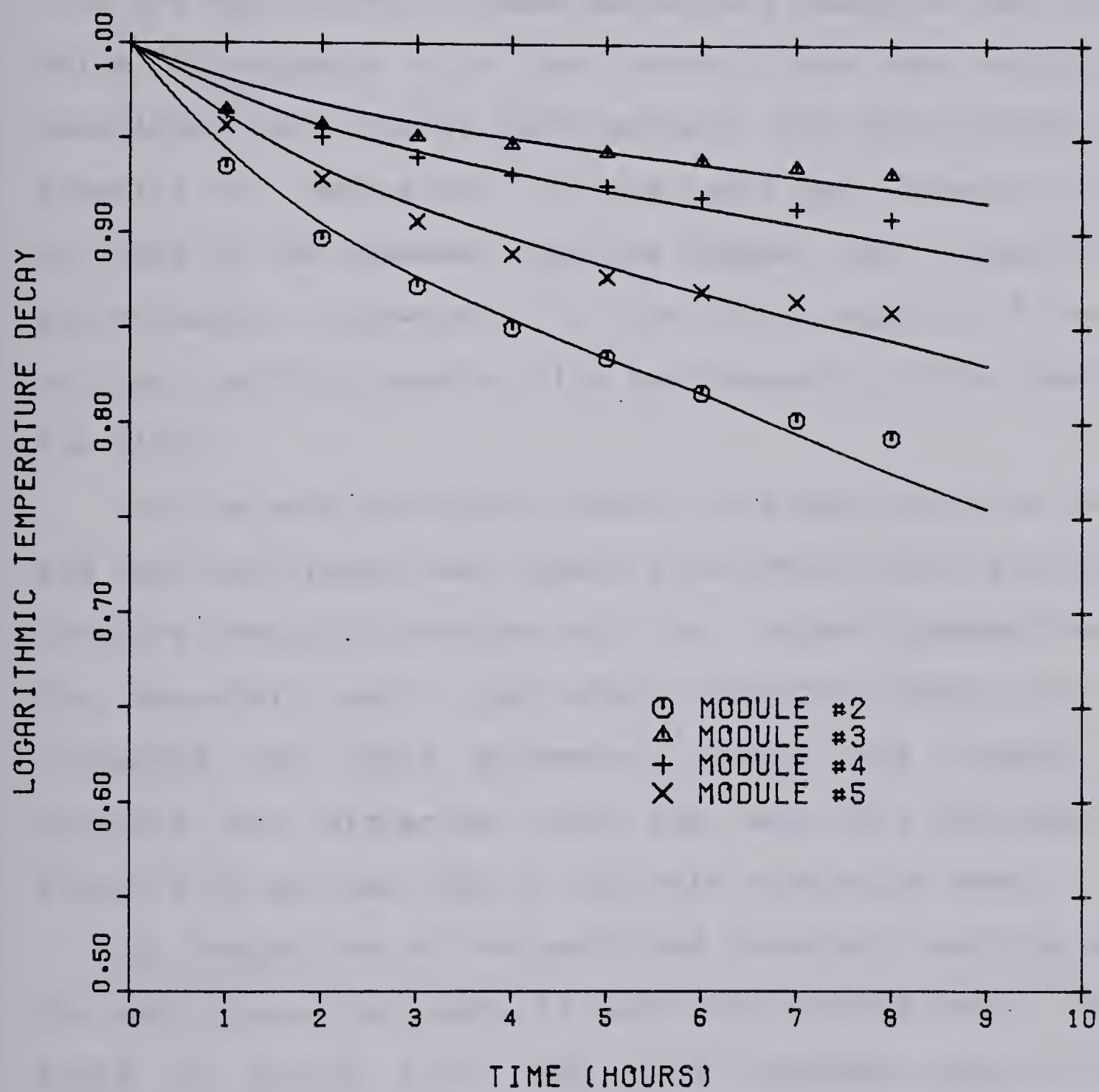


Figure 5.42 Transient response of the modules



heat capacity parameters of these modules were arrived at. These guide lines will in general be applicable to residential houses with a heated basement. An examination into the magnitudes of these parameters suggests that the UA value corresponds with the overall heat loss coefficient calculated using steady state methods. The distributed heat capacity is equivalent to the total heat capacity of the concrete in the basement, and the lumped heat capacity is approximately equivalent to the heat capacity of the dry wall and ceiling together with heat capacity of the wood in the floor.

In the main simulation model the steady state UA value and the distributed heat capacity parameters were calculated from the overall dimensions and the thermal properties of the materials used in the module, therefore these were left unchanged. The third parameter, namely the lumped heat capacity was extracted from the best fits obtained from Figure 5.42 and was used in the main simulation model.

A comparison of the predicted transient response using the main simulation model is made with another set of decay tests in Figure 5.43. The good agreement shown in this figure indicates that the uncertainties involved due to such factors as nonhomogeneity of materials and the heat capacity effects of the wood in the structure can be largely overcome with a simple strategy such as performing transient temperature decay tests.



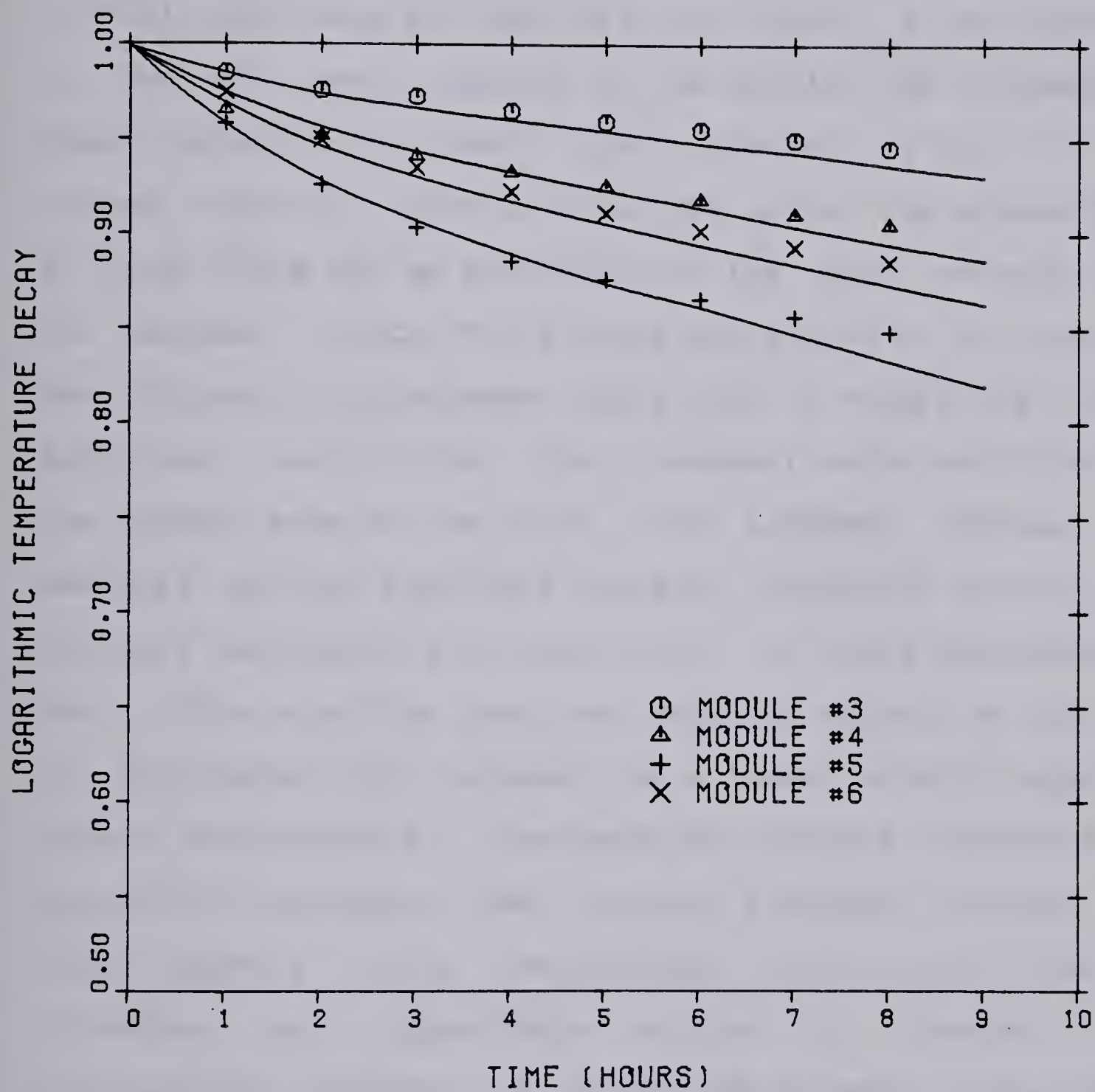


Figure 5.43 Transient response of the modules



Some observations can be made from Figure 5.43. As suggested in reference [29], there appears to be three probable regions of differing slopes in these figures. The initial rapid drop for the first two hours is attributable to the air heat capacity in the module. The intermediate decay resulting in a short time constant is due to the lumped capacity effects of the dry walls. The slower decay at large times can be attributed to the heat release from the basement walls. The diurnal variations in the measured heat fluxes to the basement walls seen in Figure 5.44 is an additional verification that basement walls contribute to the thermal mass of the house. The agreement between the measured and the predicted transient behaviour is still not entirely satisfactory in the initial two hours for modules 3 and 4. This signifies that heat capacity effects of the room air introduced into the model via a lumped capacity approach cannot satisfactorily represent the complex convective and radiative interplay of heat transfer processes. However, the error appears to be insignificant and is not likely to introduce any appreciable errors in heating load calculations. However, a study can be made of the errors resulting in the overall heating load calculations due to a change in the magnitudes of the lumped and the distributed heat capacities. This discussion will be later followed up in Chapter 6.



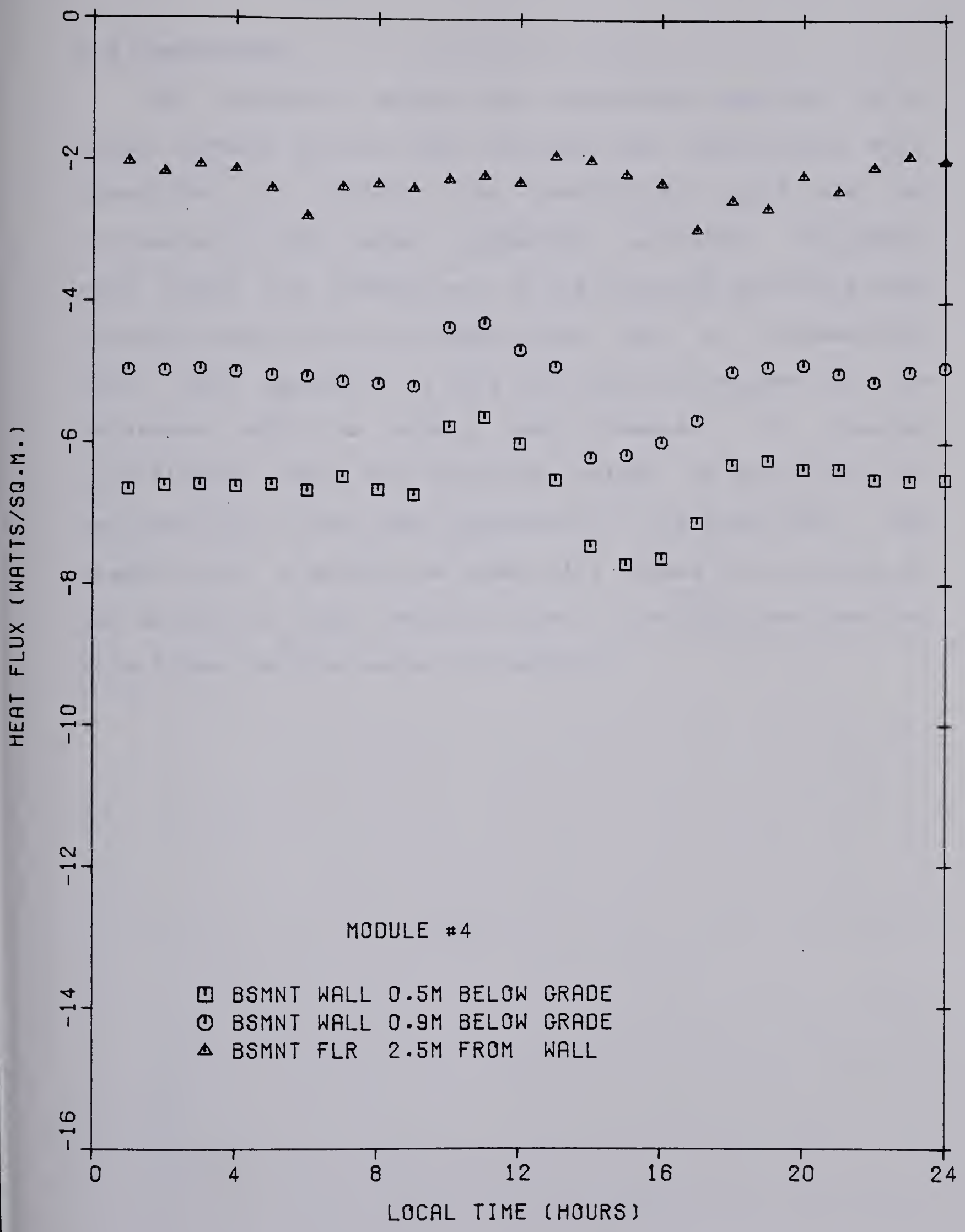


Figure 5.44 Diurnal input heat flux to the basement walls



## 5.8 Conclusions

The component models were extensively analyzed. In so doing, several factors that influence the predictions were identified. In addition the predictions could also be influenced by the thermal properties selected. Throughout this study the properties of the building materials were directly taken from the ASHRAE Hand Book of Fundamentals [55]. This approach is very much desired because this the reference which is widely used. However, of greater significance than the absolute values is the effects of perturbations in the input parameters on the house heat loss predictions. A parametric study will indeed give an idea of the effects of these uncertainties on the predicted results. This forms the discussion of Chapter 6.



## 6. PARAMETRIC STUDY

### 6.1 Introduction

In Chapter 5, the component models were tested and analyzed. As a result of the analysis, it was possible to show that several factors could affect the house heat requirement calculations. However, it is now of interest to carry out a parametric study to determine the impact of such uncertainties on the predictions. The errors in predictions could result either from the modeling techniques or the thermal property data employed in the calculations. In either case, what is required may be an example illustrating the relative importance of the parameters influencing the predictions.

With this in view, a numerical experiment was carried out on one of the modules (module 3). The first step was to put together the component models. A rationale for the choice of the component models was drawn from the analysis of chapter 5, in that the following models were integrated for predicting the module heat requirements.

1. Steady state model for the walls and ceiling. Their transient analysis was included via a lumped capacity approach.
2. Basement first model was used.
3. The solar gains model [14] was employed for calculating the sol-air temperature effects whereas, the measured



vertical radiation data was used for predicting the solar gains through the window. The loss of transmittance due to surface layers was accounted for.

4. The empirical equation developed for the window shutter thermal resistance was used.
5. Measured air infiltration rates were used.
6. The overall thermal analysis were based on the transient response model described in section 4.7.

The second step was to let the parameters take a range of values and to examine their effects on the module heat requirements. The choice of parameters and their probable range of variations were arrived at from the experimental observations and simulation results. Three types of simulation runs were taken for evaluating the effect of each of the parameters. The first run referred to as TYPE-P was obtained from the model with the above referred component models included in it. For this run the thermal property data given in the ASHRAE Hand Book of Fundamentals [55] was used. The second run referred to as TYPE-P PLUS was obtained by allowing the parameter under investigation to take a positive range of values. The third run, TYPE-P MINUS, corresponds to the case with a negative range of values. The results of TYPE-P PLUS and TYPE-P MINUS were compared with TYPE-P. To be consistent with the previous chapter, the numerical experiment involving the following parametric changes was performed.

1. Effect of variations in wall and ceiling resistances.



2. Effect of the soil thermal properties.
3. Influence of solar gain predictive techniques.
4. Effect of thermal shutter resistance.
5. Errors due to fluctuations in infiltration rates.
6. Influence of thermal capacity.

It is desired to be stressed here that the results of the above parametric study should not be taken as general. These are as a result of a specific example and are intended to show the relative importance of certain parameters influencing the house heat requirements.

## 6.2 Effect of Variations in Wall and Ceiling Resistances

Figure 6.1 shows the variations in the typical diurnal module heat requirements due to a change in the resistance value of the walls by  $\pm 20\%$ . It can be seen from the figure that an error of  $\pm 20\%$  in the resistance level of the walls causes less than 7% change in the module heat requirements. Apparently this is because of the fact that this module has highly insulated walls and that wall losses represent a small fraction of the total loss.

## 6.3 Effect of the Soil Thermal Properties

Figure 6.1 shows the effects of variations in the soil conductivity on the module heat requirements. The soil conductivity was allowed to vary over a range of  $\pm 50\%$ . It is apparent from the figure that the module heat requirements



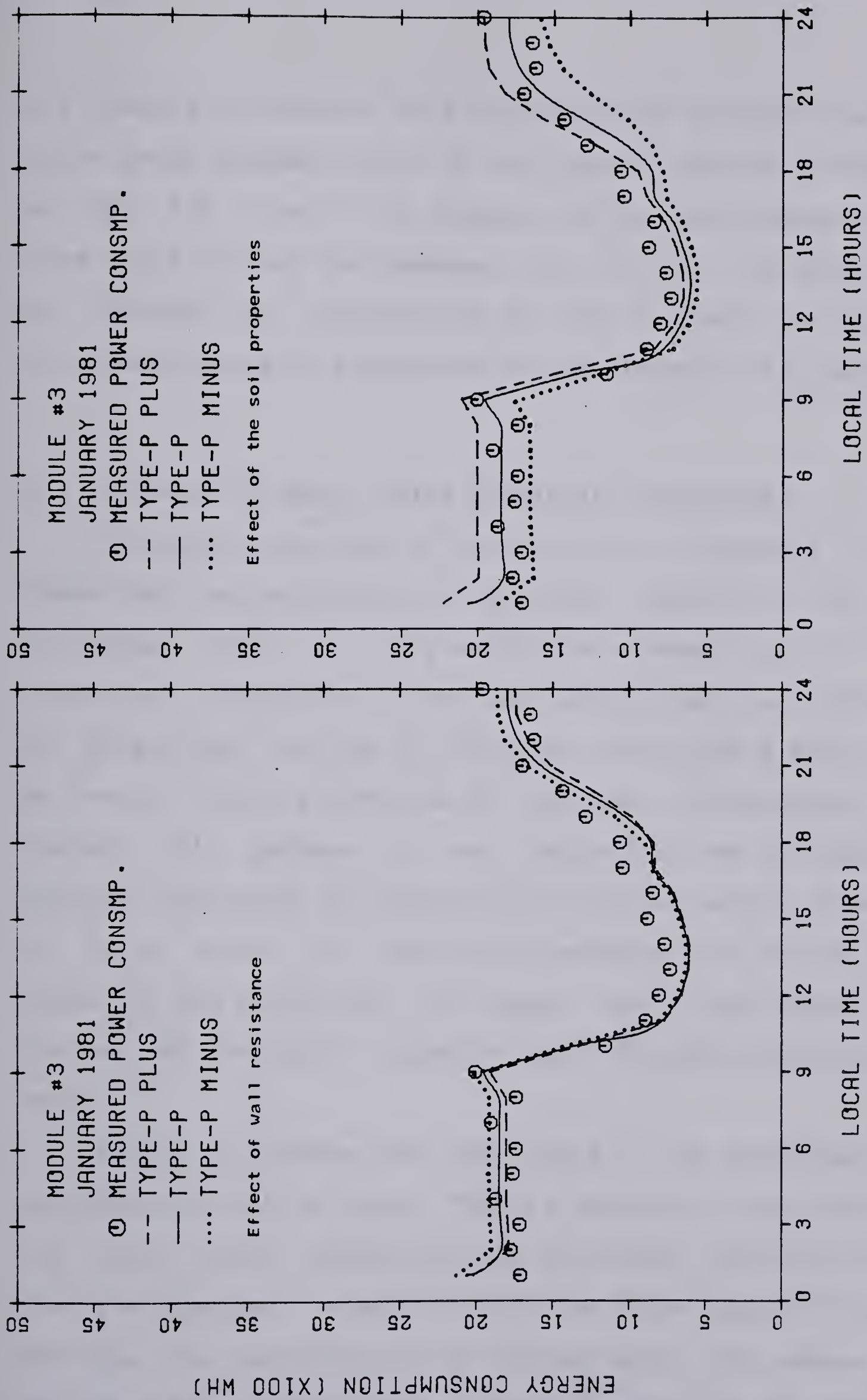


Figure 6.1 Effect of wall resistance and the soil properties  
on module 3 heat requirements



are greatly influenced. This is inspite of the fact that the below grade basement walls in this module have an insulation of RSI 3.5. One of the reasons for the high basement heat loss could be that the basement floor is not insulated and an increase in conductivity by  $\pm 50\%$  is likely to increase this loss almost in proportion to the conductivity changes.

#### 6.4 Influence of Solar Gains Predictive Techniques

During the analysis of solar gains in Chapter 5, it was shown that the calculation of vertical radiation from the horizontal total is very sensitive to modeling of diffuse radiation. In addition it was speculated that the influence of anisotropic nature of reflected light from a snow cover at low sun angles might also be important. Consequently, to elevate this problem it was decided to use the measured vertical radiation for predicting the solar gains. However, it is a matter of interest to examine what errors would result in the prediction of module heat requirements if instead of vertical radiation data the horizontal data is used.

Figure 6.2 shows that the errors in the predicted heat requirements will be large. This is because of the fact that the solar gains predicted from horizontal total are lower than the measured. In addition the low solar gains will also decrease the contributions of thermal mass. The reasons for the lower than expected solar gains appear to be due to



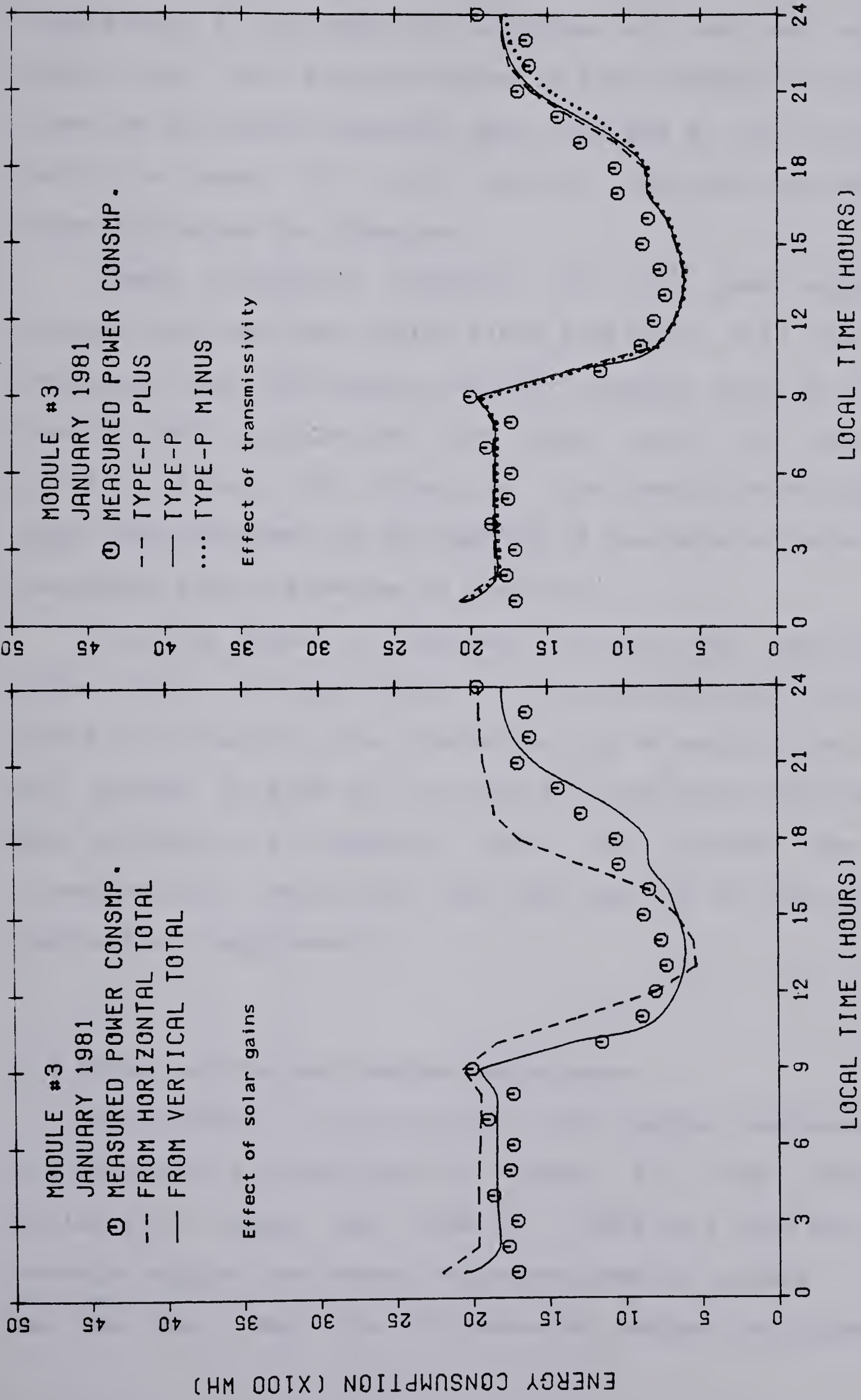


Figure 6.2 Effect of solar gains and transmissivity on module 3 heat requirements



sensitivity of the modeling techniques at low sun angles. Apart from this another source of error seems to resulting from the horizontal radiation data recorded at the facility which is about 15 to 20 percent less than the average expected values for Edmonton.

These arguments together with the good agreement between the predicted (solid lines in figure 6.2) and the measured heat requirements strongly suggest that for hourly heating load calculations the solar gains be based on vertical total. For otherwise, the prediction of passive solar contributions to the heating of the modules cannot be evaluated with any degree of certainty.

A second aspect of interest concerning the capture of solar gains through windows is the transmittance of window glass. In Figure 6.2 the transmissivity of each of the glass was varied by  $\pm 20\%$  and its effect on the heat requirements was plotted. It appears that the errors due to transmissivity variations are less than 3% in terms of the module heat requirements.

### 6.5 Effect of Thermal Shutter Resistance

The effect of variations in the thermal resistance of the shutters is illustrated in Figure 6.3. The range of variability chosen was from a + 200% to a -25% over the average shutter resistance value measured on module 3. It can be seen that the influence of shutter resistance is



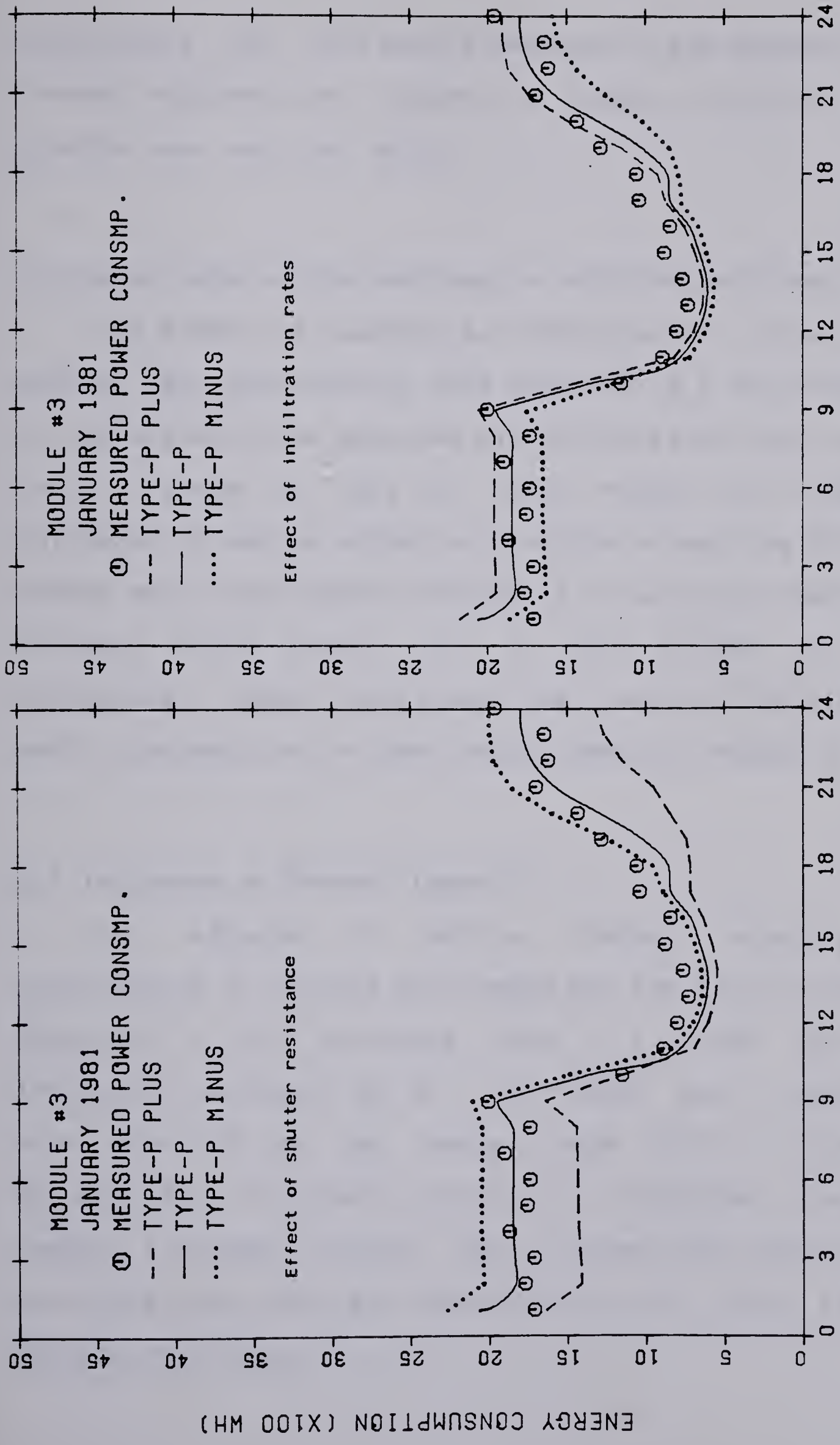


Figure 6.3 effect of shutter resistance and infiltration rate on module 3 heat requirements



significant for this module because in the absence of good thermal shutters the windows in highly insulated houses provide near zero net gains.

#### 6.6 Errors due to Fluctuations in Infiltration Rates

The effect of changing air infiltration rates on the module heat requirements were examined in a very simplified way by allowing the measured air infiltration rates to vary over a range of +30% to -50%. Figure 6.3 shows that influence of such a variation could be as much as 20% on the module heat requirements. Though it is unlikely that such an increase would prevail for a large period of time, nonetheless, these curves show the limits of the effects of such transients on the heat requirements of module 3.

#### 6.7 Influence of Thermal Capacity

The effects of module thermal capacity were investigated by varying the lumped and the distributed heat capacity in the structure from 0 to 100%. The results indicated that about 16% of the module heat requirements were provided by the thermal mass during the month of January 1981. It should, however, be recognized that this number increases rapidly due to large solar gains and low heat loss rates that are representative of early and late winter conditions.



## 6.8 Conclusions

Figures 6.1 through 6.3 give an impact of the variations in the input parameters on module 3 heat requirements. It is to be noted that the behaviour of these curves to changing input has to be read together with the range of variability chosen. A summary of the results of the parametric changes discussed thus far are listed in Table 6.1. These results give the relative importance of the parameters influencing the module 3 heat requirements for the mid winter conditions. The effect of the parametric changes were compared with the reference case (TYPE-P) and were expressed as the ratio of the difference in heat requirements caused by the change in the parameter to the heat requirements with no change. This ratio is referred to as an influence factor in Table 6.1.

In order of importance therefore it appears that the heat requirements of module 3 are influenced by thermal shutter resistance, the soil thermal conductivity, infiltration rate, thermal capacity, wall resistances etc. Depending upon the thermal resistance and capacitance combinations in the structure, the order of these parameters may change. In this regard an attempt was made to generalize the study so that the influence of several parameters of interest could be studied from a set of curves referred to as the general design curves. A brief discussion on this subject will be presented in Chapter 8.



Table 6.1 Summary of parametric study

Input parameter	Percent range	Influence factor
Shutter resistance	+200 to -25	0.337
Soil conductivity	+50 to -50	0.214
Infiltration rate	+30 to -50	0.183
Thermal capacity	+100 to -00	0.162
Wall resistance	+20 to -20	0.066
Ceiling resistance	+20 to -20	0.030
Transmissivity	+5 to -15	0.030



## 7. MODULE PERFORMANCE

### 7.1 Introduction

Various component models were developed and tested in Chapters 4 and 5. These models were put together to form a main simulation model. Using this main simulation model it is now of value to predict the module performance as a total system. The tests for these predictions from the main simulation model will be the module temperatures and most importantly the module heat requirements on hourly basis.

Apart from the module performance several results of interest will be presented. Some alternative methods of data analysis will also be discussed. With this in view, the organization of this chapter is divide into the following sections:

- 7.2 Solar gains from South facing windows.
- 7.3 Module performance.
- 7.4 Passive solar contributions.
- 7.5 Component heat losses.

### 7.2 Solar Gains From South Facing Windows

A topic of much current interest is solar heat gains through the south facing windows [100]. However, in heating load calculations net gains through the windows are of importance. The calculation procedure for net window gains from the measured horizontal insolation data was described



in [14]. The procedure is relatively straight forward provided, the magnitude of radiation incident on the window, the transmissivity and the thermal resistance of the window are known precisely. In section 5.3, methods for predicting the above three quantities were analyzed in parallel with the measured data.

It is now of value to present the net solar gains as a function of horizontal insolation in a graphical form. An examination into Figures 5.32 and 5.37 suggests that the most physically plausible technique for presenting net window gains is to explore the window-shutter characteristics. Consider for example an ideal window-shutter combination the equation describing the net window gains can be written as.

$$\text{Net Gains} = \text{SHG} - \text{Heat Losses.} \quad (7.1)$$

On a monthly basis

$$\int Q_{\text{net}} = \int \text{SHG} - \int Q_L \quad (7.2)$$

Comparing the heat losses to the heat gains,

$$1 + \frac{Q_{\text{net}}}{Q_L} = \frac{\text{SHG}}{Q_L} \quad (7.3)$$

This linear relationship is shown plotted in Figure 7.1. The difference is instead of SHG, the incident radiation on the window surface was chosen as an independent variable. The window gain factor (WGF) is defined here as:

$$\text{WGF} = \left( 1 + \frac{Q_{\text{net}}}{Q_L} \right) / \bar{\tau} \quad (7.4)$$



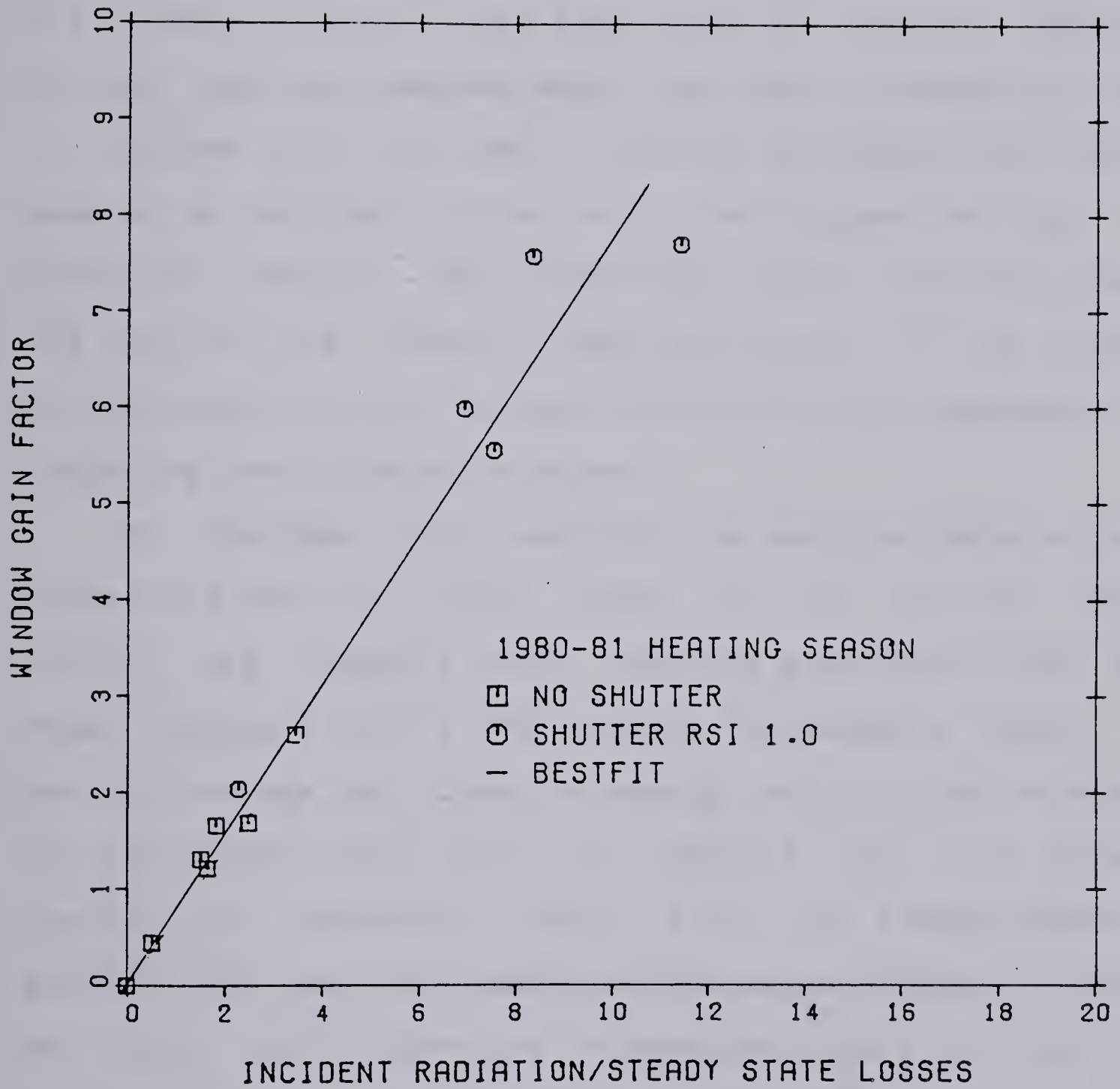


Figure 7.1 Window gain factors resulting from south facing windows



Where  $\bar{\tau}$  is the average transmissivity of the window.

Even though the assumption of an ideal shutter was made in generating results of Figure 7.1, it is reasonable to expect that on a long term basis, such as monthly averages, the linear relation will hold. What is, however, important is that from the measured data, the three correlations shown in Figures 5.32, 5.37 and 7.1 can be developed which can be used as an excellent criterion for testing and refining the predictive models. The window gain factor which represents the ratio of its thermal characteristics to its optical characteristics can be used as an efficiency parameter for comparing the different windows.

To conclude this section, the measured data on solar fluxes and the net window gains for the heating season 1980-81 are compared with readings and calculations from other sources [100,75]. The numbers indicated in Table 7.1 are the average net fluxes of energy per unit area of window for the months shown. First it appears that the present reading of horizontal total is on an average about 20 percent less than the reading at the meteorological station at Stony Plain. There are no measured totals on a vertical surface to compare with, however, the present measurements are roughly consistent with the predictions of Hay [75] and Barakat [100]. It will be noted that the solar gains measured for March and April 1981 were substantially below those predicted by Barakat. This is at least in part due to the fact that the window overhangs on the modules 3 and 4



Table 7.1 Calculated and measured heat fluxes

Month	Description	Hays' long term Avg.	Barakats' 70/71	Our Data 80/81
Nov.	1. Deg. days		850	574 (664)*
	2. Total Horizontal (W/Sq.m)	46	-	26.5
	3. Inv. vertical (W/Sq.m)	101	100	83
	4. Solar gain (W/Sq.m)		76	72
	5. Cond. losses (W/Sq.m)		86	55
	6. Net gain (W/Sq.m)		-10	17
Dec.	1.		1143	996 (1089)*
	2.	31	-	22.5
	3.	7	96	46
	4.		73	41
	5.		86	92
	6.		-10	-51
Jan.	1.		1142	730 (832)*
	2.	46	-	33.3
	3.	101	87	122
	4.		66	111
	5.		108	67
	6.		-42	44
Feb.	1.		769	683 (767)*
	2.	81	-	34.6
	3.	139	162	115
	4.		122	85
	5.		84	70
	6.		38	15
Mar.	1.		821	622 (715)*
	2.	144	-	89.4
	3.	179	228	142
	4.		168	96
	5.		83	57
	6.		85	39
Apr.	1.		447	425 (514)*
	2.	202	-	138
	3.	172	203	104
	4.		145	49
	5.		52	40
	6.		3	9



were designed to start cutting Sun out some time in March. One surprising result is that the highest net gain was recorded in January 1981. In fact on a long term average one would expect a net negative value. This gives some indication of weather variability from one year to the next and suggests that a number of years data may be necessary to arrive at average values for net window gains.

### 7.3 Module Performance

Before attempting to compare the predicted and the measured module performance, it is instructive to develop a method of data analysis. A natural choice would be to assess the module performance for small and large values of time. A rationale for this approach can be drawn from the physical nature of the problem. The physics of the problem such as the diurnal and annual climatic variations, suggest that the choice for small value of time should correspond to diurnal scale and that of the large value of time should correspond to yearly cycle.

An application of this concept allows the module performance to be investigated at two independent levels. The main simulation model developed in this study works exactly on this principle, i.e. calculating the parameters of interest over a small time interval and integrating these values for large values of time. However, the concept of working with large values of time alone can be used to



develop simple practical methods for heating load calculations.

Following the above approach, it is of interest to first analyze the measured module performance for large values of time. Undoubtedly, the module heat requirements can be taken as a direct measure of module performance. Table 7.2 summarizes the heating degree days, the energy consumption of the modules on the basis of monthly and heating season totals for the years 1980-81, 1981-82. First thing to note from the table is that the total heating degree days for the two consecutive years under consideration varied by about 15.5% with a maximum and minimum monthly variations of 36% and 0.5% respectively.

Note particularly that the maximum variation occurred in January 1981 and 1982. This observation suggests that a number of years data taking may be necessary to arrive at an average heating season performance in a climate as variable as of Edmonton.

Secondly, as a direct consequence of the concept of large values of time, it is possible to determine an average U factor (heat loss coefficient) for the modules, which can be defined as the ratio of cumulative heating requirements to cumulative heating degree days [15]. Following this approach, the overall U factor for the modules one through six obtained from the measured data are tabulated in Table 7.3. As an example Figure 7.2 shows the overall U factor for the modules 2 and 4.



Table 7.2 Summary of heating degree days and energy consumption for the modules during 1980-81 and 1981-82 heating season

Month	D. Days		Module (Energy consumption in KWH per month)					
	(21Deg. C base)		1	2	3	4	5	6+
Nov.	1. 80-81	644	2139	2753	1087**	1209**	2121	2149
	2. 81-82	665	1884	2505	804	908	2031	1656
Dec.	1.	1089	3519	4688	1693**	2690**	3611	4007
	2.	969	3052	3265	1146	1497	2940	2730
Jan.	1.	823	2603	3534	1055	1671	2851	2761
	2.	1305	4029	4626	1719**	2588**	3818	3933
Feb.	1.	767	2419	3353	1124	1618	2468	2675
	2.	982	2724	3786	1328*	1757*	2947	2695
Mar.	1.	715	1950	2700	896	1275	2177	1897
	2.	840	2293	3327	1196*	1746*	2680	1998
Apr.	1.	514	1534	2181	870	1150	1775	1358
	2.	649	1640	2374	887	1224	2154	1145
Total	1.	4572	14164	19209	6725	9613	15003	14847
	2.	5410	15622	19883	7080	9720	16570	14157

\* Shutters were closed during the day and as well as the night

\*\* Shutters were open during the day as well as the night

+ Active air system.



Table 7.3 Comparison of the measured and predicted overall U factors for the modules

Module	Heat loss coefficient (W/°C)			Measured relative heat loss coefficients
	Steady state calculations*	Measured	% Error	
1	172	130	24	0.722
2	222	180	9	1.00
3	61	58	5	0.334
4	120	95	21	0.527
5	149	145	3	0.805
6	154	140	9	0.777

\* Reference (15)



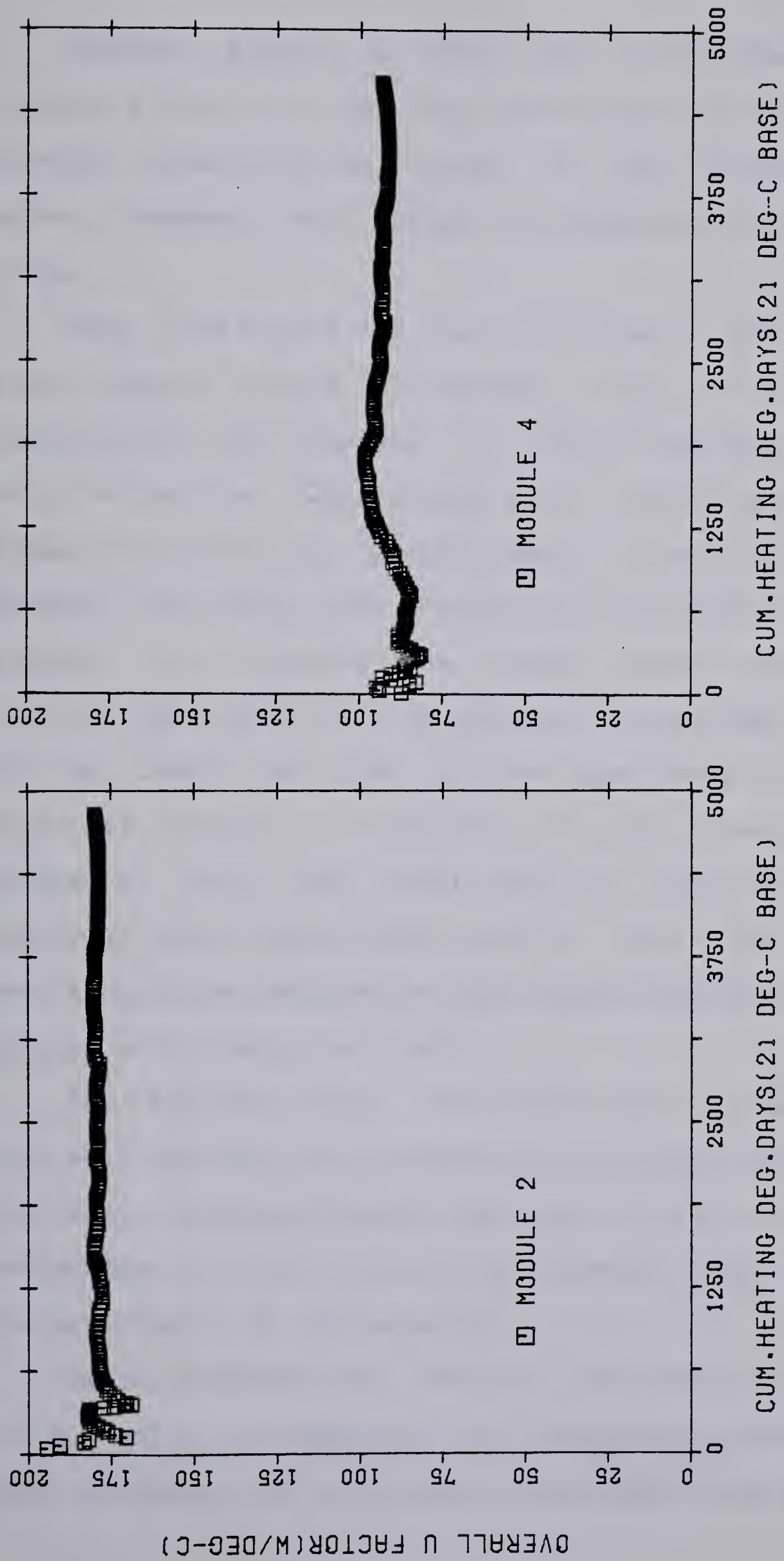


Figure 7.2 Overall U-Factors for modules 2 and 4



Ideally, Figure 7.2 would show a constant value of overall U factor or heat loss coefficient. Divergence from a constant value would be caused by such things as solar gains, basements heat losses, and changing air infiltration rates.

Note from Figure 7.2 that a minimum of 1000 degree days were elapsed before a constant value of heat loss coefficient was obtained. A little consideration here is very instructive. Under steady state conditions, the heat losses are directly proportional to heating degree days. However, the actual heat losses are influenced by transient effects. By imposing the steady state concepts on a transient phenomenon, it is possible to get some indication of the length of time a given experiment must be run in order to derive a reasonable accurate measure of the effective heat loss coefficient of the modules. This otherwise also implies the length of time over which the result could be averaged so that simplified methods could be applied with greater accuracy.

The building heat loss coefficient can be used as an excellent parameter for comparing the thermal performance of different envelope designs. Because it is to a large extent independent of local climate and depends only on thermal characteristics of the envelope.

Table 7.3 shows the relative performance of modules 1,3,4,5 and 6 in comparison with the standard module 2. As a basis of comparison module heat loss coefficients were used.



It can be seen that improved design strategies can effectively reduce the heating requirements by as much as 50-65% of the heat requirements of a standard module without internal heat gains. As was shown in reference [14], with internal heat sources this reduction could be as high as 80-90%.

Finally, it is of interest to compare the calculated module heat loss coefficients using steady state techniques with that of the measured heat loss coefficients. It can be seen from Table 7.3 that for large values of time i.e. on an annual basis, the errors involved are within the accuracy desired for simple practical calculation. However, on a shorter time scales and with increasing solar gains, the steady state calculations can lead to large errors [45].

Of considerable challenge in verification of the simulation model is the insitu module performance for small values of time. Because, if a model can accurately predict the building thermal performance for small values of time, it will obviously give more accurate predictions for large values of time.

To illustrate, consider for example the module 4. Large temperature swings associated with solar gains could make this module an ideal choice for verifying the thermal performance for small values of time. The choice of time interval itself should be consistent with the time interval between two consecutive measurements. In the present study, this time interval was an hour.



Figure 7.3 shows the predicted and the measured module heat requirements and the air temperatures on hourly basis for three consecutive days. It can be seen that the diurnal fluctuations are closely predicted by the simulation model. Note, however, that the predicted heat requirements, (the solid lines in Figure 7.3) do not follow the measurements point by point, instead tend to take a mean value. This is due to the fact that the predicted module heat requirements were excluded from the dynamics of the furnace duty cycle. Recently, McBride [101] in his thesis has developed models for including the system dynamics. Yet another reason for the difference could be due to the complex effect of air infiltration on module heat requirements.

The variation in module air temperatures during afternoons, is due to the maximum temperature limit of  $24^{\circ}\text{C}$  set in the simulation model. Another source of error could be due to the assumption of constant heat transfer coefficient used in the main simulation model. Nevertheless, the agreement seems to be quite satisfactory considering the complexities involved.

To compress the data to a manageable amount, the results are presented as typical diurnal variations of module temperatures and furnace heat requirement on a hourly basis for each month and for each module. The typical diurnal variation was obtained from all the measurements, for example, the heat requirements at a particular hour of the day during one month. These comparisons check time



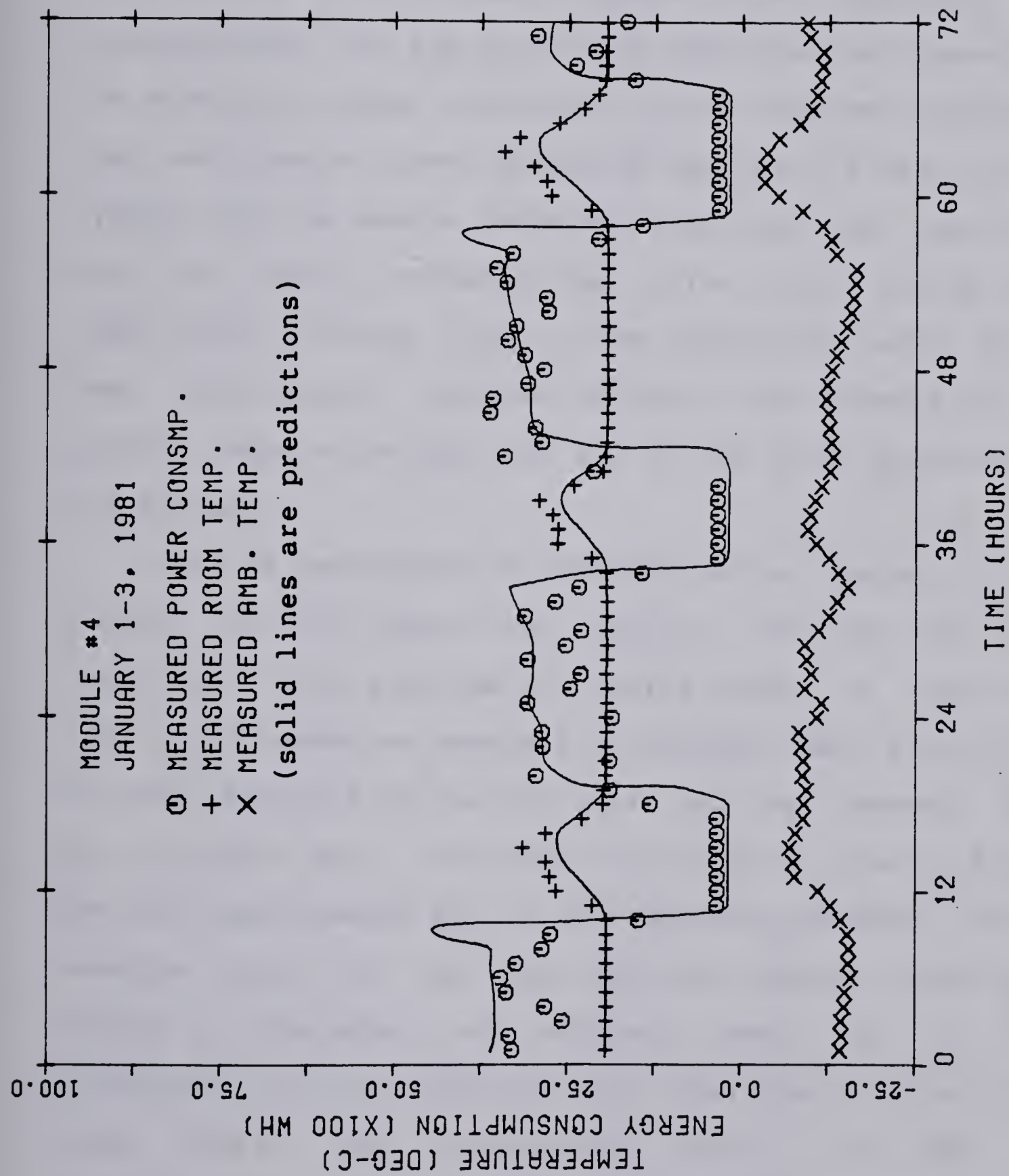


Figure 7.3 Comparison of the predicted and the measured module temperatures and furnace heat requirement on a hourly basis



constant behavior, solar gains as well as the module heat losses.

Predictions and measurements are compared in Figures 7.4 through 7.12. These figures were obtained after incorporating all the previously described refinements into the simulation model and hence are the improved versions of the performance curves presented earlier [54,102]. During a typical day the module temperature and the heat requirements are very nearly constant during the night. During the day light hours a slight rise in room temperature and a drop in heat requirements recorded is due to the effects of higher outside temperature and also due to the solar gains entering the modules.

Also of importance in determining the shapes of these curves is the module heat capacity. The slow rise in heat requirement over a period of several hours in the evening (16 to 21 hours for module 4 in January 1981) is the result of heat release from the dry walls and the basement walls. For the most part, the predictions (solid lines in Figures) and the measurements are in satisfactory agreement with an average error of less than 5%. Note however, that for the months of December and February there is a slight discrepancy in the predicted heat requirement during the day light hours. The interesting thing is that this inconsistency can be noticed in both the modules 3 and 4. The cause for this error is believed to be error in radiation data. However, the magnitude of the error in the



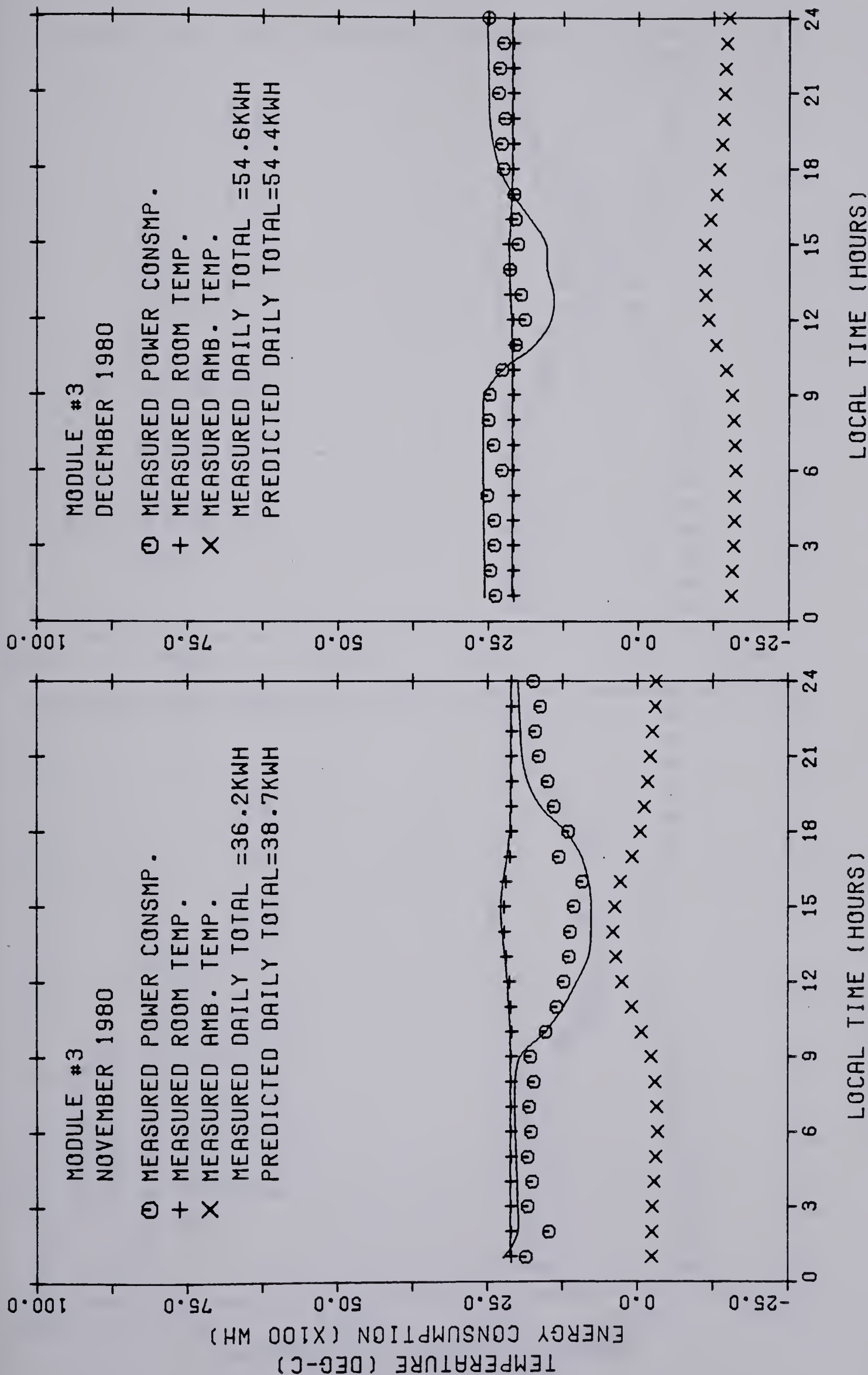


Figure 7.4 Performance of module 3 for various months of the heating season (solid lines are predictions)



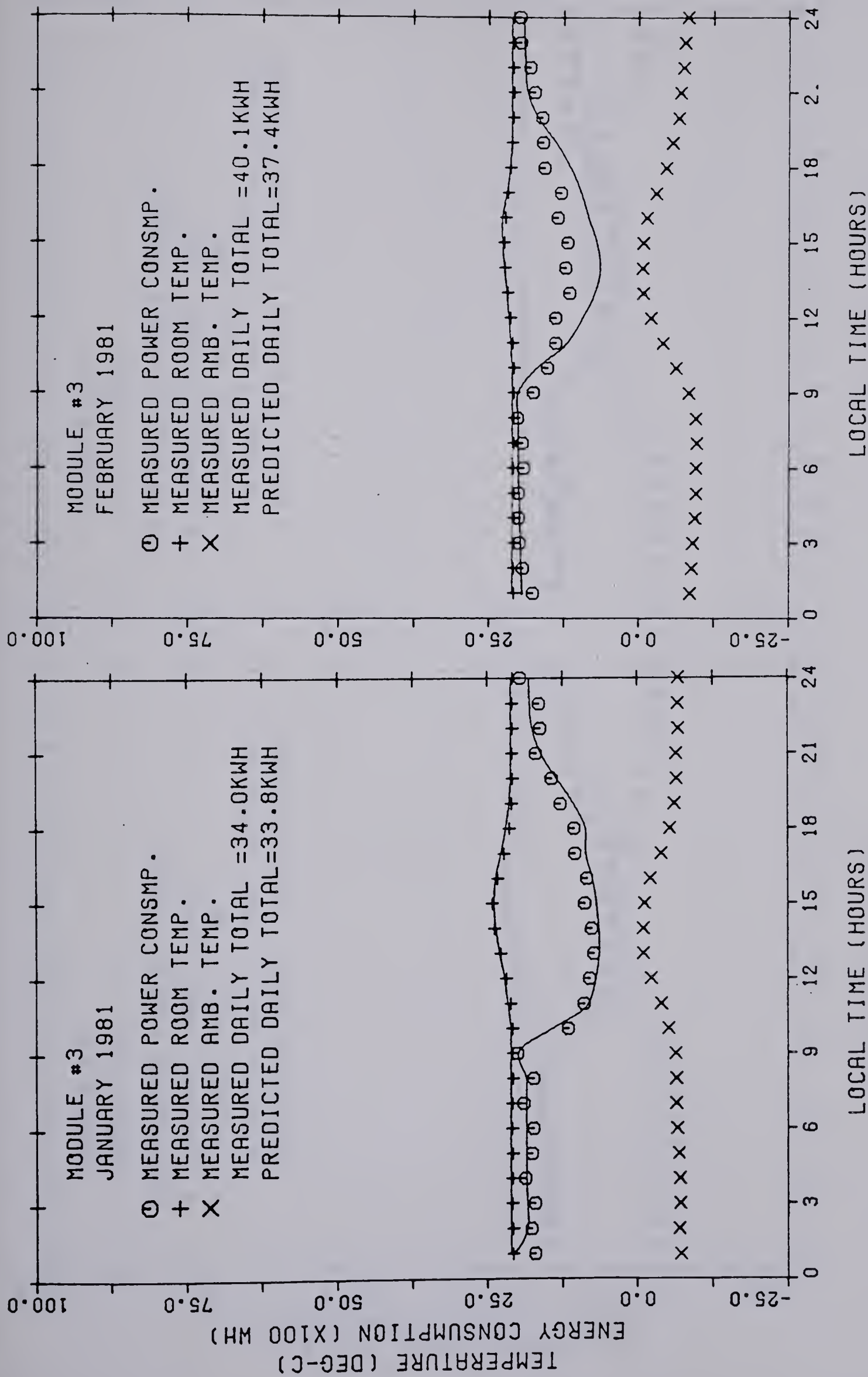


Figure 7.5 Performance of module 3 for various months of the heating season (solid lines are predictions)



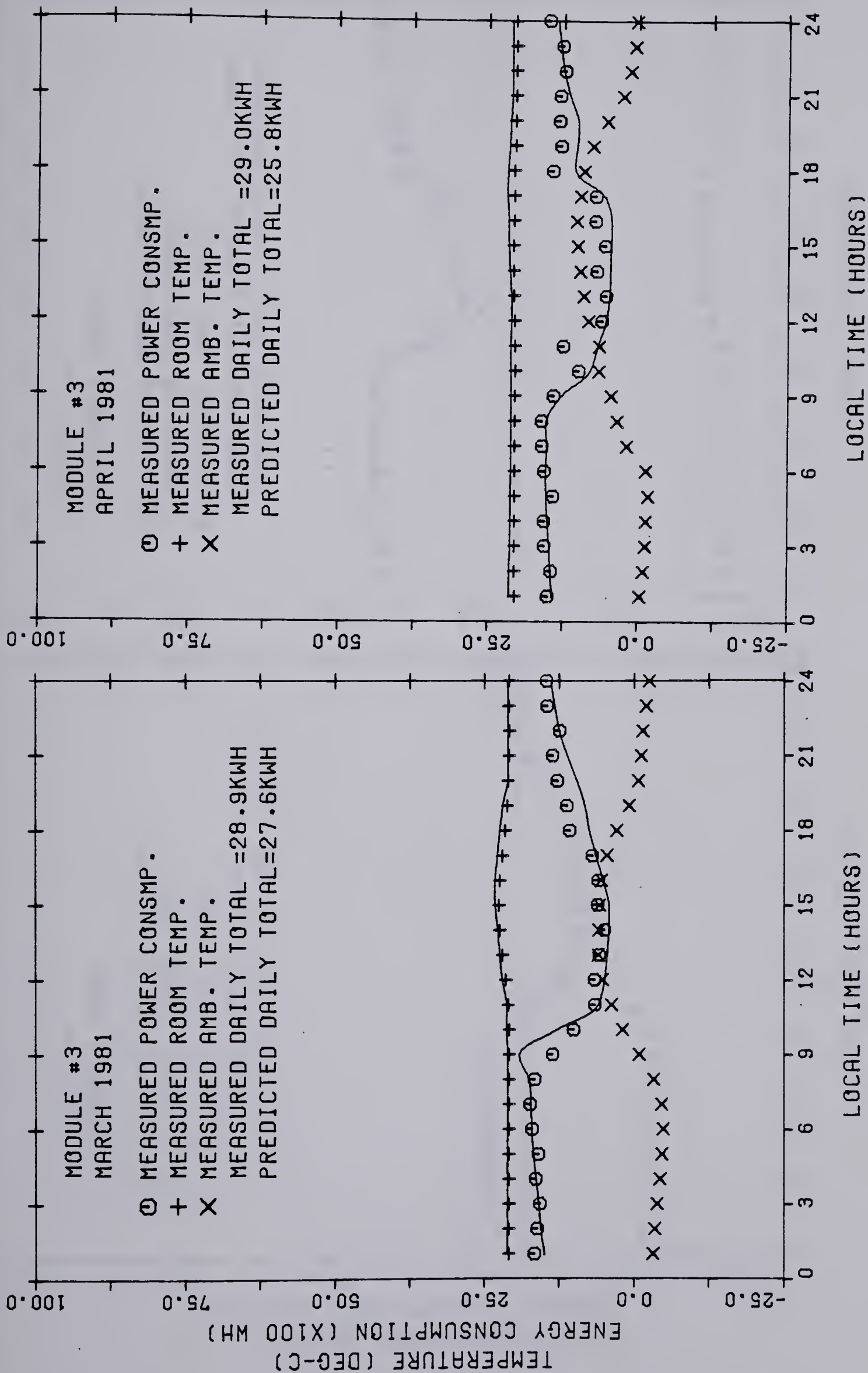


Figure 7.6 Performance of module 3 for various months of the heating season (solid lines are predictions)



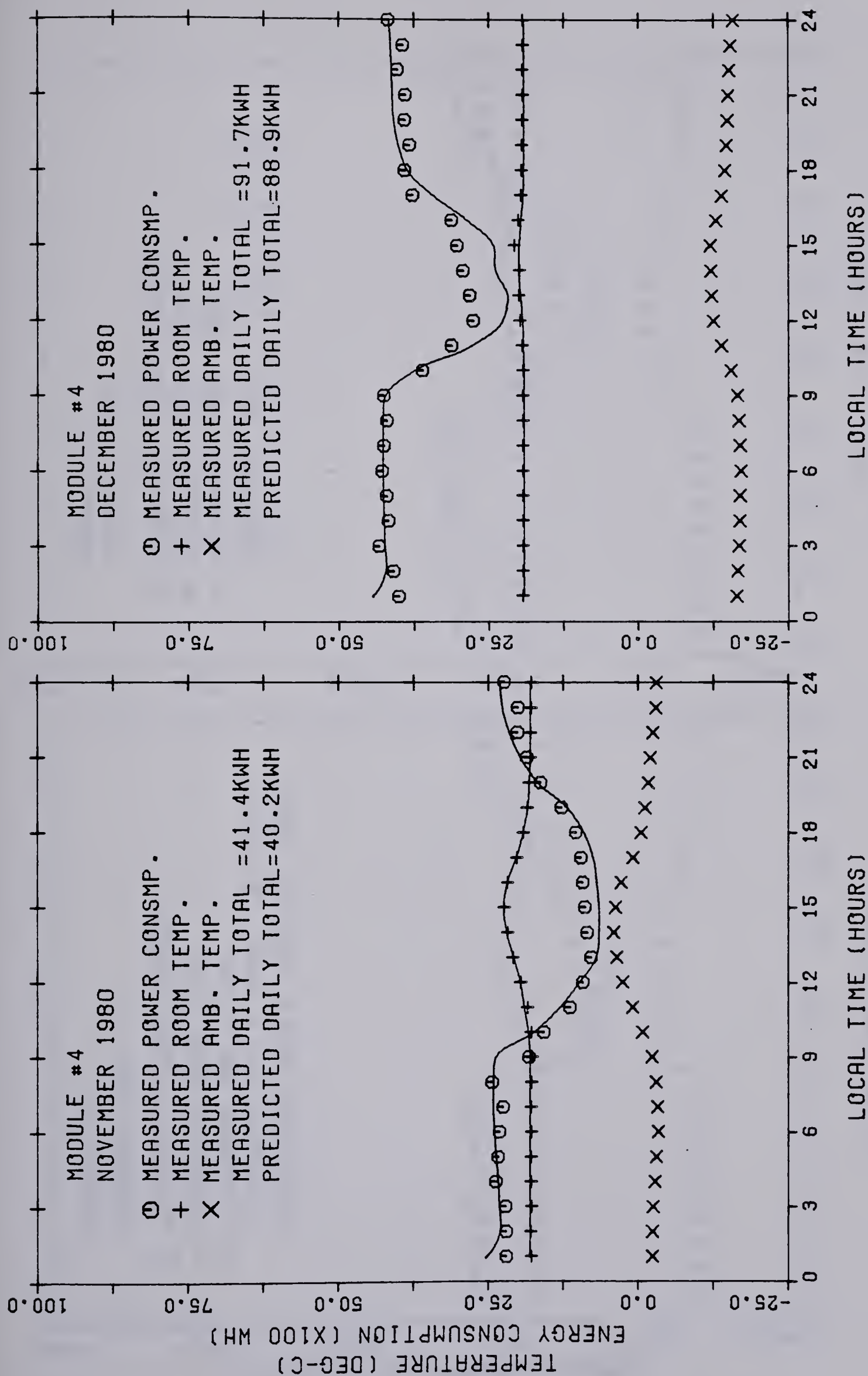


Figure 7.7 Performance of module 4 for various months of the heating season (solid lines are predictions)



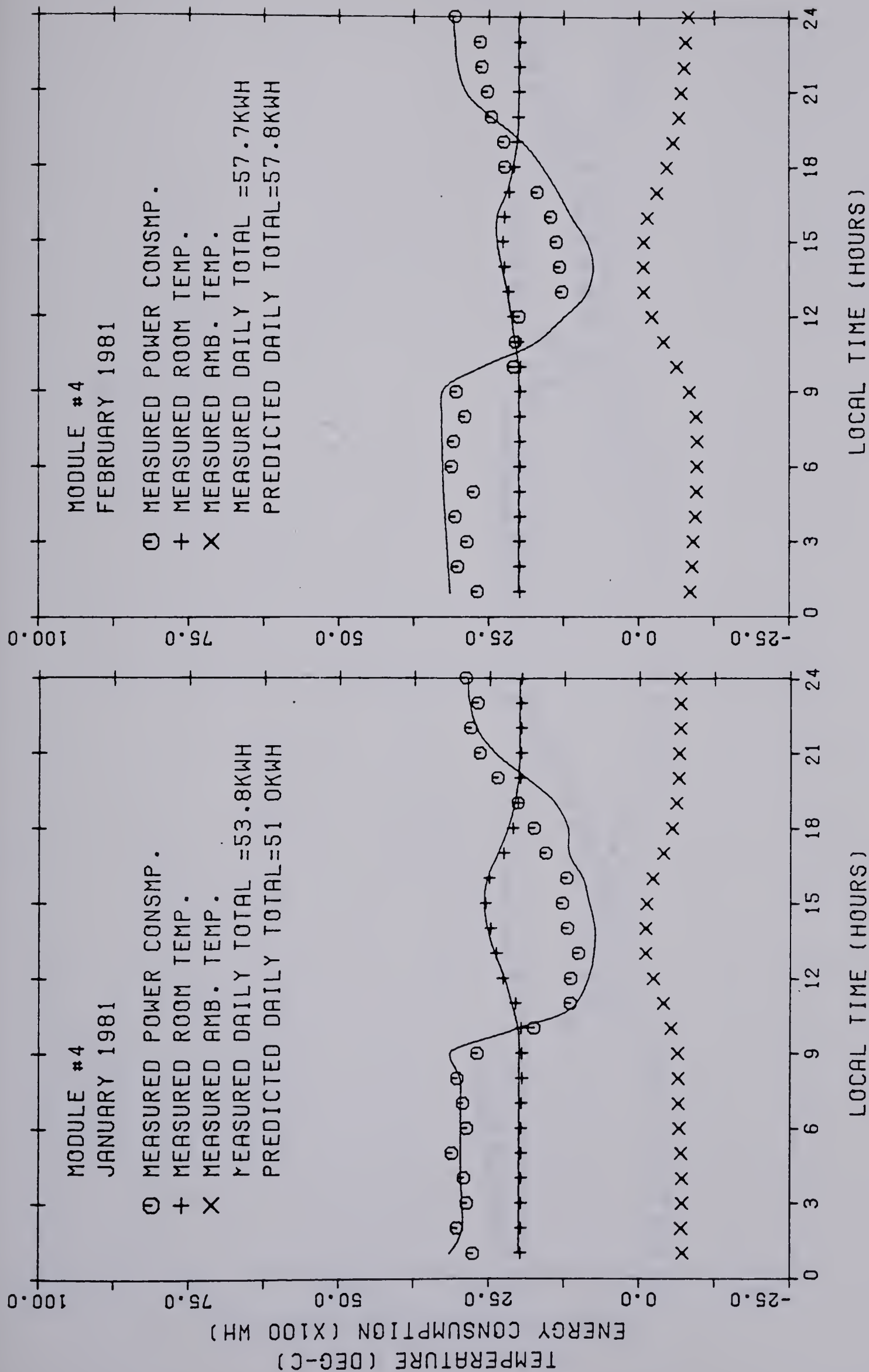


Figure 7.8 Performance of module 4 for various months of the heating season (solid lines are predictions)



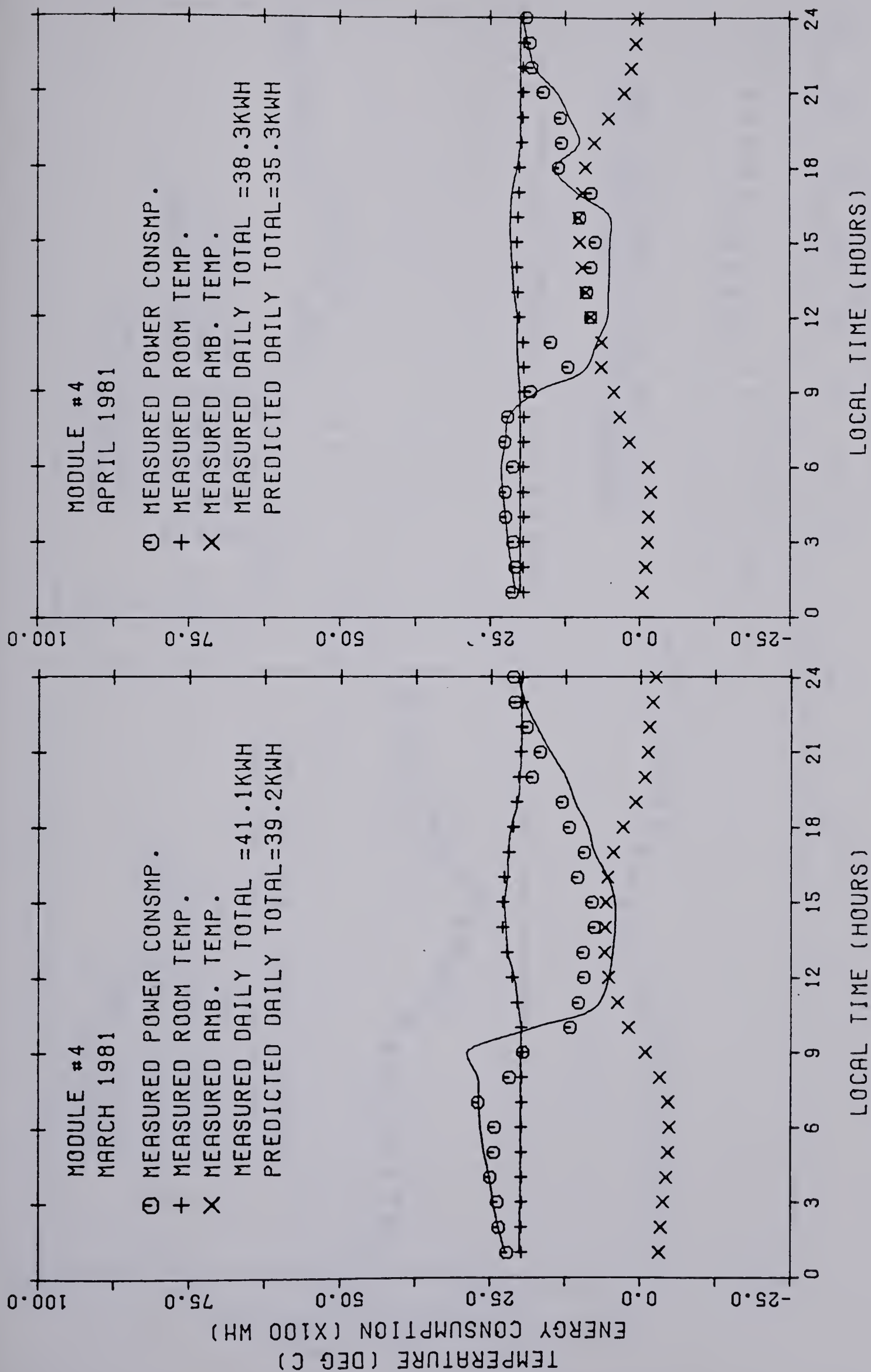


Figure 7.9 Performance of module 4 for various months of the heating season (solid lines are predictions)



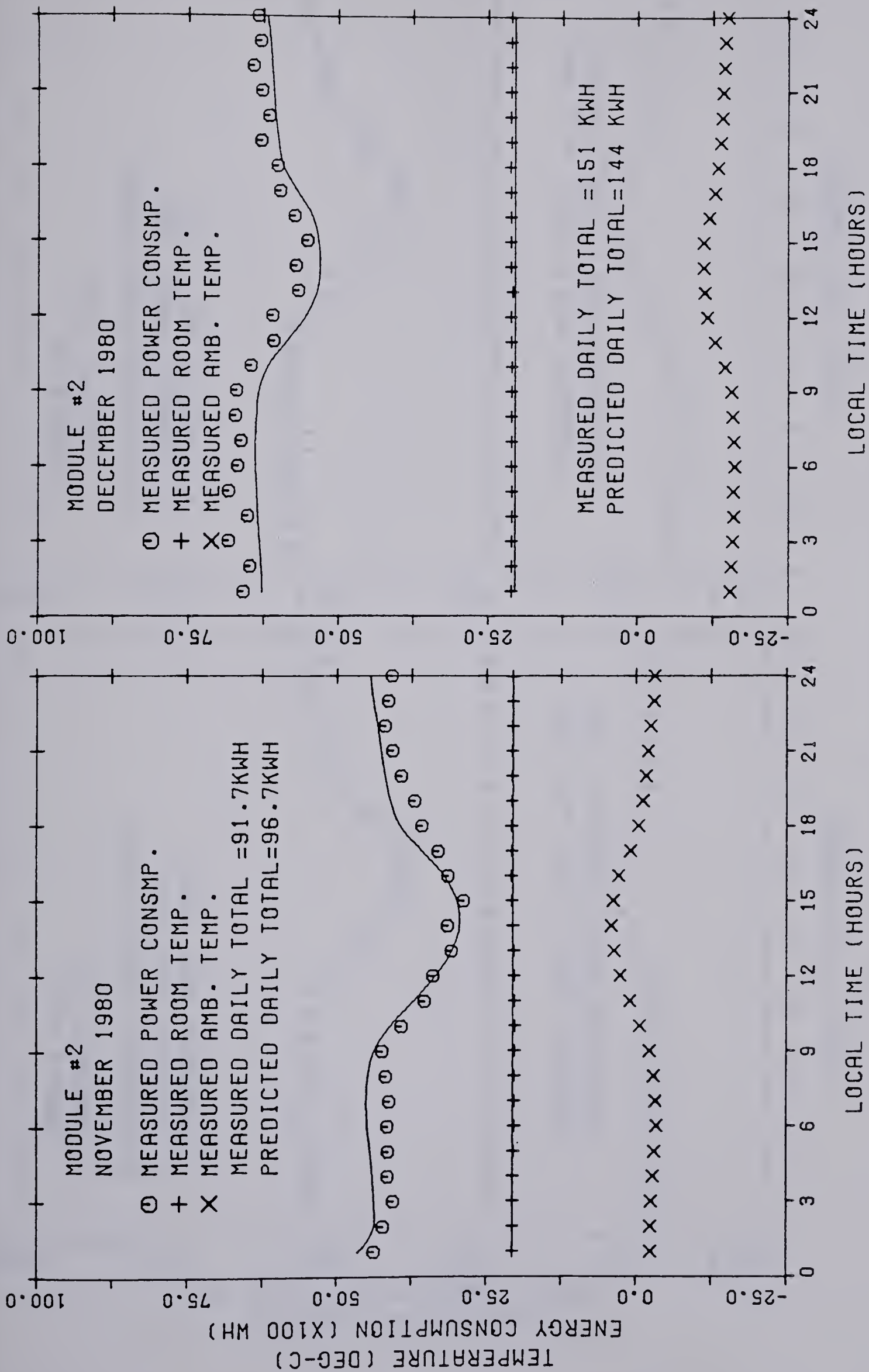


Figure 7.10 Performance of module 2 for various months of the heating season (solid lines are predictions)



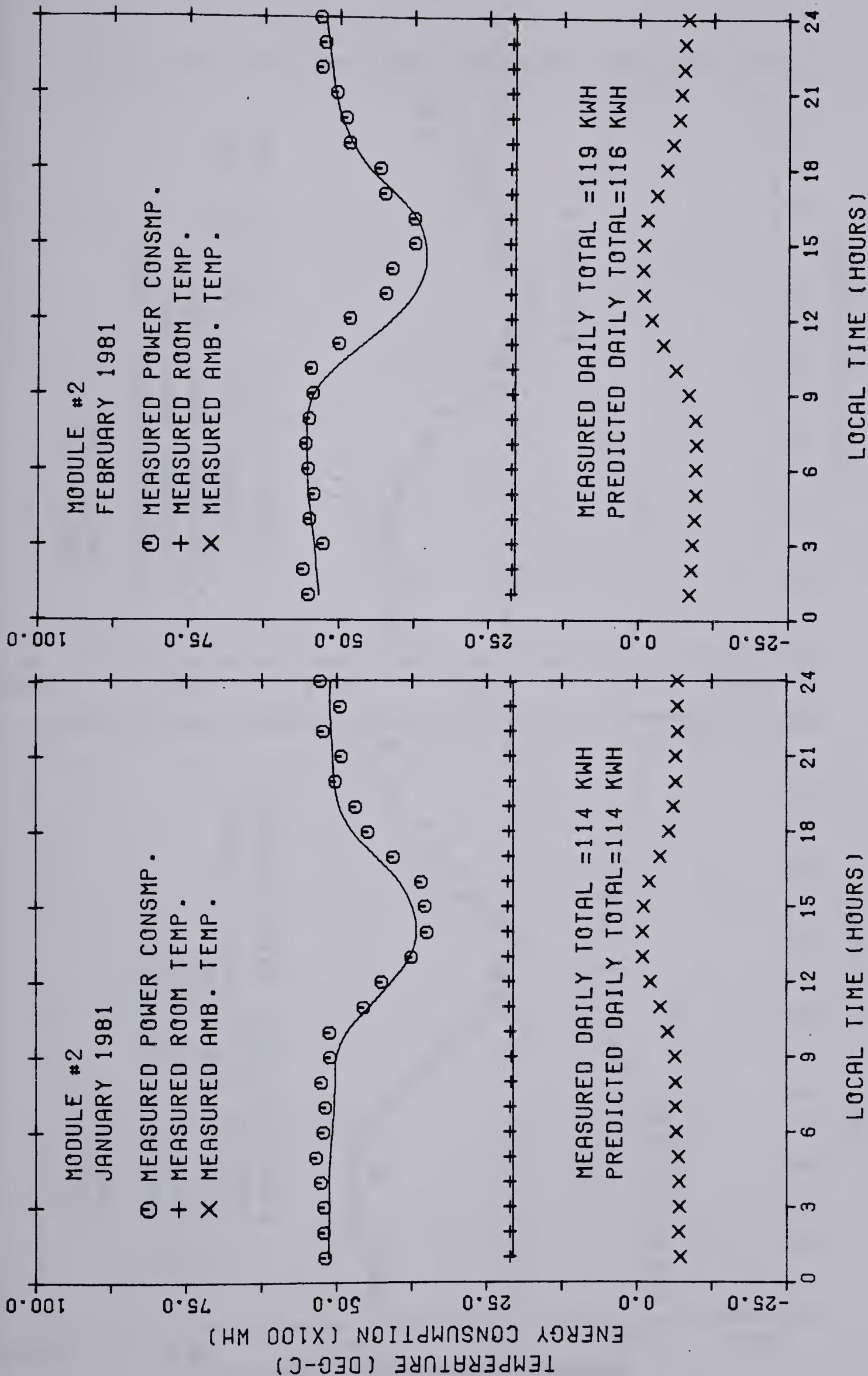


Figure 7.11 Performance of module 2 for various months of the heating season (solid lines are predictions)



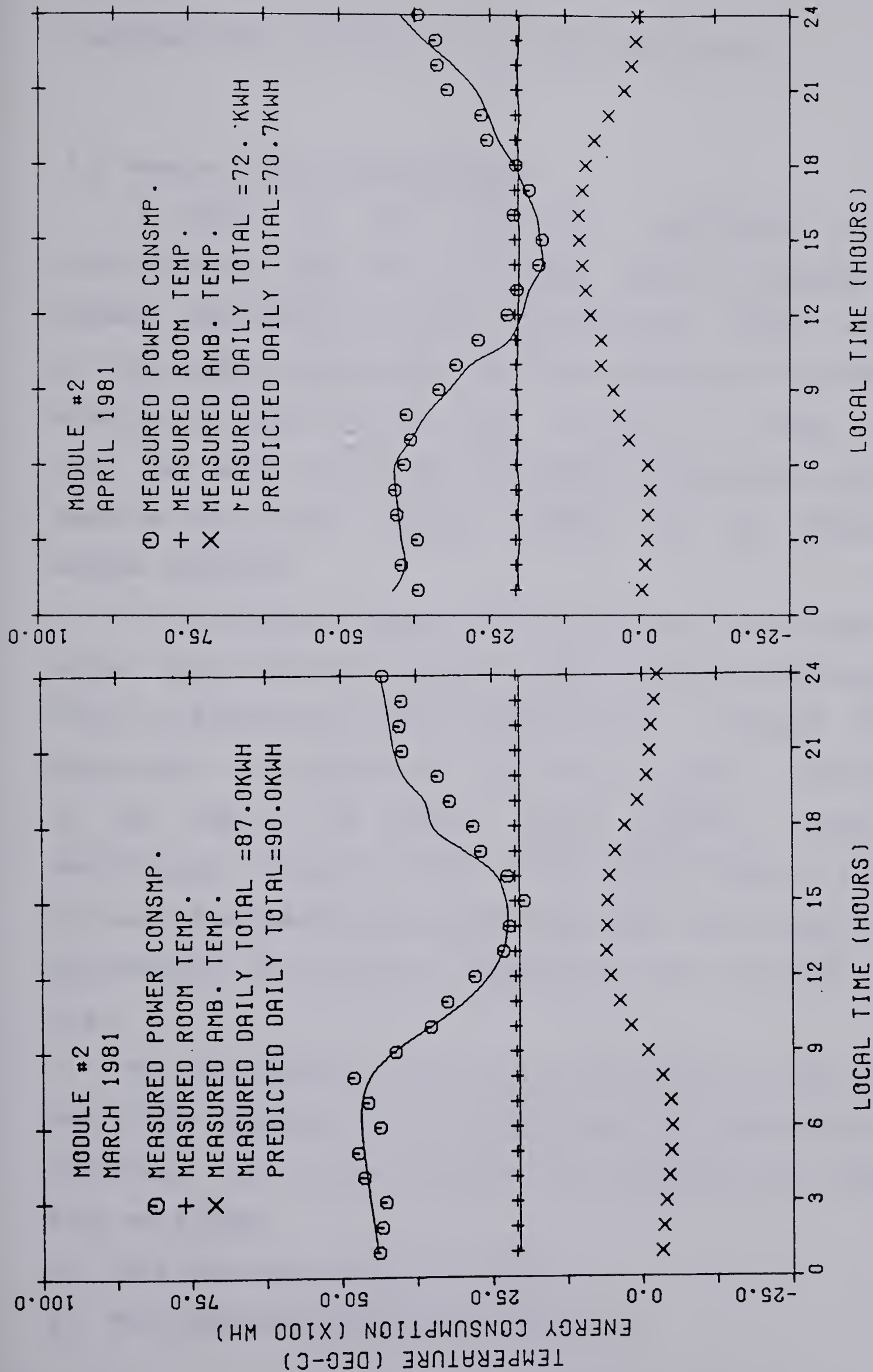


Figure 7.12 Performance of module 2 for various months of the heating season (solid lines are predictions)



predicted heat requirements is relatively small.

#### 7.4 Passive Solar Contributions

A topic of very practical importance is the contributions made by the solar gains in heating of the houses. The effects of solar gains and the window shutters on the module performance can now be analyzed. The computer simulation model which has been verified in great detail will be used to extract seasonally averaged contributions made by solar gains through windows and the effects of window shutters.

The increased furnace heat requirements that occur when solar gains are set to zero or when shutters are eliminated from the simulation can be used to give a measure of the percentage contributions these factors made to the heating of the module. To obtain these effects solely by measurements directly on the modules would require a number of years data taking and would leave open the question of variability of climatic conditions from one year to the next.

For the modules 3 and 4 the contribution of solar gains and window shutters can now be analyzed with some degree of certainty. For these modules the following four computer runs were made.

1. With shutters and solar gains
2. With shutters but no solar gains



3. Without shutters and with solar gains

4. Without shutters and without solar gains

Runs with no solar gains were used as reference and the heat requirements obtained for other runs were expressed as a percentage of this value. These percentages are heating load reduction factors [103]. A summary of monthly heating load reduction factors for the modules 3 and 4 for the year 1981 is given in Table 7.4.

The rationale for this approach was drawn from the theoretical considerations presented in developing the general design curves [14]. To show the similarity between the AHLR factors obtained from the general design curves and the AHLR factors obtained from the above approach, it is worth examining the definitions of SIG (Solar and Internal Gain) and AHLR (Annual Heating Load Reduction) factors introduced in reference [14]. A more rigorous theoretical approach to developing the SIG and AHLR factors will be presented in Chapter 8.

Solar and Internal Gain Factor:

$$\text{SIG} = \frac{\text{ISHGF} * \text{WA} + \text{If} * \text{HHR}}{\text{U} * \text{HDHr}} \quad (7.5)$$



Table 7.4 Effects of solar gains and shutters on module performance: monthly results

Energy consumption per month in KWH							
Module	Description	Nov.	Dec.	Jan.	Feb.	Mar.	Apr.
3	1. With shutters & solar gains	936	1496	1048	1048	855	755
	2. With shutters no solar gain	1218	1662	1492	1350	1346	1058
	3. Without shutters with solar gains	1161	1686	1491	1466	1274	1119
	4. Without shutters no solar gains	1420	1878	1941	1772	1771	1439
	5. HLR with shutters	0.7684	0.9001	0.7024	0.7763	0.6352	0.7325
	6. HLR without shutters	0.8176	0.8977	0.7681	0.8273	0.7194	0.7776
4	1.	1004	2351	1573	1619	1216	1060
	2.	1532	2667	2413	2198	2125	1582
	3.	1206	2756	2200	2211	1802	1558
	4.	1774	3076	3051	2798	2730	2116
	5.	0.6553	0.8815	0.6518	0.7365	0.5722	0.6700
	6.	0.6798	0.8959	0.7210	0.7902	0.6600	0.7362



Annual Heating Load Reduction Factor

$$\text{AHLR} = \frac{Q_{fu} + I_c * \text{HHr}}{U * \text{HDHr}} \quad (7.6)$$

Time constant:

$$\tau = \frac{C * (T_{\max} - T_{\min}) \text{HHr}}{U * \text{HDHr}} \quad (7.7)$$

In the above equations:

ISHGF is the integrated solar heat gain factor

WA is the window area

If is the fluctuating component of the internal load

HHr is the heating hours per year

U is the steady state heat loss coefficient

HDHr is the heating degree hours

C is the total heat capacity

Tmax and Tmin are the allowable temperature limits

Ic is the constant component of internal load.

To draw an analogy between the two approaches, consider for example the first two modes of module simulation runs.

1. with shutters and solar gains

2. with shutters but no solar gains.

The SIG factor is zero for case 2, because in the absence of



solar gains and internal heat sources, Equation 7.5 reduces to zero.

Zero SIG factor implies that AHLR factor is unity. Substituting in Equation 7.6,

$$1 = \frac{Q_{fu}}{U * HDHr} \quad (7.8)$$

or

$$U * HDHr = Q_{fu} \quad (7.9)$$

Notice from the Equation 7.9, that the furnace heat requirement for no solar gain case reduces to steady state heat loss. Therefore the ratio of cases 1 and 2 defined as Heating Load Reduction Factors in this study corresponds to the annual heating load reduction factors defined earlier. Therefore,

$$\frac{\text{Heating load with shutters + solar gains}}{\text{Heat requirements with shutters + no solar gains}} = \frac{Q_{fu}}{U * HDHr} \quad (7.10)$$

Comparing Equations 7.6 and 7.10 it is evident that conceptually, both approaches are the same.

The length of time over which the Equations 7.5 and 7.6 have to be integrated has to be large enough from the point of view of the accuracy of the results. Ideally it should be about an year. However, as a first approximation the monthly



integrals will be used. Therefore, the information presented in tables 7.4 and 7.5 and the figure 7.13 of this chapter imply that the heating load reduction factors are based on monthly results, where as the AHLR factor was obtained from the heating season average of the monthly HLR factors.

With this reservation in mind, the monthly HLR factors for modules 3 and 4 are shown on the general design curves in Figure 7.13. First thing to note from the figure is the distribution of HLR factors around the line joining the condition for which  $SIG = AHLR = 1.0$ . This condition implies that for each time constant, there is a broad minimum in the AHLR as a function of SIG.

Secondly, the time constants of the modules 3 and 4 calculated from Equation 7.7 are approximately 25 and 15 hours. From the limited data points it can be seen that there is a definite grouping of HLR factors according to the module time constants.

A complete verification of the general design curves solely from measurements would be a very expensive and time consuming endeavor. Even though the above analysis rely on computer simulations for extracting seasonally averaged AHLR factors, a fair degree of confidence can be put into the results. This can be argued from two considerations: firstly, the model has been verified in great detail; secondly, the model is closely predicting the diurnal module heat requirements and space air temperatures for the two modes of module operation, for which data is available



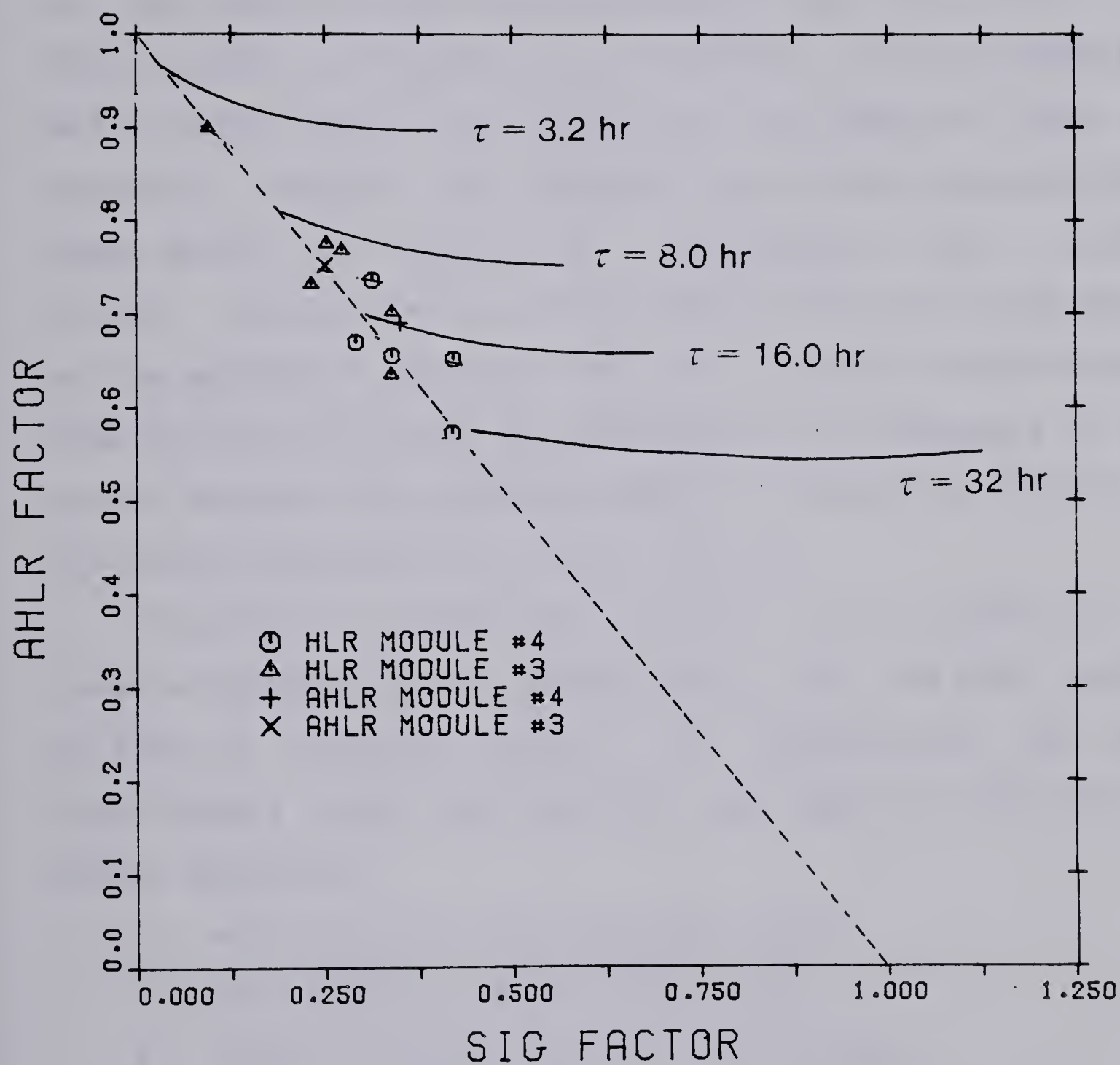


Figure 7.13 Monthly heating load reductions produced by modules 3 and 4



namely:

1. Without shutters and with solar gains (Nov.-Dec. 1980)

2. With shutters and with solar gains (Jan.-Apr. 1981)

This is shown in Figures 7.4, 7.7 and 7.5, 7.8 for modules 3 and 4 respectively. This implies that the model is able to correctly simulate the dynamic fluctuations introduced by solar gains and ambient air temperatures under varying thermal characteristics of the envelop such as the presence or the absence of shutters. Results from such a verification step can be very useful in understanding the dynamics of the system because this approach tends to isolate the effects of the solar gains and the thermal shutters.

Therefore, an additional criterion for validation of computer programs can be prescribed in that the model should be able to correctly predict the temperatures and heat requirements under the following four modes of test cell or module operation.

1. with shutters and with solar gains.
2. with shutters but no solar gains.
3. without shutters and with solar gains.
4. without shutters and without solar gains.

It is believed that application of these concepts could prove to be very valuable in extracting the passive solar contributions, because the test modules can be monitored with relative ease for each of the above four modes of operations.



A comprison of AHLR factors with the resistive losses through the windows is made in Table 7.5. With solar fractions noted in Table 7.4 these windows are very nearly neutral as far as their effect on the module heat requirements is concerned when no shutters are used. With shutters the windows make a net positive contribution to the heating of the modules between 10 to 20 percent of the heating load.

### 7.5 Component Heat Losses

Using the data thus far developed it is of interest to compare the magnitudes of the various components of the heat losses for the modules. Such a study will not only aid in identifying the relative magnitudes of the component heat losses, but will also help in establishing guide lines for further research in its order of importance. However, the more fundamental nature of contribution resulting from this type of investigation is of great value in performing a check on the logical errors in the computer models.

Consider for example, the main simulation model used in this study. As stated before, the individual component models were put together to simulate the building as a whole. A necessary condition for this integration step is that the overall energy balance equation be governed by the first law of thermodynamics. Often, however, a common problem with building load analysis programs is that they



Table 7.5 Effect of solar gains and shutters on module performance: heating season results

Module	AHLR Factor	Fraction solar gain	Resistive losses through window (fraction total loss)	Net window gain (fraction total heat required)
3	Without shutters	0.20	0.22	-0.02
	With shutters	0.25	0.14	+0.11
4	Without shutters	0.25	0.21	+0.04
	With shutters	0.31	0.14	+0.17



are quite large and complex and that updating or refinements are done over a period of time by addition or replacement of subroutines to the main simulation model. This practice is easily susceptible to errors resulting from the violation of the first law of thermodynamics. A second source of error is likely to come from the numerical instabilities. Therefore, by drawing pie charts of the heat losses and gains, the overall energy balance can be checked and any errors can at once be corrected. Figures 7.14 through 7.18 examine the component losses as a percentage of the heat requirements for modules 2, 3, and 4.

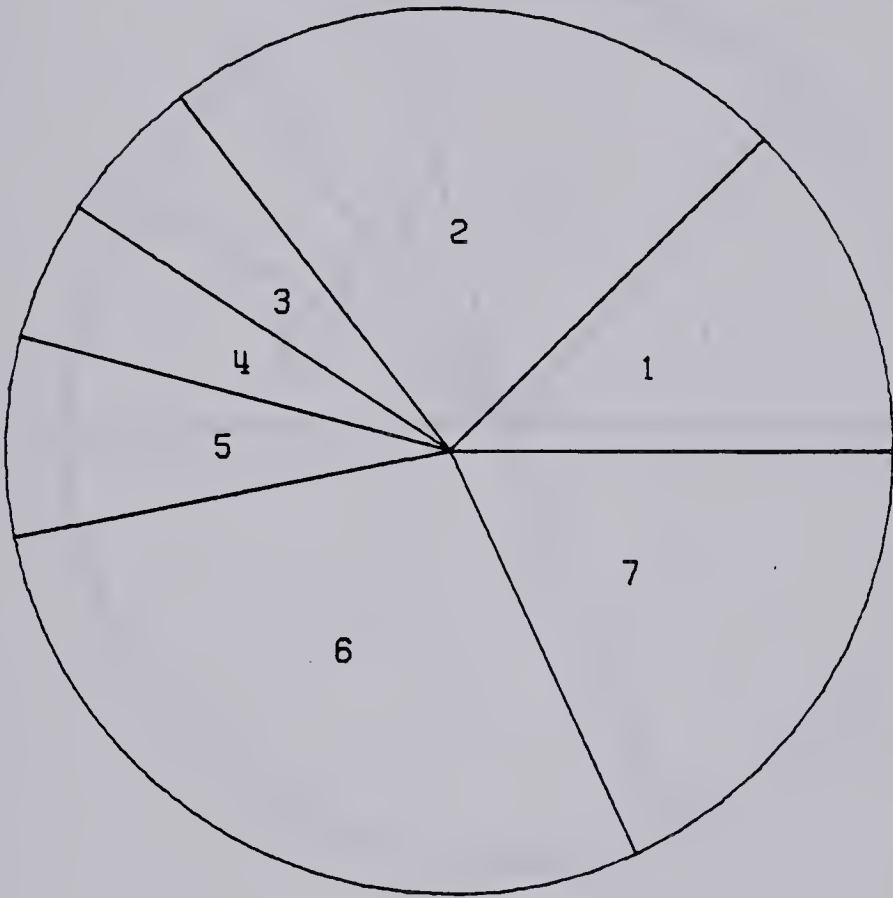
In these Figures the most striking feature is that the below grade basement heat losses for modules 3 and 4 account for by far the greatest single component heat loss. This is in spite of the fact that the modules 3 and 4 have insulation to the full height of the basement wall with an RSI 1.76 in module 4 and an RSI 3.52 in module 3. Obviously in these modules which have highly insulated above grade walls even more insulation than this may be required in the basement in order to achieve really low energy consumption.

After the basement heat losses the next two highest heat losses are infiltration and window heat losses. The window heat losses could be cut somewhat by designing better thermal shutters with good seals.

Another observation that can be made is that basement losses and infiltration account for 50 percent or more of the total losses for these highly insulated modules. Since



MODULE #3 - COMPONENT HEAT LOSSES WITHOUT SHUTTERS

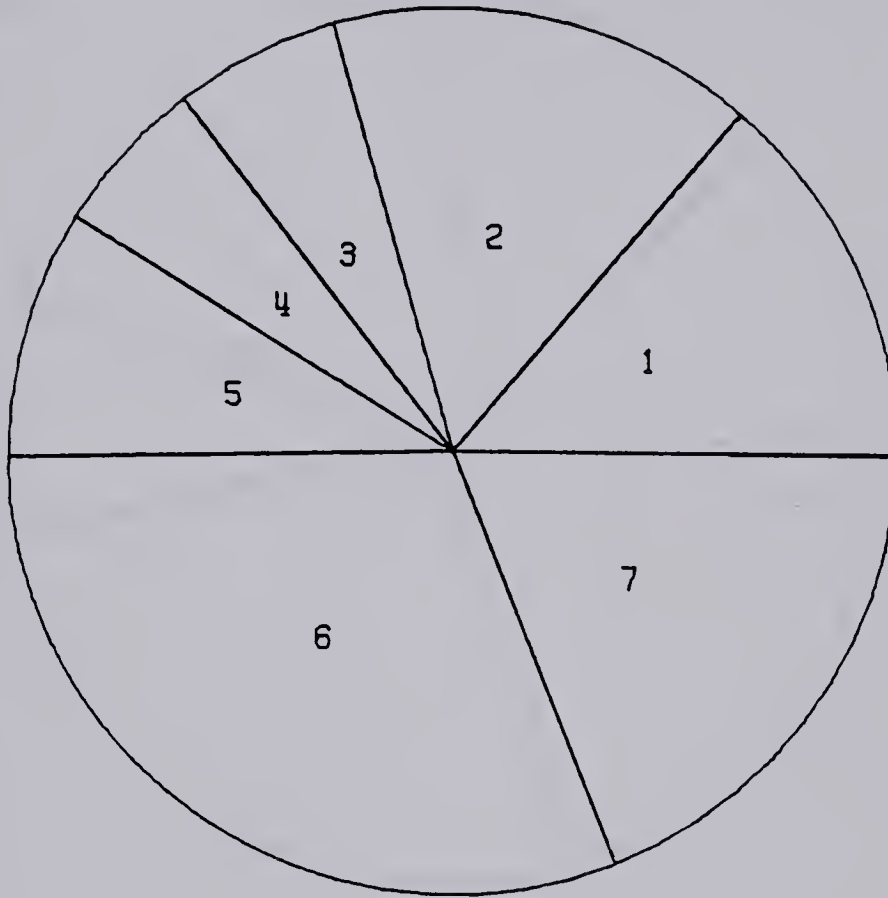


1. Walls (12.4%)
2. South facing window (22.9%)
3. Ceiling (5.4%)
4. Door and remaining windows (5.1%)
5. Above grade basement walls (7.2%)
6. Below grade basement (28.7%)
7. Infiltration (18.3%)

Figure 7.14 Component heat losses for module 3 without shutters



## MODULE #3 - COMPONENT HEAT LOSSES WITH SHUTTERS

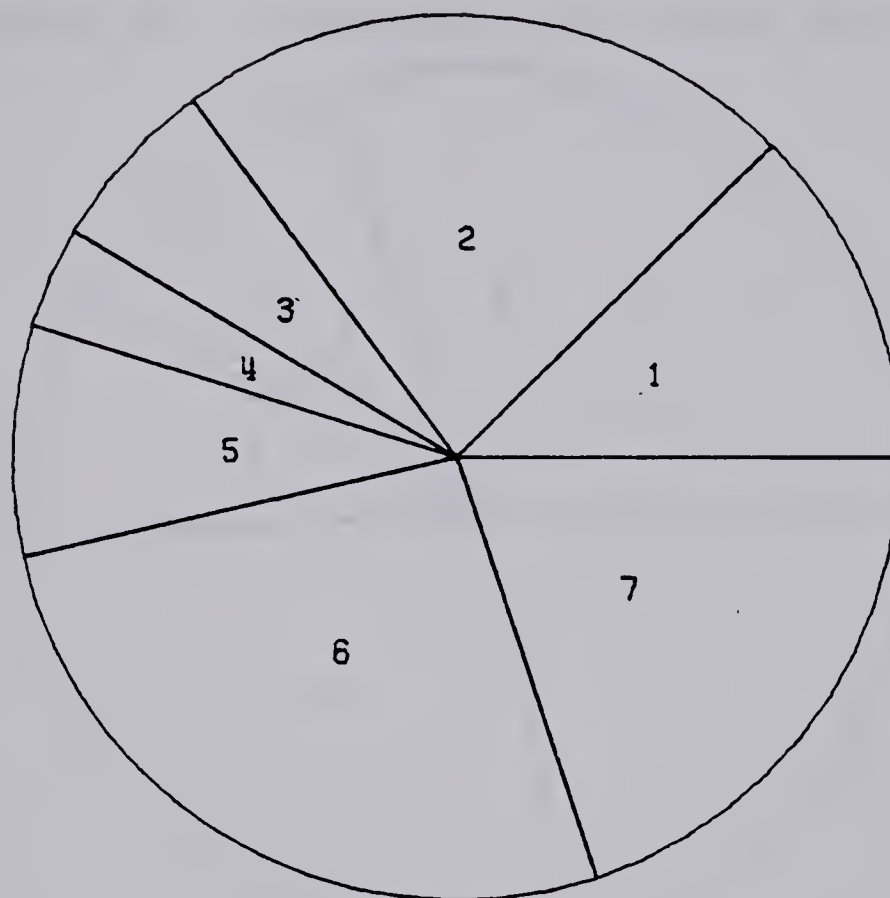


1. Walls (14.0%)
2. South facing window with shutter (15.7%)
3. Ceiling (6.1%)
4. Door and remaining windows (5.8%)
5. Above grade basement walls (8.1%)
6. Below grade basement (31.0%)
7. Infiltration (19.3%)

Figure 7.15 Component heat losses for module 3 with shutters



## MODULE #4 - COMPONENT HEAT LOSSES WITHOUT SHUTTERS

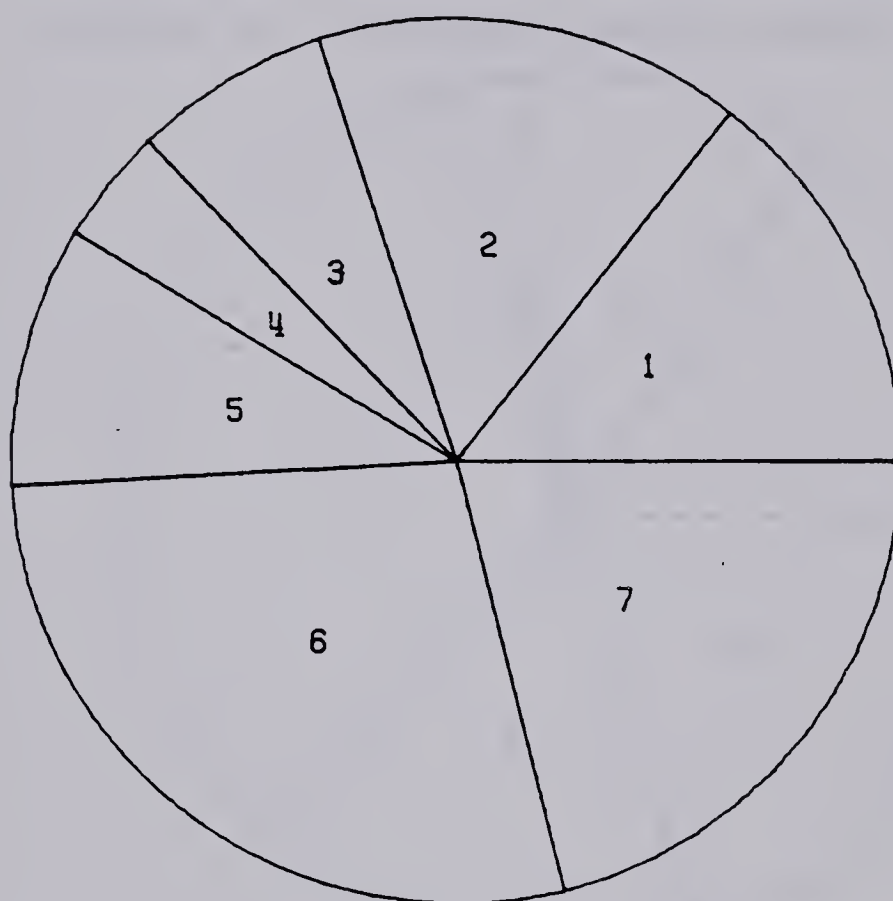


1. Walls (12.4%)
2. South facing window (22.7%)
3. Ceiling (6.4%)
4. Door and remaining windows (3.7%)
5. Above grade basement walls (8.4%)
6. Below grade basement (26.5%)
7. Infiltration (19.9%)

Figure 7.16 Component heat losses for module 4 without shutters



## MODULE #4 - COMPONENT HEAT LOSSES WITH SHUTTERS

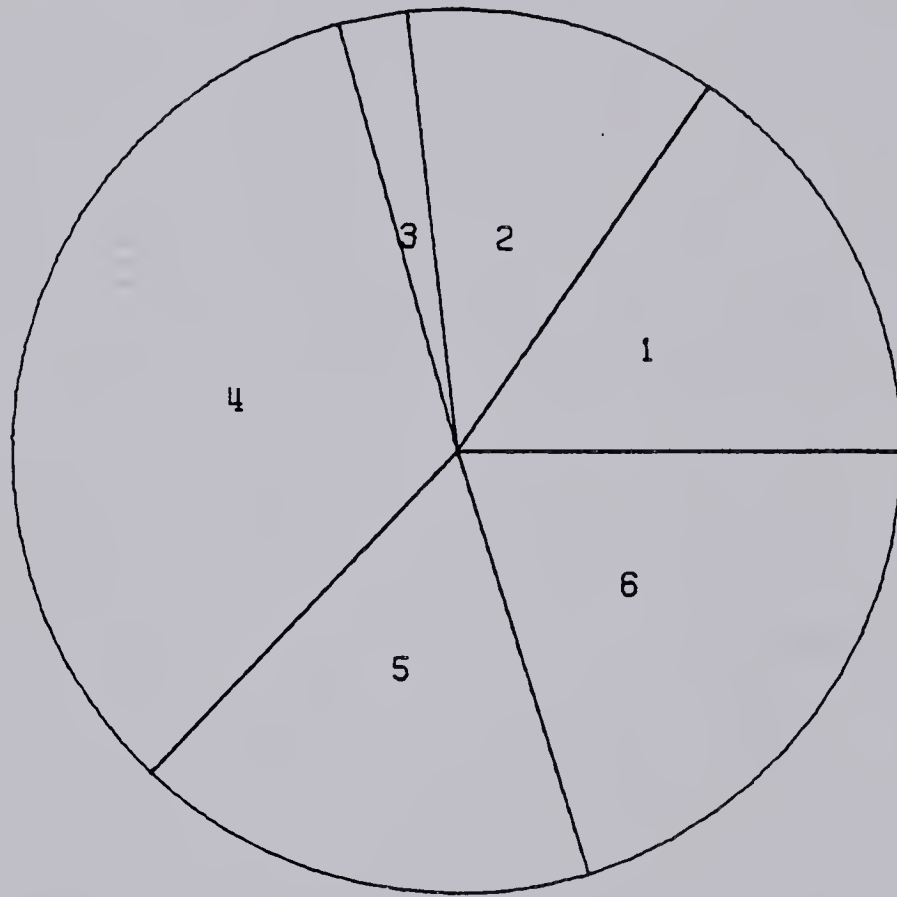


1. Walls (14.4%)
2. South facing window with shutter (15.6%)
3. Ceiling (7.2%)
4. Door and remaining windows (4.2%)
5. Above grade basement walls (9.5%)
6. Below grade basement (28.0%)
7. Infiltration (21.1%)

Figure 7.17 Component heat losses for module 4 with shutters



## MODULE #2 - COMPONENT HEAT LOSSES



1. Walls (15.4%)
2. Ceiling (11.4%)
3. Door and remaining windows (2.5%)
4. Above grade basement walls (33.6%)
5. Below grade basement (16.9%)
6. Infiltration (20.2%)

Figure 7.18 Component heat losses for module 2



these are the most difficult losses to predict the calculation of heat requirements of houses built to similar specifications remains challenging area of endeavor.



## 8. APPLICATIONS

### 8.1 Introduction

In the previous chapters the simulation model developed in reference [14] was refined and tested. In order to determine the passive solar contributions to the heating of the modules it was first necessary to accurately simulate the thermal behaviour of the modules. In so doing a number of parameters that influence the heat requirement predictions were indentified during the modeling of walls, ceilings, basements, solar gains and transient response. On the other hand some specific problems relating to the module thermal shutter performance and window transmisivity were also identified. These specific problems, may or may not be applicable to all houses. However, they had to be taken into account for accurately simulating the module thermal response.

The experience gained from these studies on the modules at least partially suggest that the present simulation model can be used to speculate certain guidelines for the design of passive solar houses. These guide lines will be developed in a general way so that they are not limited to any particular design. To develop such guide lines the house designs given in Table 8.1 were evaluated using the simulation model. The results of these numerical experiments were put in a form of a set of curves. This excercise was



Table 8.1 Specifications of the house designs used for numerical experiments

House Name	Walls RSI	Walls Area (Sq m)	Ceiling RSI	Ceiling Area (Sq m)	Basement RSI	Basement Area (Sq m)	Infiltration Air changes per hour	Overall U-Factor W/deg.C
R7	1.23	135	2.46	124	2.64	198	0.50	331
R15	2.64	135	4.40	124	4.40	198	0.50	220
R25	4.40	135	7.39	124	4.40	198	0.25	141
R40	7.04	135	12.3	124	7.04	198	0.10	76



already initiated in the author's previous work [14,103]. Since then several concepts have been refined. The discussion of the present chapter will therefore attempt to rationalize the whole study. First the general design curves will be developed and their physical significance will be explored. This will be followed by a discussion on design of direct gain passive houses.

## 8.2 General Design Curves

Simplified methods for determining the passive solar contributions have been suggested in the literature [33,34,104]. These studies are more or less empirical in nature and lack theoretical basis. In the present study a theoretical approach will be taken and attempts will be made to make it more generally applicable.

In general the auxiliary heat required to maintain a house at a certain preset temperature is a function of several variables. The complex relationships among these factors makes optimum design a non-trivial matter. However, in order to understand the overall problem it is instructive to consider a very simplified version of the thermal model of a house [14] as shown in Figure 8.1. In this simplified model the entire thermal mass is assumed to be at the room temperature,  $T_R$ , and the room receives three time varying heat inputs - the solar heat gain, SHG, the internal loads,  $I$ , and the furnace output,  $Q_{fu}$ . The difference between these



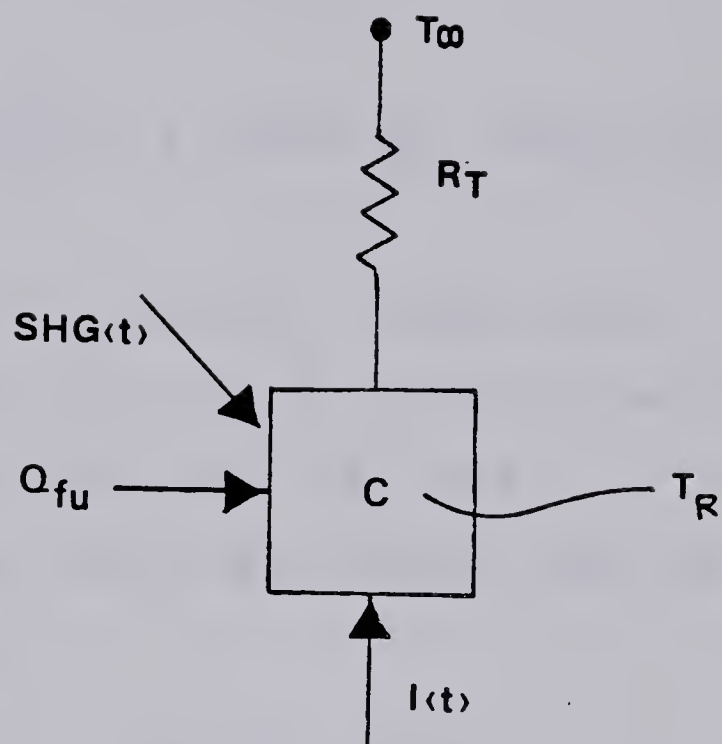


Figure 8.1 Simplified Version of the Thermal Model



heat inputs and the heat loss rate,  $U (T_R - T_\infty)$  is equal to the rate of change of heat stored in the total thermal capacity of the house,  $C_T$ . The heat balance equation describing this model would be

$$C_T \frac{dT_R}{dt} = I + SHG + Q_{fu} - U(T_R - T_\infty) \quad (8.1)$$

To extract the appropriate normalization parameters from this equation each term or group of terms will be compared in some way with the heat loss rate.

First the total heat energy that can be stored in the thermal mass is

$$C_T (T_{\max} - T_{\min}) \quad (8.2)$$

Where  $T_{\max}$  and  $T_{\min}$  are the upper and the lower set point temperatures. This value should be compared with the typical rate of heat loss during the heating season which is  $U * HDHr / HHr$  where HDHr (heating degree hours)

$$\int_{1 \text{ yr}} (T_{\min} - T_\infty) dt ; (T_\infty < T_{\min}) \quad (8.3)$$

and HHr (heating hours)

$$\int_{1 \text{ yr}} dt ; (T_\infty < T_{\min}) \quad (8.4)$$

The ratio HDHr/HHr is just the mean temperature difference  $(T_{\min} - T_\infty)$  during the heating season. The ratio of the



amount of heat storage to the mean rate of heat loss is a storage time constant,

$$\tau = \frac{C_T * (T_{\max} - T_{\min}) * \text{Hr}}{U * \text{HDHr}} \quad (8.5)$$

The heat inputs,  $I$ , SHG and  $Q_{fu}$  should also be compared to the heat loss rate. These three inputs can be combined and expressed as two parameters if some thought is given to the matter. Consider the internal loads. The internal loads can be thought of as consisting of a constant component that occurs day or night,  $I_c$ , plus a fluctuating component,  $I_f$ , that peaks during the day or early evening. That is  $I = I_c + I_f$ . During the heating season the constant component,  $I_c$ , directly relaces part of the furnace heat requirement,  $Q_{fu}$ , and thus these two components should be combined. Alternatively, the fluctuating component,  $I_f$ , acts in a very similar way to the solar heat gain, SHG, and it is appropriate to combine these components. In both cases it is the integral of these heat fluxes over the heating season that is important. The two parameters that result from these manipulations are the

Solar and Internal Gain (SIG) factor

$$\frac{\text{ISHGF} * \text{Window Area} + I_f * \text{Hr}}{U * \text{HDHr}} \quad (8.6)$$

Where Integrated Solar heat Gain (ISGH) factor

$$\int_{1 \text{ yr}} \text{SHG} dt ; (T_{\infty} < T_{\min}) \quad (8.7)$$



and the

Annual Heating Load Reduction (AHLR) factor

$$\frac{\int_{1 \text{ yr}} Q_{fu} + I_c * HHr}{U * HDHr} \quad (8.8)$$

However, a more appropriate way of calculating the constant and the fluctuating internal loads is given by

$$I'_c = \int_{1 \text{ yr}} I_c dt ; (T_\infty < T_{\min}) \quad (8.9)$$

$$I'_f = \int_{1 \text{ yr}} I_f dt ; (T_\infty < T_{\min}) \quad (8.10)$$

In such an event the SIG and AHLR factor equations can be modified as

$$SIG = \frac{ISHGF * \text{Window Area} + I'_f}{U * HDHr} \quad (8.11)$$

$$AHLR = \frac{\int_{1 \text{ yr}} Q_{fu} + I'_c}{U * HDHr} \quad (8.12)$$

The SIG factor thus relates the potential heat gain from solar and fluctuating internal loads to the heating required. The AHLR factor is the output parameter which describes how much furnace or auxiliary heating is required. The annual heating requirement,  $\int_{1 \text{ yr}} Q_{fu} dt$ , is related to the value one would obtain from a static



calculation neglecting solar gains,  $U * HDHr$ , through this latter parameter.

There are three meteorological parameters which appear in these expressions. These are the ISHG factor, The heating degree hour index,  $HDHr$ , and the number of heating hours,  $HHr$ . These are to be calculated from meteorological data using some test year as a reference.

Thus from a simple thermal model it was possible to visualize the interactions among the heat gains and the heat losses. It is therefore apparent that using the results of numerical experiments a function of the following form can be sought.

$$AHLR = f ( SIG, \tau ) \quad (8.13)$$

The results of this exercise which was carried out in reference [14] are shown in Figure 8.2. The figure shows that different levels of house insulations are properly normalized. Several curves were drawn through the computer simulated results to indicate the general dependence of AHLR factor on the SIG factor for different values of time constant. One would expect that (dashed lines in figure) for a house with a large time constant the heating requirement would approach zero.  $AHLR=0$  for  $SIG = 1$ . The data shows that as the time constant is increased this value is approached.

For each time constant there is a broad minimum in the AHLR as a function of SIG. This implies that there is a



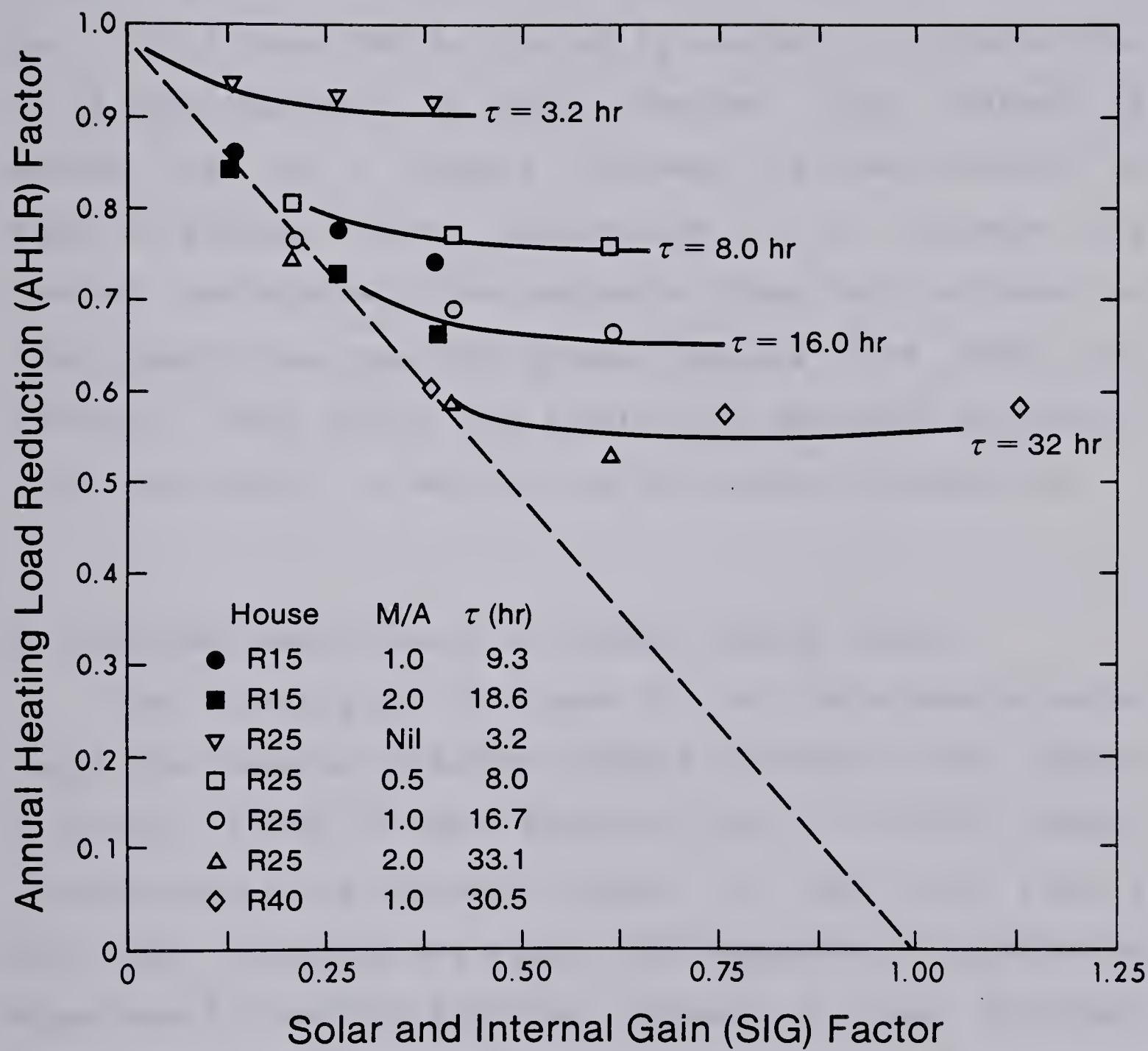


Figure 8.2 General design curves for estimating heating load reduction produced by passive solar gain



technical optimum window area for a given time constant. As the time constant can be increased the window area can be increased as well with a resulting reduction in heating load. In practice, however, the amount of mass that can be put into a house may be limited by economic considerations. It is very important to note, however, that instead of adding mass to a house to increase its time constant, an equal or perhaps better alternative is to increase the thermal resistance of the enclosure. They both increase the time constant and thus the dynamic capture from solar and internal loads while the latter also decreases the static heat requirement. It may also be the cheaper alternative.

### 8.3 Physical Significance of General Design Curves

The curves given by figure 8.2 in a more general sense imply that several different designs of direct gain houses differing either in their physical size or in their thermal characteristics are thermally similar if their SIG factors and time constants are equal. The independent variables in Equations 8.5 and 8.6 might be allowed to take different magnitudes and yet their SIG factors and the time constants can be held constant. Here is a concept which can be referred to as a criterion for thermal similarity between the houses. The definition of SIG factor also suggests that the functional relationship between AHLR and SIG factor is independent of the location. That is the weather variability



from one location to the other or from one year to the next does not alter the character of these curves.

The SIG and AHLR factors can be also be understood by visualizing them as input and output parameters. That is the SIG factor can be thought of as an input parameter and the AHLR factor is the output parameter. This approach leads to efficiency or utilization concept. To illustrate consider the utilization factor defined in reference [100]

$$\text{Utilization Factor (UF)} = \frac{\text{Fraction Net Gain}}{\text{Solar Gains}} \quad (8.14)$$

In terms of SIG and AHLR factors the utilization factor can be expressed as,

$$\text{UF} = \frac{(1 - \text{AHLR})}{\text{SIG}} \quad (8.15)$$

$$\text{IF } \text{AHLR} = (1 - \text{SIG}); \text{UF} = 1.0$$

Ideally, one would like to have an utilization factor of 1, which represents the condition at which all the solar gains will be fully utilized without causing potential overheating.



Another important application of the general design curves can be explored in carrying out a parametric study. The definitions of SIG factor and the time constant given by Equations 8.5 and 8.6 suggest that these parameters represent the ratio of variables involving the input parameters to design parameters. Therefore, by varying one parameter at a time a number of design decisions can be evaluated from these curves.

#### 8.4 Design Considerations for Passive houses

The general dependence of AHLR on SIG and  $\tau$ , at least theoretically can be extended one step further. This can be explained by observing the design curves. As noted before, the design curves indicate that there is a broad minimum in the AHLR as a function of SIG. This implies that there is a technical optimum window area for a given time constant. Thus it is possible to obtain this technical match by a simple empirical equation. An equation of the following form was found to represent this optimum condition for the range of data given in Figure 8.2.

$$\text{SIG} = 0.17 + 0.375 \log_{10} \tau \quad (8.16)$$

$$\tau = 1.48 * \left( \frac{\text{SIG}}{0.375} \right) \quad (8.17)$$

This suggests that for an optimum design the proper balance



between the thermal mass, overall resistance, window area as well as the meteorological parameters will be dictated by Equation 8.17. However, in practice, the amount of mass may be dictated more by economics than by technical considerations, mitigating toward the selection of an amount less than that suggested by Equation 8.17.

#### 8.4.1 Window Overhang

Another feature that a designer may be able to use to advantage in a passive house is a roof overhang. Figure 8.3 shows the effects of adding roof overhang of various geometries on the AHLR factor and the hours of potential overheat for one particular passive house design (R25 house,  $M/A=1.0$ , 12% window). The general nature of these curves is very similar to other designs tested. The roof overhang of 1 m (3.0 Ft.) located 0.5 m (1.5 Ft.) above the window was used as a standard throughout the previous calculations. It will be noted that AHLR is 3 percent more with this overhang than with no overhang at all; however, it reduces the hours of potential overheat by one third. Even larger overhangs, for example a 2 m (6 Ft.) overhang 1 m (3.0 Ft.) above the window could be used with minimal changes to beneficial heat gain while substantially reducing overheating.



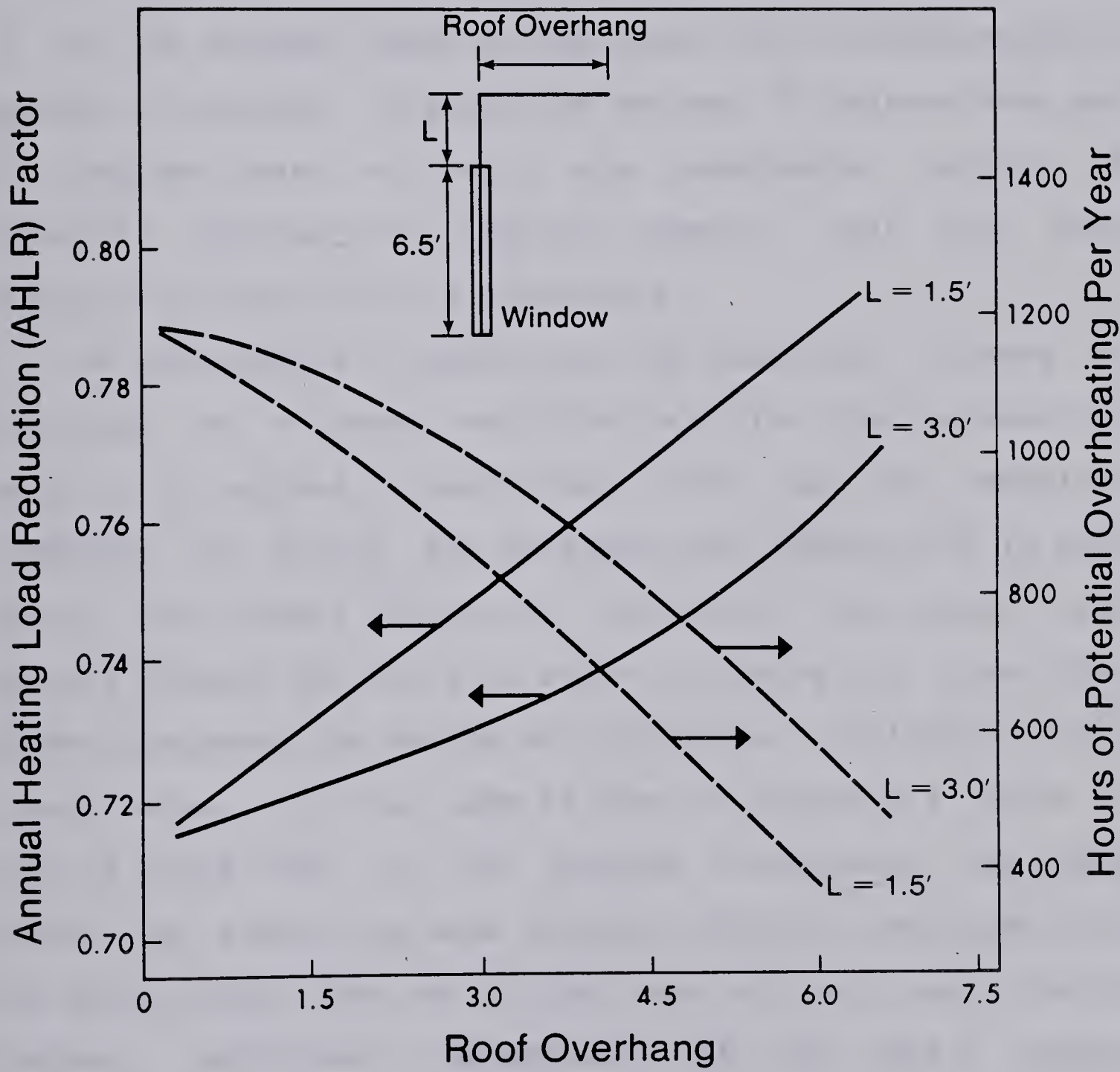


Figure 8.3 Effect of window overhang



#### 8.4.2 House Orientation

Figure 8.4 shows the effect, again only for a particular design, (R25 house,  $M/A=1.0$ , 12% window), of changing the window orientation. It can be seen that the optimum heat gain occurs for windows oriented approximately 10 to 15 degrees East of due South. For an AHLR within 5 percent of optimum, orientations between 30 degrees West and 40 degrees East of South are acceptable. Looking at potential overheating suggests however, that the more easterly orientations are preferable.

An alternative to having all the heat gain windows on one wall of a house would be to divide them between two walls at 90 degrees to each other. This has an immediate advantage of giving the designer more flexibility in plan layout. The thermal effects of splitting the window area equally between two walls is shown in Figure 8.5. Other than window placement the design of this house, including total window area, is the same as that in Figure 8.4. First it will be noted that at the optimum orientation the AHLR factor is almost the same (within 1.5%) for the house with the split window area as for the house with all south facing windows. Additional advantages of the split window configuration are that it allows a wider range in acceptable orientations and that it results in a lower amount of potential overheating. For example, a house with one-half of its window area facing East and one-half facing South has a heating requirement only 3 percent less than with all south



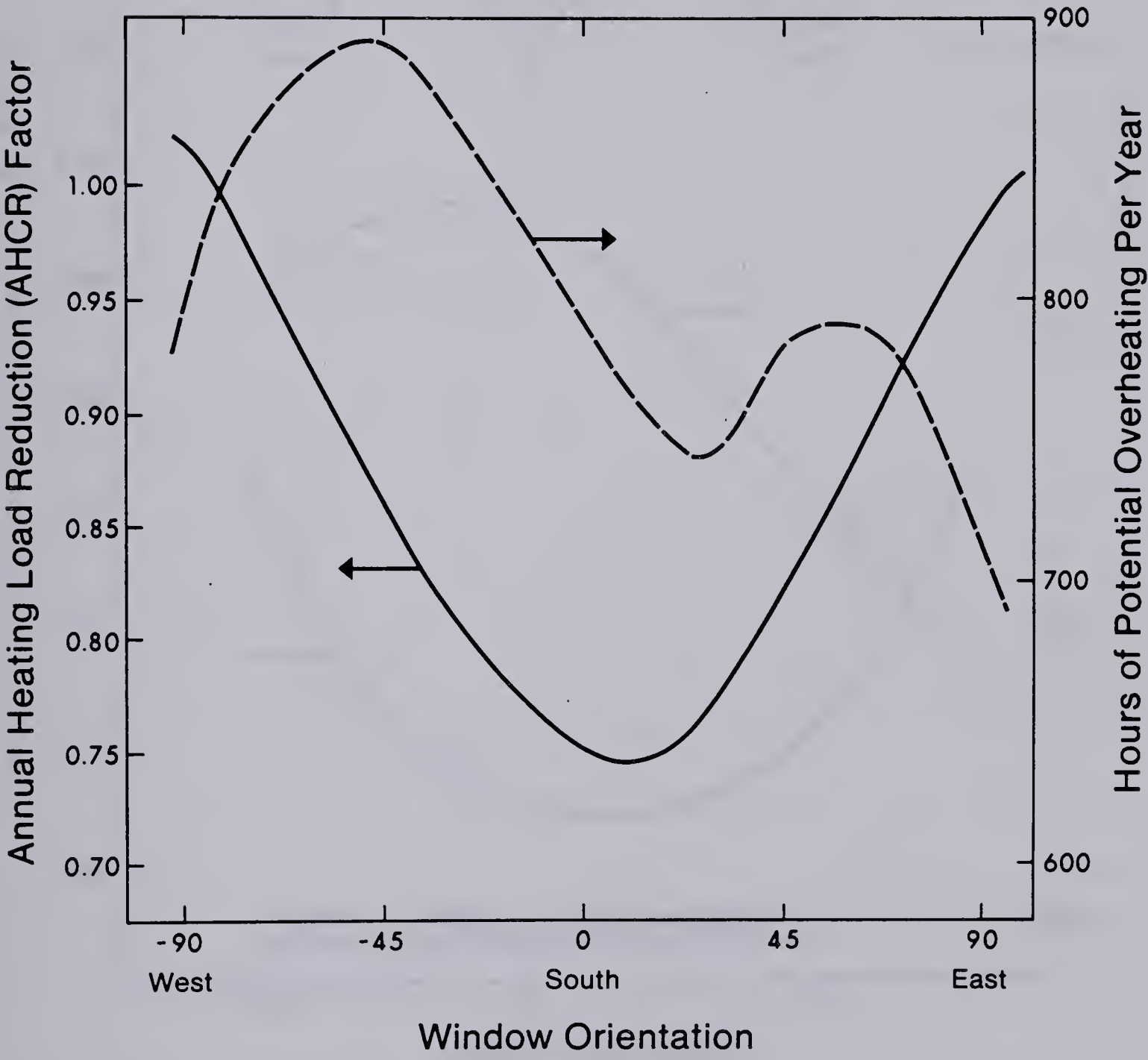


Figure 8.4 Effect of house orientation for a house with all heat gain windows in one wall



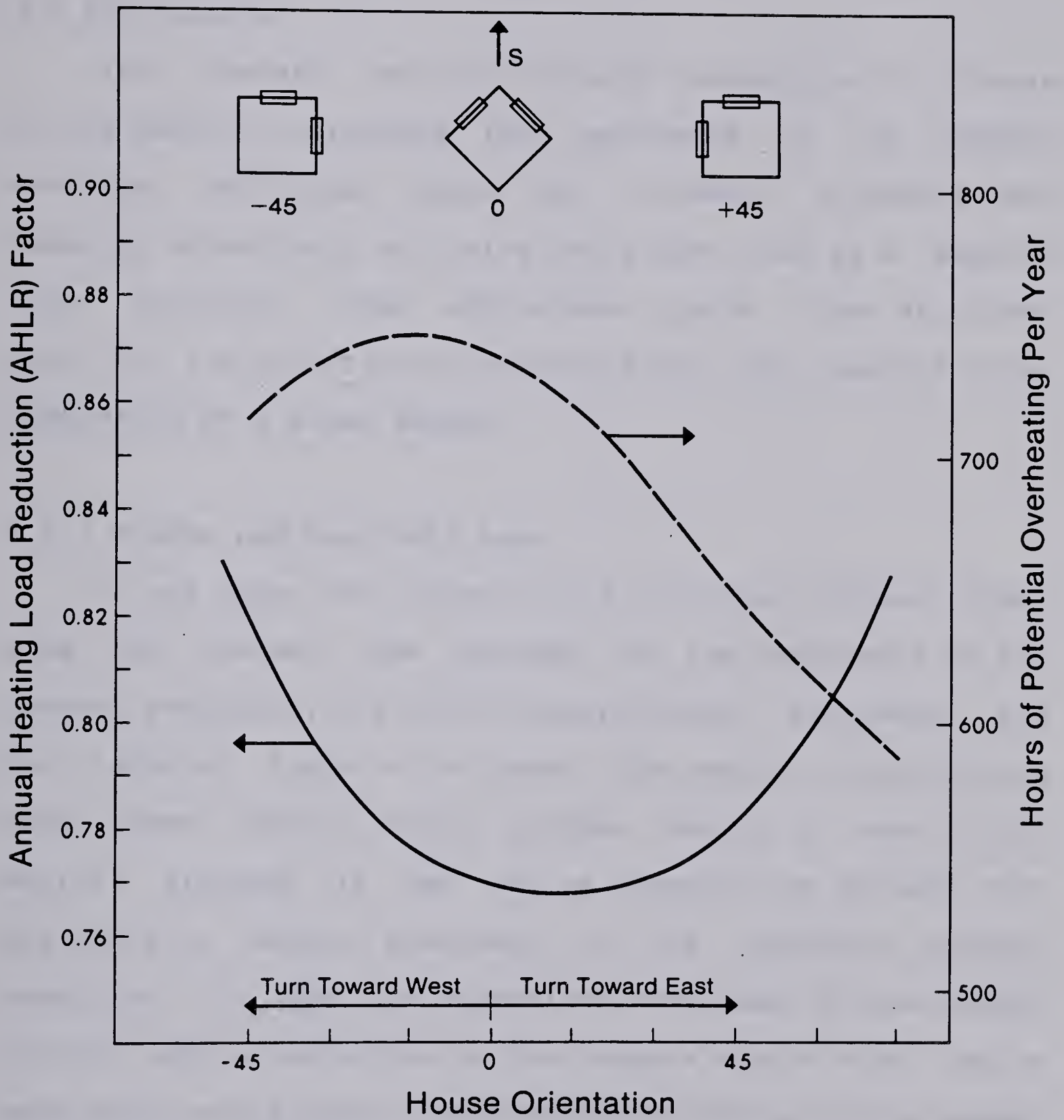


Figure 8.5 Performance of a house with window area split equally between two walls of the house



facing windows and has 30 percent less overheating.

## 8.5 Conclusions

The greatest savings in energy consumption in a house can be made by increasing the resistance of its thermal envelope. Additional gains can; however, be made in any house by effectively utilizing the window area as a passive solar collector. Some approximate guide lines are given below for the selection of various direct gain passive solar components of a house design.

### 8.5.1 Window and Mass Wall Area

It was shown that selection of technical optimum window area and thermal mass depends on the resistance of the thermal enclosure, the local meteorological parameters and the internal loads in the house. The complex relationships among these factors makes optimum design a non-trivial matter. Although it may not be necessary or perhaps even desirable to design precisely to the technical optimum condition, it must be emphasized that some obvious design errors, such as selection of too large a window area, can be made which would result both excessive overheating in summer and an increased annual heating bill. Three different designs which are close to the technical optimum conditions for their given R value are shown below.



### Technical Optimum Designs

House	Window area as	Mass wall as	Annual
Table	Fraction of	a Fraction of	Heating
8.1	Floor Area	Floor Area	Load
			(GJ)
R15	0.18 to 0.30	2.00	43.78
R25	0.12 to 0.20	1.00	19.62
R40	0.06 to 0.12	0.50	4.85

In the above table the thermal mass was assumed to be in the form of masonry walls thin enough to respond to diurnal temperature fluctuations. This means a maximum of 60 mm for a facing or a wall 120 mm thick of both sides exposed to room temperature. The measurements made at the facility suggest that the bare basement walls could provide thermal mass provided the diurnal heat inputs to the house are felt by the basement walls. Usually, this means a circulating fan may have to be used. The designs in the table also assume that an effective shutter system exists. Without such a shutter system the optimum window area is shifted toward the minimum acceptable values.

#### 8.5.2 Window Overhang

This is a component of passive design that is usually under-utilized. At high northern latitudes such as Canada's fixed window overhang can be chosen such that it has very little deleterious effect on the desirable solar gain in



winter and yet, in summer, it can very dramatically reduce overheating problems. A desirable overhang would be one located 0.5 meter above the window and extending out 1 m. An even better overhang would be 1 m above the window and extend out 2 m.

### 8.5.3 Window Orientation

For a house with its solar gain windows in one wall an orientation somewhat East of due South is optimum with orientations 30 degrees West to 40 degrees East being acceptable. If exposure over a wide enough range in sun angles is available there is some advantage to be gained by splitting the window area between two walls such as East and South facing walls.



## 9. SUMMARY AND CONCLUSIONS

The simulation model developed previously [14], was refined and tested. The procedure used to analyze the data and validation of computer model consisted of basically the following three steps:

1. The calculation of the various components of the heat loss were compared with detailed measurements from heat flux gauges, radiometers etc. These comparisons were used to test and refine the model calculations for the components.
2. The next step was to compare the predicted and the measured module performance as a whole where all of the components were involved. This was done using typical daily variations of module temperatures and furnace heat requirements. These comparisons check the time constant behaviour, solar gains as well as heat losses.
3. Finally, the heating season summary of the results were obtained which include the percentages of heating load resulting from each component of the heat loss as well as the percentage contributions to heating load reduction made by solar gains.

Conclusions drawn from the component model verification can be summarized as follows.

1. To a large extent the wood frame walls and ceilings can be considered as simple resistive elements. Their heat capacity effects can be accounted for via a lumped capacity approach for the transient analysis.



2. The analysis of basement heat losses can be greatly simplified by introducing the concept in which the heat exchange to the basement walls can be divided into two components. One with a diurnal variation and one with an annual variation. By uncoupling the annual variations from the diurnal variations, the energy balance equation can be solved with relative ease.
3. Reasonably accurate estimate of the basement heat losses can be obtained by using a two dimensional model such as the third model described in section 4.3.3. The results of this model could then be transformed to the main simulation model using the first model (section 4.3.1). This approach is reasonably accurate and requires negligible computational time.
4. A comparison of basement heat losses using the simulation model shows that relative heat losses of the basements in module 3 (RSI 3.52 full height), module 4 (RSI 1.76 full height) and module 5 (RSI 1.76, 0.6m below grade) with respect to an uninsulated basement, are of the order of 0.47, 0.58 and 0.77 respectively.
5. The available techniques for calculation of the radiation on a vertical surface are not suitable for calculation of heating loads on an hourly basis. This limits the accuracy of the hourly heating load calculations. From the results of analysis, it is speculated that the effects of anisotropic nature of reflected light from a snow cover could be important



particularly at low sun angles.

6. The insitu transmissivity of a double glass window around normal incidence was found to be about 10% less than the normally expected value for a clear double glass. The loss of transmissivity is believed to be due to surfacial layers on the glass.
7. Improper sealing of shutter around the edges causes a considerable loss in effective thermal resistance due to air infiltration. The measured window shutter resistance on the modules showed that the actual resistance was about 35% less than the expected value.
8. For accurate analysis of heating load requirements on a hourly basis the dynamics of the window shutters may have to be included in the main simulation model.
9. The effective thermal capacity of a structure can be considered to be of two types: a lumped capacity and a distributed capacity. It was shown that by developing a simple transient model, these two parameters can be extracted from the transient decay curves.

The various component models developed and tested were put together to predict the module performance as a total system. The ability of the main simulation model to predict the module performance on a hourly basis was demonstrated by comparing the module room air temperatures and most importantly the module heat requirements.

A subject of current interest is the heating load reductions that can be produced by solar gains, window



shutters, and the thermal mass. To determine these contributions directly from the measurements is an expensive and time consuming endeavor. Alternatively, a logical way of extracting the seasonally averaged contributions made by solar gains to the heating load reductions was demonstrated.

Some results of interest to house heating design and the model verification studies can be summarized as follows.

1. The measured thermal performance of the modules 3 and 4 relative to module 2 of standard construction indicates a reduction in energy consumption of the order of 66% for module 3 and 47% for module 4.
2. From the results of the measurements of diurnal heat fluxes to the basements and as well as the transient decay tests, it appears that basements which are uninsulated on the inside surface have a major effect on the thermal capacity of the house.
3. Double pane south facing windows on a well insulated house in a northern climate such as Edmonton, provide near zero net gains when averaged over the heating season. This is true for relatively small window area (less than 12% of the floor area). It is predicted that larger window areas would result in a net loss due to the inability of a house of standard construction to absorb the addition of solar gains.
4. The addition of window shutters could give the south facing windows a positive net gain. It would appear that south facing windows with shutters (RSI 1.0) could



reduce the house heating requirement of a typical house by about 20%. This is with the thermal mass provided by bare basement walls with no added mass walls.

5. The data analysis on the modules suggested that the simulation models for estimating the heat requirements may have to be subjected to a comprehensive testing procedure. Without such a testing procedure the models may not be able to distinguish the actual solar gains from the large errors that might result in due to improper modeling techniques.
6. An investigation of the component heat losses indicate that basement losses and infiltration account for 50 percent of the total loss for highly insulated modules. Since these are the most difficult heat losses to predict, the calculation of heat requirement of houses built to similar specifications remains a challenging area of endeavor.

Although not adequately demonstrated, it appears that passive house designs could be evaluated with reasonable accuracy through the use of the general design curves. Therefore, based on the simulation studies carried out for developing these curves the following conclusions can be drawn.

1. The greatest savings in energy consumption in a house can be made by increasing the resistance of its thermal envelope. Additional gains can; however, be made in any house by effectively utilizing the window area as a



passive solar collector. The general design curves could be used for this purpose.

2. A desirable overhang for the Northern latitudes, appears to be one located 0.5 m above the window extending 1 m. An even better overhang would be 1 m above the window and extending out 2 m.
3. For a house with its solar gain windows all in one wall an orientation somewhat East of due South appears to be optimum with orientations 30 degrees West to 40 degrees East seem reasonable. If exposures over wide enough range of sun angles is available there is some advantage to be gained by splitting the window area between two walls such as East and South facing walls.

### 9.1 Recommendations

Further research into the following areas would be of interest.

1. Theoretical and experimental study to develop improved predictive models for estimating the hourly radiation intercepted by a vertical surface with emphasize on the influence of snow cover at low sun angles can be a good research problem. Such a study will be of considerable importance for modeling the house heating load requirements.
2. Use of phase change materials for passive solar energy storage and their impact on the heating load reductions



that can be achieved through their use would be another potential research problem of interest.

3. A detailed experimental investigation into ceiling heat losses could be very valuable for developing improved ceiling heat loss models.
4. Finally, developing simple and yet reasonably accurate general infiltration models still remains as one of the challenging research problem.



## REFERENCES

1. O' Callaghan, P.W.

Building for Energy Conservation, Pergamon Press, New York, 1978.

2. Yellot, J.J.

Passive Solar Heating and Cooling Systems, ASHREA Trns., Vol. 83, Pt. 2, 1977.

3. Holtz, M.J., Wayne, P. and Kammerud, R.C.

A Classification Scheme for the Common Passive and Hybrid Heating and Cooling Systems, Proc. 3rd National Passive Solar Conference, ISES, Vol. 3, 282-289, 1979.

4. Kusuda, T.

NBSLD - the computer program for heating and cooling loads in Buildings, NBS, Building Science Series 69, 1976.

5. Hittle, D.C.

BLAST - The Building Loads Analysis and Systems Thermodynamics Program, Proceedings third international symposium on the use of computers for environmental engineering related to buildings, Banff, Alberta, Canada, 1978.

6. Konard, A. and Larsen, B.T.

ENCORE-CANADA: Computer Program for the Study of Energy Consumption of Residential Buildings in Canada, DBR Paper No. 859, National Research Council of Canada, NRCC 17663, 1978.

7. Kerrisk, J.F., Schnur, N.M., Moore, J.E. and Hunn, B.D.

The Custom Weighing Factor Method for Thermal Load Calculations in the DOE-2 Computer program, ASHRAE Trans, Vol. 87, Pt. 2, 1981.

8. Klein, S.A. et al.

TRNSYS - A Transient Simulation Program, Report 38-10, Solar Energy Laboratory, University of Wisconsin - Madison, June 1979.



## 9. ASHRAE Task Group

Procedure for Determining Heating and Cooling Loads for Computerizing Energy Calculations. Algorithms for Building Heat Transfer Subroutines, Energy Calculations 1, ASHRAE Task Group on Energy Requirements for Heating and Cooling of Buildings, ASHRAE Inc., 1975.

## 10. McFarland, R.D.

PASOLE: A General Simulation Program for Passive Solar Energy, Los Alamos Scientific Laboratory Report LA-7433 Ms, Oct., 1978.

## 11.

SUNCAT: Simulation Program Developed at The National Centre for Appropriate Technology, P.O. Box 3838 Butte, Montana 59701.

## 12. Chen, B., Maloney, J. and Thorp, J.

Modeling Thermal Networks with PCAP, Conference Proceedings ISES, Silver Jubilee Conference, Atlanta, Georgia, Vol. 2, PP. 1583-1587, 1979.

## 13. Goldstein, D.B.

Modeling Passive Solar Buildings With Hand Calculators, Proceedings of the 3rd National Passive Solar Conference, Sanjose, California, Jan., 1979.

## 13A. Dumont, R.S., Lux, M.E. and Orr, H.W.

HOTCAN: A Computer Program For Estimating The Space Heating Requirement Of Residences, DBR Computer Program No.49, National Research Council of Canada, Ottawa, Canada, September 1982.

## 14. Zaheeruddin, M.

Computer Simulation of Direct Gain Passive House, MSc. thesis, The University of Alberta, July 1980.

## 15. Gilpin, R.R., Dale, J.D., Forest, T.W. and Ackerman, M.Y.

Construction of the Alberta Home Heating Research Facility and results for the 1979-80 Heating Season, Departmental Report No.23, Department of Mechanical Engineering, The



University of Alberta, August 1980.

16. Gupta, C.L., Spencer, J. and Muncey, R.

A Conceptual Survey of Computer Oriented Thermal Calculation Methods, Use of Computers for Environmental Engineering Related to Buildings, Building Science Series, NBS 39, Oct., 1971.

17. Stephenson, D.G. and Mitalas, G.P.

Cooling Load Calculations by Thermal Response Factor Method, ASHRAE Transactions, 73, Part 1, 1967.

18. Mitalas, G.P. and Stephenson, D.G.

Room Thermal Response Factors ASHRAE Transactions, 73, Part 1, 1967.

19. Stephenson, D.G. and Mitalas, G.P.

Calculation of Heat Conduction Transfer Functions for Multi-Layer Slabs, ASHRAE Transactions, Vo. 77, Part II, 1971.

20. Mitalas, G.P. and Arseneault, J.G.

Fortran-1V Program to Calculate Z-Transfer Functions for the Calculation of Transient Heat Transfer Through Walls and Roofs, NRC, DBR, Computer Program No. 33, 1972.

21. Mackey, C.O. and Wright Jr., L.T.

The Sol-Air Thermometer - A New Instrument, ASHVE Transactions Vol. 52, p. 277, 1946.

22. Van Gorcum, A.H.

Theoretical Considerations on the Conduction of Fluctuating Heat Flow, Appl. Sci. Rec., Hague, Vol. A2, 1951.

23. Carslaw, H.S. and Jaeger, J.C.

Conduction of Heat in Solids, Oxford University Press, 1959.

24. Alford, J.S., Ryan, J.E. and Urban, F.O.

Effect of Heat Storage and Variation in Outdoor Temperature and Solar Intensity on Heat Transfer Through Walls, ASHVE Transactions, Vol. 45,



1939.

25. Mackey, C.O. and Wright, L.T.

Periodic Heat Flow - Homogeneous Walls and Roofs, ASHVE Transactions, Vol. 50, 1946.

26. Mackey, C.O. and Wright, L.T.

Periodic Heat Flow - Composite Walls and Roofs, ASHVE Transactions, Vol. 52, 1946.

27. Sonderegger, R.C.

Dynamic Models of House Heating Based on Equivalent Thermal Parameters, Doctoral Dissertation, Princeton University, N.J., 1977.

28. Goldstein, D.B.

Some Analytic Models of Passive Solar Building Performance: A theoretical Approach to the Design of Energy Conserving Buildings, Doctoral Dissertation, University of California, Berkeley, 1978.

29. Billington, N.S.

Building Physics - Heat, Pergamon Press, P.68, 1967.

30. Gerald, C.F.

Applied Numerical Analysis, Addison-Wesley Publishing Company, 1978.

31. Myers, G.E.

Analytical Methods in Conduction Heat Transfer, McGraw-Hill Book Company, 1971.

32. Patankar, S.V.

Numerical Heat Transfer and Fluid Flow, Hemisphere Publishing Corporation, 1980.

33. Balcomb, J.D. and McFarland, R.D.

A Simple Empirical Method for Estimating the Performance of a Passive Solar Heated Building of Thermal Storage Wall Type, Proceedings of the 2nd National Passive Solar Conference, Philadelphia, PA, March, 1978.



34. Wray, W.D., Balcomb, J.D. and McFarland, R.D.

A Semi-empirical Method for Estimating the Performance of Direct Gain Passive Solar Heated Buildings, 3rd National Passive Solar Conference, Sanjose, CA, Jan., 1979.

35. Mitalas, G.P.

Net Annual Heat Loss Factor Method for Estimating Heat Requirements of Buildings, Building Reseach Note 117, NRC, Canada Nov., 1976.

36. Mitalas, G.P.

Relation Between Thermal Resistance and Heat Storage in Building Enclosures, Building Research Note 126, NRC, DBR, Jan., 1978.

37. Monsen, W., Klein, S., Beckman, W. and Utzinger, D.

The Resistance Network Design Method for Passive Solar Systems, Proceedings of the 4th National Passive Solar Conference, Kansas city, Missouri, Vol. 4, Oct., 1979.

38. Monsen, W.A., Klein, S.A. and Beckman, W.A.

Prediction of Direct Gain Solar Heating System Performance, Solar Energy Vol. 27, No. 2, pp.143-147, 1981.

39. Gordon, J.M. and Zarmi, Y.

Analytical Model for Passively Heated Solar Houses-I Theory, Solar Energy Vol. 27, No. 4, pp.331-342, 1981.

40. Gordon, J.M. and Zarmi, Y.

Analytical Model for Passively Heated Solar Houses-II Users Guide, Solar Energy, Vol. 27, No. 4, pp.343-347, 1981.

41. Gordon, J.M. and Zarmi, Y.

Massive Storage Walls as Passive Solar Heating Elements: An Analytic Model, Solar Energy, Vol. 27, No.4, pp.349-355, 1981.

42. Hodges, L., Block, D.A. and Ward, W.O.

A Simple Methodology for Generating Solar



Percentage Graphs based on Actual Winters, Proceedings of the 4th National Passive Solar Conference, Kansas City, Missouri, Vol. 4, Oct., 1979.

43. Mazria, E. and Wessling, F.C.

An Analytical Model for Passive Solar Heated Buildings, Proceedings of 1977 Annual Meeting, ASISIS, Florida, Vol. 1, June, 1977.

44. Sonderegger, R.C. and Garnier, J.Y.

A Simplified Method for Calculating Heating and Cooling Energy in Residential Buildings, LBL-13508, Lawrence Berkely Laboratory, Energy and Environment Division, University of California, Oct., 1981.

45. Peavy, B.A., Powell, F.J. and Burch, D.M.

Dynamic Thermal Performance of an Experimental Masonry Building, NBS, Building Science Series 45, 1973.

46. Chen, B., Maloney, J., Thorp, J. et al.

Preliminary Winter Comparison Results of Four Passive Test Cells in Omaha, Nebraska, Proc. of the ISES, Silver Jubilee Conference, Atlanta, Georgia, Vol. 2, pp. 1583-1587, 1979. (Pergoman Press)

47. Arumi'-Noe', F.

Field Validation of the DEROB/PASOLE System, Proc. of the 3rd National Passive Solar Conference, PP. 152-158, 1979.

48. Hunn, B.D., Schnurr, N.M., Peterson, J.L. kerrisk, J.F. and Moore, J.E.

Application of DOE-1 to Passive Solar Heating of Commercial Buildings: Preliminary Results, Proc. 3rd National Passive Solar Conference, Sanjose, California, pp. 159-163, 1979.

49. Wheeling, T. Wardsworth, B. and Palmiter, L.

Performance of Passive Test Units during the 1978-1979 Heating Season, Proceedings of the ISES Silver Jubilee Congress, Atlanta, Georgia, Peramon Press, Oct. 2, pp.1589-1592, 1979.



50. Balcomb, J.D., McFarland, R.D. and Moore, S.w.

Simulation Analysis of Passive Solar Heating Buildings -- Comparison with Test Room Results, Proceedings of the ASISES, 1977 Annual Meeting, Florida, June, 1977.

51. Dumont, R.T., Orr, H.W., Hedlin, C.P. and Makohon, J.T.

Measured Energy Consumption of a Group of Low Energy Houses, Proceedings Solwest 80, Vancouver, Published by SESC Canada, 1980.

52. Besant, R.W., Green, G.H. and Schoenan, J.

Experimental Measurements of the Dynamic Thermal Behavior of three Passive Solar Energy Conserving Houses, Proceedings Solwest 80, Vancouver, Published by SESC Canada, 1980.

53. Moore, E.F. and McFarland, R.D.

Passive Solar Test Modules, LA-9421-MS, Los Alamos National Laboratory, New Mexico 87545, June, 1982.

54. Gilpin, R., Forest, T., Ackerman, M., Wilson, D., Sadler, G. Dale, J. and Zaheeruddin, M.

Second Annual Report on the Alberta Home Heating Research Facility: Results for the 1980-81 Heating Season, Departmental Report No. 24, Department of Mechanical Engineering, The University of Alberta, June, 1981.

- 55.

ASHRAE Handbook of Fundamentals - 1977, American Society of Heating Refrigerating and Air Conditioning Engineers, New York.

56. Dale, J.D., Wilson, D.J. and Ackerman, M.

Adaptable Modules for Air Infiltration Studies in Home Heating, Proceedings of the International Seminar on Air Infiltration and Ventilation, Building Research Establishment, Watford, U.K., April, 1980.

57. Houghten, F., Tainmuty, S., Gutberlet, C. and Brown, C.

Heat Loss Through Basement Walls and Floors, ASHVE Trans., pp.369-384, 1942.

58. Brown, W.G.



Graphical Determination of Temperature under Heated or Cooled Areas on the Ground Surface, NRC, DBR, NRC 7660, Oct., 1963.

59. Boileau, G.G. and Latta, J.K.

Calculation of Basement Heat Losses, Technical Paper 292 of the Division of Building Research, (NRC 10477), NRC, Ottawa, Dec., 1968.

60. Latta, J.K. and Boileau, G.G.

Heat Losses From House Basements Canadian Building Vol. xix No. 10, Oct. 1969, pp.39-42.

61. McBride, M., Blancett, R., Sepsy, C. and Jones, C.

Measurement of Subgrade Temperatures for Prediction of Heat Losses in Basements, ASHRAE Trans, Vol. 185, Part I, 1979.

62. Shipp, P.H.

The Thermal Characteristics of Large Earth-Sheltered Structures, Doctoral Dissertation, The University of Minnesota, 1979.

63. Swinton, M.C. and Platts, R.E.

Engineering Method for Estimating Annual Basement Heat Loss and Insulation Performance, ASHRAE Trans, vol. 87, Part 2, 1981.

63A. Mitalas, G.P.

Basement Heat Loss Studies at DBR/NRC, DBR Paper No.1045, Division of Building Research, National Research Council of Canada, Ottawa, Canada, September 1982.

64. Kusuda, T. and Achembach, P.R.

Numerical Analyses of the Thermal Environment of Occupied Underground spaces with Finite Cover using Digital Computer, ASHRAE Trans, Vol. 69, 1963.

65. Gilpin, R.R.

The Ground Temperature Boundary Condition Provided by a Moss Covered Surface, ASME 76-WA/HT-61, 1976.

66. Gilpin, R.R. and Wong, B.K.



Heat Valve Effects in the Ground Thermal Regime, Journal of Heat Transfer, Vol. 98, Nov. 1976, pp.537-542.

67. Gilpin, R.R. and Wong, B.K.

A Study of Some Factors that Influence Ground temperature, Proceedings of the 4th Canadian Congress of Applied Mechanics Montreal 1973, pp.771-772.

68. de Vries, D.A.

Heat Transfer in Soils, Heat and Mass Transfer in the Biosphere, Vol.1, De Vries, D.A., Afgan, N.H., ed, John Wiley and Sons, Scripta Book Co., Washington, D.C., 1975.

69. Philip, J.

Water Movement in Soil, Heat and Mass Transfer in the Biosphere Vol 1, De Vries, D.A., Afgan, N.H., ed. John Wiley and Sons, Scripta Book Co., Washington D.C., 1975.

70. Eckert, E.R.G., Bligh, T.P. and Pfender, E.

Energy Exchange Between Earth Sheltered Structures and the Surrounding Ground, Energy, Vol. 4, pp.171-181, Pergamon Press, 1979.

71. Meixel, G.D., Shipp, P.H. and Ramsey, J.W.

Analysis and Measurement of the Thermal Behaviour of the Walls and Surrounding Soil for a large Underground Building, Proceedings of the ASHRAE/DOE-ORNL Conference on the Thermal Performance of the Exterior Envelops of Buildings, Kissimmee, Florida, Dec., 1979.

72. Meixel, G.D., Shipp, P.H. and Bligh, T.P.

The impact of Insulation Placement on the Seasonal Heat loss through Basement and Earth Sheltered Walls, Proceedings of the ASHRAE/DOE-ORNL Conference on the Thermal Performance of the Exterior Envelops of Buildings, Kissimmee, Florida, Dec., 1979.

73. Lachenbruch, A.H.

Periodic Heat Flow in a Stratified Medium With Application to Permafrost Problems, Experimental and Theoretical Geophysics, Geological Survey



Bulletin 1083-A, Washington D.C., 1959.

74. Liu, B.Y.H. and Jordan, R.C.

The Interrelationship and Characteristic Distribution of Direct, Diffuse, and Total Solar Radiation, Solar Energy 4 (3), 1960, pp.1-19.

75. Hay, J.E.

A Revised Method for Determining the Direct and Diffuse Components of the Total Short Wave Radiation, Atmosphere 14 (4), 1976, pp.278-287.

76. Threlkeld, J.L.

Solar Irradiation of Surface on Clear Days, ASHRAE Transactions, Vol. 69, 1963, P. 27.

77. Pratt, A.W. and Ball, E.F.

Transient Cooling of a Heated Enclosure, Int. J. of Heat Mass Transfer, Vol. 6, 1963, pp.703-718.

78. Choudhury, N.K.D. and Warsi, Z.U.A.

Weighting Function and Transient Thermal Response of Buildings, Part I, Homogenous Structure, Int J. of Heat Mass Transfer, Vol. 7, 1964, pp.1309-1321.

79. Warsi, Z.U.A. and Choudhury, N.K.D.

Weighting Function and Transient Thermal Response of Buildings, Part II, Composite Structure, Int. J. of Heat Mass Transfer Vol. 7, 1964, pp.1323-1334.

80. Janssen, J.E.

Building Thermal Resistance Measurement, Paper Presented at Winter Annual Meeting of the ASME, San Francisco, California, Dec. 1978 on Energy Conservation in Building Heating and Air Conditioning

81. Brown, W.C. and Schuyler, G.D.

Insitu Measurements of Frame Wall Thermal Resistance, ASHRAE Trans., Vol. 88, Part I, 1982.

82. Sherman, M.H. Sonderegger, R.C. and Adams, J.W.



The Determination of the Dynamic Performance of Walls, ASHRAE Trans., Vol. 88, Part I, 1982.

83. Roberts, Jr., C.C. and Reinke Jr., K.

Thermal Measurements of Building Envelope Components in the Field, ASHRAE Trans., Vol. 88, Part I, 1982.

84. Jaeger, J.C.

Conduction of Heat in Composite Slabs, Quart. Applied Mathematics, 8, 1950, pp.187-198.

85. Wilkes, K.E.

Modeling of Residential Attics, Proceedings of the ASHRAE/DOE-ORNL Conference on the Thermal Performance of the Exterior Envelopes of Buildings, Kissimmee, Florida, Dec. 1979.

86. Ruth, D.W. and Chant, R.E.

The Relationship of Diffuse Radiation to Total Radiation in Canada, Solar Energy, Vol. 18 (2), 1976, pp.153-154.

87. Bugler, J.W.

The Determination of Hourly Insolation on an Inclined Plane Using a Diffuse Irradiance Model based on Hourly Measured Global Horizontal Insolation, Solar Energy, Vol.19, 1979, pp477-491.

88. Iqbal, M.

Prediction of Hourly Diffuse Solar Radiation From Measured Hourly Global Radiation on a Horizontal Surface, Solar Energy, Vol. 24, 1980, pp.491-503.

89. Bruno, R.

A Correction Procedure for Separating Direct and Diffuse Insolation on a Horizontal Surface, Solar Energy, Vol. 20, 1978, pp.97-100.

90. Orgill, J.F. and Hollands, K.G.T.

Correlation Equation for Hourly Diffuse Radiation on a Horizontal Surface, Solar Energy, Vol. 17, 1977, pp.357-359.



91. Klein, S.A. and Duffie, J.A.

Estimation of Monthly Average Diffuse Radiation,  
Presented at the National Solar Energy  
Conference, 1978.

92. Hill, J.E. and Kusuda, T.

Dynamic Characteristics of Air Infiltration, Trans,  
ASHRAE, Vol. 81, Part I, 1975, pp.168-185.

93. Hunt, C.M. and Burch, D.M.

Air Infiltration Measurements in a Four-Bedroom  
Tower House Using Sulfur Hexafluoride as a  
Tracer Gas, ASHRAE Trans, Vol. 81, Part I, 1975,  
pp.188-198.

94. Kumar, R., Ireson, A.D. and Orr, H.W.

An Automated Air Infiltration Measuring System  
Using SFG Tracer Gas in Constant Concentration  
and Decay Methods, ASHRAE Trans, Vol. 85, Part  
II, 1979, pp.385-394.

95. Sherman, M.H., Grimsrud, D.T. and Diamond, R.C.

Infiltration-Pressurization Correlation:  
Surface Pressures and Terrain Effects, LBL, No.  
8785, 1979.

96. Sherman, M.H., Grimsrud, D.T. and Sonderegger, R.C.

Low Pressure Leakage Function of Building,  
Proceedings ASHRAE/DOE-ORNL Conference on  
Thermal Performance of Exterior Envelopes of  
Buildings, Published by ASHRAE, New York, 1979.

97. Stewart, M.B., Jacob, T.R. and Winston, J.G.

Analysis of Infiltration by tracer Gas  
Technique, pressurization tests and Infrared  
Scans, Proceedings ASHRAE/DOE-ORNL Conference on  
Thermal Performance of Exterior Envelopes of  
Buildings, Published by ASHRAE, New York, 1979.

98. Reeves, G. McBride, M. and Sepsy, C.

Infiltration Models for Residences, Trans.  
ASHRAE Vol. 85, Part 1, 1979.

99. Ackerman, M., Dale, J., forest, T., Gilpin, R., Wilson,  
D., Sadler, G. and Zaheeruddin, M.



The Alberta Home Research Facility - Update III  
- 1981-1982 Heating Season, Energex' 82, Solar  
Energy Society of Canada Inc., Regina, August  
1982.

100. Barakat, S.A.

Solar Heat Gains through windows in Canada. DBR  
Paper No. 944, National Research Council of  
Canada, Division of Building Research, Canada,  
1980.

101. McBride, M.E.

Dynamic Modeling of System Transients By  
Computer Simulation for Prediction of  
Residential Energy Consumption. Ph.D.  
dissertation, the Ohio State University 1979.

102. Forest, T., Gilpin, R., Ackerman, M., Sadler, G., Dale,  
J. and Zaheeruddin, M.

The Alberta Home Heating Research Facility -  
Update II - The 1980-1981 Heating Season, Solar  
Energy Society of Canada Inc., Annual Meeting  
Montreal, August 1981.

103. Gilpin, R.R. and Zaheeruddin, M.

Optimum Design for a House Employing Direct  
Solar Gain: A Computer Simulation Study, Proc.  
Sol West 80, Vancouver, British Columbia, August  
1980, pp.433-437.

104. Barakat, S.A. and Sander, D.M.

Utilization of Solar Gain through Windows for  
Heating Houses Building Research Note 184, NRC,  
Ottawa, March 1982.





B30376